NASA/CR—2008-215479

Seal Technology Development for Advanced Component for Airbreathing Engines

Philip H. Snyder
Rolls-Royce North American Technologies, Inc., Indianapolis, Indiana

December 2008

NASA STI Program . . . in Profile

Since its founding, NASA has been dedicated to the advancement of aeronautics and space science. The NASA Scientific and Technical Information (STI) program plays a key part in helping NASA maintain this important role.

The NASA STI Program operates under the auspices of the Agency Chief Information Officer. It collects, organizes, provides for archiving, and disseminates NASA's STI. The NASA STI program provides access to the NASA Aeronautics and Space Database and its public interface, the NASA Technical Reports Server, thus providing one of the largest collections of aeronautical and space science STI in the world. Results are published in both non-NASA channels and by NASA in the NASA STI Report Series, which includes the following report types:

- TECHNICAL PUBLICATION. Reports of completed research or a major significant phase of research that present the results of NASA programs and include extensive data or theoretical analysis. Includes compilations of significant scientific and technical data and information deemed to be of continuing reference value. NASA counterpart of peer-reviewed formal professional papers but has less stringent limitations on manuscript length and extent of graphic presentations.

- TECHNICAL MEMORANDUM. Scientific and technical findings that are preliminary or of specialized interest, e.g., quick release reports, working papers, and bibliographies that contain minimal annotation. Does not contain extensive analysis.

- CONTRACTOR REPORT. Scientific and technical findings by NASA-sponsored contractors and grantees.

- CONFERENCE PUBLICATION. Collected papers from scientific and technical conferences, symposia, seminars, or other meetings sponsored or cosponsored by NASA.

- SPECIAL PUBLICATION. Scientific, technical, or historical information from NASA programs, projects, and missions, often concerned with subjects having substantial public interest.

- TECHNICAL TRANSLATION. English-language translations of foreign scientific and technical material pertinent to NASA's mission.

Specialized services also include creating custom thesauri, building customized databases, organizing and publishing research results.

For more information about the NASA STI program, see the following:

- Access the NASA STI program home page at *http://www.sti.nasa.gov*

- E-mail your question via the Internet to *help@sti.nasa.gov*

- Fax your question to the NASA STI Help Desk at 301–621–0134

- Telephone the NASA STI Help Desk at 301–621–0390

- Write to:
  NASA Center for AeroSpace Information (CASI)
  7115 Standard Drive
  Hanover, MD 21076–1320

NASA/CR—2008-215479

Seal Technology Development for Advanced Component for Airbreathing Engines

Philip H. Snyder
Rolls-Royce North American Technologies, Inc., Indianapolis, Indiana

Prepared for
National Aeronautics and Space Administration
Glenn Research Center, Cleveland, Ohio

Prepared under Contract NAS3–01143, Task Order 5

National Aeronautics and
Space Administration

Glenn Research Center
Cleveland, Ohio 44135

December 2008

This work was sponsored by the Fundamental Aeronautics Program
at the NASA Glenn Research Center.

Level of Review: This material has been technically reviewed by NASA technical management.

Available from

NASA Center for Aerospace Information
7115 Standard Drive
Hanover, MD 21076–1320

National Technical Information Service
5285 Port Royal Road
Springfield, VA 22161

Available electronically at http://gltrs.grc.nasa.gov

Statement of Work Tasks

I. Preliminary Design

a. Study and evaluate candidate gas dynamic wave cycles for the ORC/WR, including consideration of various modes of combustion.

b. Select an agreed upon gas dynamic wave cycle of the ORC/WR, including the mode of on-rotor combustion, as necessary to establish the preliminary aero-design size of the wave rotor, ports spacing, and thermal and pressure fields for the engine product application. The combustion mode must be consistent with high thermodynamic performance.

c. Produce a practicable preliminary mechanical design applicable to the required rotor and casing. Internal unsteady and steady thermal and mechanical loads are to be considered plus the required adaptive ducting or peripherals for the fuel/ignition system. The design is to assure operation within realistic mechanical constraints.

II. Develop Seal Strategies

a. Identify and develop seals to mitigate leakage or clearance flows that detrimentally impact aerothermodynamic performance. The seal strategies will be applicable to the general geometry of an on-axis, partial-admission/emission wave-rotor in which ducts port flows to and from surrounding full-annulus turbomachinery components. These are to include the seal strategies that reflect and build upon prior contracted efforts. The effort is to accommodate comprehensively new seal concepts and challenges posed by the on-rotor combustion at engine operating conditions. Seal strategies must address the realities of mechanical design and be targeted at the product engine application.

b. Apply seal strategies and technologies to the geometry required for the agreed upon engine demonstration.

c. Identify new technology requirements and corresponding development plans.

III. Apply Developed Seal Strategies

Apply developed seal strategies and technologies to the NASA SE-17 four-port wave rotor, which will represent an agreed upon concept development/demonstration vehicle unless another seals POC experiment is identified by contract midterm with NASA concurrence. Develop seal designs at sufficient level to enable manufacture, build-up, and test in POC experiment in the second year.

Program Summary

This program addressed key aspects of the design of sealing systems for On Rotor Combustion/Wave Rotor (ORC/WR) systems. The first step was to arrive at a proper context in which to attempt a sealing design. With no historical base of generally accepted ORC/WR design from which to draw, the work proceeded to identify specifics within a relevant product engine, a suitable demonstrator engine, and a useful proof-of-concept (POC) rig. Thus work proceeded from turbofan engine cycle analysis centered on a regional jet application to detailed design of POC seals for a rig test.

In the regional turbofan context, the potential gains for an ORC system capturing a high degree of the full pressure gain capabilities, cycle work showed the level of specific fuel consumption (SFC) benefits to be 17%. Sensitivity studies then showed that, to the extent that either design compromises or additional leakage or both reduce these capabilities, SFC gains are diminished, but gains of 10% remain available even at levels 50% below the available pressure gain levels.

Narrowing of the ORC/WR design space on which to apply seal technology was then made through a careful study of a wide-ranging set of design approaches for the combustion events within the system. This work revealed that while designs reaching the full potential may require further development addressing deflagration-to-detonation (DDT)-related issues, a nearer term candidate design is available that promises to deliver good pressure gain performance and that is also highly suitable for a regional turbofan application.

Technology readiness level of this ORC/WR approach is presently at 2.0. Moving this approach to the next level requires that a relevant demonstrator engine application be identified, toward which design attention can be placed—one leading to generation of a relevant rig hardware set. To this end, a demonstrator engine search determined that the industrial version of the T56 turboprop engine, the Model 501, possessed many of the characteristics required. Cycle work showed that performance gains were substantial while the engine carcass contained the space claim and turbomachinery options needed. Upon this base, a preliminary design of the ORC/WR and required sealing system was performed. The work was supported by an extensive investigation into the sealing approaches available. This work was also directly relevant to developmental testing of this same ORC/WR approach in an atmospheric rig.

Even nearer term is the need to demonstrate a high level of sealing within an existing and relevant wave rotor system. To this end, the identified sealing technologies targeted for application in the demonstrator setting were analyzed for application to an existing wave rotor rig. The NASA GRC SE-17 pressure exchanger rig was seen as an advantageous opportunity to apply both expanded analytical modeling capabilities developed within this program and to identify and fix identified leakage issues found within this rig. Because of the close coupling of the wave solution and the leakage at the rotor endpoints, and due to the need for a detailed tracking of leakage flows in a network of leak paths external to the rotor, these two solutions were solved together in a new procedure. To this end, an extensive leakage analysis of the rig was performed and a detailed design of additional sealing for this rig was generated and seal drawings produced.

Contents

List of Figures

List of Tables

Seal Technology Development for Advanced Component for Airbreathing Engines

Philip H. Snyder
Rolls-Royce North American Technologies, Inc.
Indianapolis, Indiana 46207-7162

Introduction

The goal of the work for this program is to develop technology applicable to a broad class of constant volume combustion engines utilizing wave-rotor configurations. The primary effort is to develop sealing technology generally applicable/adaptable to multiple wave-rotor configurations. Specifically, the work reported here was devoted to developing comprehensive seal strategies and technologies that are applicable to an On Rotor Combustion/Wave Rotor (ORC/WR) based product, an engine demonstrator, and the NASA SE-17 four-port wave rotor. Secondary objectives include preliminary design/layout of the ORC/WR, identifying appropriate and realistic combustion mode, fueling system, and ignition system. This effort was a one-year design effort study. The seal tasks were specifically aimed toward and are seen as enabling technology required for use in a future engine demonstration. This final report documents research effort and findings, including the developed seal strategies and identified technologies required to mitigate leakage flows in wave-rotors with on-rotor combustion that are applicable or adaptable to a product turbofan engine, demonstrator engine, and NASA four-port wave-rotor experiment. A proposed design for demonstration of seal technology in a proof-of-concept experiment at NASA GRC in the four-port wave-rotor test facility is put forward. This follow-up proof-of-concept (POC) wave rotor seal experiment was a key objective.

Context for work elements:

- The wave rotor component of the ORC/WR based product will be embedded on-axis between a compressor and turbine and will have an inlet port(s) from the compressor and an exhaust port(s) to the downstream turbine as dictated by the wave-rotor gas dynamic wave cycle.
- Combustion for the ORC/WR-based product will take place within the wave rotor. The combustion mode is not specified but exploration of a rapid, gas dynamically driven mode of combustion is preferred.
- The wave-rotor wave dynamics and combustion mode must be consistent with thermal and mechanical constraints of materials used in advanced turbomachinery components.

I. Preliminary Design

Development of seal technology for ORC/WR systems must be developed while considering a relevant context and environment within an engine. Multiple options exist for the basic combustion events to be accomplished within the rotor. Each will impose sealing environments unique to that cycle of events and will also deliver unique engine cycle benefit according to pressure gain developed. A rational selection must thus be made regarding combustion cycle design. A suitable starting point is to establish the sensitivity of product engine performance to pressure gain for a generic ORC/WR device. This information is then used as a guide in selection of an appropriate cycle by considering the pressure gain capability of candidate cycles.

The engine into which this cycle will be inserted, while ultimately a product engine, will initially be that of a suitable demonstrator engine. Thus selection of a suitable demonstrator engine is also relevant to seal design and must be selected for a proper study of specific seal design.

1.1 Study Alternate Gas Dynamic Wave Cycles

In the context of a hybrid turbine engine, a number of options exist with respect to ORC/WR in the specifics of the series of combustion events that occur within the design. Thus, in the study of the various wave cycles, the trade-offs involved must be systematically addressed. In general the performance benefits to be derived for utilization of an ORC/WR combustor depend on the pressure gain generated across the device, with the degree of rise in the relevant discharge pressure reflecting the benefit to the engine cycle. A characterization of this type lumps all benefits into the pressure and thus assumes that any dependency of the turbine efficiency upon the wave cycle is included in the pressure gain. Using this approach, performance estimates of a demonstrator engine were generated at incremental levels of pressure gain achieved in the combustor. These levels are representative of the range expected for the candidate ORC/WR gas dynamic wave cycles.

1.1.1 Product Engine Cycle Study

Specifically, an engine cycle study was performed to assess the degree of improvement in SFC achievable by the incorporation of a potential ORC/WR into a derivative of the AE 3007 turbofan, an 8,000-lb thrust class engine. The AE 3007 was developed to provide a turbofan member of the AE common core family for the growing regional jet and medium/large business jet markets. The AE 30XX engine is viewed as a next-generation engine and as such is a candidate for incorporation of a pressure gain combustor. The baseline 30XX for the purposes of this study utilizes a 1.6 pressure ratio fan, a 15:1 core overall pressure ratio (OPR), and a turbine inlet temperature (TIT) of 2600R.

The approach used in this study built upon the results of the NASA Ultra Efficient Engine Technology (UEET) work performed within Rolls-Royce North American Technologies Inc. (RRNAT) by Won and Waters (Ref 1), which considered the impact of introducing a number of technologies, both evolutionary and revolutionary in type, into a regional turbofan engine. In that study, the pressure gain performance of a constant volume combustor of wave rotor type was modeled as a function of overall temperature ratio (downstream/upstream) of the combustor based on previous combustor analysis work. The pressure gain performance was formulated into an equation:

$$\frac{p_3}{p_2} = 0.502 \cdot \frac{T_3}{T_2} + 0.445 \cdot CVC\_k\_factor$$

where:

$\frac{p_3}{p_2}$ -- combustor pressure ratio

$\frac{T_3}{T_2}$ -- combustor temperature ratio

The *CVC_k_factor* is a parameter variable between 0.55 and 1.0, which can be varied to consider differing levels of performance of such a device. Changes in level of performance may be considered to be due to a number of possible influences such as differing candidate cycles, changes in level of performance of a given candidate cycle due to level of leakage, or, as in the case of the Won and Waters work, an uncertainty of attainment of performance to a goal level prior to actual component development. The study reported here utilized that same approach, with analysis performed at four levels of *CVC_k_factor (*0.55, 0.75, 0.9 and 1.0), which are sufficient to reveal the trends of engine performance. Figure 1 compares the pressure gain characteristics of the above equation to analytical predictions made for various types of wave rotor based combustion cycles. The study reported here was undertaken holding turbine inlet temperature and fan diameter constant. This caused fan bypass ratio, core size, and net thrust to vary, although net thrust of each engine was found to be within 10% of each other.

The results in terms of thrust specific fuel consumption (TSFC) reductions were determined for cruise operation and indicated reductions in SFC up to 17%. The results were viewed as significant in that they show that there are large gains in SFC to be made even with a pressure gain significantly less than the highest performing CVC. Additionally, it was noted in the study that core size was 0.8 that of the baseline engine for a *CVC_k_factor* equal to 1.0. At *CVC_k_factor* equal to 0.55, the core size raised modestly to 0.84. The engine with CVC produced more power per unit of core air mass flow, which in turn required a smaller compressor and turbine. The core is only a portion of the turbomachinery of the engine, however any reduction in turbomachinery size results in a lighter engine. Although no in depth engine weight studies were made, these results show the potential for reductions in engine weight with use of an ORC/WR in a turbofan.

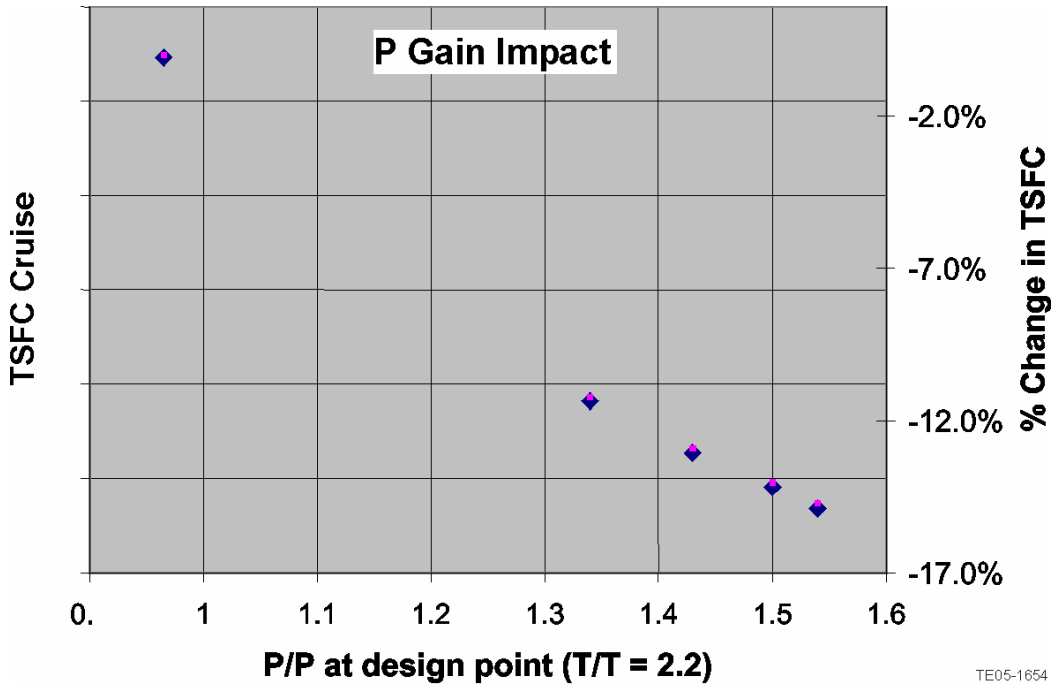

Figure 1. Cycle Work Added P Gain Characteristic to AE 30XX.

1.1.2 Candidate ORC/WR Cycle Study

On rotor combustion can be placed within a wave rotor in a number of differing ways. A study was done to examine the known candidate cycles using available analysis results for candidate cycles, including those for alternate modes of on-rotor combustion. The analysis was accomplished using the NASA one-dimensional non-steady code for simulation and analysis of wave rotors with combustion due to Paxson and Nalim (Refs 2-5), a code highly suited to modeling of the cycles. The 1-D approach captures the most important features of the flow processes while having the option to model a complete set of known loss-producing mechanisms. The code has been the subject of extensive development and validation, as reported.

The study included available analysis results for candidate cycles, including those for alternate modes of on-rotor combustion. Four main types of cycles, as follow, were analyzed, and their typical wave diagrams are shown in the figures:

1. Conventional forward-propagation pulse detonation engine (PDE) type of cycle (Figure 2)
2. Forward-running propagation exit valved PDE (Figure 3)
3. CVC cycle with gas reinjection port for energy redistribution (Figure 4)
4. Shock reflection cycle driven by backward detonation propagation (Figure 5)

All cycles involved a rapid gas dynamic mode of combustion. The available data were limited to modeling cycles utilizing instantly initiated detonation propagation. To make the performance evaluation more realistic, an attempt was made to simulate deflagration-to-detonation (DDT) for each type of cycle. The available data for a range of overall temperature ratio were considered, and were appropriately extrapolated for the estimated temperature ratio of a product engine (approximately 2.1).

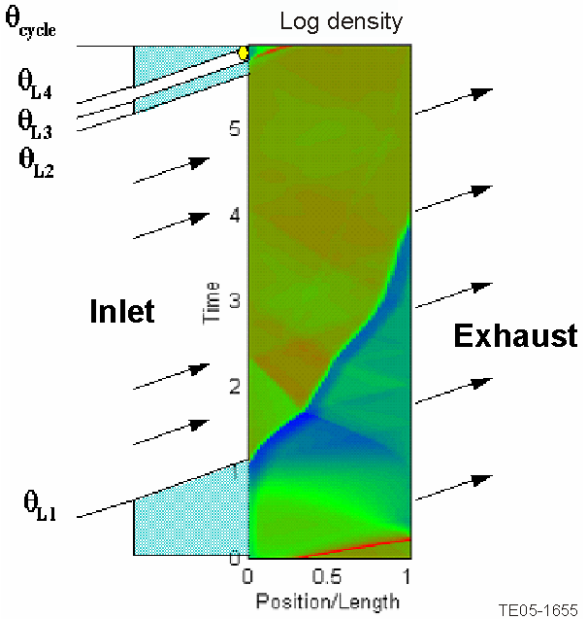

Figure 2. Conventional Forward-Propagation PDE Type of Cycle.

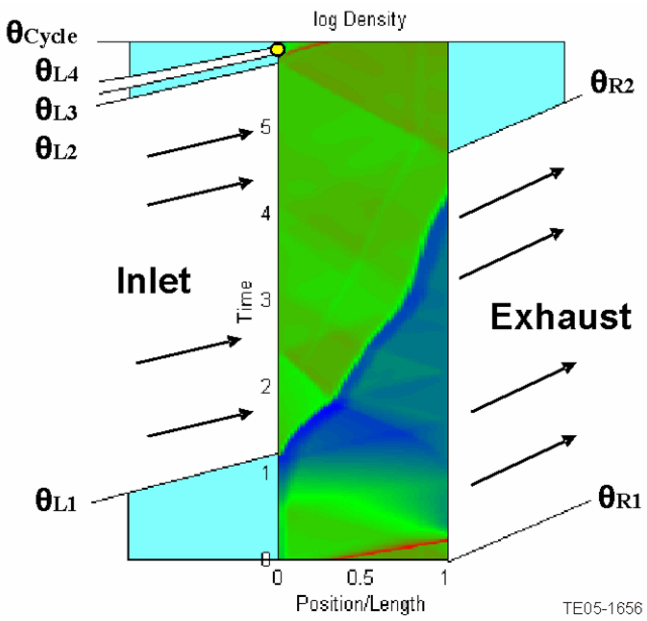

Figure 3. Forward-Running Propagation Exit-Valved PDE.

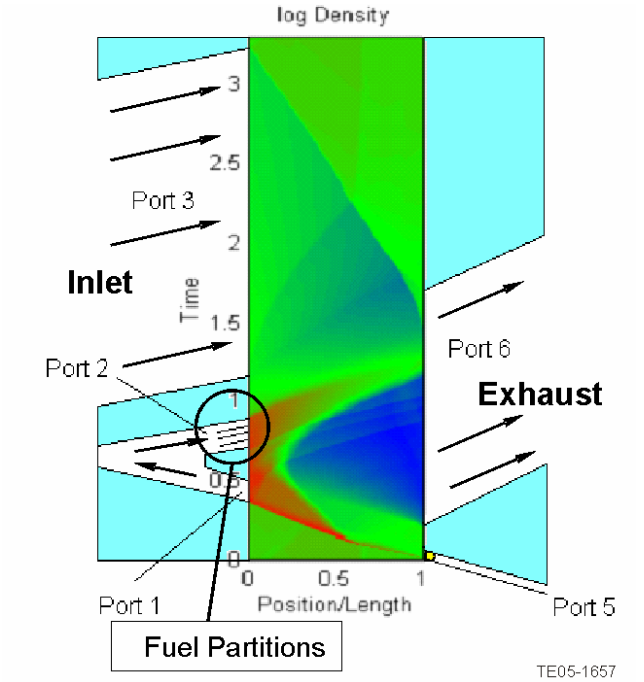

Figure 4. CVC Cycle with Gas Reinjection Port for Energy Redistribution.

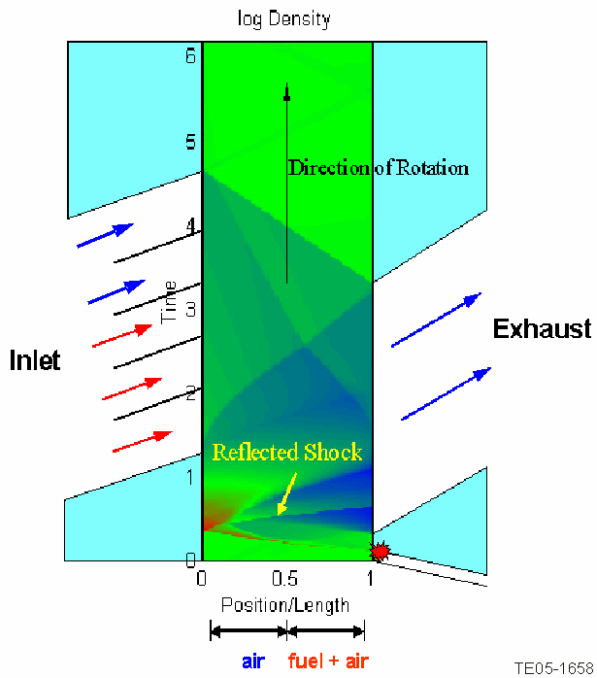

Figure 5. Shock Reflection Cycle Driven by Backward Detonation Propagation.

1.1.3 Select ORC/WR Cycle

The information generated was assessed qualitatively regarding arrival of strong pressure spikes to the discharge or inlet ports, the relative duration of expeditious deliver rates of gas into and out of the device, and the relative duration of residence of hot gases within the tubes in that it influences rotor temperature. The relative merits and demerits of each cycle are presented in Table 1. The available pressure-gain performance predictions for the cycles, using a range of parameters, are shown in Figure 6. Information regarding rotor temperature, port velocity profile, and detonability were qualitatively assessed. On this basis, the CVC cycle shows strong performance potential relative to the conventional and exit-valved PDE, along with lower potential thermal loads and emission (Refs 6-8). However, the shock reflection cycle combines reduced but similar performance with realistic accommodation of DDT.

$$\frac{p_3}{p_2} = 0.502 \cdot \frac{T_3}{T_2} + 0.445 \cdot CVC\_k\_factor$$

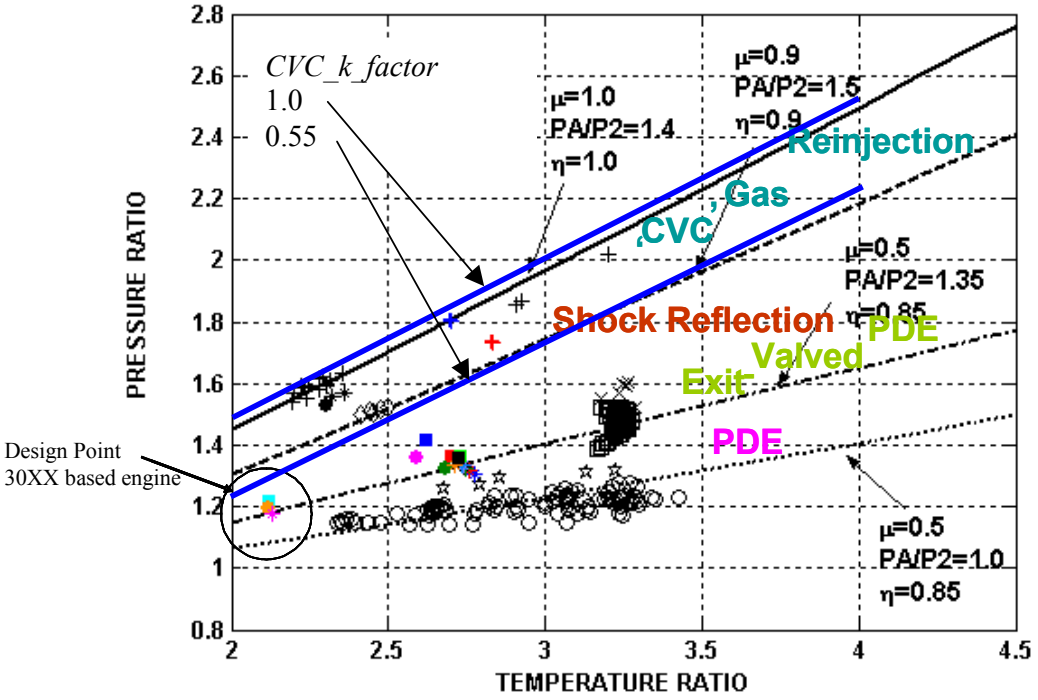

Figure 6. Performance Map for Four Candidate Cycles.

Table 1. Candidate Cycles for On-Rotor Combustion Wave Rotor Turbine Engine Demonstrator.

Conventional PDE cycle	High nonuniformity, flow losses, high wall temperature, poor performance
Exit-valved PDE cycle	Low-velocity outflow excluded
Shock reflection cycle	Relatively uniform outflow velocity and pressure, low wall temperature, accommodates deflagration-to-detonation transition (DDT)
CVC gas reinjection cycle	High performance, low wall temperature, uniform outflow, requires rapid detonation

Based on these results, a selection process was undertaken to arrive at an agreed upon cycle for the constant volume combustor. From the summary performance data and the current state of knowledge about DDT and combustion processes in a wave rotor, we determined that the best present candidate for a demonstrator engine was the shock reflection cycle of Figure 5. Considered in this assessment was the degree to which each wave cycle is generally consistent with both mechanical constraints and the attainment of high thermodynamic performance.

Summary: Studies modeled the effect of DDT on the WR and CVC cycles. The results indicated that the best wave cycle to select was the "Shock Reflection Cycle with DDT."

1.1.4 Demonstrator Engine Embodiment Selection

The application of the ORC/WR to a bypass fan engine is fully consistent with Rolls-Royce and RRNAT strategic planning as one of the ultimate applications of the technology. Further, excellent synergy exists between NASA and the company in terms of a mutual appreciation for the critical nature of the seals involved in making a successful ultimate product reach the potential theoretically possible in terms of performance.

Selection of an engine as a platform for demonstration of ORC/WR is guided by the ability to match turbomachinery corrected flows, the available real estate for integration, and the cost of the engine. The program reported here weighed carefully the use of either the Model 250 engine or the AE 3007 engine as the candidate for a suitable demonstrator base. The Model 250 has been considered a suitable platform in past wave rotor efforts due to the ability to mix and match turbine and compressor from the several models within the Model 250 line of product and thus match corrected flow of the components with a pressure gain combustor placed in between. However, the Model 250 flow size is relatively small in relation to the targeted application within a turbofan engine. Even more important is the influence of the flow size in selection of the passage dimensions of the rotor in an ORC/WR device. Larger corrected flows result in the ability to select larger rotor passage size. The ability to obtain a detonation within the tubes of an ORC/WR is judged to be more conducive within the larger passages of an engine. The exact lower limit for detonation is a subject of current research in various PDE programs.

For these reasons, the larger AE 3007 engine was selected as the preliminary engine for consideration as a demonstrator. The AE 3007 is an 8917-lb thrust 5.5 bypass-ratio (BPR) turbofan engine presently in commercial service on the Embraer ERJ 135/140/145 aircraft. The program goals were for RRNAT to develop comprehensive seal strategies and technologies applicable to an ORC/WR-based product (herein AE 30XX), an engine demonstrator (herein AE 3007), and the NASA SE-17 four-port wave rotor (NASA four-port rig).

Strategic planning at Rolls-Royce/RRNAT has included a measured approach to the application of ORC/WR technology to civil or military products. The first step in this approach is to materially assist NASA to make the four-port wave rotor rig function as intended and to fully understand, to the greatest extent possible, the lessons learned from the rig. Next in the Rolls-Royce/RRNAT plan is to progress to an atmospheric ORC/WR. This rig has already been designed in a partnership with Indiana University-Purdue University in Indianapolis (IUPUI) to operate at the Purdue University blow-down facility in West Lafayette, IN. The rig provides many special features to assist in evaluating the combustion process as it is affected by the wave rotor aerodynamics.

The next step in the technology development is to progress to a representative gas turbine. As reported in section 1.1, a negative aspect to utilizing the AE 3007 series of turbofans as a base for a demonstrator was disclosed by the results of the initial engine cycle work. Physically scaling the core down to match fan diameter constraints is unfeasible for a demonstrator engine. Absorbing of the higher power of the hybrid core by an existing fan stage is not feasible either, and matching the fan exit conditions to the core exit conditions is problematic due to the presence of a mixer that must obey static pressure matching of the two streams. These factors would seriously compromise such an engine to the extent that measurable benefits could not be demonstrated while holding modifications to surrounding turbomachinery to reasonably inexpensive levels.

Based then on the comparative candidate cycle study results and the results of the AE 30XX cycle study, an alternate to the AE 3007 engine as a demonstrator candidate was sought. We wanted to identify a safe, stable, and reliable gas turbine engine that could easily be adapted for ORC/WR technology development and overall cycle benefit demonstration.

Rolls-Royce is perhaps unique in that, when it gained ownership of the former Allison Engine Company in 1995, it also acquired ownership of the venerable Allison Model 501 engine. The Model 501, designed and developed in the 1950s from earlier engines, has an architecture is easily adaptable in terms of its potential for use as a demonstrator of an ORC/WR. The 14-stage compressor rotor is straddle mounted with a bearing in front (in the inlet housing) and a thrust bearing aft of the last stage supported by the compressor diffuser housing. Likewise, the four-stage turbine is straddle-mounted with its own thrust bearing having structural frames on both sides of the turbines. A floating lay shaft links the two rotors. Combustion takes place in six cans in a can-annular space between the compressor and turbine. The cans are long by modern standards, providing an unusual expanse for the location of the ORC/WR rotor. Engine rotor dynamics are fully developed and known to be completely acceptable with this relatively long rotor. Finally, the Model 501 has more than 40 million hours in service to its credit as the T56 Series, where four turboprops power the C-130 and P-3 aircraft. The durability and reliability of the engine is well established. In addition, the engine power section is designed to run at constant speed.

Following the most common approach to applying of pressure gain combustion, the most feasible option is to hold the turbine inlet conditions at the design level of 2033°F. By reducing the number of working stages in the compressor, accommodation of the pressure gain could be made while retaining the existing turbomachinery to the highest degree possible. To this end, a second demonstrator engine-directed cycle effort was undertaken. The pressure gain characteristic utilized is that of the shock reflection cycle as determined previously. The pressure gain characteristic of the cycle was curve fit, as shown in Figure 7.

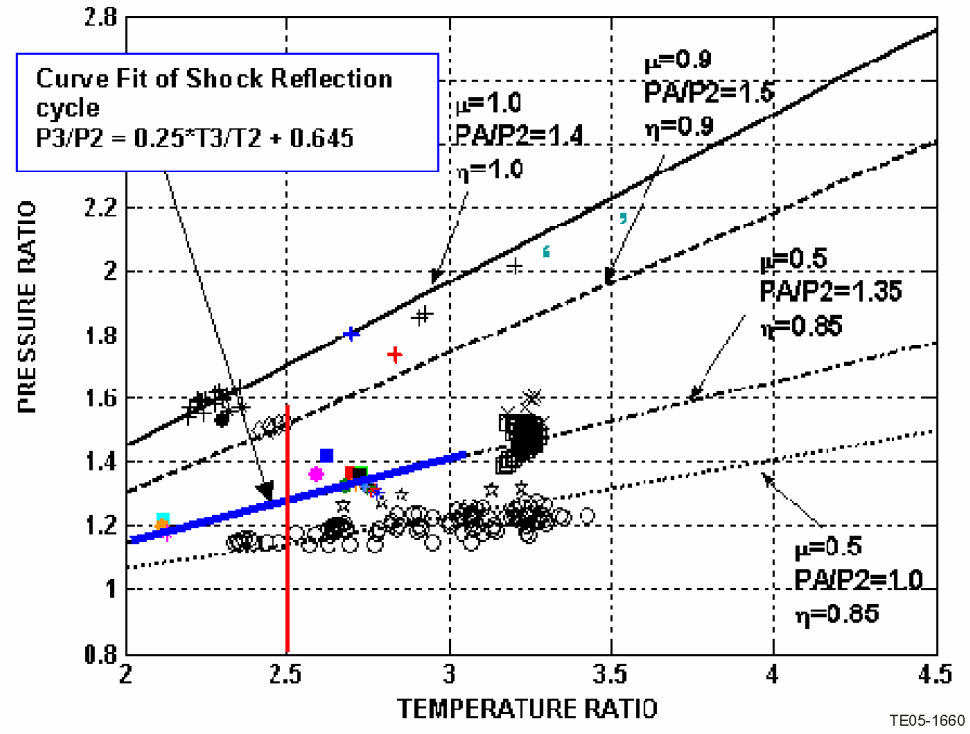

Figure 7. Curve Fit of Pressure Gain Characteristic of Shock Reflection Cycle.

The original overall pressure ratio (OPR) of the engine was 10.3 and that of the demonstrator engine is 8.0. This is between a second- and third-stage reduction in stages, which increases output power by 20% and reduces SFC 12%. No estimates of the performance were made for the engine with reduced stage count but without ORC/WR, since this combination does not result in a matched set of components with respect to corrected flow.

Refinements to the study were then made to include reduced performance of the compressor diffuser due to higher exit Mach number for the last compressor stage (+1.2% loss). Also, an additional pressure drop penalty for the exit transition duct was added (+4% loss) and the work output was debited for cooling air compression (23.8 hp). Adjusted levels of improvement are 18% power increase and 11% SFC reduction, as summarized in Figure 8.

A prudent technology development plan is to progress from the atmospheric rig to a demonstration (at approximately 10:1 atm.) in a modified Model 501 engine. As previously stated, this path takes the innovation to a real-world gas turbine that can be adapted to accommodate the new device with minimal change. In addition, testing the ORC/WR in a Model 501 potentially provides a short path to product as an industrial aero-derivative engine. Our assessment is that such a unit would produce more power than the current Model 501KB5 industrial derivative engine, and do so with reduced SFC as well. Certainly this represents an attractive combination with commercial possibilities as the technology is demonstrated to fulfill its theoretical promise.

After a review of this planning with NASA, approval was granted to shift our emphasis on initial application of the ORC/WR to the Model 501. RRNAT selected the Model 501KB5 industrial gas turbine engine for further study.

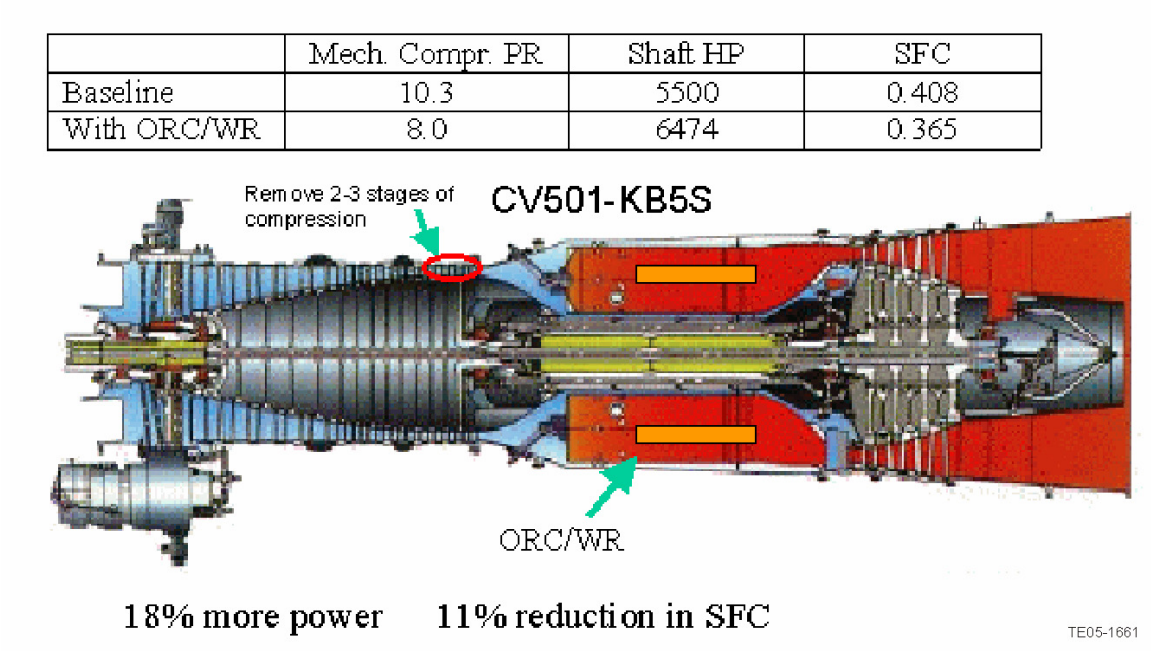

Figure 8. Selected Demonstrator Engine Based on 501KB5S.

In this selection, we considered the potential for problems presented by the wave rotor aerodynamics in a demonstrator engine. The obvious considerations were the following:

- The wave rotor is a pressure-gain device. This means that if the on-board combustion/wave rotor is substituted for a "conventional" combustor, i.e., placed between an existing gas turbine high pressure (HP) compressor and turbine components that have been sized for a conventional "pressure-loss" combustor, either the compressor or turbine would have to be modified significantly in design to account for the presence of the wave rotor in the cycle.
- The wave rotor operates based on transient flow phenomena at very high frequency. Even though we can envision coupling the wave rotor with more conventional rotating machinery (all of which operates in a more or less steady-state mode), the effect of a dynamic content in the flow on the airfoils commonly found in modern gas turbines is unknown.
- Initially, at least, the aerodynamics of the on-board combustion/wave rotor cause us to seek an application with which we have considerable liberty in terms of space claim for the device and its instrumentation. As we gain more understanding of the device and its characteristics, it may be possible to make the hardware much more compact by including more cycles per revolution or more than one flow path on board the wave rotor.

All of these considerations favor the Model 501 as the best candidate for the initial application of the technology. The desired wave rotor is expected to provide a pressure increase from compressor exit to turbine inlet of 1.22 at a temperature ratio of 2.44. The pressure rise per stage of the Model 501 is quite modest, particularly near the aft end of the compressor. It appears that, by removal of the rotor blade airfoils from the last three stages (replacing the blades with blade root sections without airfoils) and modifying the vanes to accommodate the swirl out of the last rotor into the diffuser, we will be able to match the corrected flow ($Wa\sqrt{T}/P$) into the turbine with the ORC/WR in place. The vanes all feature inner bands providing structure to locate the inner flow path. The compressor blades in the Model 501 are quite robust and operate in service with 6 blunt struts in the downstream diffuser and 6 discrete cans in the combustor. The 501 configuration invites the use of some multiple of 6 cycles per revolution for the wave rotor.

This seems a fairly modest modification of the existing turbomachinery components in that there is no change to bearing location, thus the rotor dynamic characteristics of the Model 501 engine would be retained. Further, no change is envisioned in the major cases or structural members of the engine that are known to be fully capable of accommodating the added load from the rotating ORC/WR. Finally, it retains the Model 501 bearings, sumps, and lubrication system intact, although it is planned to break into the existing system for lubrication services for the bearings of the ORC/WR component.

The first three stages of the four-stage Model 501 turbine feature tip shrouds. The rotor blades are highly mechanically damped. Data from the 501 program show that the 6 combustors create a large sixth order response mode for the turbine airfoils. The operating durability and reliability of the Model 501 demonstrates that the turbine airfoils were developed to withstand this aggressive dynamic environment. Our opinion is that the Model 501 has an excellent chance of surviving the new elements likely to be introduced in the exhaust of the ORC/WR. In the absence of definitive dynamic data from an ORC/WR operating at the correct aerodynamic conditions, the development of suitable gas turbine components to operate in concert with the ORC/WR is a process we can only anticipate. But the Model 501 record of durability gives us reason to expect that this configuration is a good place to start.

The linear distance from the compressor outlet guide vane (OGV) to the leading edge of the turbine nozzle guide vane (NGV) is 32.1 in. The compressor diffuser contains 6 blunt struts but the passages manage the flow, diffusing in a controlled manner so that at the "dump" point the velocity is below Mn = 0.2. The turbine forward frame is made up of 6 narrow struts. This combination of 6 and 6 led us to

consider the number of cycles to place on the ORC/WR device. For the Model 501 demonstrator we selected 3 cycles per revolution of the rotor. This allowed us to design similar ducts for all three ports, yielding a duct with a strut in each of the three ducts. The linear distance provided plenty of room for the rotor (length = 10.87 in.) plus seal plates, bearings, and ducts without disruption of the Model 501 lubrication system or having to tamper with well-established rotor dynamic characteristics of the existing hardware.

1.2 Design Selected Cycle—Shock-Reflection Combustion Cycle with Major Loss Mechanisms and DDT

Goal: Perform preliminary aero-design of the selected wave-rotor cycle for the engine demonstrator using current quasi-1-D unsteady flow wave rotor model. Simulate the agreed upon gas-dynamic wave cycle of the constant volume combustor using current quasi-1-D analysis model, including the mode of on-rotor combustion, to establish the preliminary aero-design size of the wave rotor, ports spacing, and thermal and pressure fields.

1.2.1 Preliminary Aero-Design of the Selected Wave-Rotor Cycle

The preliminary aero-design of the selected wave-rotor cycle for the engine demonstrator was determined using the current quasi-1-D unsteady flow wave rotor model. The shock reflection cycle was simulated to establish the preliminary aero-design size of the wave rotor, ports spacing, and thermal and pressure fields. Each cycle achieves balancing of the inlet and exit mass flow, fully repeating cycle of wave events, and achievement of the desired overall temperature ratio.

Characteristics designed into the cycle to accomplish desirable features are as follows:

- Opening of the exit port before arrival of the reflected wave formed by the detonation
- Filling of each passage with fuel air mixture such that the mixture arrives at the exit end as the passage is closed
- Closing of the inlet port at the arrival of the hammer shock formed by the closing of the exit port

Simulations with progressive inclusion of loss mechanisms and DDT with best-known parameters and manually optimized timing are illustrated in Figures 9 through 12. Modest adjustments to the required port placements can be noted as each of the inclusions is added. It should be noted that retention of highly uniform port velocity profiles and fuel placement is accomplished. The most realistic prediction (Figure 12) shows that relatively uniform exit velocity profile and reasonably short cycle time is possible, upholding recommendation of this cycle. Cycle pressure gain performance change with the incremental inclusion of losses is documented in Figure 16.

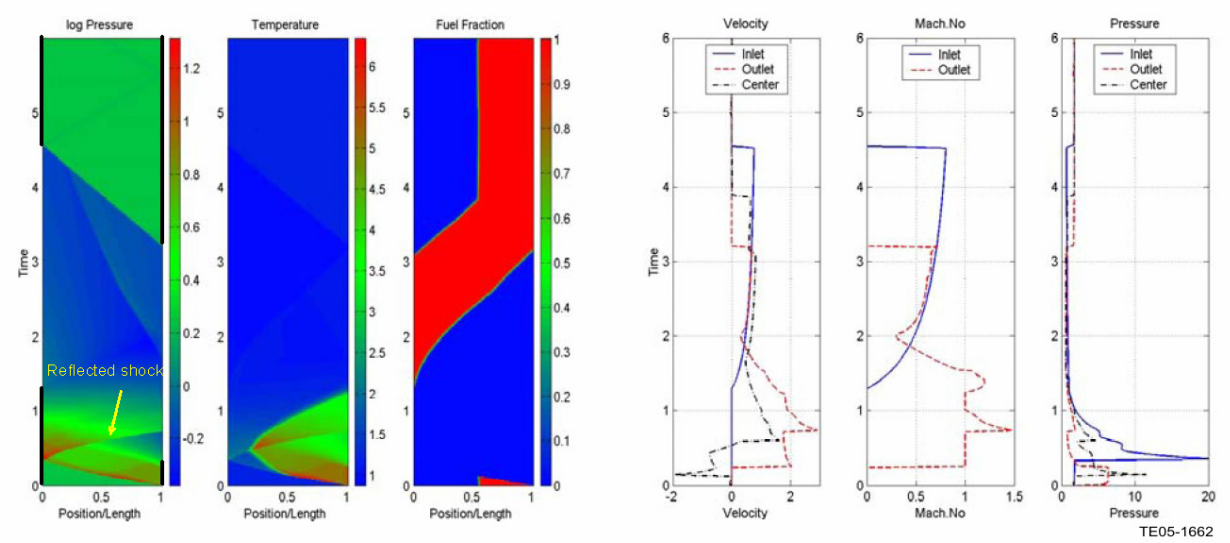

Figure 9. Instantaneous Detonation Simulation for Shock Reflection Cycle without Any Loss.

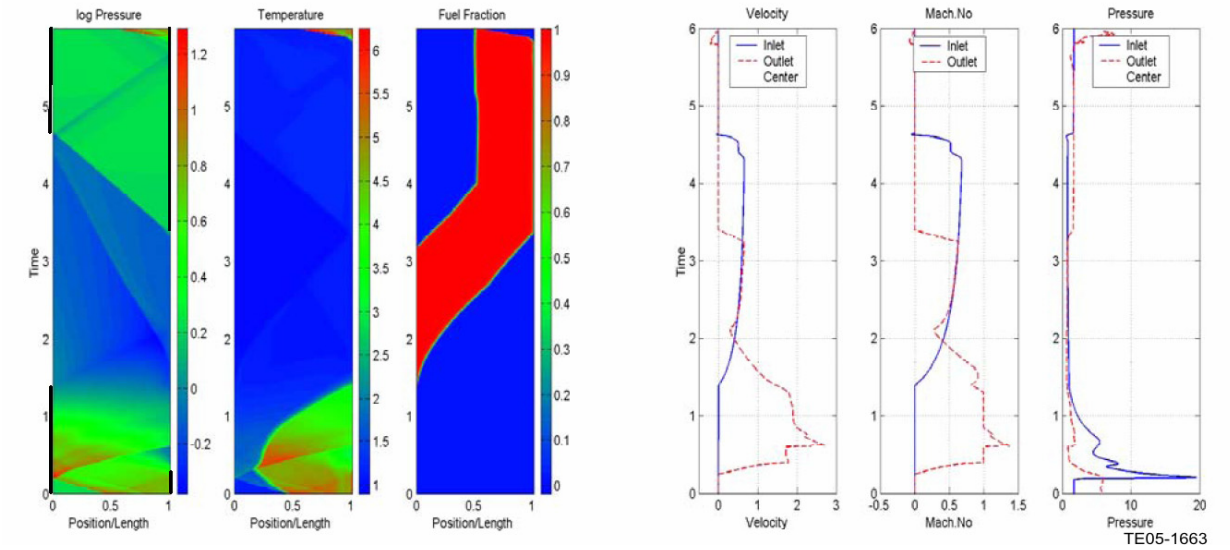

Figure 10. Instantaneous Detonation Simulation for Shock Reflection Cycle including the Effects of Friction, Gradual Opening, and Leakage.

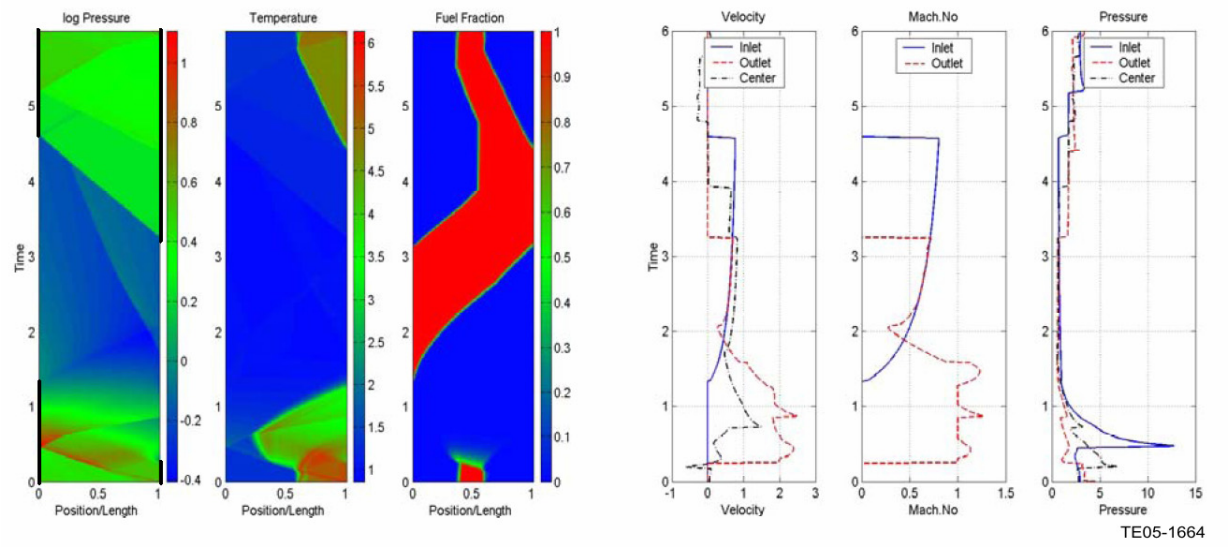

Figure 11. DDT Simulation for Shock Reflection Cycle without Any Loss.

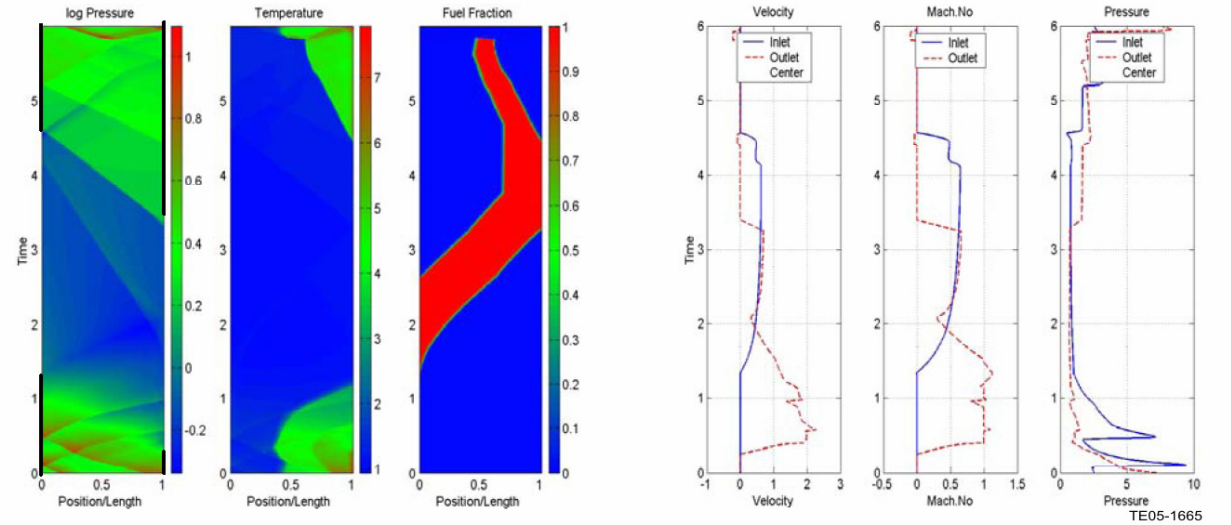

Figure 12. DDT Simulation for Shock Reflection Cycle including the Effects of Friction, Gradual Opening, Heat Transfer, and Leakage.

1.2.2 Preliminary Rotor Heat Transfer Analysis

Using the current quasi-1-D model for design point transient flow (covering one wave rotor aerodynamic cycle within rotor), a preliminary rotor heat transfer analysis was performed at the design point to estimate steady-state wall temperatures. Resulting wall temperature is shown in Figure 13, where Twall is the wall metal temperature normalized by the compressor discharge temperature, both expressed in the form of absolute temperature. Assuming the rotor has negligible conductivity, the peak temperature is below the turbine inlet temperature. With good rotor conduction, it would be possible to reach even lower low average rotor temperatures with this cycle. The impact of the temperature profile of Figure 13 is assessed in section 2.2 of this report.

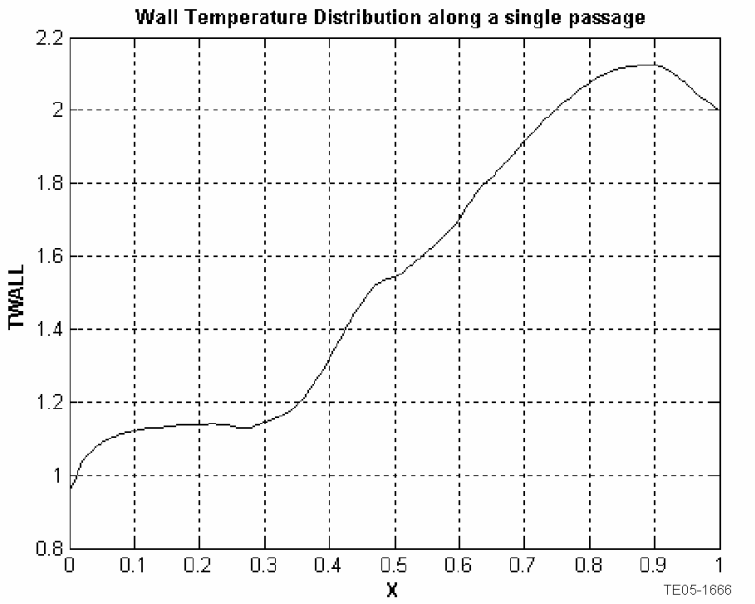

Figure 13. Wall Temperature Distribution along a Single Passage, DDT Case for Shock Reflection Cycle.

1.2.3 Preliminary Rotor Leakage Analysis

The sensitivity of pressure gain to leakage is an important consideration in seal design in that it establishes the utility in achieving lower levels of leakage. A parametric variation of leakage gaps was performed to establish impact of leakage on design-point pressure-gain performance, and provide useful information for redesign. The analysis also identified limitations from inadequacy of the current wave rotor leakage analysis tool capabilities, leading to the improved code discussed in the next task. Figure 14 shows the non-dimensional rotor-end pressures (left) and relative amounts and direction of leakage mass flow at each end (middle and right), assuming the ends encounter a uniform clearance gap with a single leakage cavity pressure. This provides guidance on the regions of the periphery that require most attention to leakage control, based on the cyclic pressure variation and leakage rate. To analyze leakage when more discriminating seals are applied, it will be necessary to create a leakage computation model that segments the rotor periphery in accordance with differently sealed regions, with different leakage path pressures.

Figure 15 shows the effect of increasing gap size and variations in assumed discharged coefficient on pressure gain, with the same gap on both ends of the rotor. For a rotor with passage height of 1 in., data presented a varied leakage gap from 0.002 to 0.006 in. Although this indicates the importance of clearance control, since a 0.004-in. change in gap reduces the pressure gain by 10% for a CD = 0.5, the discharge coefficient is currently arbitrary. This simplistic model cannot be expected to provide adequate quantitative guidance on leakage rates unless experimentally validated.

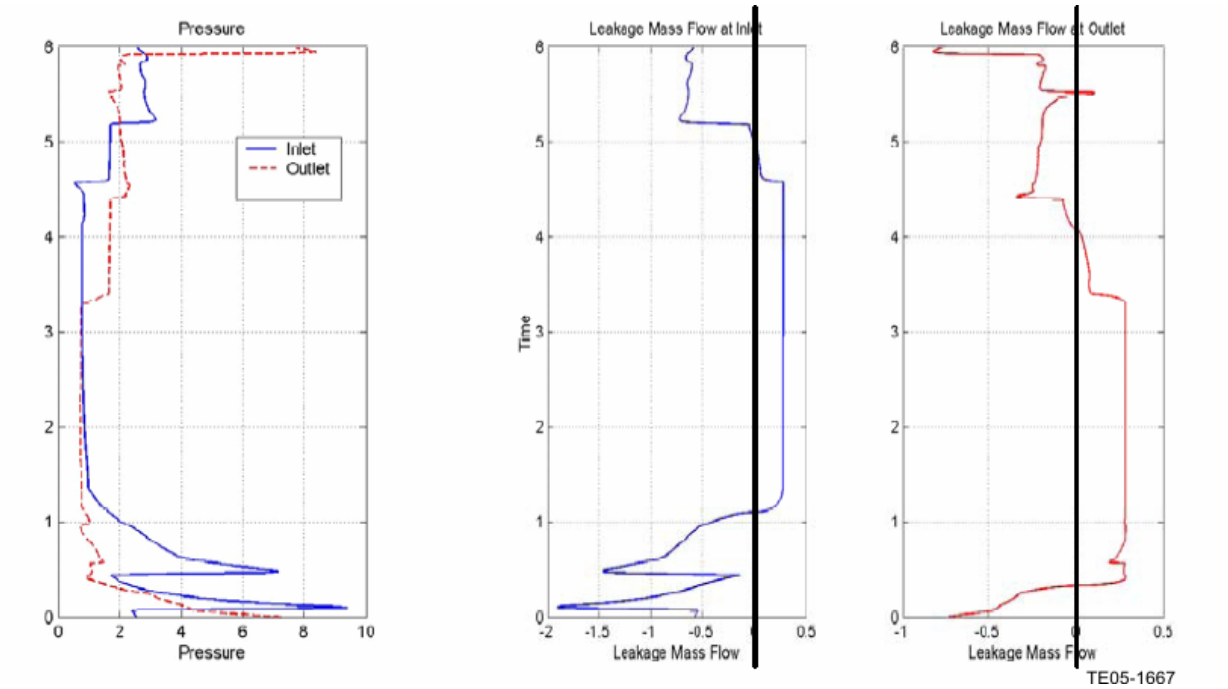

Figure 14. Leakage Mass Flow to and from Single Leakage Cavity, DDT Case.

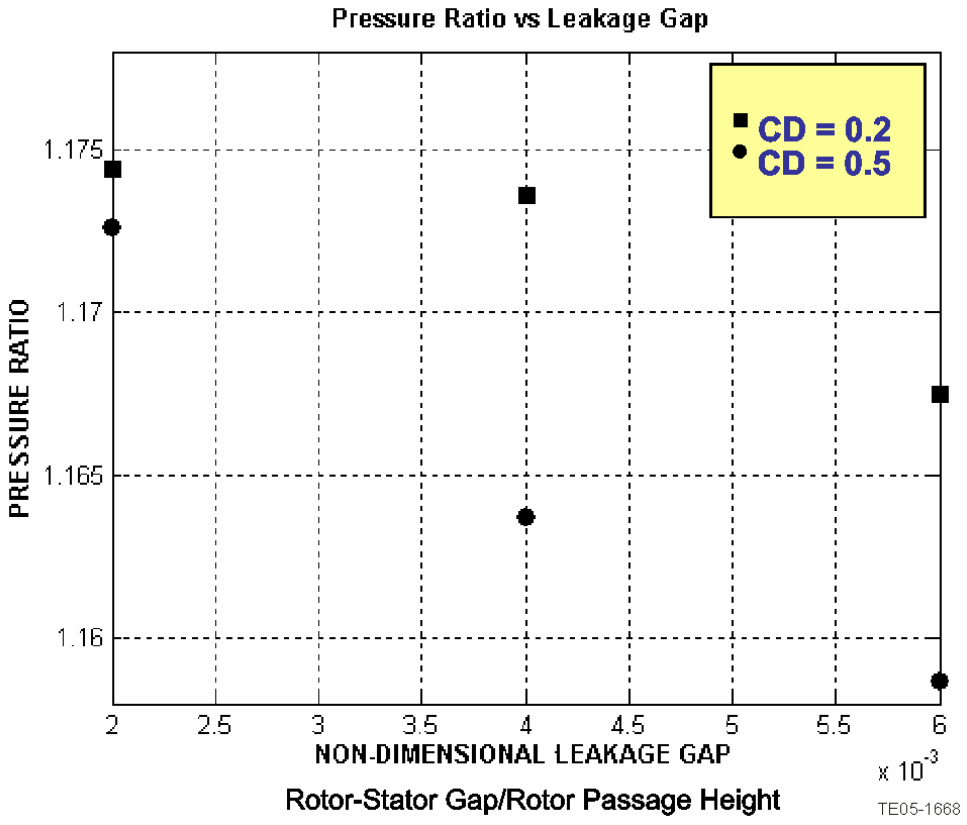

Figure 15. Leakage Gap Impact on Pressure Gain, DDT Case for Shock Reflection Cycle at a Temperature Ratio of 2.12.

The effect of DDT and leakage is further summarized in Figure 16 for a temperature ratio of approximately 2.1, where the highest performance is given by the direct detonation cycle, without considering leakage. All the cases shown include the losses due to friction and finite opening time (FOT), and all consider DDT except the first case mentioned. As the gap size is progressively increased and discharge coefficient is increased, the performance falls.

The effect of DDT is significant but hardly crippling, and use of detonation may have drawbacks related to structural, thermal, and outflow quality. The seal design clearly should accommodate brief peak detonation pressures, but also hold the deflagrative pressure rise that occurs over a longer time period. Realistic fuel and gas dynamic considerations may eventually point to a design that uses mild detonation or fast deflagration. Further, the ability to seal tightly will tend to favor non-detonative combustion, and thus allow wider engine operating range.

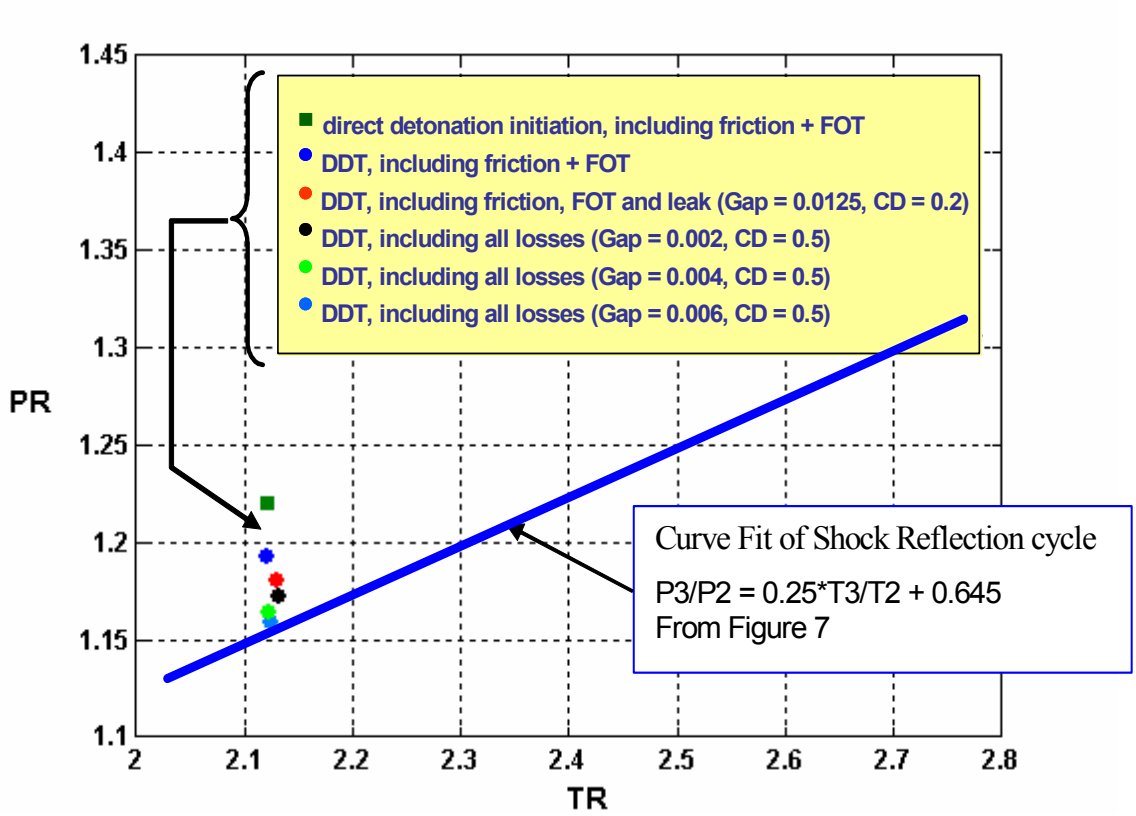

Figure 16. Shock Reflection Cycle Performance Map.

II. Develop Seal Strategies

Within the context of a demonstrator engine, seal designs originating from all available sources were examined to apply to the wave rotor.

2.1 Identify and Develop Seals to Mitigate Leakage or Clearance Flows That Detrimentally Impact Aerothermodynamic Performance

Goal: The seal strategies will be applicable to the general geometry of an on-axis, partial-admission/emission wave-rotor in which ducts port flows to and from surrounding full-annulus turbomachinery components. These are to include the seal strategies that reflect and build on prior contracted efforts. The effort is to accommodate comprehensively new seal concepts and challenges posed by the on-rotor combustion at engine operating conditions. Seal strategies must address realisms of mechanical design and be targeted at the product engine application. Apply seal strategies and technologies to the geometry required for the agreed upon engine demonstration. Identify new-technology requirements and corresponding development plans.

The process in developing seal strategies for the demonstrator engine modified to accommodate the ORC/WR took three distinct paths:

a. Search the open literature to document and review seal strategies applied to wave rotors in past development efforts.

b. Review those documents available to RRNAT, but not generally available in the open literature. These came from two sources: ABB and internal Rolls-Royce reports of the internal wave-rotor development effort that took place in the UK in the mid to late 1960s.

c. Hold brainstorming meetings involving Rolls-Royce Corporation and RRNAT personnel with a proven track record in innovative thought and good background in mechanical seal problem solving.

2.2 Seal Strategies from Historical Efforts

One primary source of information used as a resource of historical wave rotor development and sealing issues is Reference 9. Table 2 contains a summary of the wave rotor efforts reviewed at the workshop and documented together with information gleaned about seals and sealing issues.

This review provided no specific new insights in that these data were already in our thinking and the most recent review uncovered no new revelations. Certainly, there is evidence that rotor to end plate sealing is critical to the efficient operation of the wave rotor cycle but, it appears, no organization or development program had at that time solved the problems in a definitive or comprehensive manner. Certainly, successful wave rotor devices have been built and tested and at least one concept has been reduced to commercial product status, the Comprex, and much can be learned from the approach taken.

Our literature survey extended beyond this single document to include information available on the Internet as well as various Society of Automotive Engineers (SAE), American Society of Mechanical Engineers (ASME), and American Institute of Aeronautics and Astronautics (AIAA) papers collected over the past 20 years by RRNAT personnel who have tracked this developing technology. This included a fairly comprehensive search of available patent literature relating to wave rotors and their application. Among these was the following patent giving insight regarding one approach achieving a better end plate to rotor seal: US Patent 4,529,360 Gas Dynamic Pressure Wave Supercharger for Vehicle Internal Combustion Engines (Ref 10), which describes a method for making the rotor end faces concave or convex, as appropriate to account for the observed fact that the inner shell of the rotor expands differently than does the outer shell, being at different temperature during operation. The shaping of the rotor end

faces compensates for this difference in temperature, allowing the rotor face to present a more nearly planar face to the matching end plate during operation and thus reducing operating end clearance. Textural information from Caterpillar on the Internet confirms that the Comprex-style pressure exchange charger currently in production for use with their line of diesel engines makes use of this end compensation treatment to achieve more favorable operating clearances.

A notable outcome in terms of lessons learned: the radial thermal gradient existing in the rotor during operation should be determined and the rotor face shaped to achieve a radially planar surface at the expected operating temperature to achieve the lowest possible end clearance between the rotor and end plate. (This end shaping is probably of no consequence in SE-17 due to the low temperature of operation.)

Table 2. Survey of Available Literature of Wave Rotor Sealing Experience.

NPS-67-85-008					
WAVE ROTOR TECHNOLOGY SURVEY					
AUTHOR	TITLE	SUCCESS ACHIEVED	SEAL STRATEGY	SEAL ISSUES	OTHER INFO
Krantrowitz, A	Wave Engines	Patented a "thermally actuated clearance control" in 1954	Position moveable end plate by means of actuators whose legth is contolled to achieve desired clearnce.	A bellows joint is shown to avoid back side leakage, but no details are included as to how this is accomplished in a practical device.	Difficult to tell if this device was ever built or tested.
Kentfield, J.A.C.	The Pressure Exchanger; an Introduction, Including a Review of Work of Power Jets (R&D) Ltd.	Power Jets hardware ran at Imperial College in London 1952-1965	Outer sleve telescopes to permit the end plates to retain their clearnce.	None addressed in document.	Dr. D.B. Spalding of Imperial College was consultant. OBR/WR described in principal.
Berchtold, M.	The Comprex	Proceeded thru development and into production as supercharger.	Thermal growth in case and rotor are similar allowing one thrust bearing to set clearance	Rotor is overhung from "cold" housing. Rotor faces are "coned" to accommodate radial thermal growth differences.	Still in production for Diesel Engine supercharger in Brazil and by Caterpillar Engine Co. in the US.
Matthews, L.	Gas Dynamics of Pressure Wave Superchargers	Ran a device but little detail revealed.	Unknown		
Thayer, W.	The MSNW Energy Exhanger Research Program.	Built and tested a 2 cycle per rev device	Reports running with 0.004/0.005 in clearance	None reported. Uncertain how the clearances were achieved.	Reports 80% efficiency.
Moritz, R.	Rolls-Royce Studies of Wave Rotors (1965-1970)	Two generations of rigs built and tested, a third designed but not tested.	End plates located to rotor by thrust bearings; casing has bellows.	None reported. Coating used to minimize effect of contact.	RR reports avaialble to AADC.
Pearson, R.	A Gas Wave-Turbine Engine Which Developed 35 HP and Performed over a 6:1 Speed Range.	Arrangement similar to COMPREX.	Same as COMPREX.	Encountered large leakage problems due to excessive end clearance.	Pearson's is one of the most complete accounts.
Mathur, A.	A Brief Review of the G.E. Wave Engine Program of 1958-1963	A test program was conducted with some success.	End plates are located by means of thrust bearings. Ducts are sealed by sliding joints.	Few details were made available about the mechanical design of the test article.	G.E. abandoned the work in 1963.
ISABE-2001-1222					
AUTHOR	TITLE	SUCCESS ACHIEVED	SEAL STRATEGY	SEAL ISSUES	OTHER INFO
Okamoto, A. et. al.	Rotor-Wall Clearance Effects upon Wave rotor Passage Flow	Cell Fixed, Ports Rotate. 4-port rig	Each end plate positioned to static test cell by thrust bearing.	Minimal, due to short running times.	Verified importance of close clearnce.

2.1.2 Seal Strategies from Sources Not Generally Available

This part of the seal strategy development effort concentrated on two sources. The first of these are two papers documenting work done at ABB in the early 90's. The second of these is the library of reports that document the effort completed by Rolls-Royce in the UK in the mid to late 60's. Both sources provided specific insights of value to the current effort.

ABB: The ABB reporting of "Project 426" in References 11 and 12 summarizes the effort. The rather short paper (Ref 11) provides a good overview of the company's experimental program involving on-rotor combustion with a wave rotor of their own design. The second paper (Ref 12) is a much more comprehensive technical report and provides much more detail about what was accomplished and some of the problems that were encountered with the ABB device.

The purpose of the ABB work was to investigate constant volume combustion in a pressure wave machine, recognizing that this is one of the most advanced thermodynamic processes that might be available for gas turbines today. It was anticipated that the extremely fast unsteady combustion in a cell rotor would allow low NOx emissions at high combustion temperatures.

Significant findings of the work are as follows:

- After being investigated in a fixed cell machine, the feasibility of the constant volume process was demonstrated in a rotating cell machine.
- Axial recirculated hot gas jet from the stator turned out to be reliable for igniting the fuel-air mixture in the rotor cell during continuous operation.
- The mixing of the gaseous fuel with incoming air could be improved by applying vortex generators in the premix zone.
- Honeycomb seals on the rotor showed the best results in retaining the pressure in the cell during the combustion time.
- Starting with an inlet pressure of 2 bars, operation up to 9 bars in-rotor pressure was achieved.
- Testing was done with propane and with natural gas enriched with hydrogen.
- The machine operated with values according to expectations.
- A number of improvements were made to achieve useable results.
- Active clearance controlled the gap between stator and rotor.
- Massive water-cooling of the stators, made of copper alloy (very high thermal conductivity), was necessary to control thermal expansion of the stationary seal plates and thus achieve desired rotor to stator clearances.

ABB found that the design of the device limited its operation at higher pressures. The following is a list of ABB conclusions regarding the shortcomings of the 36-cell test device that was the workhorse for most of its testing.

- There was no collection or removal of leakage gas.
- The consequence was that air/fuel mixtures and hot exhaust gas could meet and mix in the space between the rotor and stator, igniting at elevated power settings.
- There was insufficient cooling of the rotor.
- The consequence was that the rotor temperatures were too high and air/fuel mixtures were ignited upon entering the rotor causing premature firing.

- One-sided suspension of the rotor by one bearing only turned out to present mechanical difficulties.
- The report states, “The operation of the machine for a longer time at full thermal load has not yet been possible due to local hot spots or instabilities of the process.” No reporting of operating time or the nature of instabilities was furnished.
- The electronic clearance control was too complex and delicate and the sensors were unreliable.
- There was frequent contact and too much leakage.

In terms of information of direct interest or benefit to the current program, there was specific information of value to an application of the technology to a product. (Less so for information of direct use in solving the problems of the NASA four-port rig.) Specifically, we elected to adopt the ABB-invented honeycomb seal for the Model 501 demonstrator engine rotor to reduce leakage. ABB explored the honeycomb-like seal by adding one row, then two rows, and subsequently a covering of the face of the rotor that runs in close proximity to the stator wall. The honeycomb structure was achieved by drilling holes in the face, thus creating cavities. This is shown in Figure 28. Also, their experience with getting the fuel on board the rotor is of direct interest to the follow-on effort to develop OBC/WR technology. Clearly the ABB efforts are well in advance of our current state of development.

2.1.3 Rolls-Royce Development Experience

Rolls-Royce conducted experiments involving wave rotor construction during the decade of the 1960’s at which time Rolls-Royce maintained a working relationship with Dr. Max Berchtold of the Technical Institute in Zurich, Switzerland. The clear intent of the Rolls-Royce work was to achieve application of the technology to gas turbine engines as a way to improve their performance. Studies from this time period include mention of an on-rotor combustion wave rotor used as a topping cycle for a high bypass fan engine. A 17% improvement in SFC was projected over the then-state-of-the-art engine for this device.

Early in the decade Rolls-Royce conducted fundamental pressure-exchange experiments followed by a “Phase II” rig. It is this rig and its operation that was covered very briefly by Robert Moritz and is documented in the 1985 ONR/NAVAIR Symposium (Ref 9). Subsequently, Rolls-Royce designed in detail a “Phase III” rig that was never built. Significantly, the Phase III rig addressed all the identified shortcomings of the Phase II rig and incorporated all features needed to permit it to be adapted to the then Allison Model 250 engine as a four-port wave rotor. The Phase III rig was not set up for on-rotor combustion, however.

Here is a summary of problems being addressed in the Phase III rig design:

- Rotor integrity is listed first. The Phase II rig rotor was a brazed assembly that was inadequate for service as a pressure-exchange device due to its lack of structural integrity.
- Pressure-exchange sealing, in particular the sealing of the rotor ends was identified as a difficult and unresolved problem.
- Pressure loss in the low-pressure discharge duct (exit to the turbine) was identified as a problem that might be addressed with better design effort.
- The prediction method for performance was thought to be inadequate from the Phase II rig and an improvement in technology was identified as being needed.

Each of these was addressed to one level or another by the design of the Phase III rig. Of particular interest to this program is the approach taken by the Rolls-Royce engineers of nearly 40 years ago regarding the matter of rotor end sealing.

The Phase III rig is still considered by Rolls-Royce (UK) to be proprietary, so a copy of the general arrangement could not be included. However, we have included an operating schematic as Figure 17 that makes the point worthy of discussion. For comparison in terms of a schematic we have included a schematic of the NASA 4-port rig, SE-17 as Figure 18.

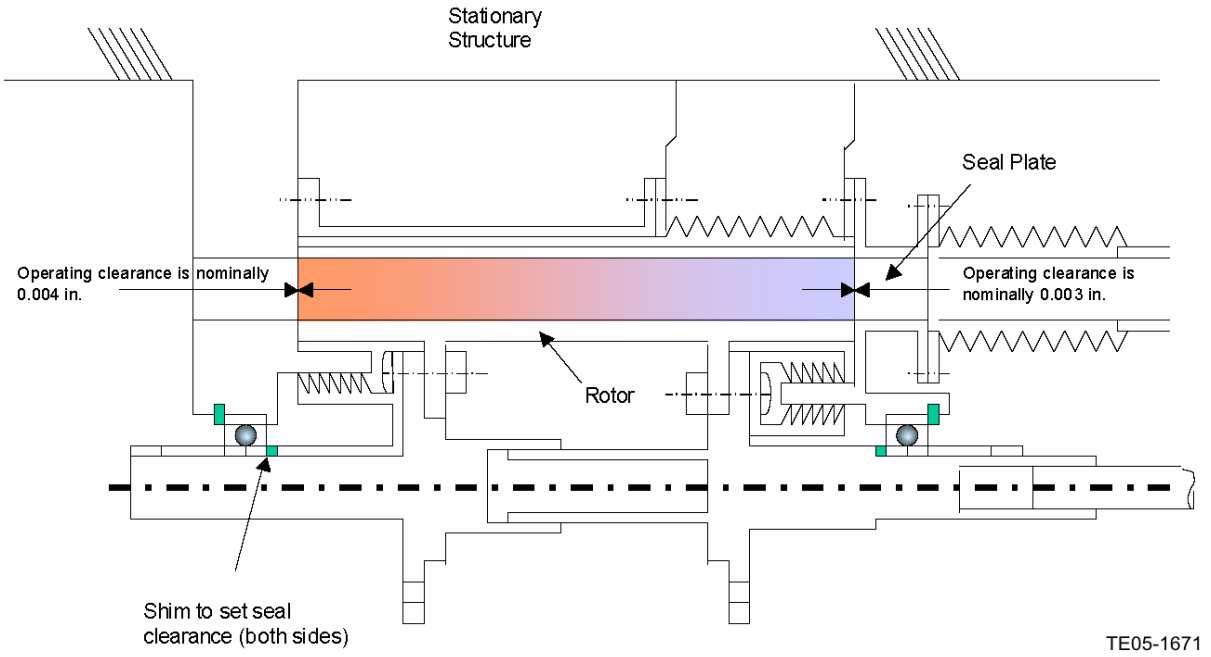

Figure 17. Rolls-Royce (Proposed) Phase III Rig Circa 1968.

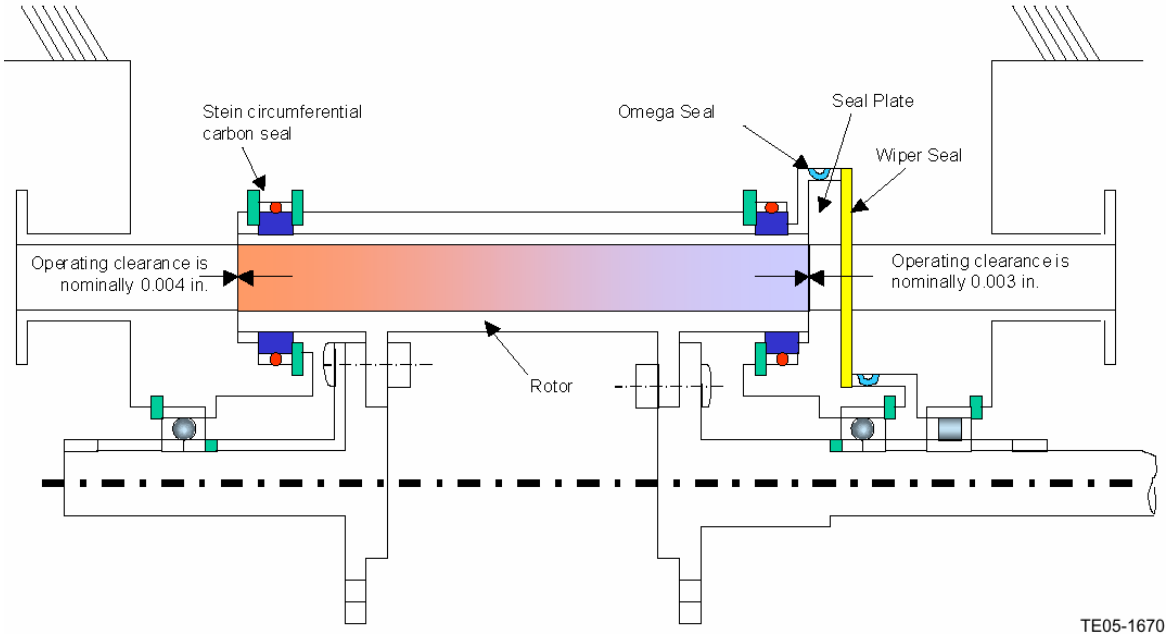

Figure 18. NASA SE-17 Rig Schematic.

The primary innovation of note in the Phase III rig is the way the movable end plate is supported and guided mechanically. The plate is free to follow the rotor, being positioned to the rotor by means of a thrust bearing, as is the case for the SE-17 rig. The floating end plate is attached to the ductwork through a bellows joint. It is also guided by a flexible mount to structure and is soft-mounted to the outer case through another flex joint. The ends of the rotor shaft are guided through a slip joint so that the movable plate is restrained from "pitching" about the engine centerline while being free to move with the rotor. The floating end plate is positively sealed to both the outlet duct and the outer case. This leaves the sealing of the rotor ends to be established by the interface between the rotor and stator. (Note that there is no "shunt flow" path, defined in section III, for leakage to bypass the gas stream as is the case in the SE-17 design.)

2.1.4 In-House Brainstorming

Brainstorming sessions involved personnel of the following disciplines:

- Secondary flow specialist
- Chief design engineer
- Engine design consultant with wide experience in sealing
- Compressor component design supervisor
- Combustor/nozzle design supervisor
- Senior design chief
- Wave rotor specialist with secondary flow experience
- Program manager
- Seal technology specialist
- Engine design consultant

The group forwarded the following ideas:

- Brush seals for the radial seal application
- Labyrinth seals for the radial seal application
- Adapt a regenerator compliant seal to the "smile" of the CVC using mineral-filled, nickel sponge leaf seals as a feature
- Make use of the apex seal materials developed for the Wankle rotary engine as a primary seal for the rotor to stator interface
- Place a small tapered roller bearing radially outward at the end of each tube and use this in contact with the stationary surface of the "seal plate" to effect a seal like a needle bearing. A corollary to this idea is to place the tapered roller bearing on the stationary seal plate to accomplish the same effect.
- Make the seal a film-riding seal like an air bearing of a leaf-type.
- Use ceramics to overcome thermal stability problems as well as rub tolerance problems—perhaps silicon nitride (rotor) and lithium/alumina/silicate (LAS) stator
- Make use of a toothed gear penetrating the rotor openings to seal the critical high-pressure region.
- Employ a flapper-type compliant seal with a suitable wear coating for light continuous contact. This could be pressure-balanced to avoid heavy contact where high pressures are not present. This idea could be combined with the film-riding seal idea for the inner and outer rings.

Also ideas surfaced after the brainstorming meeting as shown in Figures 19 and 20.

This pocket seal was suggested as a way to provide sealing in the local area where high-pressure spikes occur and to make use of the leakage in this area to energize a similar pocket seal on the opposite end of the rotor. An adaptation of this idea was subsequently adapted in the demonstrator engine concept.

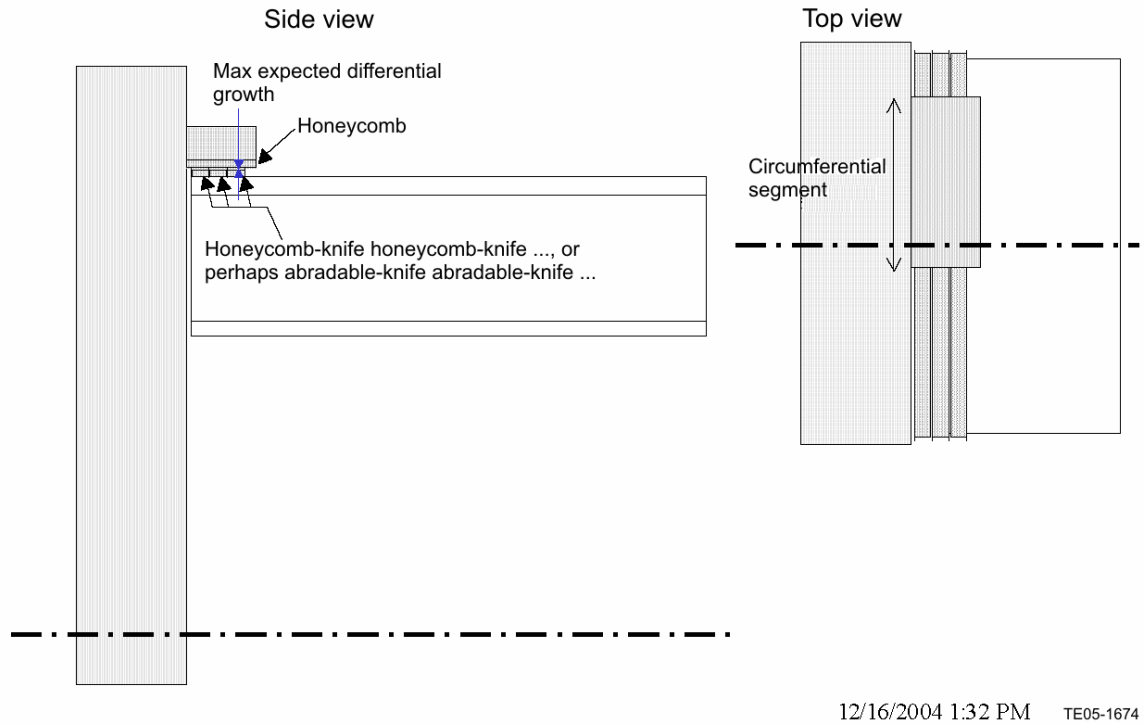

Figure 19. Pocket Seal.

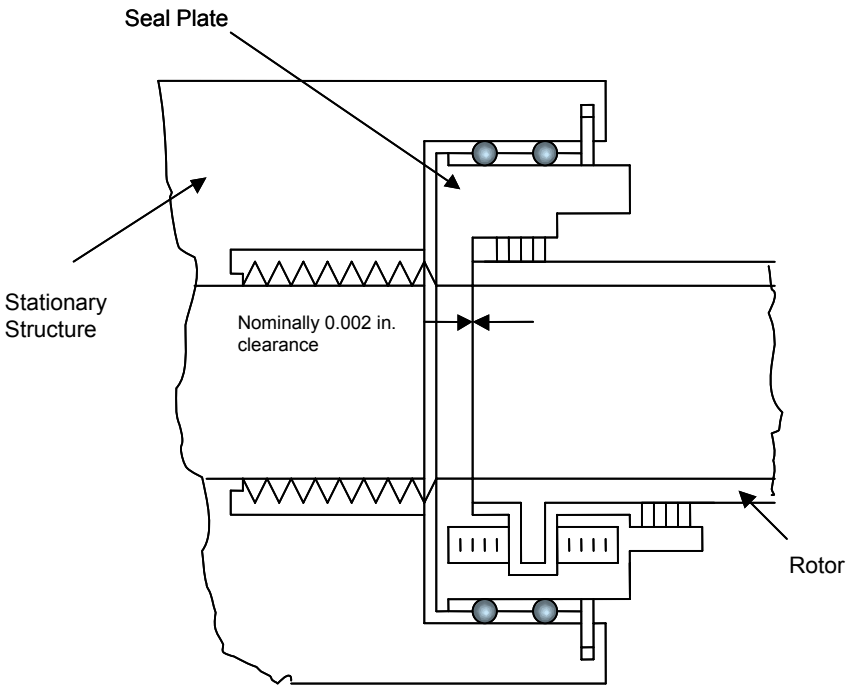

Figure 20. Magnetically Actuated Seal.

The magnetically actuated seal depends on a successful bellows-type joint to seal the gas stream and holds potential to actively react to the variable forces tending to "pitch" the movable end plate in relation to the rotor. This interesting idea has been shelved at present, but holds potential for future development.

In addition, configuration information from all available wave rotor rigs were compared with those conceived using the ideas from the brainstorming session. Ideas were ranked by the participants of the session according to consensus for 7 categories as shown in Table 3. A cumulative average was then used to identify the top candidates as shown in bold type. Information from this part of the program was used later to develop the seals for both the demonstrator engine and SE-17 rig.

Table 3. Ranked Results of Brainstorming.

#	CVC Seal Options	Mech. Complexity	Aero. Compatibility	Leakage	Overall Practicality	Life	Weight	Cost	Cumulative Average Score
1	Brush Seals	4	3	7	3	4	9	4	**4.86**
2	Leaf Seal	4	3	4	3	4	9	3	**4.29**
3	Labyrinth	9	2	2	10	10	9	10	**7.43**
4	Regenerator – Type	2	5	2	1	1	5	2	**2.57**
5	Wankle Apex Seal Tech.	4	7	7	2	2	8	2	**4.57**
6	Roller Bearing for Radial Portion	1	7	3	1	3	3	2	**2.86**
7	***Film-Riding Seal***	***10***	***10***	***7***	***10***	***10***	***8***	***6***	***8.71***
8	***Ceramic to give Stability***	***10***	***10***	***8***	***10***	***10***	***10***	***9***	***9.57***
9	Toothed Penetrating	4	8	10	4	4	2	3	**5.00**
10	Pressure Balanced Flapper	8	9	7	4	8	9	4	**7.00**
11	Controlled Clearance (NASA)	5	5	5	5	5	5	5	**5.00**
12	Rotary Valves	1	7	8	1	1	1	1	**2.86**
13	Poppet Valves	1	7	10	1	1	1	1	**3.14**
14	***Endplates contoured to compensate for combined thermal and mechanical loads***	***10***	***8***	***8***	***8***	***10***	***10***	***7***	***8.71***
15	***Magnetic Thrust Bearing to Control Clearance***	***7***	***10***	***9***	***8***	***10***	***7***	***5***	***8.00***
16	***Film-Riding Segment Actively Positioned Spring Stabalized***	***7***	***8***	***6***	***10***	***10***	***10***	***7***	***8.29***
17	***Actuated Endplate to control Clearance***	***10***	***9***	***9***	***9***	***10***	***7***	***9***	***9.00***
18	Mechanical Contact	8	8	9	7	6	8	9	**7.57**

2.2 Application of ORC/WR to the Demonstrator Engine

Sealing the rotor was of primary importance in the design of adapting the ORC/WR to the Model 501KB7 engine. Design of a sealing system depends on many factors directly influenced by the details of the rotor design. The rotor design task was accomplished through a process of manual examination of the available design variables resulting in a rotor size and speed. The process utilized as its basis the Q1-D analysis results. A spreadsheet-based procedure was used to employ the dimensionless parameters from the Q1-D output and input data describing geometric, fuel, inlet conditions, and resulting performance, and use them together with design variables to arrive at a suitable selection of rotor length, radius, passage dimension, and rotor speed. The design variables are number of passages per cycle, rotor web thickness, passage outer to inner radius ratio, rotor tip Mach number, and number of cycles per revolution. Several internal iterative solutions are required within the calculation.

The cycle analysis of the preliminary design task established the inlet and exit conditions for the candidate engine. Using the prescribed inlet temperature, pressure, and mass flow, the design space was examined. Tip Mach number was varied over a narrow range from 0.2 to 0.3 as guided by previous pressure exchanger design work. Basic rotor length is determined largely by the number of cycles per revolution selected. The radius ratio determines the mean radius of the rotor flow path. The number of passages is adjusted to result in an approximately square set of passages on the rotor. No iteration with the

Q1-D solution was undertaken to explore an optimum performing design. The output of the design calculation for the demonstrator engine is summarized in Table 4.

Table 4. Wave Rotor Flow Path Calculation Based on Q1-D Analysis.

3 cycles per revolution
Rotor diameter 16 in., length 10.9 in. Rotor speed 4735 rpm
40 passages dimensions 1.12 in. height by 1.17in. width

The rotor temperature profile as determined by the Q1-D analysis indicates that the rotor will basically operate with the inlet end at 560°F and the exit temperature at 1680°F uncooled. At the rotor speed of 5487 rpm, stress levels are acceptable for a monolithic rotor constructed of common turbine materials such as a number of currently available turbine alloys with good structural properties and acceptable characteristics for high volume manufacture using the investment casting process. Suitable materials are Inco 713 LC, Mar M 246, Mar M 247, Inco 718, IN 100, and Inco 635. The thermal gradient will cause the rotor to grow at the exit end and take on the shape of a cone at temperature. It may be possible to mitigate this by building in the appropriate negative cone in the cold condition so that hot and running we are flat and square. Further refinement of the design was outside the scope of this program.

2.2.1 Exit Ducting

Many issues were encountered in developing the concept design. The first of these was where to place the rotor. General wisdom called for the rotor be placed as near the turbine end as possible to minimize the extent of hot metal transition duct to the turbine. Early in the process, we studied a number of approaches to accomplish this.

Figure 21 shows one of these ideas. In this idea, the exit gasses are "dumped" into a "collector" or chamber where flow is mixed and then re-accelerated to the turbine nozzle guide vane. It has the desirable feature of thoroughly mixing the flows at the exit of the ORC/WR, but has the disadvantage of loosing the full velocity head in the exiting gas stream, which for this type device would be substantial.

Another variant was generated. In the approach of Figure 22, the hot gasses are ducted directly into the turbine nozzle guide vane. In this case, all the variability expected in the exit flow from the ORC/WR is fed directly into the turbine. This was considered to be undesirable at best and intolerable at worst. Inspection of the velocity profile at the exit of the wave rotor in Figure 12 shows how non-uniform this flow is expected to be. This analysis shows that the flow is very hot with high velocity in half of the port.

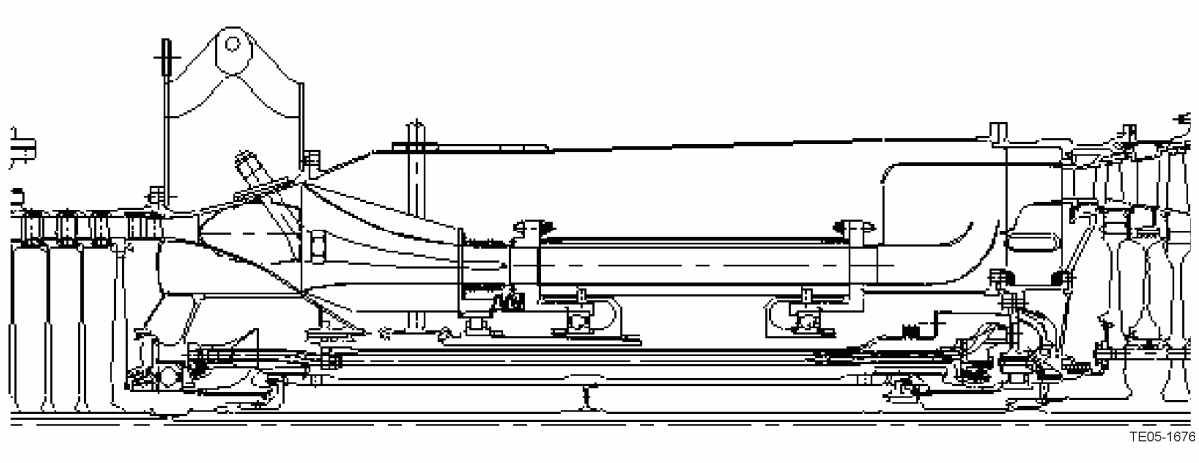

Figure 21. "Dump" Exhaust Duct Concept.

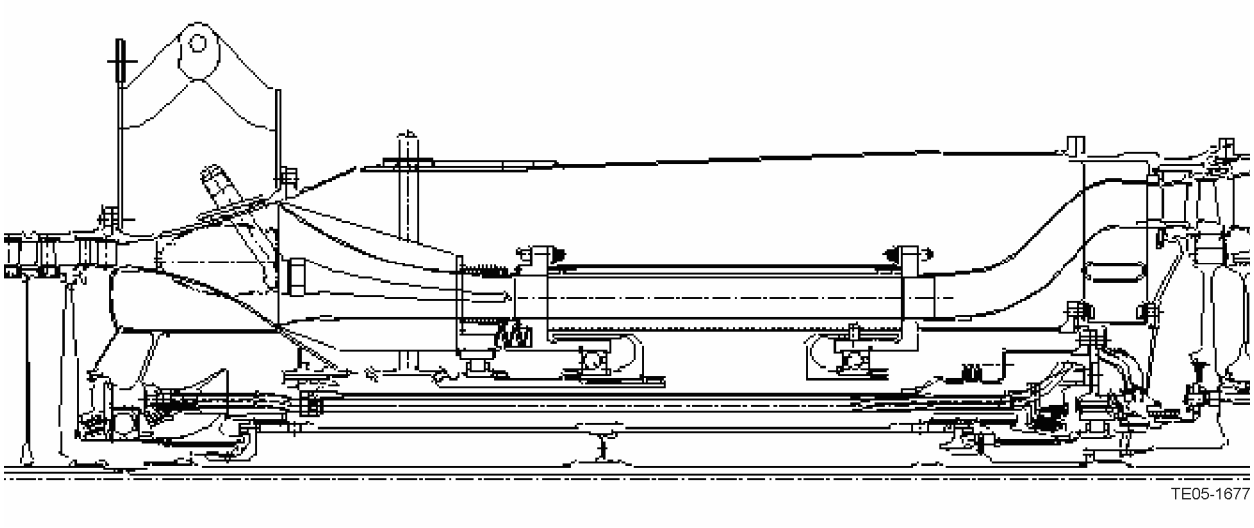

Figure 22. Smooth Exit Duct Concept.

while the flow from the other half of the port is relatively lower in both velocity and temperature. Ducting such wide variation directly into the turbine would create an even more challenging environment for the rotating turbomachinery than would otherwise be the case. Our desire was to thoroughly mix the flows so that the gases entering the turbine would be as uniform as possible

This led to discussions of some suitable mixer. Since the concept of Figure 21 was considered to involve too much pressure loss to the cycle, a potentially lower loss idea was to incorporate some variant of a "pipe" diffuser for the hot-high Mach number flow ducting it into the cool-low Mach number flow. While this had merit, it became mechanically complex in execution. The design team finally decided to adapt the type mixer commonly employed in a mixed flow turbofan. In that case, the cool, relatively slow fan flow was efficiently mixed with the hot, relatively fast flow from the exit of the turbine. The device is known as a "lobed" or "daisy" mixer in which the cold-slow air is interspersed with the hot-fast flow in a series of radial wedges. Of course for the ORC/WR, the design had to be highly adapted. Instead of radial mixing, as is the case for the fan engine, the ORC/WR exit required circumferential mixing of the two halves of the exit port flow. The resulting design is shown in Figures 23 and 24 and should be understood as a notional mixer design.

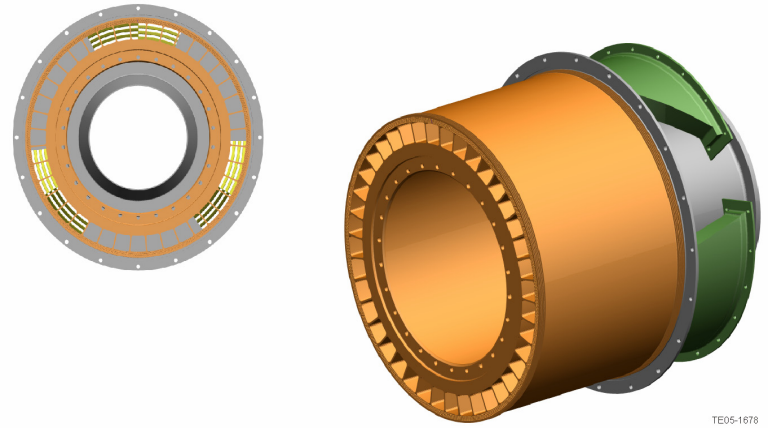

Figure 23. View Looking Aft Thru Rotor Showing How the Mixer "Splits" the Exit Duct Side to Side.

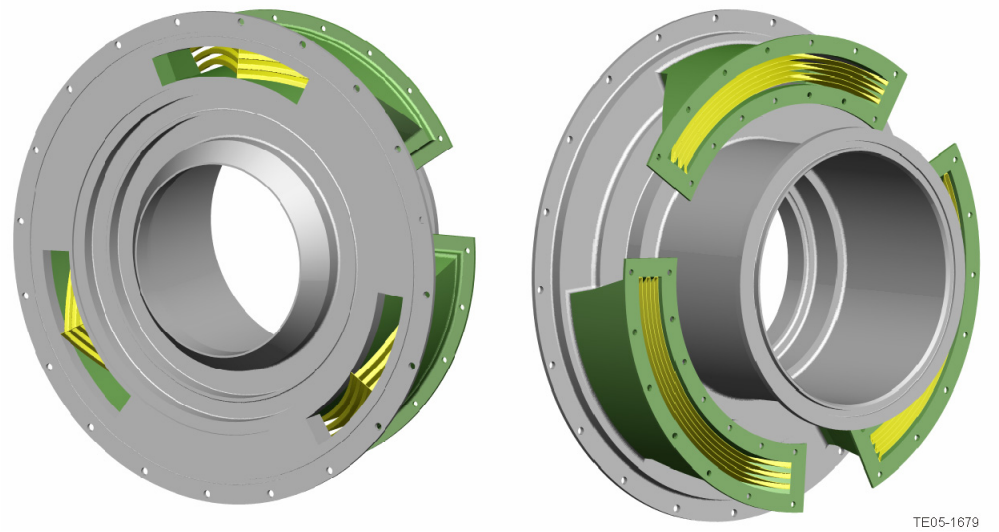

Figure 24. View of the Exit Ports with the Mixer Installed.

The exit duct mixer is difficult to describe, but this thin sheet metal mixer ducts the low temperature, low Mn flow from half the port to circumferential slots interspersed with similar slots carrying the high temperature, high Mn flow, thus providing effective mixing of the two streams off the trailing edge of the sheet metal. The mixer is shown installed with the rest of the final design system in Figure 25. In this first estimate of the mixer, no attempt was made to incorporate its function with the subsequent transition duct to the turbine. This was left to a second attempt at the design of the demonstrator system.

The design of the exit duct mixer and connecting duct to the turbine nozzle guide vane established the location of the wave rotor between the compressor and turbine. The ductwork needed to both mix and transition to the turbine became so long that we moved the radial drive that supplies the speed control to the rotor from the cold end (mid-term arrangement) to the hot end of the rotor. There was still plenty of room between the exit ducts for the shafting, but this meant that the inlet duct must be shorter than we originally planned. One additional benefit of moving the radial drive was that the exit or hot end of the

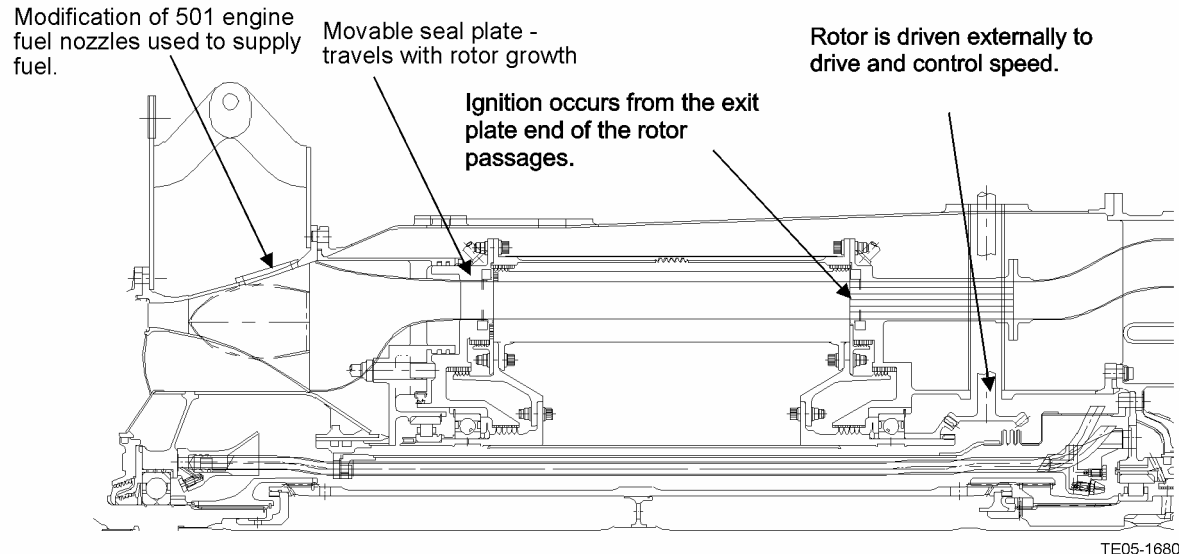

Figure 25. Final ORC/WR Concept Showing Exit Mixer and Transition Duct to Turbine Section.

ORC/WR system is the non-moving sealing end plate and contains the prime thrust bearing for the rotor. This means that the gear setup is maintained without a second bearing and working spline as would have been required had we located the radial drive gear at the moving plate end of the rotor. The drive was envisioned to be powered by a speed controlled electric drive coordinated with the control system of the engine.

Turning to the inlet end duct design, we elected to control the critical rotor to stationary end plate clearance with a thrust bearing on each end of the rotor using the same mechanical arrangement as employed in the NASA SE-17 wave rotor rig. On the hot or discharge end, the thrust bearing locates the rotor to the rest of the engine and is the solid (non-moving) end of the structure. On the inlet or cold end of the rotor, the thrust bearing locates a movable end plate to the rotor, while the rotor bearing to the stationary structure centers the rotor.

2.2.2 Inlet Ducting

The inlet duct is trapped mechanically between the existing diffuser struts and the inlet ports in the movable end wall. Compressed air at relatively high subsonic conditions enters the engine diffuser as it exits the compressor outlet guide vane. The Model 501 engine diffuser is designed to decelerate the low to an exit Mach number of approximately 0.2 in a controlled and uniform manner. As shown in Figure 26, the approach taken was to design the three inlet ducts leading to the ORC/WR to pick up the flow from between two of the six blunt struts in the compressor diffuser and accelerate the flow uniformly to the front face of the rotor. In this scheme, one of the blunt struts forms the forward part of an airfoil, the back half of which is part of the inlet ductwork. The other two strut walls are continued and contract to accelerate to flow.

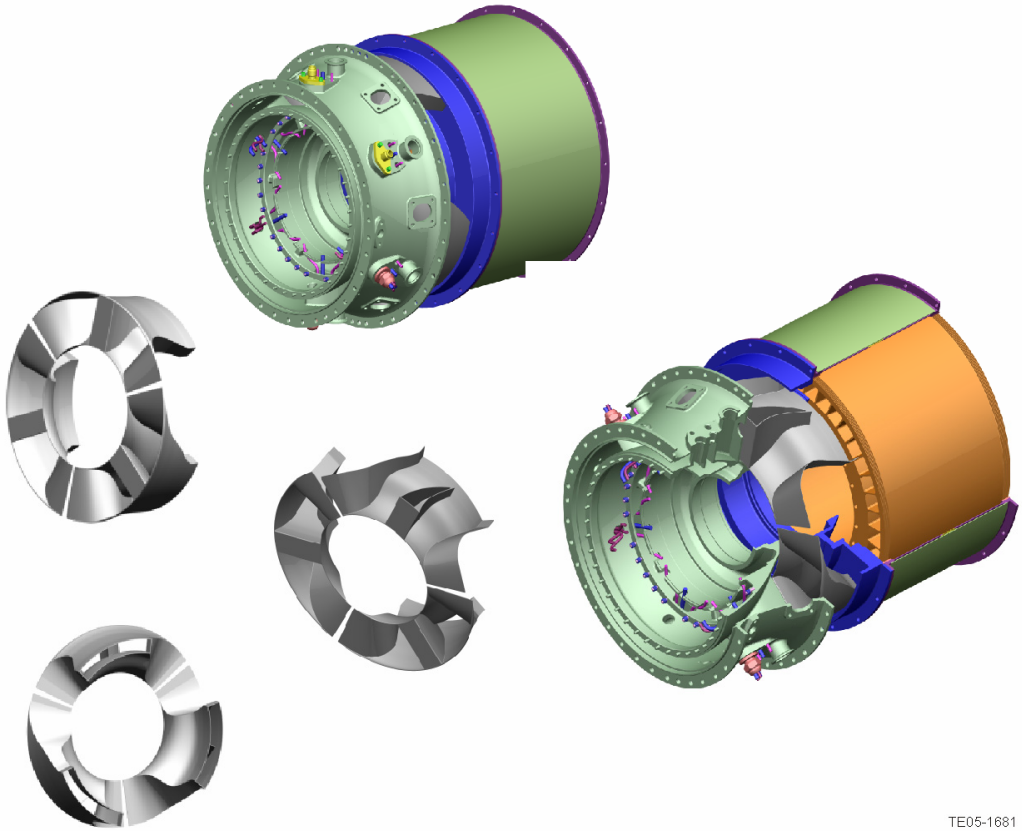

Figure 26. Inlet Duct Design Showing Transition from Compressor to Three Inlet Ports.

Mechanically, the movable end wall carries the ducts inserted as shown in Figure 27. There is no seal between the inlet duct and the stationary diffuser. Instead, the inlet ducts project into a sealed chamber defined between the diffuser outlet and the movable end wall. The movable end wall is sealed to the stationary support structure shown by means of multiple piston rings. The chamber between the diffuser and the new stationary support structure will reach an average pressure established by the static pressures at the exit of the diffuser.

The movable end plate is positively loaded toward the rotor face and into the thrust bearing by means of hydraulic rams. These cylinders provide load to locate the movable end plate to the rotor face with the load being carried through the thrust bearing. A spacer machined to produce the desired clearance at assembly establishes the end wall-to-rotor clearance. An alternate to this would be to attempt to position the movable end plate to the rotor face by means of actuators (the hydraulic cylinders) acting to drive the plate into the rotor to achieve a predetermined clearance established by means of data obtained from proximity probe data. While this remains an option, the ABB experience is discouraging.

The movable end plate must be both mechanically and thermally stable to provide the planer surface needed for the tight running clearance required. Mechanically, the plate is inherently balanced by the three-cycles-per-revolution layout of this arrangement. Should analysis done at the time of demonstrator engine design indicate that unbalanced moments may occur due to gas loads from the aerodynamics of the wave rotor under some of the anticipated operating conditions, another (non-rotating) bearing could be added between the movable plate and the stationary support to react the pitching moment.

Lubrication and scavenging of the ORC/WR bearings is provided by adapting into the engine lubrication system.

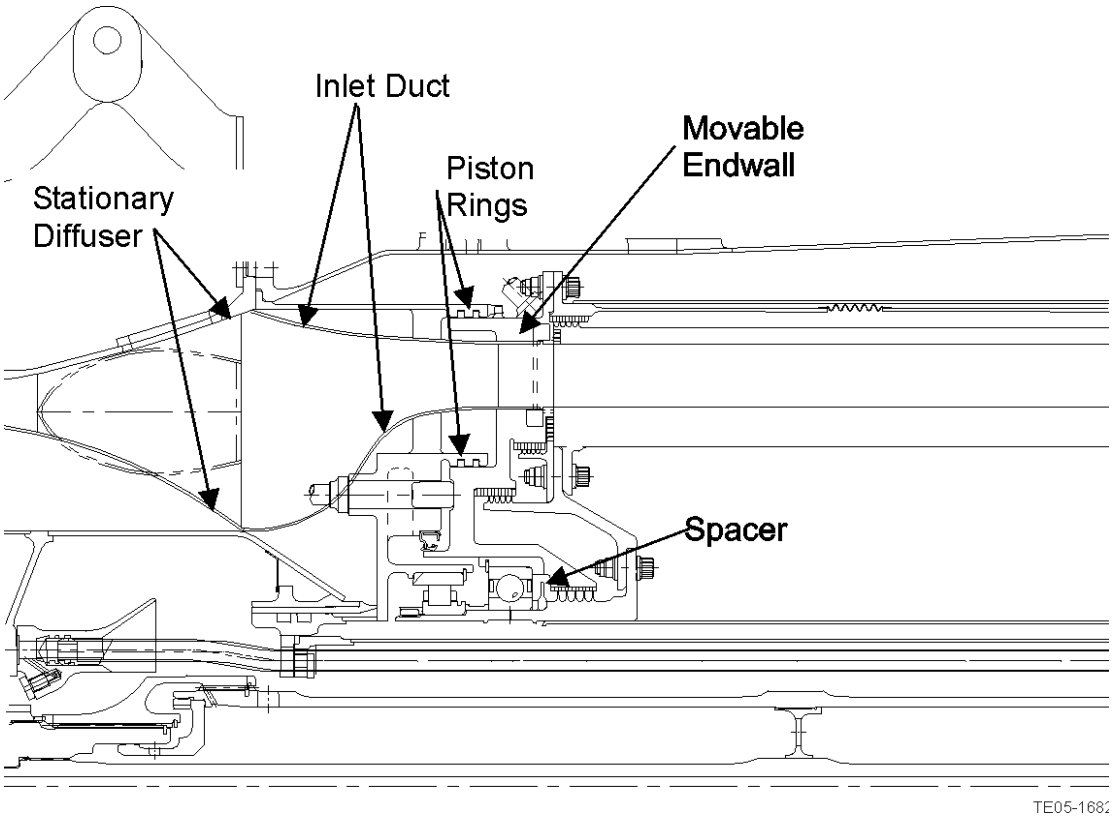

Figure 27. Detail of ORC/WR Inlet Ductwork and Movable End Wall.

2.2.3 Primary Sealing

The demonstrator engine contains a number of features to ensure that the primary sealing clearance is maintained and that the primary seal is as effective as possible during operation. As previously stated, the clearance is established at the time of assembly by the machining of a spacer taking out all part tolerance. The stationary structure will be coated with a suitable, abatable coating, such as a nickel-graphite thermal sprayed coating. Our plan is to incorporate a "honeycomb" seal in the face of the rotor as shown in Figure 28.

This feature was shown to be quite effective in reducing leakage from the gas path by the work accomplished by ABB in Reference 12. Following the work, this feature was added to the demonstrator engine rotor in both the inner and outer faces of the rotor.

In addition, in recognition of the fact that pressure varies dramatically circumferentially around the inner and outer faces of the rotor, and that the pressure on the inlet end is higher than the pressure in a similar location on the exit end, we have incorporated bleed chambers in the design of the movable end plate as well as in the exit end stationary structure. Bleed slots are provided in the seal surface face so that flow leaking from the rotor, through the small gap between the rotor and stator, can be drawn off on the inlet end and ducted through suitable piping to the exit end, where it is introduced as a "buffer" flow to inhibit the leakage of hot gases from the exit gas path. The rotor with bleed arrangement is shown in Figure 29. Further, these chambers carrying reasonably hot high-pressure air will act to cause the end plate and stationary structure on both ends of the rotor to be more uniform thermally than would have otherwise been the case.

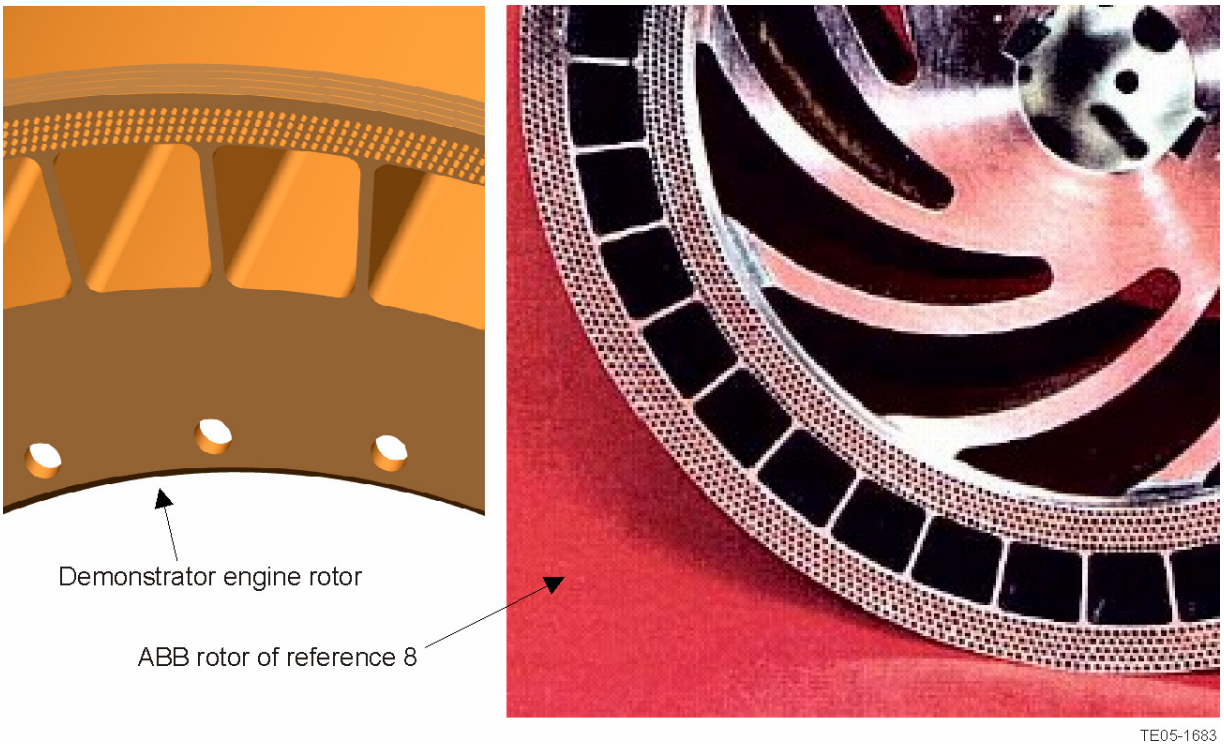

Figure 28. "Honeycomb" Geometry in Outer Face of Rotor.

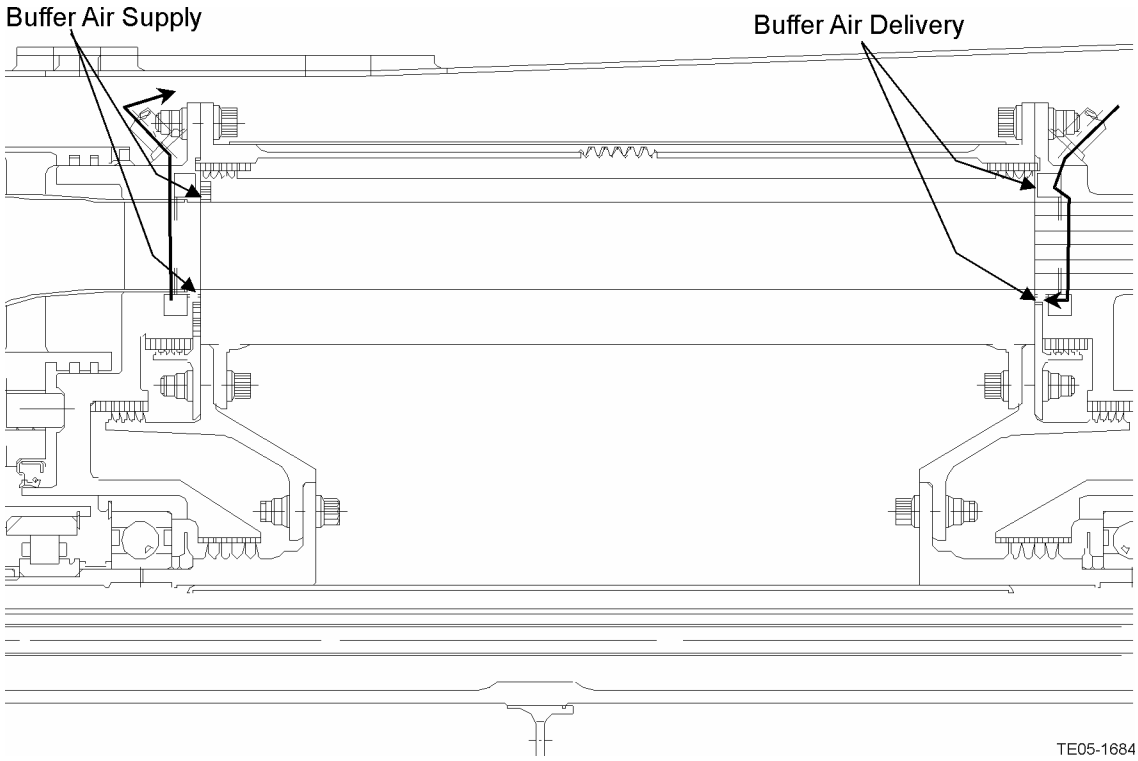

Figure 29. Bleed Flow for Leakage Control.

This leads us into a discussion of the thermal stability of the movable end plate (as well as the exit stationary end plate thermal stability). Thermal warpage of the movable end plate and stationary structure interfacing the wave rotor at both ends of the rotor is of immediate concern and must be addressed. In the current program, our team was unable to carry the design to this level of refinement, but certainly we easily recognized how important the thermal stability of the interfacing stationary plates were to the maintenance of the desired close clearance between the rotor and stator hardware and develop strategies to address the issue. For the Model 501 industrial engine application, it is entirely feasible to water cool the plates, and this was our approach for the demonstrator. If need be we could even consider using copper plates as was done by ABB in their rig. Should development prove the water-cooled plate approach to be viable, the resulting industrial product could incorporate water-cooling since the units are land-based.

For future application of the technology to flight-rated hardware, we must explore other ways to ensure the thermal stability of the critical end plates. High on this list of concepts is fuel cooling of the plates (fuel prior to use in combustion) and/or the development of low thermal coefficient materials for use as a seal plate. These materials, such as the currently available industrial hot pressed ceramics, silicon nitride and silicon carbide, could potentially provide a solution to the end plate design problem. Silicon nitride is being considered for use as a potential rotor material in wave rotor application, Reference 6. In that same vein, Rolls-Royce had good experience with lithium/alumina/silicate in the same development program. This material is not particularly strong, when compared with the previously mentioned ceramics, but has the advantage of being able to be made to exhibit no thermal coefficient of expansion over a useful temperature range and might be a candidate for the stationary rotor-interfacing parts.

2.2.4 Model 501 Engine Rotor Design Considerations

As a part of the design work toward a demonstration of ORC/WR technology in an engine, we considered the design of the rotor itself. As previously mentioned, Rolls-Royce experienced rotor

integrity problems with the fabricated rotor design used in the Phase II rig. The Phase III rig report contains an extensive section addressing 19 ideas brought forward for consideration. In those days, finite element heat transfer and structural analysis were not available, so the analytical work done at the time provided little insight into the details of the problems inherent in many of the designs. Included in the mix was a rotor produced in one piece, as is the SE-17 rotor. Also considered was the addition of a mid-span ring or web, much as is done in the current Comprex rotor.

The final design from the Rolls-Royce Phase III rig study effort was to produce the blades as individual elements and to mount them in the rotor in a dovetail groove as might be done in a turbine or compressor. Following this idea, we produced a model of such a design for the demonstrator engine that is shown in Figure 30.

The blades are located by means of a flow-path part interlaced to the rotor with a long pin that passes through tabs on the rotor and alternating tabs on the underside of the platform part. The outer "band" is formed by the shroud on the blade and is set up so that centrifugal force causes one blade to lean on the next, thus closing the gap and providing damping. The designers thought that the damping aspects of this design might be of considerable benefit in the highly transient dynamic environment expected in the wave rotor.

For our study, this concept was eventually abandoned as it introduced leak paths that would be detrimental to performance. In effect, the multipiece rotor design acted to decrease the desirability of the ORC/WR concept at a time when we had not established that a monolithic rotor could not be made to work. Certainly the Comprex rotor is one piece and the ABB rotor that ran successfully in its ORC/WR test program was produced of one piece, although the running time was limited.

The final design of the rotor is shown in Figure 31 without the honeycomb seal detail already discussed.

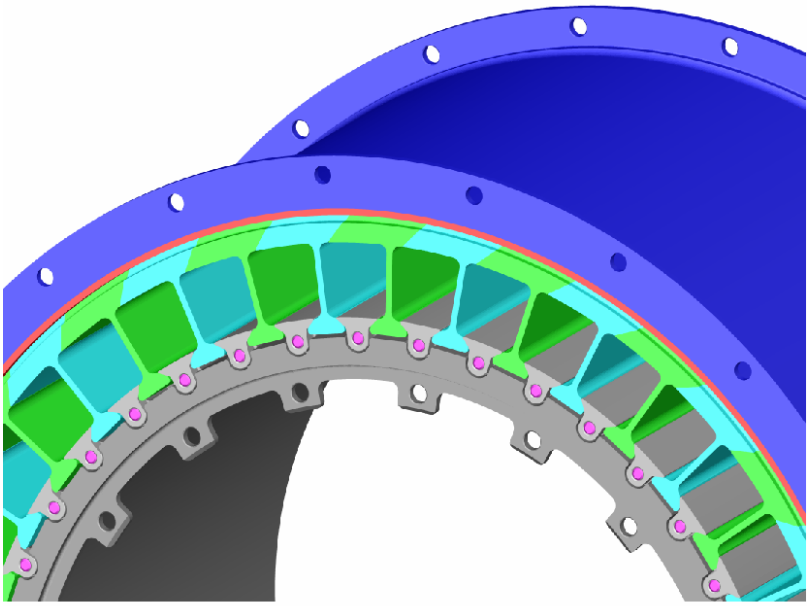

Figure 30. Model 501 Demonstrator Engine Rotor Concept with Individually Replicable Blades Shown Assembled into the Rotor.

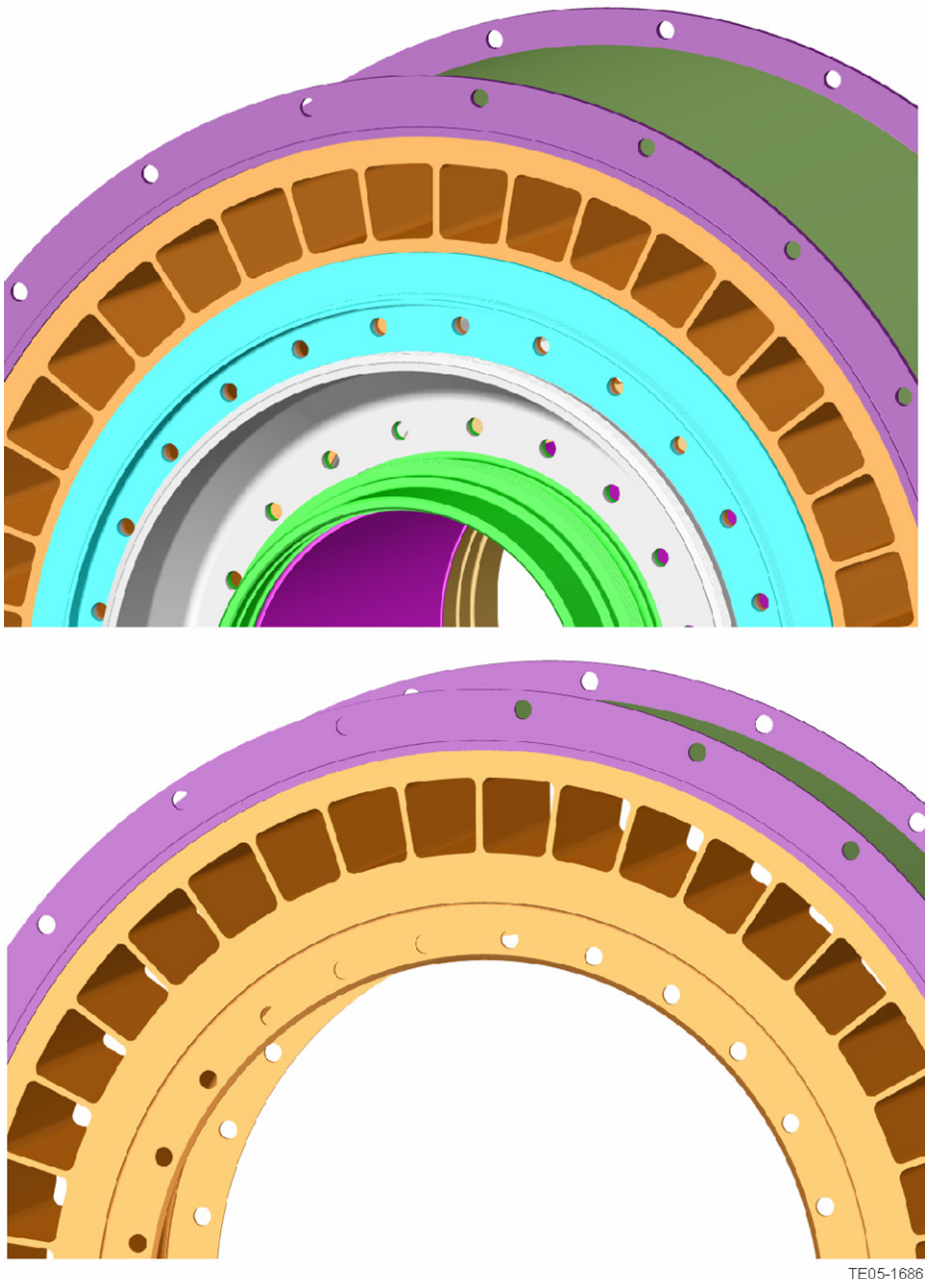

Figure 31. Final Design of the Rotor Selected for the Model 501 Demonstrator Engine.

III. Apply Developed Seal Strategies for POC Test Phase

Goal: Apply developed seal strategies and technologies to the NASA SE-17 four-port wave rotor, which will represent an agreed upon concept development/demonstration vehicle. Develop seal designs at sufficient level to enable manufacture, buildup, and test in a proof-of-concept (POC) experiment.

The most suitable machine for a POC test currently is the NASA four-port rig in SE-17 at NASA Glenn Research Center. While this is a pressure-exchange device rather than an on-board combustion device considered as the product, it has similar sensitivity to leakage and requires an improved seal design itself. It is initially desired to apply an improved leakage modeling capability to examine the performance of the existing seals in this rig, as a major step toward modeling and eventually testing new seal designs for it. This was accomplished by analyzing both the leakage flow constituents in detail and in analyzing the effect of leakages on rig operating characteristics; i.e., its ability to generate pressure gain. We then modified the Q1-D flow solver code to include the influences of interdependency of the leakage within the passages and the network of leakage paths external to the passage.

3.1 Perform Leakage Assessment using Network Flow Tool

Based on available reports, papers, and presentations concerning the NASA GRC SE-17 wave rotor test rig and previous wave rotor leakage analysis models utilizing secondary flow system analysis tools, a methodology was developed for leakage analysis. Leakage analysis within gas turbines is generally conducted utilizing analysis tools that employ a one-dimensional restrictor and chamber element network solving method. The modeling approach favored is one of determining key potential leak paths and then developing a series of common regions with definable pressures. Connecting them are discreet flow restrictions having defined geometry and predictable pressure loss characteristics. RRNAT utilizes a highly effective method of generating pressure loss characteristics using the geometrically based K factor loss method, or alternatively using an empirical loss flow curve based on test data. In the resulting network of elements, unknown pressures and flows are solved for with boundary value pressures set to known values, typically atmospheric or gas flow-path values. This is the approach applied to the ORC/WR.

Unique to the wave rotor is the strong three dimensional aspects to the leakage flow in contrast to the two-dimensional axisymetric nature of leakages in a gas turbine. This is inherent to the wave rotor in that the strongest pressure gradients presented to leakage prone regions is in the circumferential direction rather than in the axial direction, as found in the majority of gas turbine engines. Such a set of elements configured around a wave rotor configuration is schematically represented in Figure 32. As is noted in the figure, the circumferential aspects are included by dividing each end of the rotor into distinct segments in the circumferential direction. This allows regions of similar pressure to be identified and treated as separate leakages within the network analysis solution of the leakage. Figures 33 and 34 show the rig hardware and provide a familiarity with the rig construction.

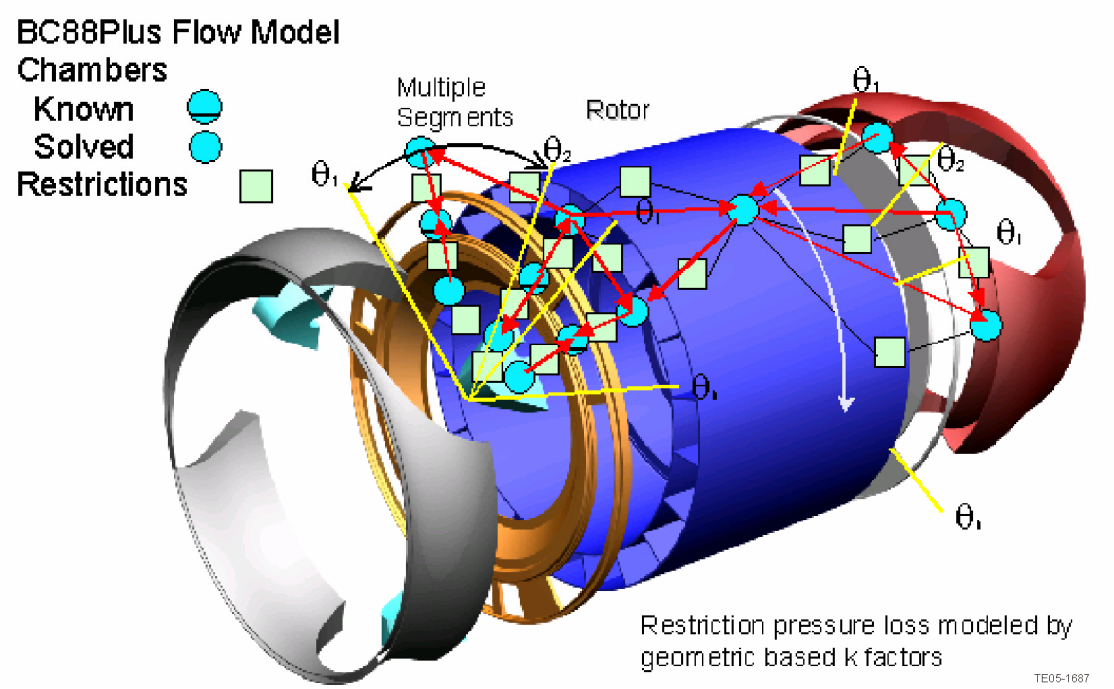

Figure 32. Schematic of Methodology Used in Applying Leakage Network Solver to a Wave Rotor Configuration.

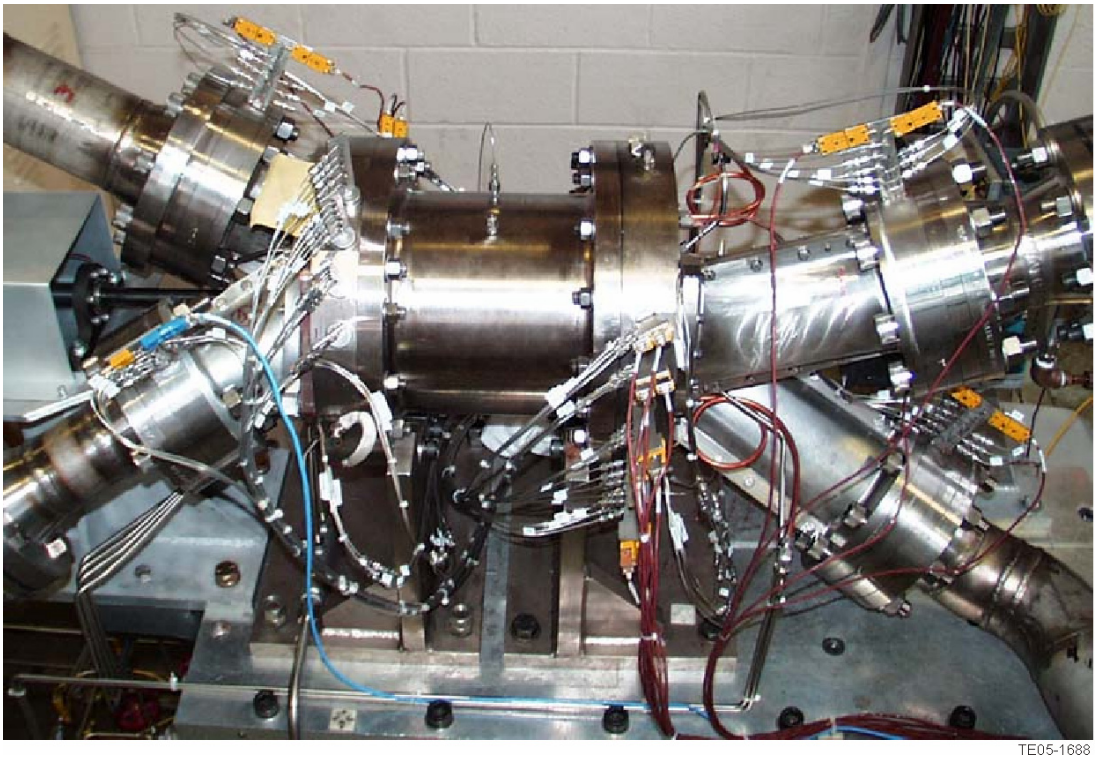

Figure 33. SE-17 Rig Installed in NASA GRC Test Cell.

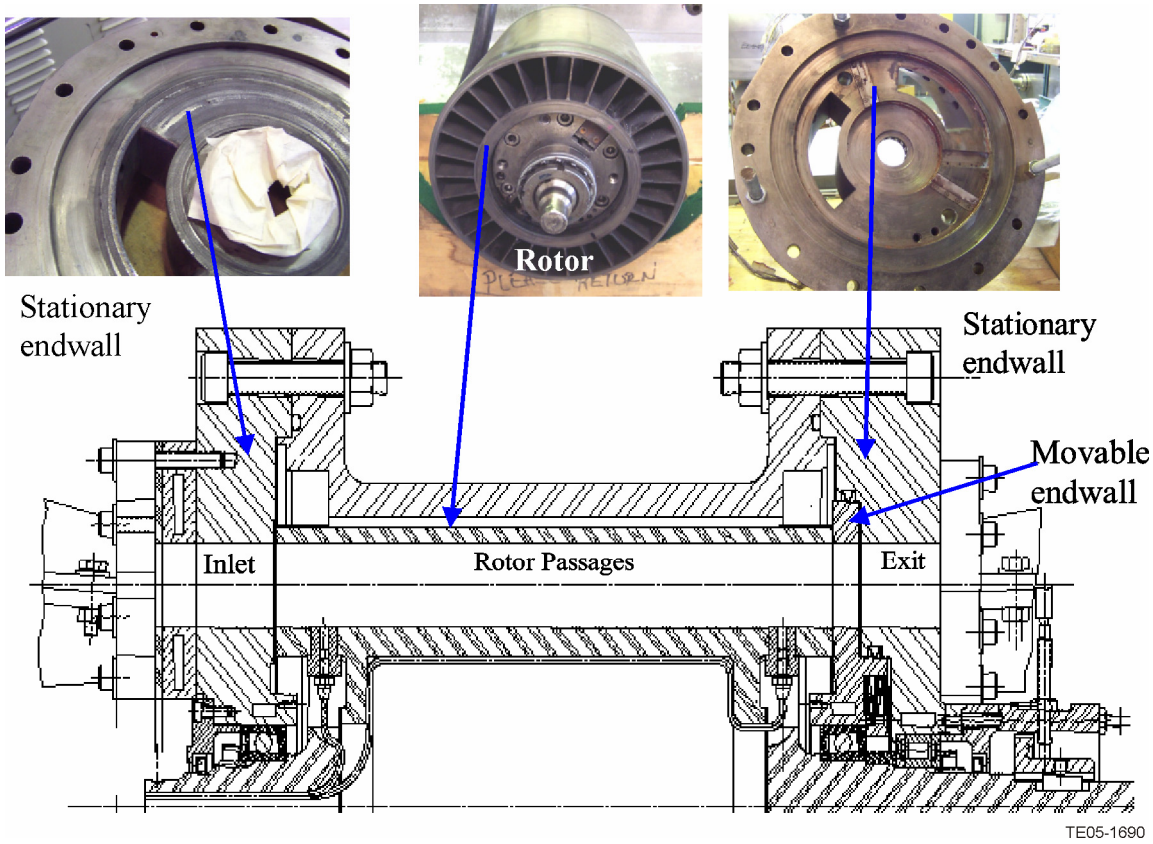

Figure 34. SE-17 Rig Familiarization.

The SE-17 rig cross sections, drawings, and the main gas path Q1-D flow solutions available along with test pressures measured on the rig were reviewed to determine an appropriate set of such elements. Leakage modeling work began with laying out the network model for the rig. The resulting network model can best be expressed as dividing the rig into three planes: the rotor to stator inlet interface, the rotor to movable endwall exit interface, and the movable endwall to stationary endwall interface. These are shown in detail in Figures 35 and 36. Shown are the element identification numbers for the chambers and restrictors. Connection of the three planes can be traced by identifying elements common to two of the planes.

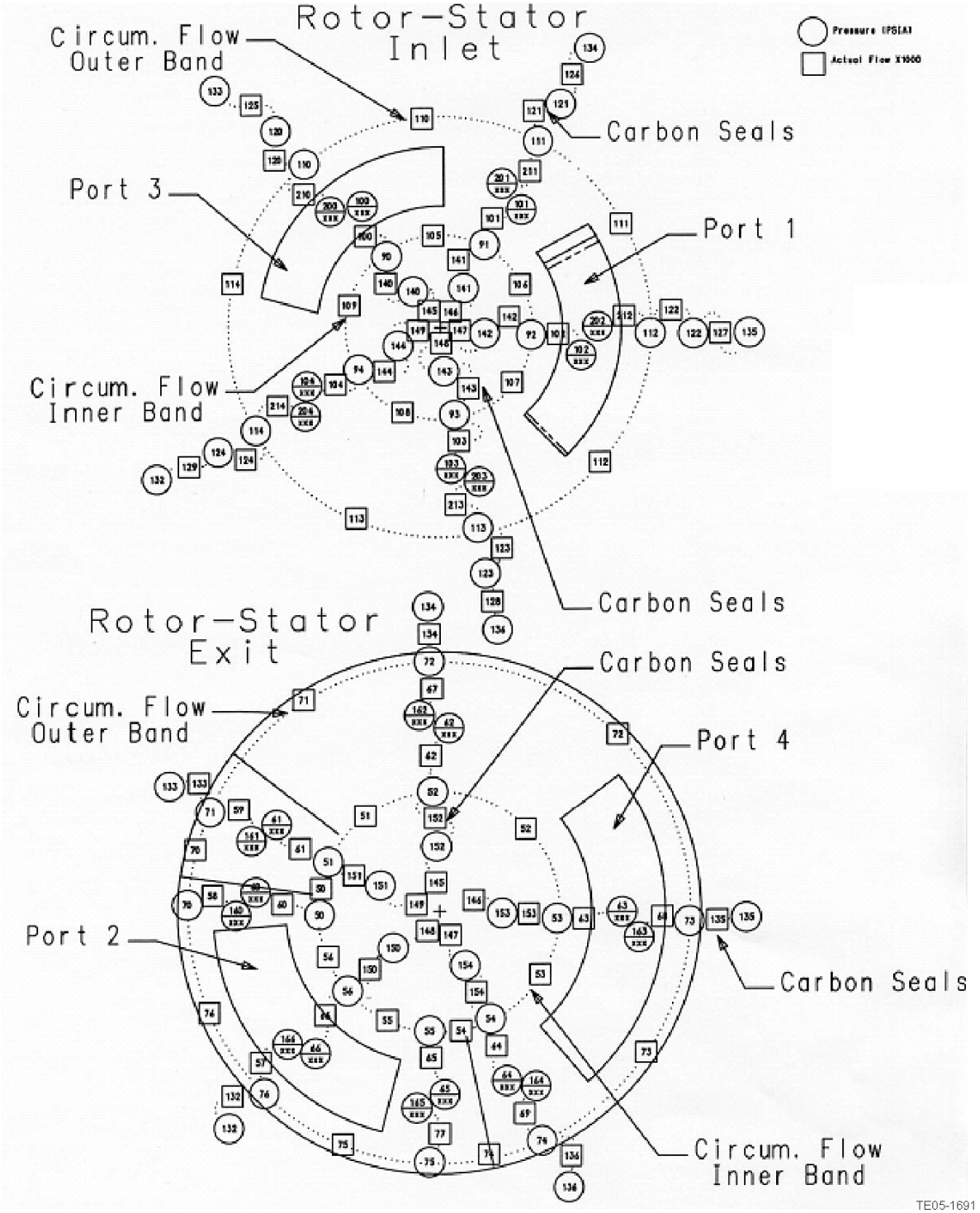

Figure 35. Network Modeling Elements between Rotor and Stationary Endwall on Inlet and Exit End.

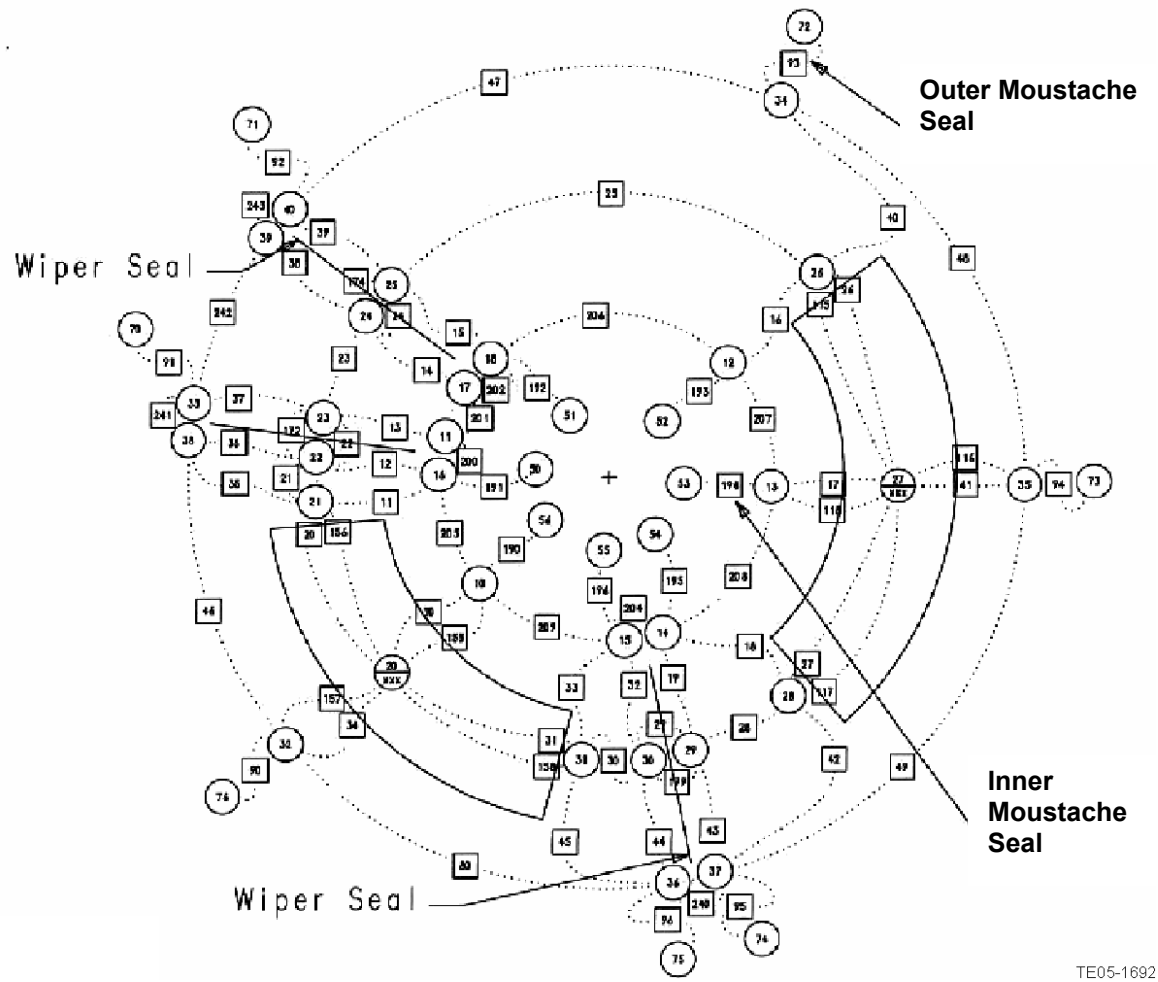

Figure 36. Flow Leakage Network Elements at Station Between Stationary Endwall and Movable Endwall on Exit End.

Also unique to the wave rotor is an anticipated close coupling of the levels of gas leakage to the gas-path flow solution. Within gas turbine design and analysis, basic leakage levels are generally established using estimates of gas-path pressures and temperatures; then the gas flow-path solutions, whether they be compressor or turbine, are generated using applicable tools independent of any changes in the leakage levels resulting from the gas-path flow solutions. Within the wave rotor it has been observed that gas path solutions can be driven significantly by leakage flows. Hence, a methodology was sought to link and iteratively solve for the solution of both leakages and gas flow-path properties together. To this end, a methodology was outlined that will allow the leakage solutions of the computational fluid dynamic (CFD) model to converge to levels common with the leakage network analysis being conducted at RRNAT. This method is explained in detail in section 3.2. It uses the Q1-D program and the BC88 program independently to step through a series of iterations by sharing common leakage information. A commonality of gap resistance modeling strategy between the two is required. The leakage pressure loss calculation methodology of Q1-D was reviewed and the preferred methodology of BC88 was then employed in an expanded capabilities version of Q1-D.

Analysis of the SE-17 rig was aided by an observation visit to the rig. On 12 July 2004, the team met at NASA GRC to examine the NASA SE-17 four-port wave rotor hardware. The unit had just completed a series of tests and was in partial disassembly. The RRNAT trip report provided to NASA at that time is included as Appendix A. With the additional insights gained added to information provided by NASA

about the unit (a description of the unit and a complete set of drawings), the following conclusions were drawn by the team:

- The NASA four-port wave rotor general arrangement presented some unique sealing issues that might be avoided by design in application of the On Rotor Combustion/Wave Rotor (ORC/WR) in the proposed demonstrator engine.
- The most salient of these features was the location of both low and high-pressure ports on each end of the rotor. The design of the movable end plate on the discharge end incorporated a number of seals to defeat the obvious potential paths for flow that might communicate between the high and low pressure exit ports. Our examination of the hardware confirmed that flow might be expected to bypass the seals and thus act to adversely affect the overall performance.
- The four-port unit operated at quite low temperatures compared to the anticipated application of a wave rotor or ORC/WR device to a gas turbine engine. This was done by design to eliminate a number of troublesome variables, thus simplifying rig operation and data acquisition. The potential for thermal distortion of the end plates during operation was greatly diminished.
- Operating evidence was that the desired (very small) rotor to stator gap was being achieved in practice, thus effectively eliminating the incentive to introduce changes to the rig to improve the primary source of sealing.

The team was left with a few items that would later be resolved by analysis at NASA:

- The team recorded "witness marks" where the wiper seals between the movable end plate and the stationary structure had worn into the movable end plate surface. This was later answered by a dynamics analysis (by NASA GRC) of the end plate and shown to be of no particular interest or impact regarding the effectiveness of the seals or operation of the plate.
- The team questioned the fact that the movable end plate was bisected by an internal passage that carried water to cool the bearing. The speculation was that this might cause thermal distortion of the plate, thus affecting operating clearance. A NASA-generated thermal and stress analysis later showed that while the water passage did indeed affect the temperature of the plate, the thermal gradient was sufficiently small so the plate distortion was small enough to result in no concern. It is thus expected that the movable plate thermal distortion will have little effect on operating clearances.

Attention was directed toward an analysis of the internal leak flow paths within the rig and particular attention was given to the potential leak path between the high-pressure and low-pressure port on the backside of the movable end plate at the discharge end. This leakage was termed "shunt" leakage because it provided a direct gas flow path from high to low pressure.

Detailed rig leakage circuit modeling was formulated using the geometric data available. Leakage assessment using the model first centered on static rotor leakage modeling. Several diagnostic tests on the SE-17 rig were performed at NASA to determine the potential leakage rates occurring within the rig. These tests were run with the rotor fixed (nonrotating) and high and low pressures supplied to the exit high-pressure port 2 with the inlet high-pressure port blocked off. Atmospheric pressure was allowed to supply the other two ports. The configuration is represented in Figure 37.

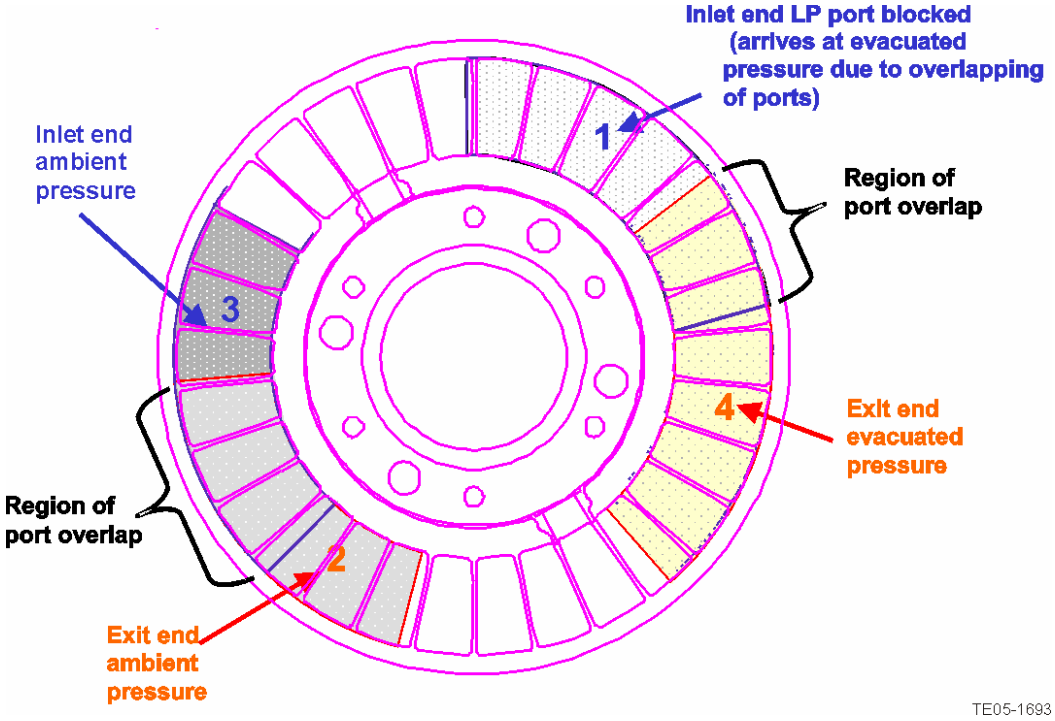

Figure 37. Representation of Static Leak Test.

As Table 5 shows, results from several static rotor tests on the SE-17 rig were used to ground the detailed rig circuit leakage model. For the static rotor case, the passage-to-passage leakage paths were determined to be important and were included in the model for this case only. The NASA static rotor leakage test results were most useful, despite limitations due to uncertainties from measurement of small mass flows using instrumentation out of the range of calibration. The uncertainties in leakage flow measurement arise from Reynolds number effects on loss coefficients when employing large orifice plates to measure small flow rates. Agreement between the test and predicted results was deemed adequate.

Table 5. Leakage Modeling Results Compared to Static Rotor Tests on SE-17 Rig.

NASA Reading No.	Predicted Flow (#/s)	Measured Flow (#/s)	R-S Inlet Gap (in.)	R-S Exit Gap (in.)	S-S Exit Gap (in.)	% Diff
3417	0.0314	0.033	0.003	0.004	0.026	~5%
3423	0.0253	0.026	0.	0.004	0.029	~3%
3426	0.0285	0.033	0.0015	0.004	0.0274	~16%

3.2 Analyze Leakage Sensitivity of Performance of NASA SE-17 Rig

The effects of the leakage on the rig operation were initially determined by utilizing the Q1-D code in its form using the single-cavity method to establish sensitivity of the rig-to-rotor endwall gap. Figure 38 shows the predicted pressure and temperature wave diagrams, and rotor-end properties for the four-port rig cycle, where the temperature ratio was targeted at approximately 2.0 under conditions of the design point of operation, assuming no leakages. The pressure gain performance predicted is shown in Figure 39 for zero leakage, as well as for the estimated leakage using the prior model with equal gaps. Figure 39 also shows the effect of varying gap at the inlet end, while the outlet end gap is kept fixed as given. This is the expected actual range of gap size in operation, corresponding in particular to Run 3468 of the NASA experiment. However, the model is based on a single leakage cavity, and does not allow for variable sealing along the periphery or include the possibility of shunt leakage as described later.

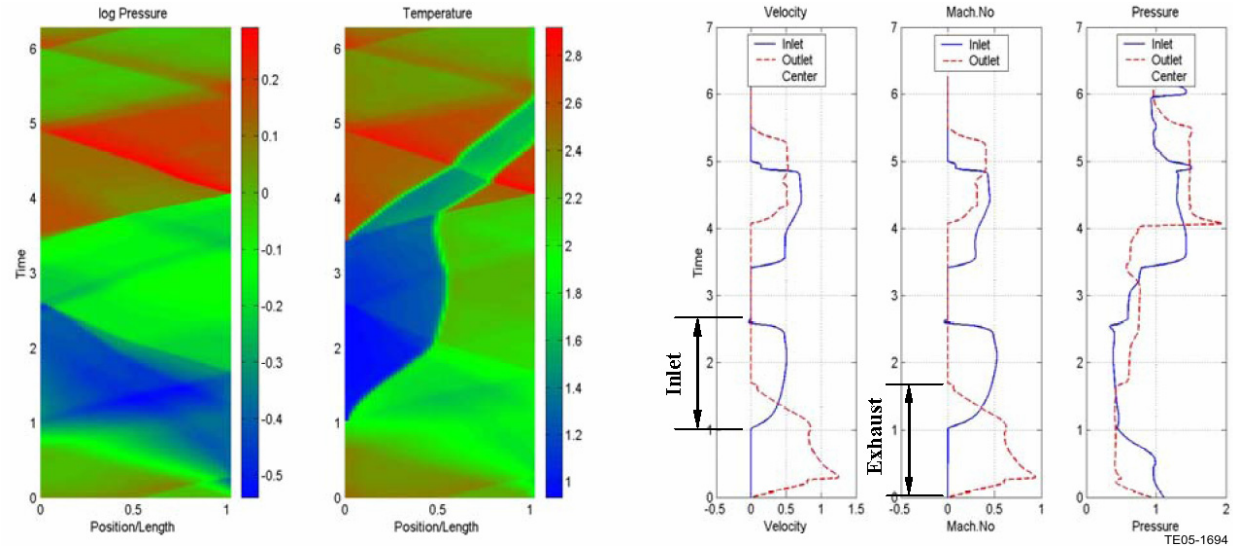

Figure 38. NASA Four-Port Cycle Design-Point Simulation with Major Losses: Temperature Ratio of 1.97.

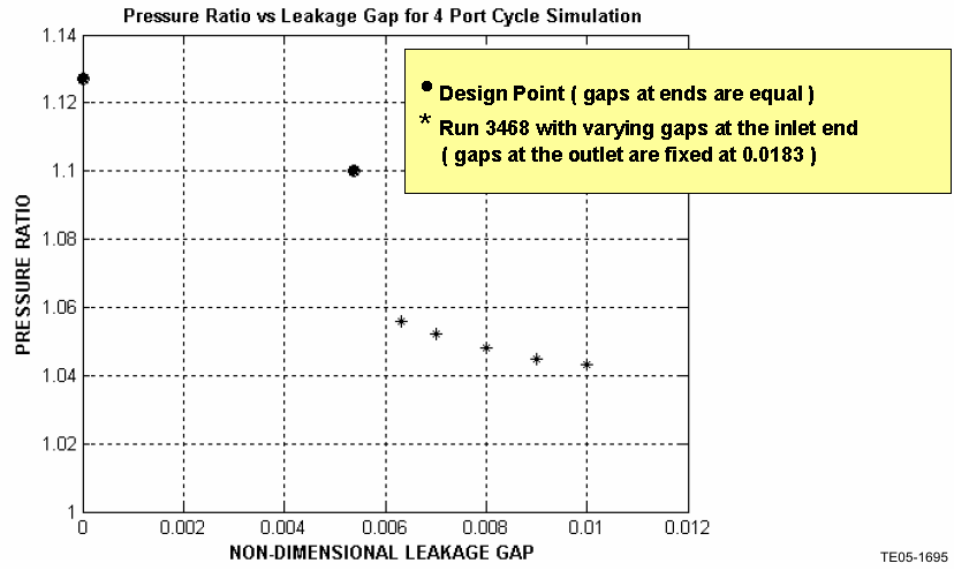

Figure 39. Pressure Gain versus Leakage Gap for Temperature Gain of 2.0 and C_D = 0.8.

3.3 Modify Q1-D Analysis Code

Goal: Modify analysis code as needed to include model for comprehensive leakage circuit, balancing secondary flows and control volumes, and/or interface with RRNAT secondary flow code with appropriate fidelity.

Control of leakage within wave rotors has been recognized as a key requirement for efficient operation. Numerical simulations suggest that experimentally observed performance degradation is substantially due to flow leakage. It is therefore important to understand the sensitivity of wave rotor performance to leakage, as well as to other design and operating parameters. However, simple one-cavity leakage models are not adequate to either capture the complexity of the current seal design leakage phenomenon or provide sufficient guidance in improved seal design. Thus a new leakage modeling approach capable of calculating mass flow rates through the gaps at the end of the rotor holding the rotating channels and stationary endplates, both inlet and exit end, was required. This was accomplished by introducing multiple leakage chambers arranged around the outer and inner radii of the rotor ends, as schematically shown in Figure 40.

In contrast to the previous single-cavity modeling used in the Q1-D code, the new model takes into account the differences in pressures and temperatures at the local leakage sites within the wave rotor to which and from which gas is exchanged. When combined with a flow network solver, as is commonly employed in examining cooling and leakage flows within gas turbines, the new approach creates a powerful tool for the control of leakage flows and in the design of improved wave rotor based engines. This model was successfully incorporated in the Q-1D wave rotor CFD code.

Shunt Leakage Modeling

The new leakage model also included the effects of leakage flow that may shunt directly between ports on one end of the rotor, as illustrated in Figure 41. Such a leakage path appeared to exist in the NASA SE-17 rig behind the movable stator or false endwall used for rotor-stator clearance control. Direct stator-stator leakage on the exit side of the device from the high pressure to the low-pressure port reduced the rig performance as shown in this section. To describe the modeling, the numbering shown in Figure 42 is used to specify inlet and outlet ports, consistent with the Q-1D code. In the following, indices 1, 2, 4, and 5 represent state of the flow at the rotor-stator plane of ports connected to compressor discharge, burner outlet, turbine inlet, and burner inlet, respectively.

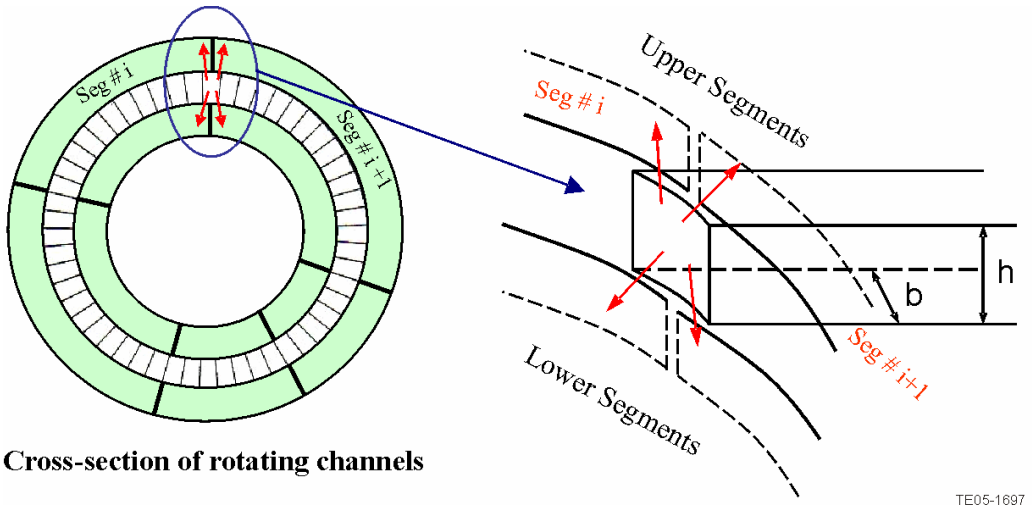

Figure 40. Schematic of Leakage Phenomenon from Rotating Channels to Leakage Chambers.

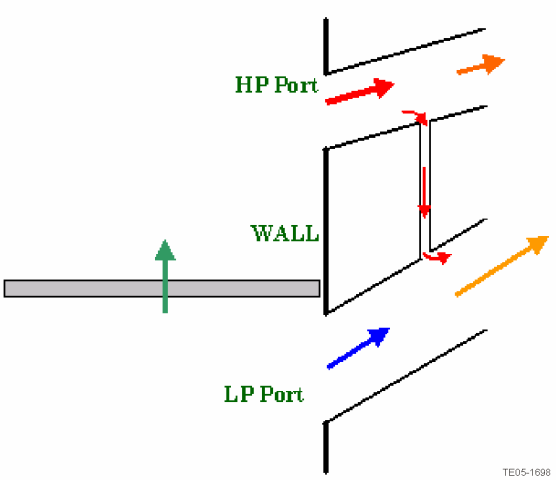

Figure 41. Simulating Leakage from High-Pressure Port into Low-Pressure Port.

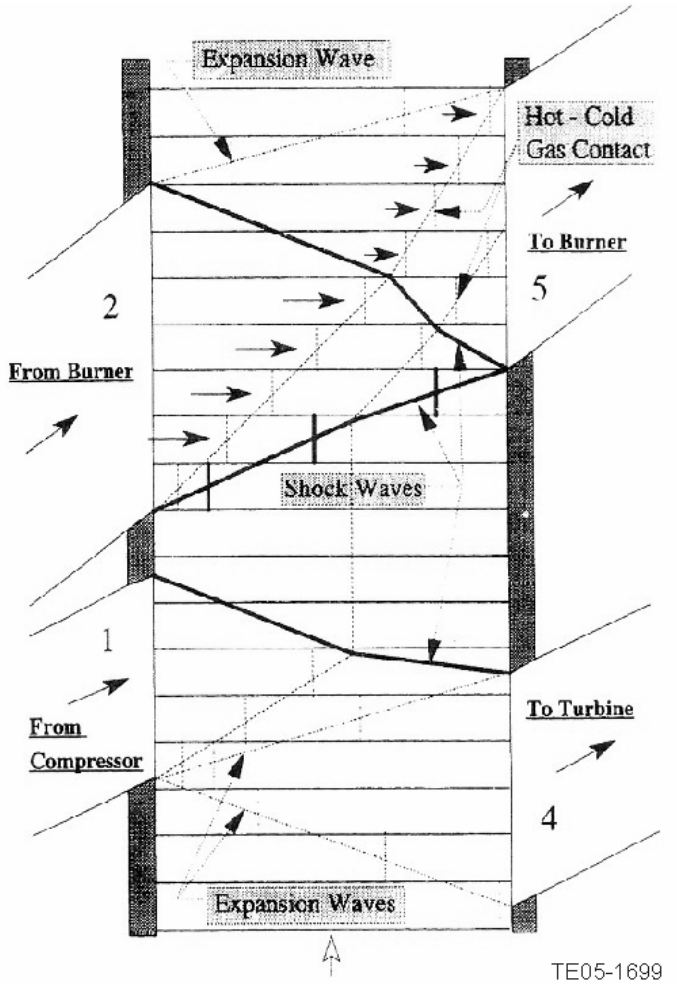

Figure 42. Port Numbering Used in the Q1-D.

Table 6 shows some outputs of Q1-D, which attempt to match NASA experiment run 3468, assuming flows to and from burner are equal, without stator-stator leakage. At this point, no attempt was made to match the predicted values with measured data. MF represents non-dimensional mass flow rate at each port. As shown, the code predicted pressure gain of P4/P1=1.065, and it converged when the mass balance occurred between ports 1 and 4 (MF = 0.268) and also between ports 2 and 5 (MF = 0.409). The corresponding wave diagrams are shown in Figure 43.

Considering severe stator-stator leakage from port 5 to port 4 equal to 5% of compressor discharge flow (MF5 = MF2 + 5% MF1, and also MF4 = 95% MF1), the code predicted lower performance (P4/P1=1.036 without adjustment for re-mixing), as indicated in Table 7. Also, leakage lowered the pressures of the entire high-pressure part (P02 and P05), degrading pressure gain. Q1-D generated wave diagrams for the 5% leakage case are shown in Figure 44.

Table 6. Output of Q1-D without Stator-Stator Leakage.

	MFCORR	P4/P1	T4/T1	OMEGA
	0.43372	1.06497	1.99497	0.97975

	MF	EF	MO	UB	PB	TB	P0	T0
1	0.268	0.267	0.550	0.505	0.428	0.965	0.512	1.016
				0.421	0.422	0.961		
2	0.409	1.140	1.596	0.659	1.343	2.723	1.499	2.810
				0.585	1.340	2.722		
4	0.268	0.537	0.668	0.857	0.415	1.878	0.541	2.025
				0.787	0.418	1.882		
5	0.409	0.870	1.480	0.573	1.426	2.082	1.590	2.148
				0.473	1.430	2.084		

NOMENCLATURE (after Paxson)

MFCORR: corrected mass flow rate
OMEGA: non dimensional rotor speed
MF: integrated mass flux from/to port
EF: integrated total energy flux from/to port
MO: integrated momentum flux from/to port
UB: absolute/relative mixed mean velocity
PB: absolute/relative mixed static pressure
TB: absolute/relative mixed static temperature
P0: absolute mixed stagnation pressure
T0: absolute mixed stagnation pressure

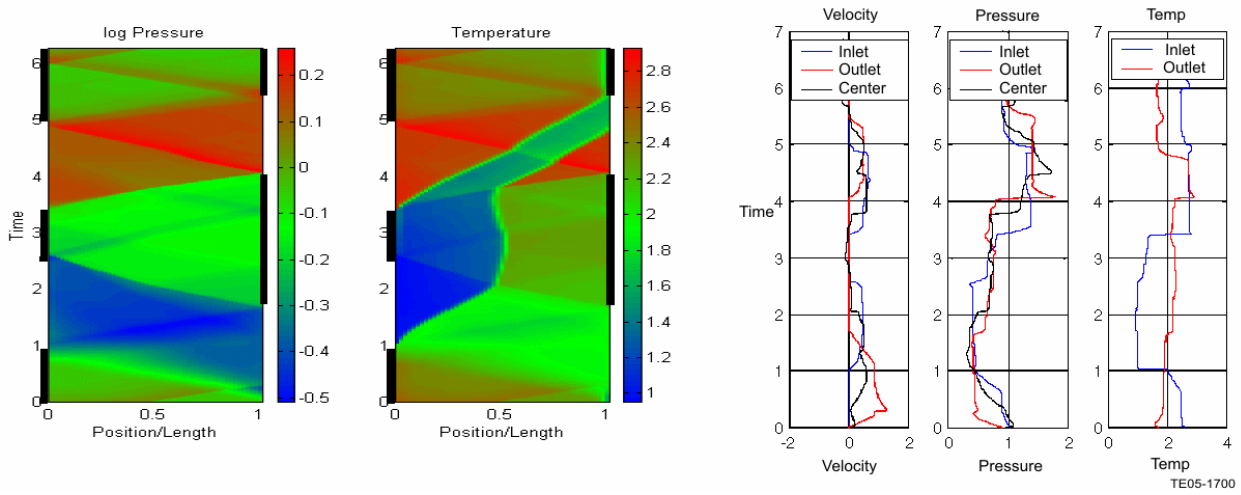

Figure 43. Wave Diagrams without Stator-Stator Leakage.

Table 7. Output of Q1-D including 5% Stator-Stator Leakage.

				MFCORR 0.43524	P4/P1 1.03625	T4/T1 1.99211	OMEGA 0.97975	
	MF	EF	MO	UB	PB	TB	P0	T0
1	0.269	0.268	0.550	0.508	0.427	0.965	0.512	1.016
				0.423	0.421	0.961		
2	0.409	1.112	1.572	0.653	1.322	2.653	1.476	2.738
				0.580	1.319	2.651		
4	0.255	0.502	0.644	0.808	0.415	1.854	0.526	2.022
				0.745	0.414	1.854		
5	0.422	0.878	1.442	0.605	1.359	2.025	1.539	2.098
				0.497	1.369	2.029		

Nomenclature: see Table 6.

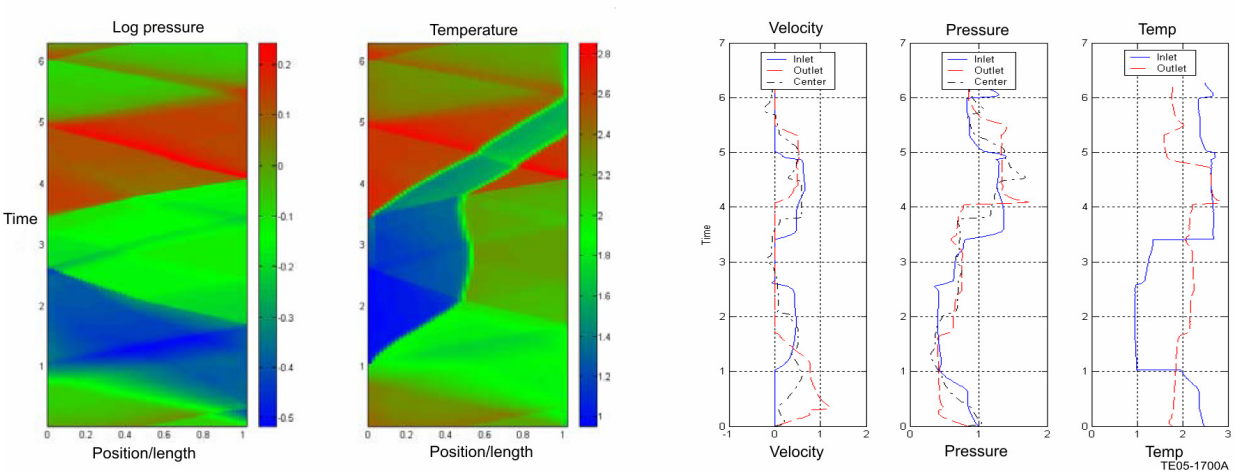

Figure 44. Wave Diagrams with 5% Stator-Stator Leakage.

Note that in calculating the temperature gain, the effect of shunt leakage was taken into account. Penetration of the hot gas from the HP outflow port increased total temperature at the exhaust port. To calculate corrected exhaust temperature, a control volume shown in Figure 45 was used to calculate this temperature using energy balance across this control volume as:

$$\dot{m}_{in} T_{total-in} + \dot{m}_{leakage} T_{total-leakage} = (\dot{m}_{in} + \dot{m}_{leakage}) T_{total-out}$$

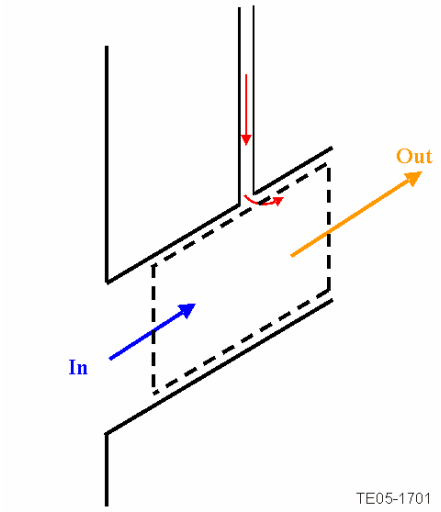

Figure 45. Calculation of Exhaust Temperature Due to Shunt Leakage.

Segmented Boundary Leakage Model

Figure 46 depicts an unwrapped view of the rotor shown in Figure 40 surrounded by multiple leakage chambers arranged around the outer and inner radii of the rotor ends. Five leakage segments were located on each clearance gap at outer and inner radii at the inlet end, and seven leakage segments were located at each gap of the outlet rotor end. Similar to the logic of Q1-D, only one channel was considered in the analysis, but mass flow rates will be calculated by taking into account the number of channels.

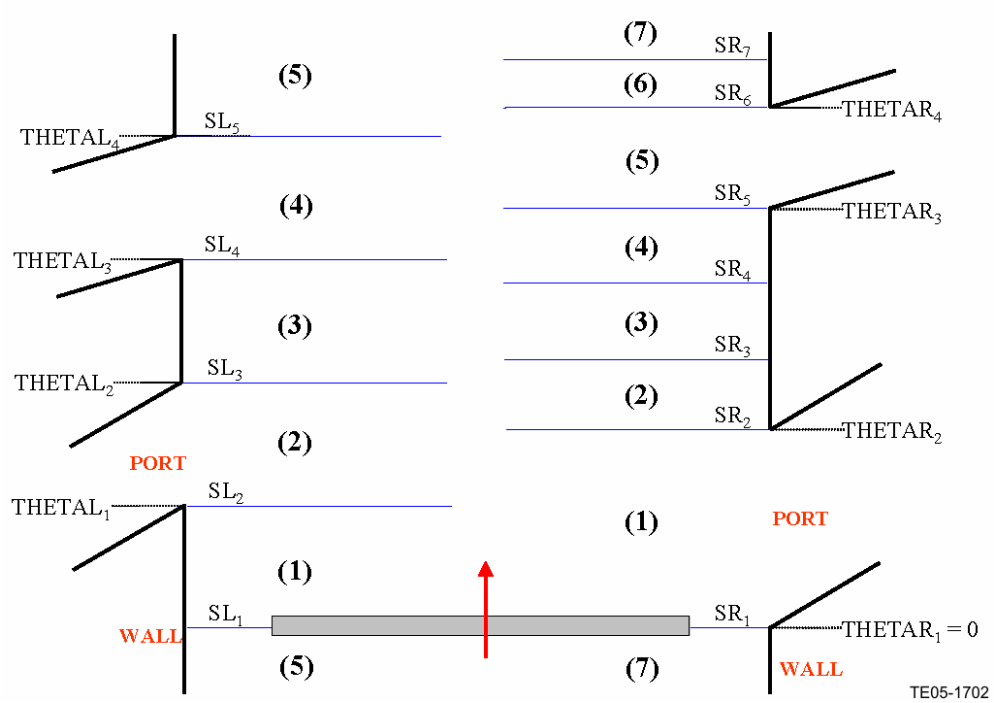

Figure 46. Developed View of the Rotor Indicating Port and Leakage Chamber Locations.

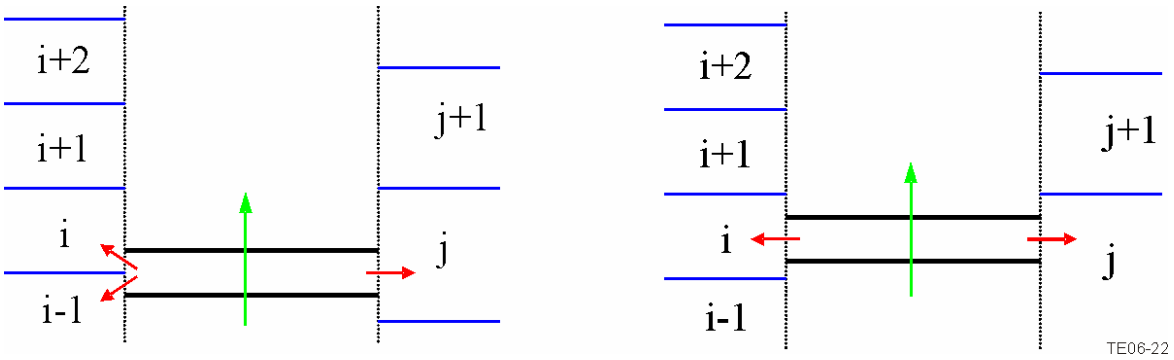

Figure 47. Two Possible Positions of a Channel Relative to Segments.

At any instant, each end of the channel may encounter a single pair of leakage chambers (inner and outer), or it could be positioned between two sequential chamber pairs (gradual opening and closing). This is schematically shown in Figure 47, where the left picture represents the gradual opening/closing between two arbitrary segments i and i-1 at the left side, while the right picture represents encountering only segment i at the left side.

Fractional Opening/Closing

As an example, Figure 48 represents the more general case when the upward moving channel of total width THETAOT is leaving segment 5 and entering segment 1 at the inlet side of the rotor. X and Y are used to represent the portion of the channel width exposed to the upper and lower chambers, respectively. Here, DTHETAX and DTHETAY are exposed arc lengths to the upper segment 1 and lower segment 5, respectively. THETA represents the distance between the upper section of the channel and the code reference point ($THETAR_1 = 0$ in Figure 46). In fact, THETA is equivalent to the time step in the code. At each time step, all these positional variables are calculated measuring from the code reference point.

The main goal was to calculate leakage mass flow rates between the rotating channel and stationary segments. Leakage rates with the upper segment ($\dot{m}_X$) and the lower segment ($\dot{m}_Y$) were obtained using the loss curves specified by Rolls-Royce, given the upstream static pressure and temperature, downstream pressure, channel geometrical characteristics such as width and height, and portion of the channel width opened to the segment. Consistent with Q1-D, positive mass flow rate was obtained when the flow entered the channel and vice versa. The direction of the flow was specified by comparing chamber pressure and channel end pressure. The described procedure was conducted for both inner and outer radii, at the inlet and outlet rotor ends. Therefore, the total leakage flow at each time step was expressed as:

$$\dot{m}(t) = [\dot{m}_X + \dot{m}_Y]_O + [\dot{m}_X + \dot{m}_Y]_I$$

where indices "O" and "I" refer to outer and inner radii, respectively. The amount of leakage mass accumulated at each leakage chamber for sequential leakage chambers j and j-1:

$$\dot{m}_j = \sum_{\theta=\theta_j}^{\theta=\theta_{j+1}} \dot{m}_X \times \left(\frac{\Delta\theta}{\theta_{Cycle}}\right)$$

$$\dot{m}_{j-1} = \sum_{\theta=\theta_j}^{\theta=\theta_{j+1}} \dot{m}_Y \times \left(\frac{\Delta\theta}{\theta_{Cycle}}\right)$$

where $\Delta\theta$ and θ_{Cycle} were the time step and cycle period, respectively.

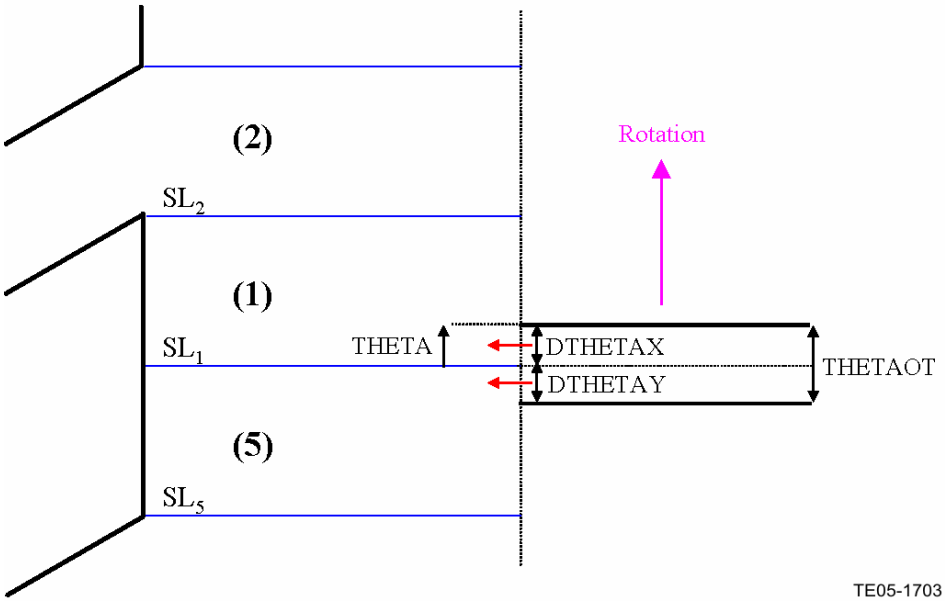

Figure 48. Schematic Model for Gradual Opening/Closing.

At each leakage chamber, it is also useful to calculate the average temperature and pressure of the entering and leaving flows. Such averages are meaningful only if the flow direction is fixed; yet in several segments, the leakage flow reverses direction as the pressure in the channel changes with the unsteady gas flows inside it, while the channel traverses the particular segment. Therefore, the code calculates average pressure and temperature separately for the positive flows (entering the channel) and negative flows (leaving the channel) comparing the pressure of channel ends and leakage chamber pressure. Pressures in the channels are those of the moving frame of reference (relative pressure). Pressures in the leakage chambers are in the stationary frame of reference. Rotation effects are ignored.

The original Q-1D code calculated leakage rate at each end to a single common cavity, and these constituted the leakage source terms (S_1 and S_3) for the computational cells at the channel ends. The well-known St. Venant's orifice equation was used. In the new model, the leakage source terms were calculated as:

$$S_1 = \frac{\left[\dot{m}_X + \dot{m}_Y\right]_O + \left[\dot{m}_X + \dot{m}_Y\right]_I}{\Delta x}$$

$$S_3 = \frac{\left[\dot{m}_X T_X + \dot{m}_Y T_Y\right]_O + \left[\dot{m}_X T_X + \dot{m}_Y T_Y\right]_I}{\gamma - 1}$$

where T_X and T_Y are total temperature of the flow at the upper and lower sections of the channel, respectively. If the flow enters the channel, the chamber temperature is used. If the flow leaves the channel, the channel cell total temperature is used.

Single Segment Pair Encounter

This scenario is a simple version of the previously described scenario. The same methodology was used by setting $\dot{m}_Y = 0$ in the entire calculation.

In the original Q1-D, the converged solution was obtained when single cavity properties equilibrated and the total net leakage tended to zero, and port flows reached steady state. With segment properties now fixed, the convergence criteria now are satisfied when changes in all leakage mass flow rates from one cycle to the next become small:

$$\left| \frac{\dot{m}_j(t_{cycle+1}) - \dot{m}_j(t_{cycle})}{\dot{m}_j(t_{cycle})} \right| \leq \varepsilon$$

where j represents each leakage chamber. ε is a small value, e.g., 0.01.

Iterative Leakage Assessment Algorithm

The algorithm shown in Figure 49 describes a summary of leakage assessment procedure using the modified Q1-D and BC88 calculations.

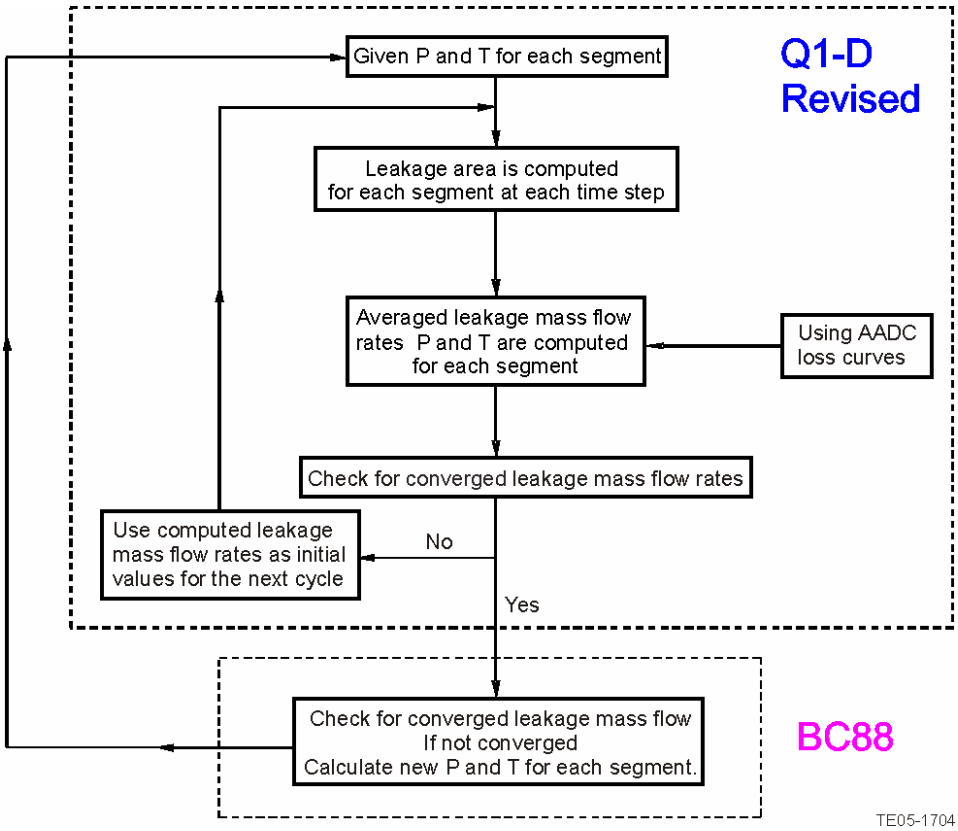

Figure 49. Summary of Leakage Calculation by Q1-D and BC88.

Verification

To test the validity of the segmented leakage model, comparison of the results of the code using the new model and the NASA Q1-D wave rotor code single cavity model was made. In this comparison, we attempted to match experimental test run 3468 using both models. At first, the difference in physical loss curves between the two models was examined using the same pressure and temperature leakage boundary condition, set to the calculated cavity pressure and temperature by the Q1-D code, i.e., $P_{camber} = P_{cav}$ and $T_{chamber} = T_{cav}$. While minor differences were observed, the general trends were identical, and good agreement was observed when the two codes used the same physical model.

Checks were performed to establish the validity of the new model by examining the instantaneous leakage flow direction. This is shown in Figure 50, where the instantaneous variation of leakage mass flow rates, rotor end pressure, and chamber pressures at the inner and outer radii at the outlet wall are shown as a function of time. The correspondence of the pressure difference with the mass flow is examined in Figure 51, where the leakage mass flow rates as functions of pressure difference (chamber pressure minus channel pressure) were plotted in dimensionless form. Per the intended method, the leakage flow followed a flow curve characteristic except for that portion that departured from the postulated full flow loss curve due to partial opening.

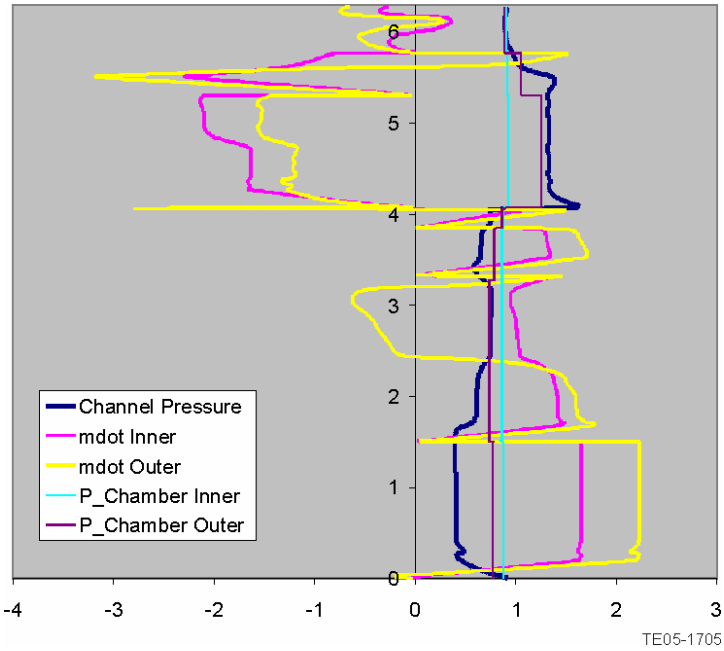

Figure 50. Validation of Flow Direction at the Outlet End.

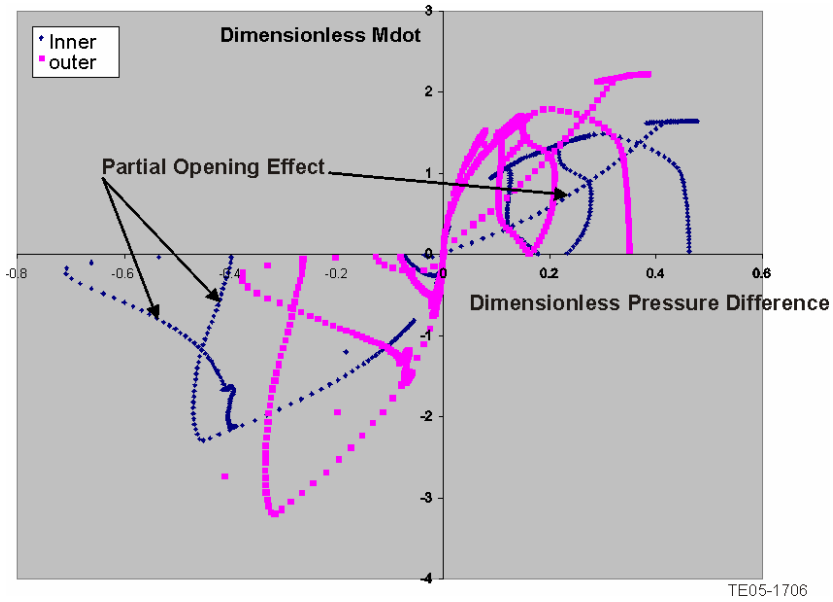

Figure 51. Leakage Mass Flow Rates as Function of Pressure Difference at the Outlet Wall.

Since the averaged pressures of the entering and leaving flows were calculated in the code, it was also possible to make a similar comparison for the averaged pressures. Figure 52 proves that for all five leakage segments at the inner and outer radii at the inlet wall, the leakage mass flow rates were positive values when the chamber pressures were greater than the averaged channel pressures, and vice versa. A consistent trend was also apparent at the outlet wall, as shown in Figure 53.

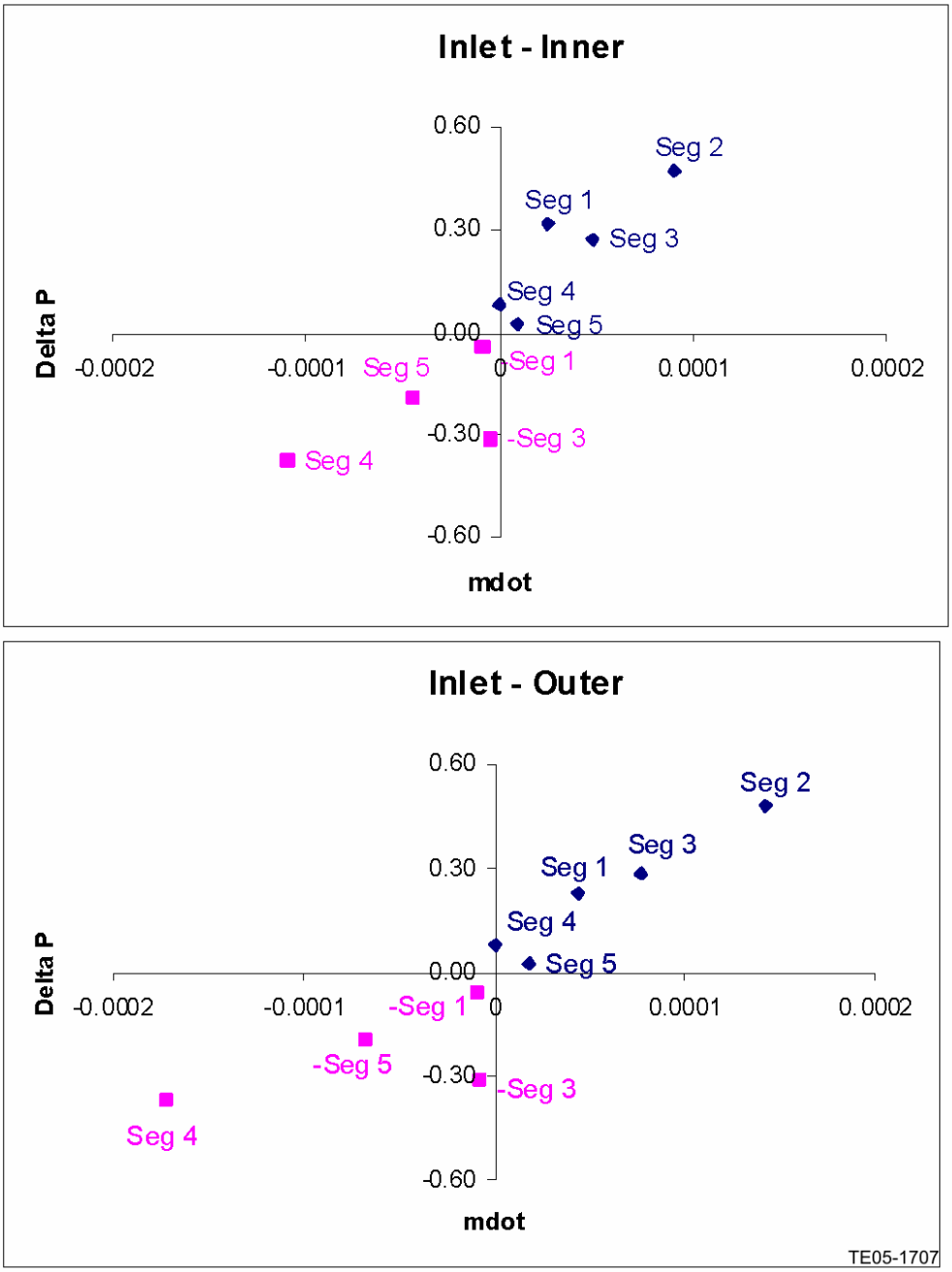

Figure 52. Averaged Pressure Difference as Function of Leakage Mass Flow Rates at the Inlet Wall.

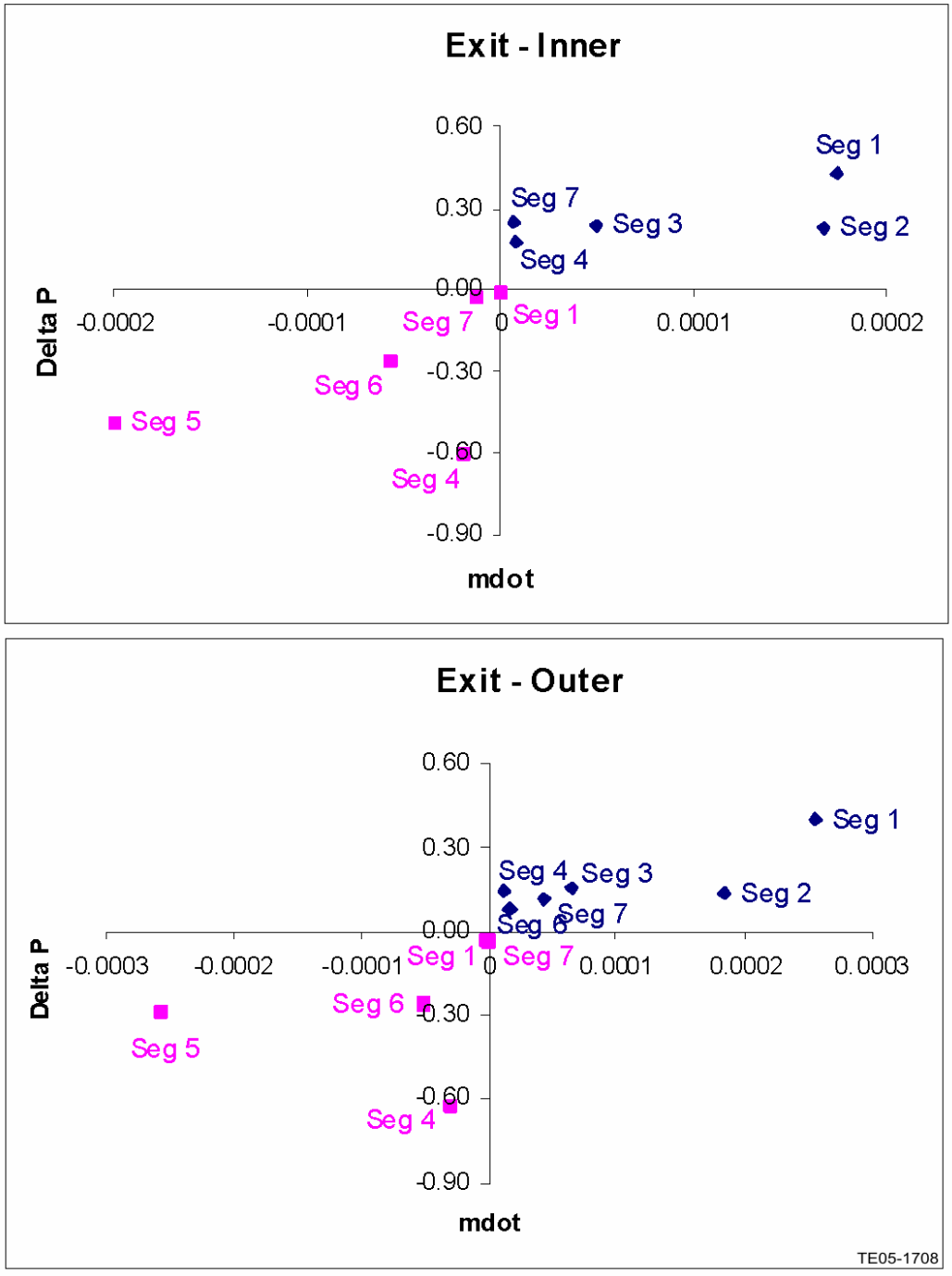

Figure 53. Averaged Pressure Difference as Function of Leakage Mass Flow Rates at the Outlet Wall.

Sensitivity Analysis

During the iteration process between Q1-D and BC88, changing the code input parameters to meet the rig measurements was important. Therefore, a systematic sensitivity analysis was made to understand how changes in the input parameters would affect the solution matching the experimental data.

In the analysis, four variables were considered as the free parameters:

- BLOSS: burner pressure drop
- QCORR: heat addition parameter
- P_4: exhaust back pressure
- Shunt flow

Four target outcomes measured by the tests were:

- Measured loop flow ratio, mass flow in combustor loop divided by inlet mass flow
- Measured overall temperature ratio: Tt4/Tt1
- Inlet mass flow, corrected: MFCORR
- Measured pressure gain: Pt4/Pt1

Running the code, changing any of the free parameters changes the targets. It is important to know which of the free parameters has the largest (or smallest) effect for each target. The reference case was judiciously assigned the following 'base' values of the free parameters:

- BLOSS = 1.1
- QCORR = 1.4
- P_4 = 0.425
- Shunt flow = 5% of the inlet mass flow rate = 0.0134

Analyzing linear sensitivity using a 5% change in each parameter, the following results were obtained for a small change in each of the free parameters. This assumed 'main effects' of each free parameter were additive to get the total effect on each target, so it neglected multiparameter interactions as well as non-linear effects. Of course, real behavior has all these complexities, so these coefficients are only valid for small changes from the reference baseline. Even so, it gives us some idea of what combination of parameters we might change to achieve a given target, rather than relying on intuition to link them in over simplistic one-on-one terms.

Fractional Change of "Loop Flow Ratio" = (-0.463) Fractional Change in "BLOSS" + (0.357) Fractional Change in "QCORR" + (0.957) Fractional Change in "P_4" + (-0.087) Fractional Change in "Shunt"

Fractional Change of "T_{t4}/T_{t1}" = (0.027) Fractional Change in "BLOSS" + (0.302) Fractional Change in "QCORR" + (0.290) Fractional Change in "P_4" + (0.019) Fractional Change in "Shunt"

Fractional Change of "MFCORR" = (0.031) Fractional Change in "BLOSS" + (0.056) Fractional Change in "QCORR" + (-0.910) Fractional Change in "P_4" + (0.004) Fractional Change in "Shunt"

Fractional Change of "P_{t4}/P_{t1}" = (0.012) Fractional Change in "BLOSS" + (0.104) Fractional Change in "QCORR" + (0.405) Fractional Change in "P_4" + (-0.018) Fractional Change in "Shunt"

The coefficients shown in the parentheses indicate that an increase in the burner pressure drop parameter resulted in a relatively small increase in T_{t4}/T_{t1}, MFCORR, and P_{t4}/P_{t1}, but a relatively high reduction in the loop flow ratio, as we might expect. Increase in the heat addition caused an increase of all the target parameters. Increased back pressure caused a significant increase in the loop flow ratio, T_{t4}/T_{t1}, and P_{t4}/P_{t1} and a significant reduction in MFCORR. Finally, increase of the shunt flow reduced both the loop flow ratio and P_{t4}/P_{t1} while it increased MFCORR and T_{t4}/T_{t1}. Surprisingly, the back pressure had the most significant relative effect among all the free parameters and the shunt flow had the least relative effect. This indicates that the solution is sensitive to the selection of the back pressure when shunt flow is considered in the calculations. To match the results of a run with the experimental data, it is wiser not to change the back pressure but make adjustments by BLOSS and QCORR for a given shunt value.

This analysis does not give us the formula for matching experimental target parameters, but this could be done with a matrix inversion to get the combination of free parameters that should match a given target set. Of course, the non-linearit(y)(ies) will require iterations. At this point, only three targets exist to match with three free parameters: BLOSS, QCORR, and P_4.

3.4 Q1-D Produced Estimates of Performance with Leakage

Performance estimates were required to guide the decision process regarding the benefits to adding additional seals to cut shunt leakage. These estimates were made with the basic Q1-D model matched to test point 3468 and run with no shunt leakage (case 1) and with shunt leakage (case 3). This seeks to bound the problem and formed a basis for evaluating the influence of techniques to reduce leakage.

Case 1

Q1-D result with 0.0025 in. (inlet) and 0.004 in. (exit) gaps
Force the measured back pressure on to port 4 by specifying P4 in the input file using the average of the 10 port static taps on the rig.
Adjust the burner pressure drop parameter BLOSS until achieving the measured loop flow ratio of 1.53.
Adjust the heat addition parameter QCORR until matching the measured overall temperature ratio TT4BAR/TTOR.
No shunt leakage. (Note that inlet mass flow is not adjusted to test levels.)

Case 3

Same as case 1 with shunt leakage model turned on.
Adjusted P4/P1 value until the performance looked like the test results.
Since the shunt leakage actually occurs upstream of where the static pressure measurement is made in the rig, the imposed back pressure is adjusted until the measured mass flow rate plus 10% for blockage is achieved.
Adjust the burner pressure drop parameter BLOSS until achieving the measured loop flow ratio of 1.53.
Adjust the heat addition parameter QCORR until matching the measured overall temperature ratio TT4BAR/TTOR.

3.5 BC88 Predictions of Leakage for Cases of Interest

Utilizing the results of Cases 1 and 3 above, and utilizing the average rotor passage pressures as boundary pressures for the 5 inlet and 7 exit segments within the gas path calculated by Q-1D, the detailed leakage prediction tool BC88 was applied. The cases considered are outlined below. For all

cases the rotor to stator gap was modeled as 0.0025 in. on the inlet end and 0.004 in. on the exit end, movable endplate to stationary end wall gap is modeled at 0.042 in. and 2 of 3 possible wiper seals (reflecting as tested configuration) are present with 0.001 contact gap. Presence of foil seals on high and low pressure ports are examined as described in section 3.7.

1. Run 3468 baseline
2. Run 3468 with high pressure port foil seal having 1 slot
3. Run 3468 with high pressure port foil seal having 2 slots
4. High pressure port foil seal with 2 slots and LP foil seal with 4 slots
5. Low pressure port foil seal with 4 slots
6. Minimum circumferential flow with gap in annulus outside rotor-to-stator interface: 0.0025 in. (inlet) and 0.004 in. (exit)
7. No circumferential flow by modeling perfect circumferential seals between segments
8. Perfect carbon seals present, carbon seals modeled as in perfect condition
9. Run 3677
10. Run 3685

For each geometry both case 1 (no shunt flow) and case 3 (with shunt flow) were predicted. Results are presented in Appendix B.

3.6 Simultaneous Solution of Wave Solution and Leakage Network

In developing the algorithms driving the solution process, two test cases were employed. The test cases were selected to examine extremes of the solution domain. In both cases the modeling of the resistance to flow between the rotor flowpath and the solution boundary chambers was maintained at the baseline values, reflecting a gap of 0.0025 inch and 0.0040 inch on the inlet end and outlet end respectively. Also the inclusion of shunt leakage was maintained, although it's interaction with the pressures on the rotor side of the movable endwall was precluded by setting the restriction to the leakage at an artificially high level. Convergence was judged to be achieved when the magnitude of Q1-D calculated leakage flows fell below 0.00005 #/s. The resulting flow solutions utilizing the simplified circuitry aided the identification of solution trends that were otherwise unexplained. These test cases proved valuable in debugging the methodology.

3.6.1 Case A

The case A examined the case of circumferential sectors of the solution boundary chambers isolated from the remainder of the leakage network. Communication between these boundary chambers and all chambers other than the rotor passage via the endwall gap were set to artificially highly restricted levels. This allowed the solution of boundary pressure levels for essentially zero net leakage flows except for that from the rotor passages to the boundary chambers within a segment.

As anticipated, the converged solution resulted in boundary chamber pressures closely matching average rotor passage side pressure levels for each of the respective segments. Figure 54 shows leakage rates for rotor inlet and exit. Note the BC88 solution predicted near zero flows due to the nature of the test case. A prediction calculation, based on previous iterations using the secant method, was manually interjected after iterations 7 and 11 to speed convergence. Traces of boundary chamber pressure for rotor inlet and exit are shown in Figure 55.

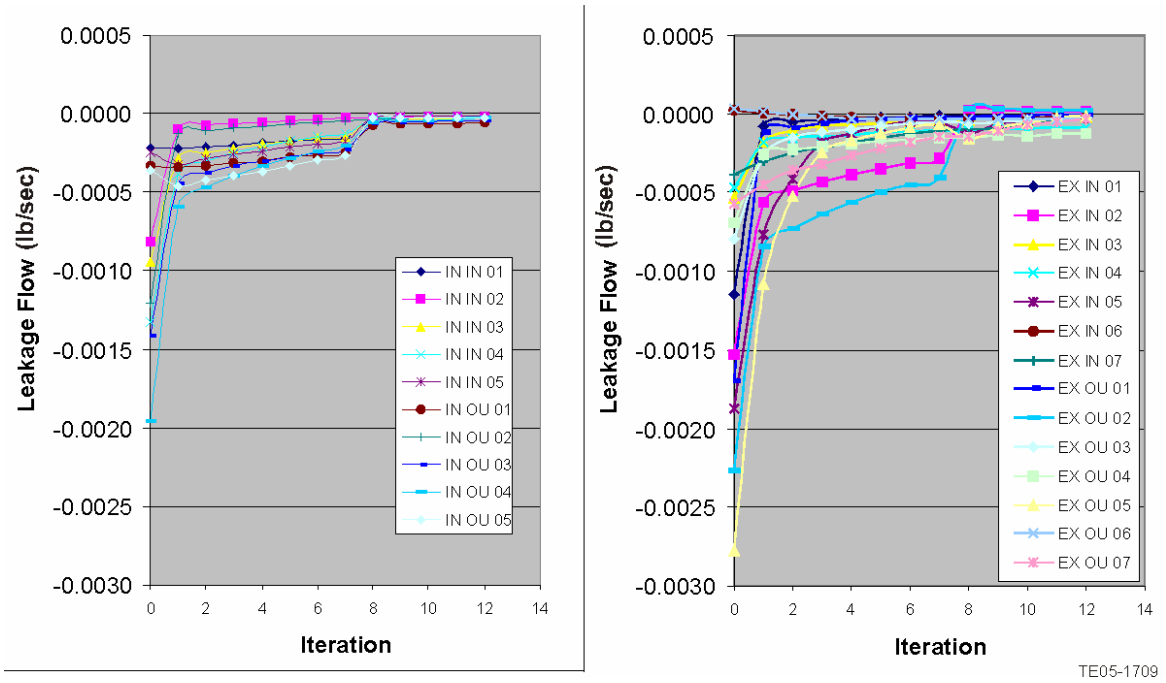

Figure 54. Solution History for the Inlet and Exit End Leakage Flows, Case A.

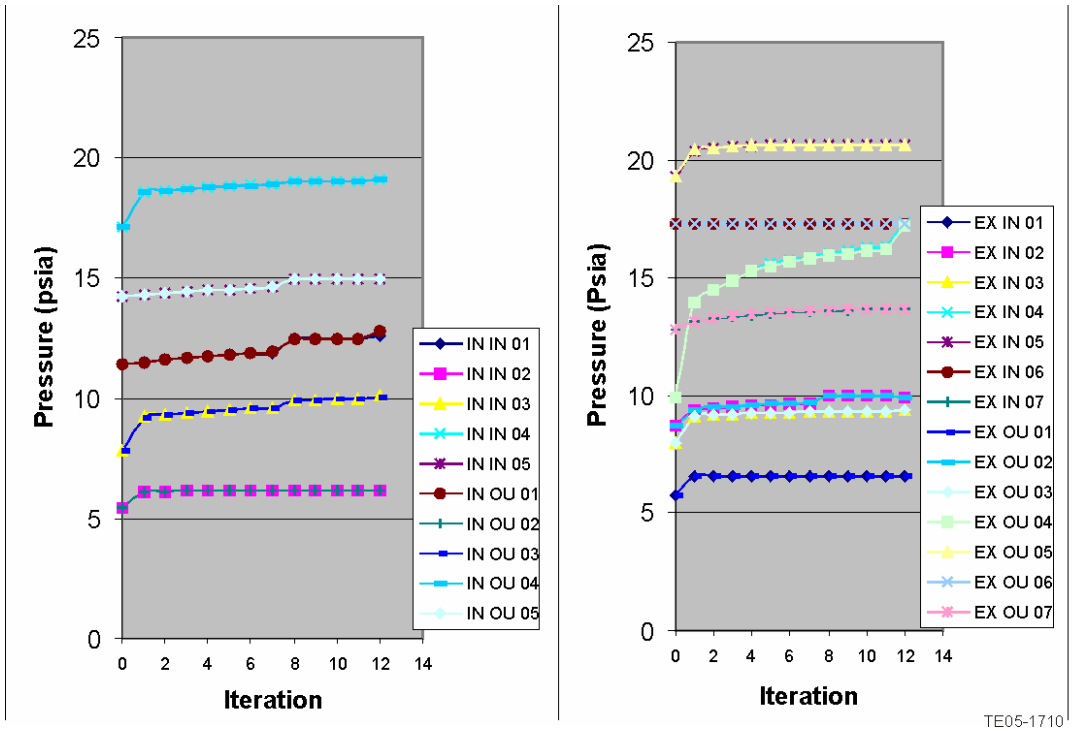

Figure 55. Solution History for the Inlet and Exit End Boundary Chamber Pressures, Case A.

3.6.1 Case B

The second case examined the situation where the restriction of flow within the network was set to an essentially zero level except that between the rotor passages and the boundary chambers, which remained at there anticipated levels. Note that only leakage paths identified in the examination of the rig are included in this relaxation of restriction of flow. Thus the result was not designed to simulate the one chamber model results of the basic Q1-D code in that all of the leakage flows are not mixed in a single chamber.

Case B resulted in boundary chamber pressures uniform both around the circumference and from rotor inlet to exit end. Traces of rotor inlet end leakage flows for Q1-D and BC88 are shown in Figure 56. Both Q1-D and BC88 predicted flow values are plotted. Traces of rotor exit end leakage flows for Q1-D and BC88 are shown in Figure 57. Note that the solution history shows an oscillating behavior prior to iteration 8. This reflects the fact that an error in automated communication of pressure information was discovered at iteration 7. This error was seriously disrupting the solution methodology for case B as can be seen from the plots of Figures 56 and 57. However, it should be noted that the error did not prevent a correct solution being reached for case A.

Following this correction to the methodology, all segments except inlet segment 1 converged to +/- 0.00005 #/s (the established convergence criteria) with in the next 2 iterations. However, the BC88 predicted direction of leakage flow for inlet segment 1 did not change to the correct direction until iteration 17 and did not converge to less than 0.00005 #/s until iteration 21.

It should be noted that, as shown in Figure 58, the results of this case predict that the boundary chamber pressure solutions at the inner and outer radial station, although not interconnected, arrived at the same uniform pressure level. This is not an immediately obvious conclusion, but one that confirms a reasoned consideration of the leakage solution.

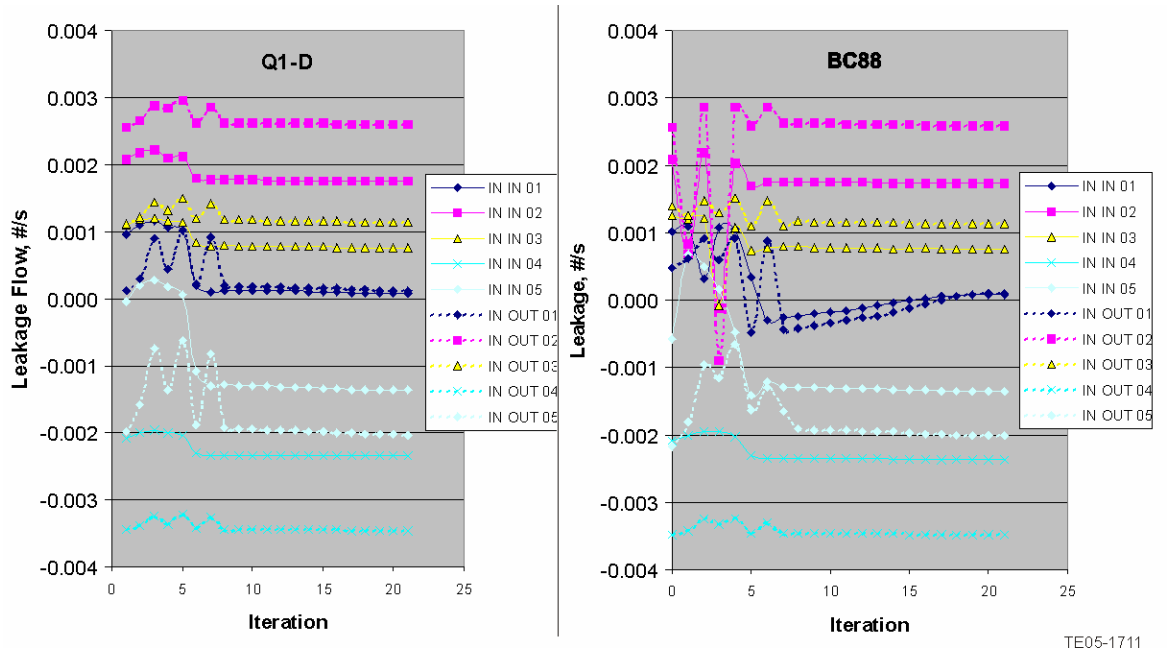

Figure 56. Solution History for the Inlet End Leakage Flows, Case B, BC88 vs. Q1-D.

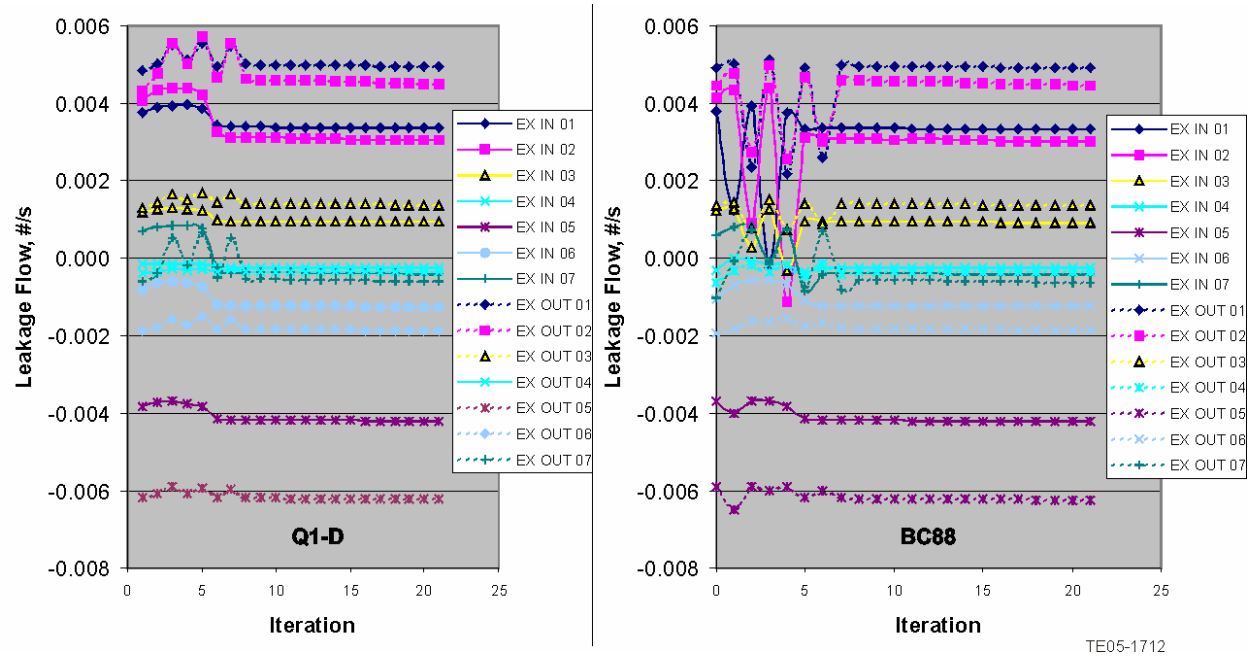

Figure 57. Solution History for the Exit End Leakage Flows, Case B, BC88 vs. Q1-D.

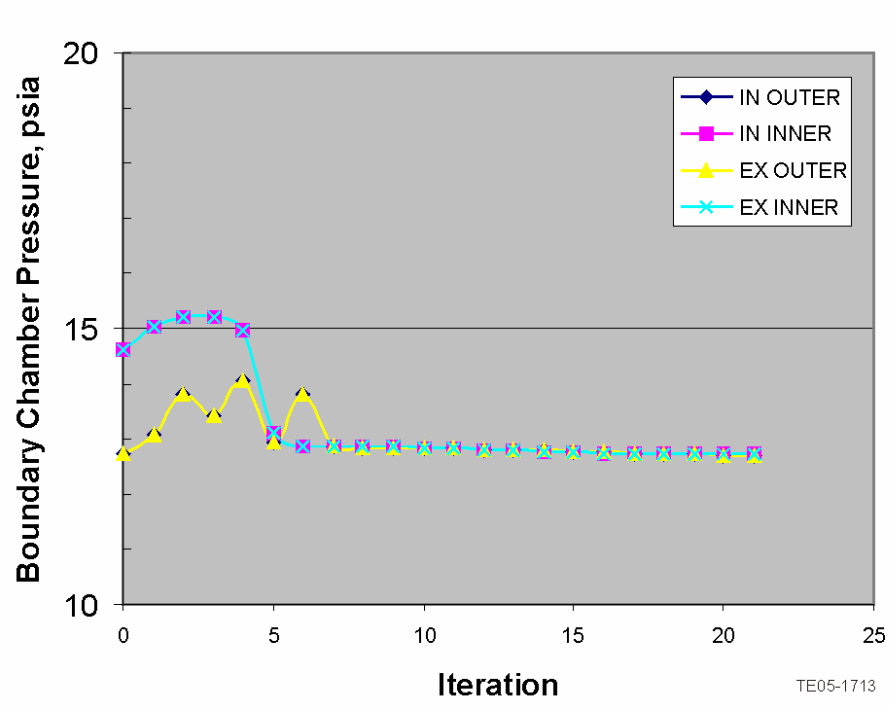

Figure 58. Solution History for the Boundary Chamber Pressures, Case B.

3.6.3 Analysis of SE-17 Test Number 3468

Using the methodology resulting from study of test cases A and B, an analysis of NASA run 3468 was performed. A Q1-D simulation of run 3468 using the standard version Q1-D single chamber leakage analysis results was performed. The value of the single chamber pressure was then used as the initial value for each boundary chamber pressure and temperature, 17.770 psia 816.7 °R, as shown in Figure 59. Based on the initial value for each of the boundary chamber pressures and temperatures and the leakage flows at the rotor to endwall gap, BC88 was used to predict a network solution (iteration zero). The BC88-predicted boundary chamber values were then used by the Q1-D program to solve for a new wave solution within the rotor and new leakage values (iteration 1). Convergence was achieved very rapidly. The solution history of Q1-D and BC88 inlet and exit leakage flows are shown in Figures 60 and 61. After the iteration zero, the leakage values change very little until convergence is achieved.

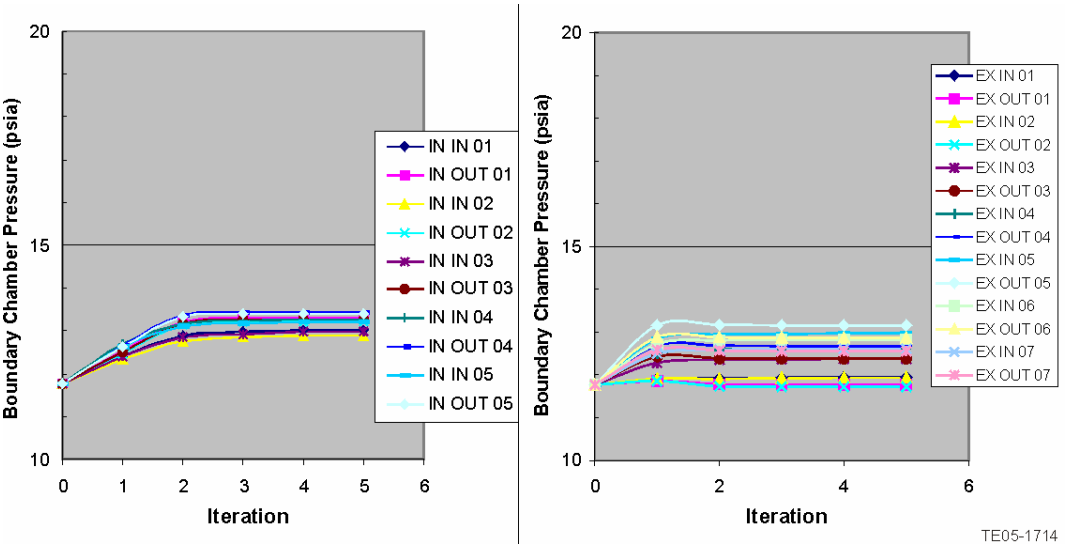

Figure 59. Solution History for the Inlet and Exit End Boundary Chamber Pressures, Run 3468.

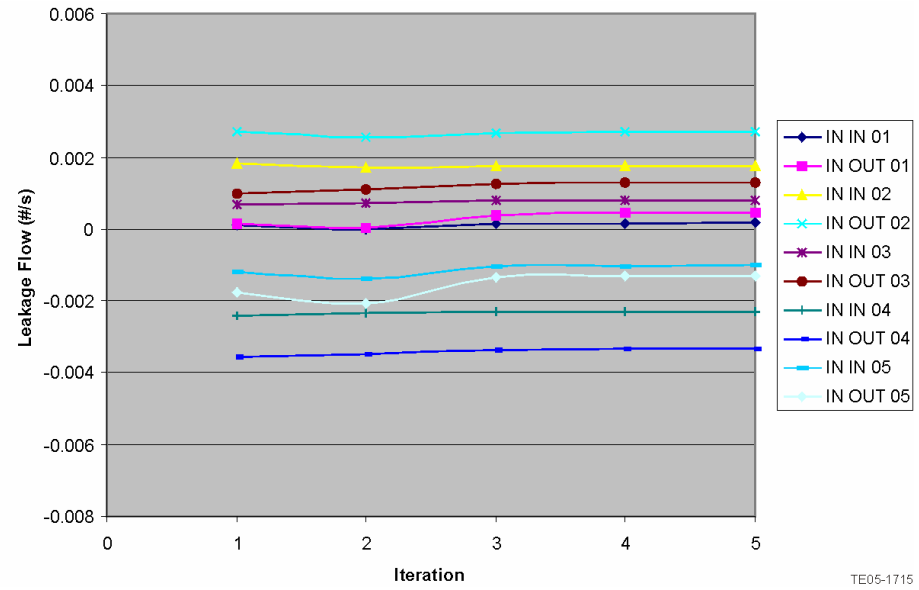

Figure 60. Solution History for the Inlet End Rotor passage Leakage Flow as Predicted by Q1-D, Run 3468.

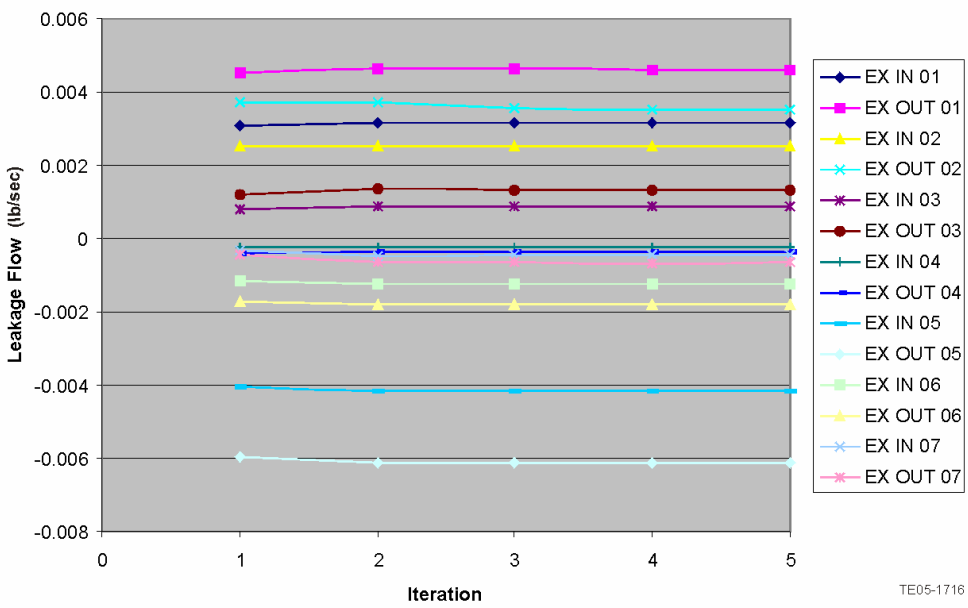

Figure 61. Solution History for the Exit End Rotor passage Leakage Flow as Predicted by Q1-D, Run 3468.

3.6.4 Comparison of Solution Cases

It is instructive to compare the resulting converged flow and pressure solutions for the three cases considered. Recall that Case A modeled rotor endplate leakage but allowed no communication between segments or any other part of the leakage circuit. Case B allowed perfect communication in each of the identified leakage paths external to the rotor endwall gap, but retained rotor endplate leakage characteristics. Run 3468 results reflected actual SE-17 conditions. Each of the cases considered identical rotor to endwall gap levels as deduced from cold build data adjusted for rotor thermal expansion.

Figures 62 and 63 present flow and boundary chamber pressure results respectively. It would be expected that the distribution of leakages and pressures for the Run 3468 case would be bracketed by the Case A and Case B results. This was indeed the trend in the modeling results. The leakage and boundary chamber pressure results for Run 3468 were very similar to those for the Case B, perfect communication case. This reflected that the leaked gas was not highly restricted in its flow either from one end of the rotor to the other, or in the circumferential direction. The distribution of the leakage around the rotor showed a significant degree transfer of gas flow from the rotor passages at the high pressure side (as indicated by a negative rotor passage flow) to the low pressure side (as indicated by a positive flow or flow into the rotor passages) at the rotor endplate interface at each end.

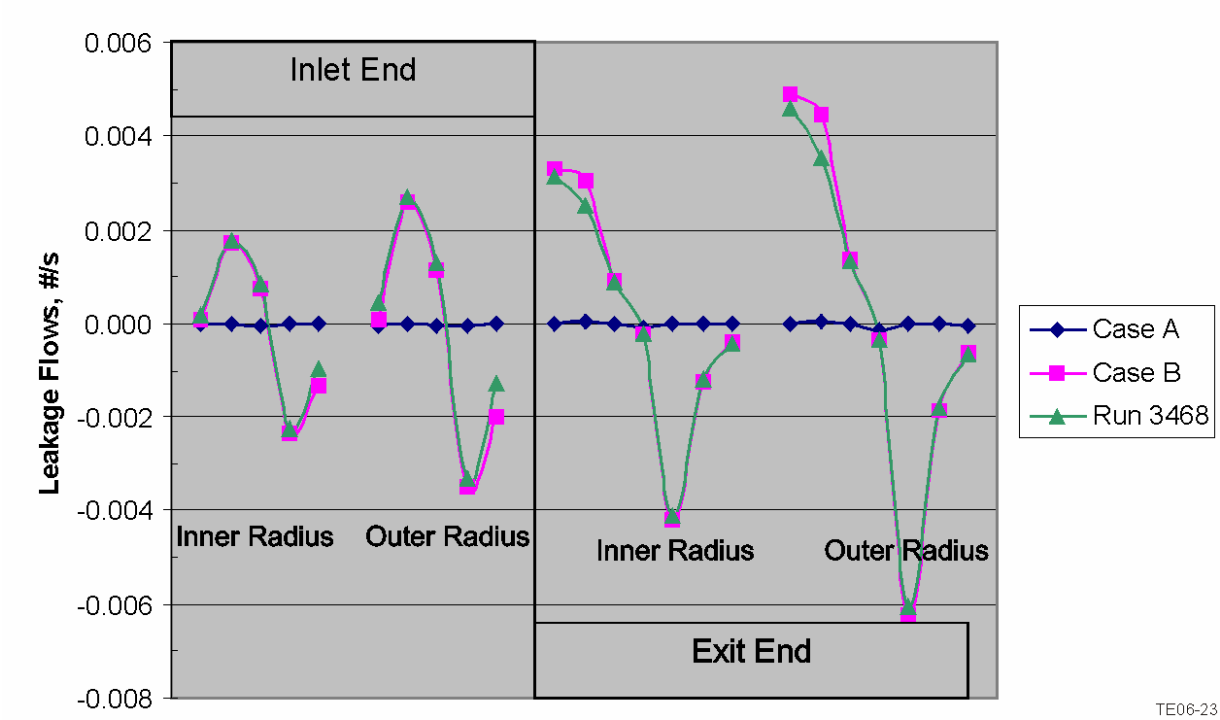

Figure 62. Comparison of Rotor Passage Leakage Flows.

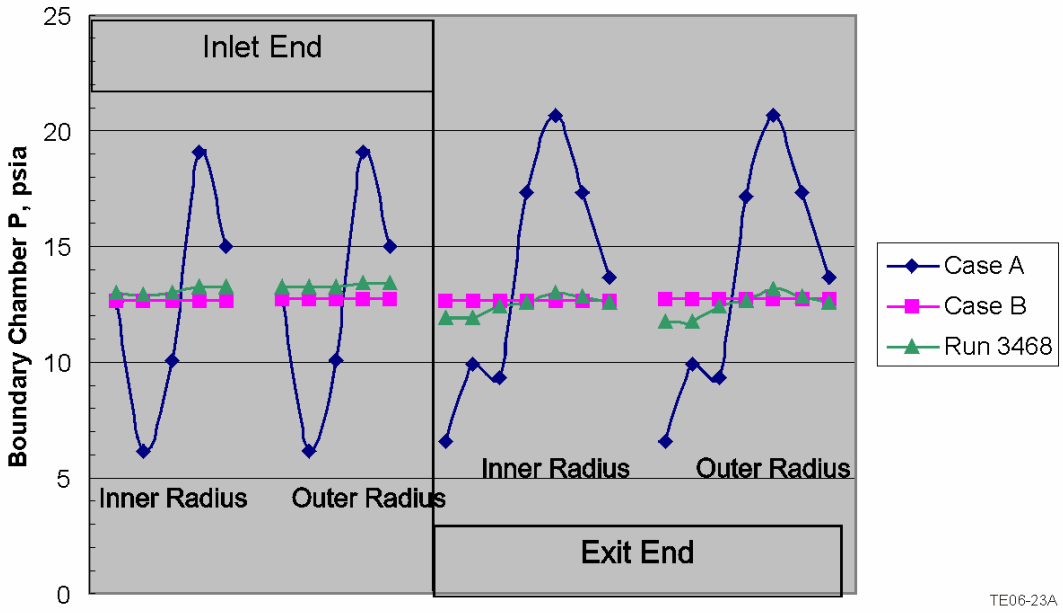

Figure 63. Comparison of Rotor Boundary Chamber Pressures.

In all cases, the net flow was from the high-pressure to the low-pressure regions within the cavities around the rotor. Table 8 tallies the net outflow and inflow components.

Table 8. Summary of Leakages and Endplate Gap, Run 3468.

	Inlet		Exit	
	Entering	Leaving	Entering	Leaving
Inner radius	0.00326	0.00276	0.00460	0.00442
Outer radius	0.00460	0.00442	0.00602	0.00654
Total	**0.00786**	**0.00718**	**0.01492**	**0.01596**
Entering minus leaving flow	**0.00068**		**-0.00104**	

Figures 64 and 65 present results for the network as a whole for the Run 3468 case. The results indicate that there is flow axially within the SE-17 rig present both within the space between the rotor and the outer case and within the rotor itself. In both cases, each component of the flow was predicted to be from the inlet end to the exit end and totals 0.00068 lb/sec. This agrees with the difference between the entering and leaving flows on the inlet end of the rotor. The unequal value of the difference between the entering and leaving flows on the inlet and exit ends of the rotor was due to the flow that crossed through the movable endplate seals into its backside region.

The effects of leakage changes on overall performance results of the wave rotor are listed in Table 9. It is significant to note that an additional pressure gain of 3% is predicted for case A, where the leakage flow is constrained within defined circumferential sections of similar rotor flow-path pressure.

Table 9. Pressure Gain Results of Three Cases.

	P4/P1	T4/T1
Case A	1.143	2.013
Case B	1.116	1.994
Run 3468	1.116	1.992

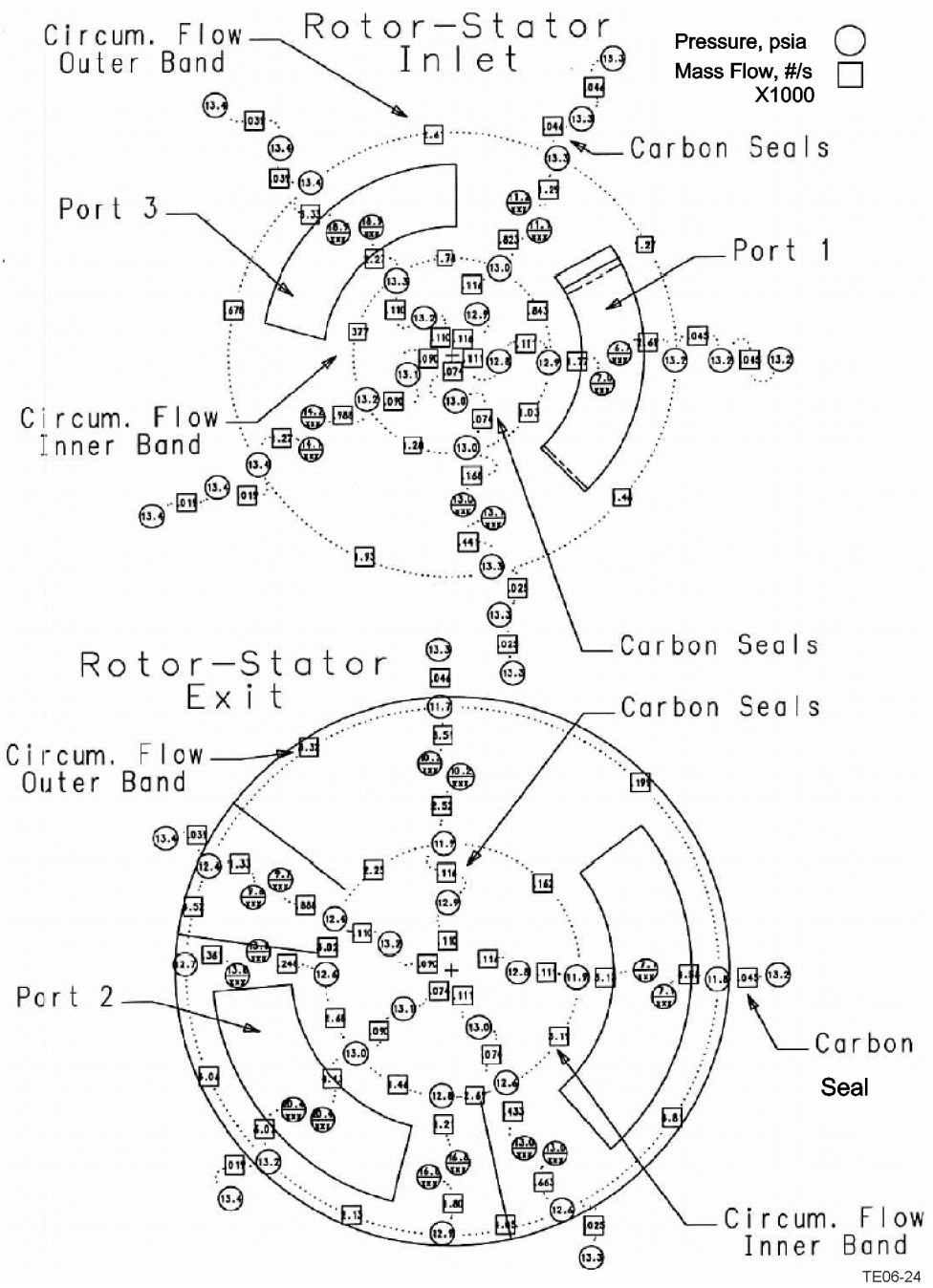

Figure 64. Network diagram SE-17 Run 3468 Modeling—Rotor Inlet and Exit Sections.

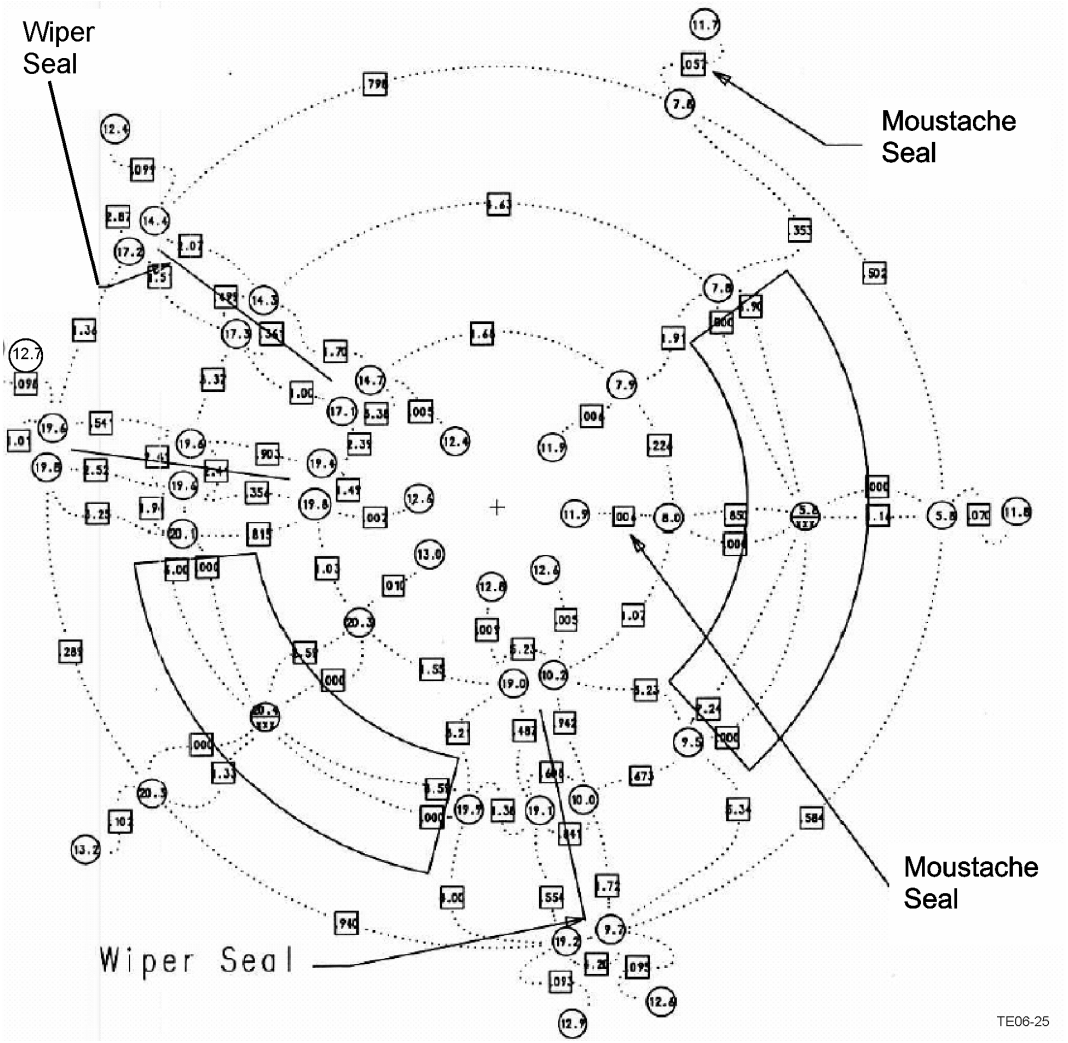

Figure 65. Network Diagram SE-17 Run 3468 Modeling—Movable Endwall, Stator Region.

3.7 Preliminary and Detail Design of Seals for NASA SE-17 Four-Port Wave Rotor Test Article

Goal: Apply developed seal strategies and technologies to the NASA SE-17 four-port wave rotor, which will represent an agreed upon concept development and demonstration vehicle unless another seals Proof of Concept (POC) experiment is identified.

In developing seal strategies, first for the demonstrator engine and then adapting these ideas to the SE-17 rig as a POC demonstration, the RRNAT team recognized basic similarities and specific differences. Evidence drawn from the examination of the SE-17 rig early in the program supported by detailed analysis by both RRNAT and NASA led to the conclusion that the primary sealing surface of the SE-17 rig (rotor to fixed endplate and rotor to movable wall) was satisfactory and not under serious question as a source of the internal loss of performance observed in the test data. The basic approach of a movable endwall has its heritage both in the SE-17and in the previous Rolls-Royce heritage work of the 1960s. The Rolls-Royce work, however, had not taken this approach to the rig demonstration stage. It is important to recognize that the NASA SE-17 rig has this critical technology needed to manage the rotor/endwall clearances embodied within it—i.e., the movable endwall approach. This approach was affirmed by the work here as viable for the demonstration and product engines.

Our attention turned to the backside (or shunt side) of the movable endplate, where "wiper" seals are employed to defeat flow from the high-pressure port directly to the low-pressure side of the circuit. From examination of the SE-17 rig hardware it is noted that both the high and low pressure port each penetrating the movable endwall. However, in the ORC/WR configuration selected for the demonstrator engine, the multiple ports that penetrate the movable endwall are all discharge ports that resided at the same pressure temperature conditions. Thus, the particular seal strategies that would be appropriate for the engine did not translate for direct adaptation into the rig. However, perfection and demonstration of the movable endwall approach will serve to validate the movable endwall approach for the demo engine. Table 10 provides a guide to our thinking on this matter.

Table 10. Comparison of SE-17 Rig with Demonstrator Engine.

Characteristic	SE-17 rig	Demonstrator Engine
Endplate gas temperature	Low: 800°F	High: 2100°F
Pressure at fwd face of rotor	Both low & high	Low
Pressure at aft face of rotor	Both low & high	High
Movable plate location	Exit end	Entrance end
Design flexibility	Limited mods	Blank sheet of paper

In the demonstrator engine, we were able to modify the geometry to eliminate the prime source of (identified) leakage in the SE-17 rig by design at the onset. We had a strong desire to minimize the amount of modification needed to solve the sealing problem in the SE-17 rig. This led to a seal design; though different in concept from the approach taken in the demonstrator engine, it served to fix a challenge unique to the SE-17 rig—one required to allow the movable endwall to function as intended.

Drawing ideas from the earlier literature reviews and brainstorming meetings, a number of seal concept studies were made to correct the seal leakage suspected to take place on the shunt side of the moveable endplate. Some of this work took place ahead of the development of the secondary flow model that later provided insight that modified the direction of the design effort. All ideas we seriously studied are included here for completeness of the record.

3.7.1 SE-17 Rig Movable Endplate Seals

The locations of the mating surfaces of the strip seals in question are illustrated in the Figure 66.

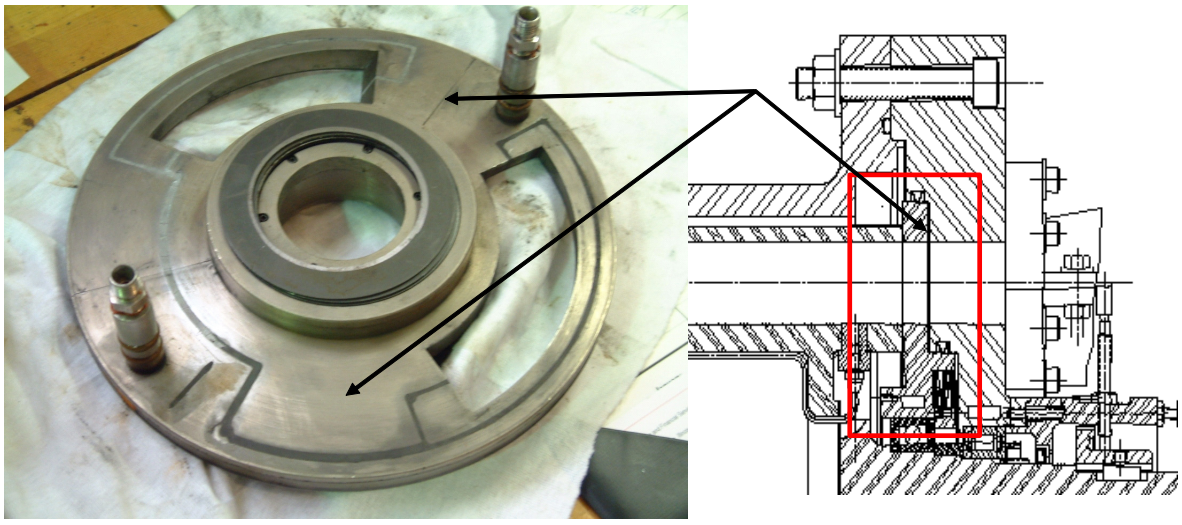

Figure 66. SE-17 Rig with Seal Locations on Shunt Side of the Movable Plate Identified.

Several issues were of concern in the shunt side leakage, as illustrated in Figure 67. The primary issue among these was the leakage around the wiper seals, shown here as flow through gap B and gap C. Gaps D and E presented no appreciable resistance to flow so that the leakage could transmit directly to the opposing port, causing a measurable loss in performance for the rig.

Concept #1: Port-Shaped Bellows Type Joint. Largely based on insights drawn from the internal Rolls-Royce Phase III Report, our initial approach to solving the suspected SE-17 rig shunt side leakage was to incorporate some form of bellows joint around each of the ports. This idea eliminated the leakage flow by providing a positive, leak-proof seal of the gas path, yet permitted free motion of the movable plate so that the primary sealing surface could continue to perform as desired.

Examination of the SE-17 rig parts showed that an application of the desired bellows joint would be difficult, at best. Unlike the Rolls-Royce rigs, where bellows joints are used extensively to control leakage, the joints could not be located in the ductwork leading to the ports permitting the bellows to be circular in form. Rather, for the SE-17 rig, the bellows would have to be the shape of the ports themselves. With some searching, we found that bellows can, in fact, be fabricated in this shape, although their "travel" is somewhat limited by the geometry in the "corners". The tighter the radius in the corners, the less motion can be achieved without buckling the bellows. More flexibility can be achieved, however, with more convolutions.

With the hope of bellows fabrication in hand, we attempted to fit the port-shaped bellows to the rig. The leading idea for the concept is illustrated in Figure 68.

As illustrated, the seal would first be attached to the movable endplate. During assembly, it would fit through an enlargement of the port and be fastened on the backside of the stationary structure. This is illustrated with the models in Figure 69.

Slot A = Wiper seal thru leakage

Slot B = Wiper outer end leak gap

Slot C = Wiper inner end leak gap

Slot D = Stator to stator gap inner (0.025 in.)

Slot E = Stator to stator gap outer (0.025 in.)

Slot F = Mustache clearance inner

Slot G = Mustache clearance outer

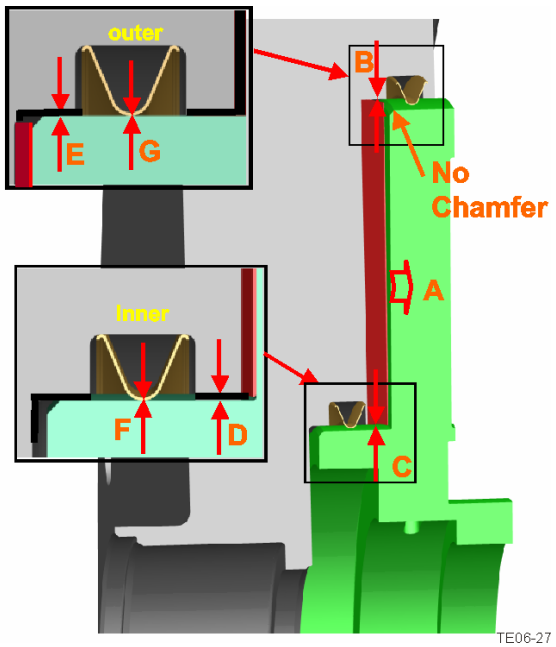

Figure 67. Movable Endplate Seal Issues.

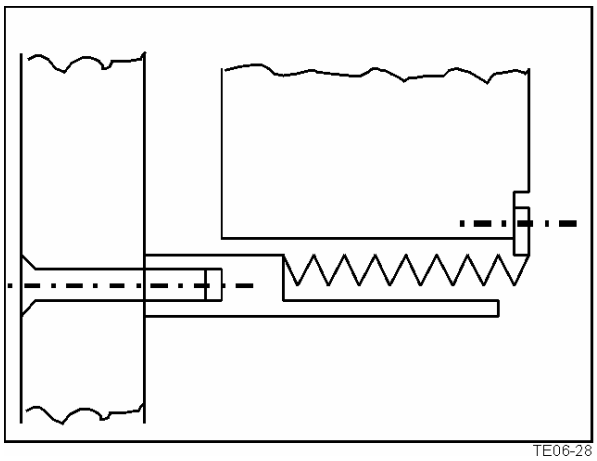

Figure 68. Schematic of Bellows Seal Installation in SE-17 Rig.

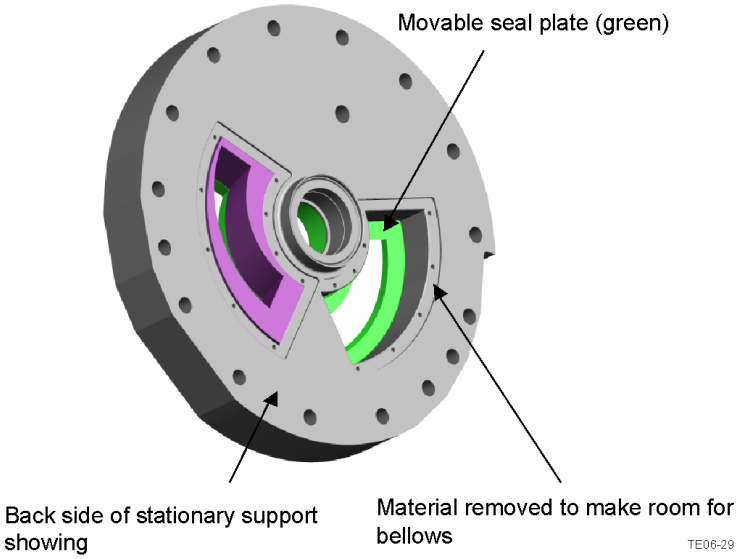

Figure 69. Concept Showing the Amount of Modification Needed to Install Port-Shaped Bellows to the SE-17 Parts.

In attempting to fit the bellows seal to the existing parts, we encountered a problem we were unable to resolve. As shown in Figure 70, this involved the space needed at one of the corners of each of the ports. The ports do not break through the aft side of the stationary structure in a manner that is concentric with the innermost projection at the bearing. This physical feature resulted in a small amount of real estate at this extreme corner that simply precluded the fitting of the port-shaped bellows assembly in the extreme corner location.

Further, the amount of material that had to be removed from the stationary structure interfered with access ports for gas-path instrumentation, making the insert even more complicated to fabricate. The bellows-type joint idea was subsequently abandoned as a strategy for the SE-17 rig.

Concept #2: Turbine Type Strip Seal. An alternate concept was based on gas turbine engine experience relating to the sealing of turbine vane gas path joints involving the capture of a sheet metal strip seal in a sealing groove, thus presenting a tortuous, low clearance path for leakage. This type seal, when applied to the SE-17 rig, is illustrated in Figure 71.

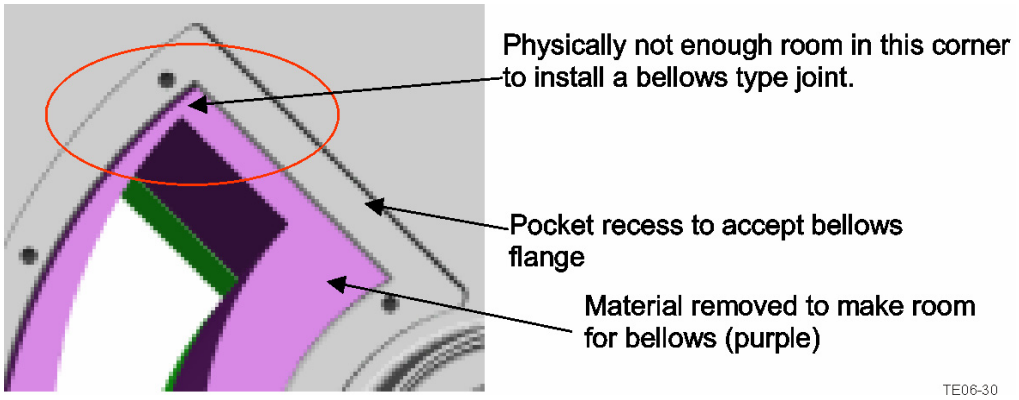

Figure 70. This Shows Insufficient Room to Install the Port-Shaped Bellows Joint.

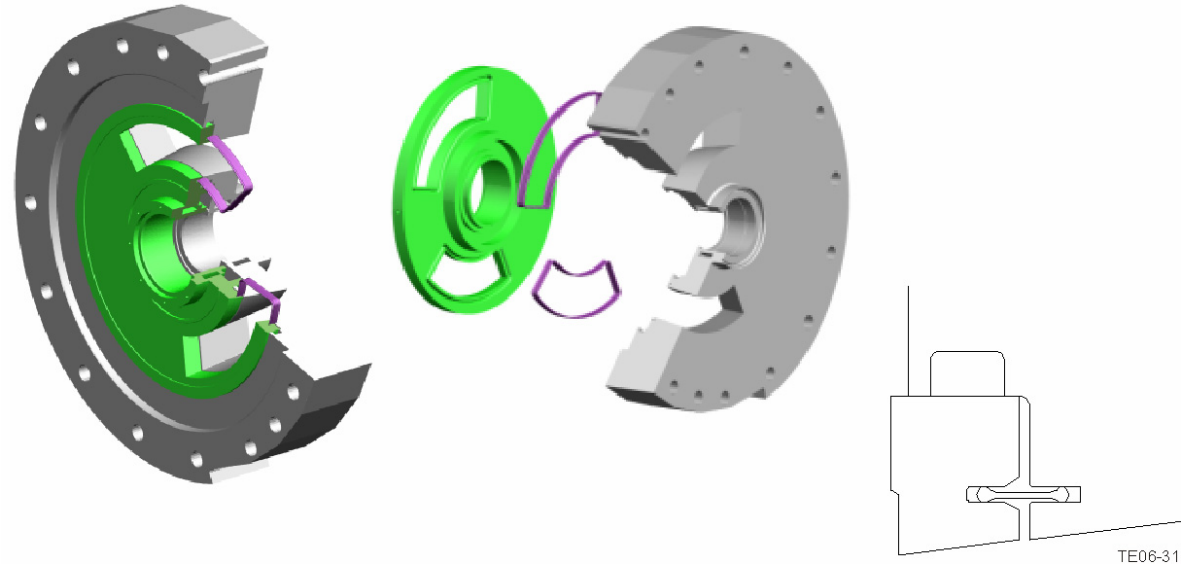

Figure 71. Strip Seal Concept Applied to the SE-17 Rig Parts.

The original assessment of this type seal showed that with the 0.0025-in. clearance being assumed we could expect a 58% reduction in shunt leakage flow compared to the current configuration of the SE-17 rig. Subsequent assessments of the probably fit-up of seal strip with groove indicated that the best fit would be more like 0.013 to 0.0025 in. for an average clearance of 0.008 in. This "finding" made the strip seal idea much less attractive.

Further, we could anticipate assembly issues with the heavy SE-17 parts (which are horizontally assembled) and the delicate nature of the strip seals. Work was done to define a system of guide pins and jacking screws that could potentially overcome this issue.

A further refinement to the strip seal idea was developed to produce the strip seal itself as a projection from an insert as illustrated in the model shown in Figure 72.

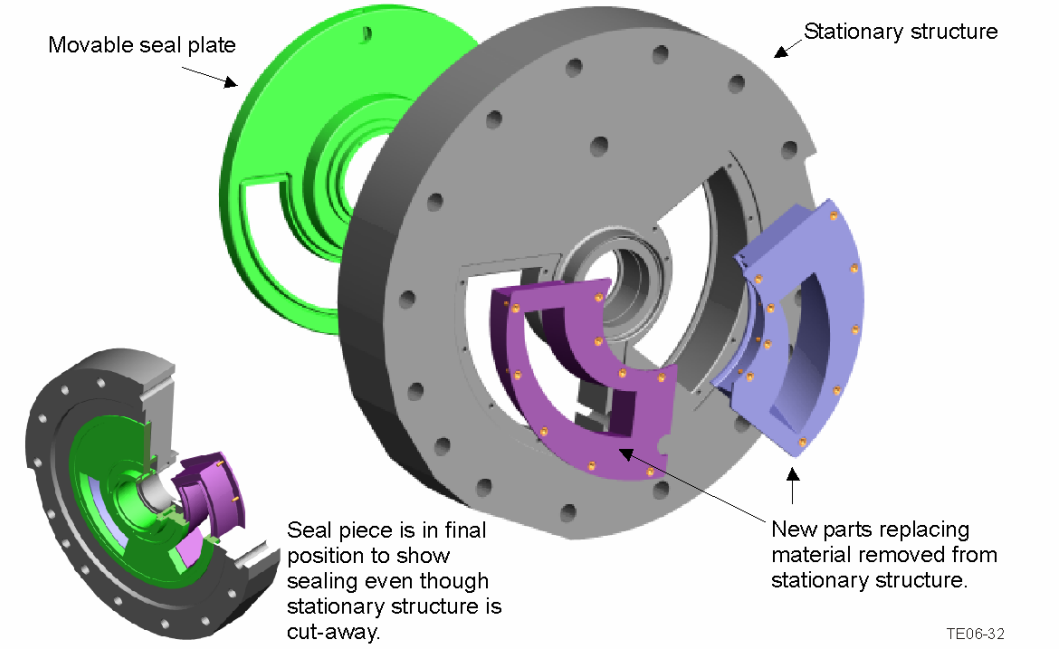

Figure 72. Sealing Concept in which the "Strip" Seal Is Produced as a Projection on an Insert to Eliminate Half the Leakage.

This scheme has the same inherent assembly difficulty as did the prior concept, and, while cutting the potential leak path in half, involved much more radical "surgery" in terms of the amount of machining of the existing parts. Thus this scheme could be reasonably expensive to implement.

The seal strip idea was shelved as we sought other, potentially more effective concepts that might be somewhat easier to implement.

Concept #3: Foil Seals. One of the ideas from our brainstorming sessions early in the program was to make use of the type seal used in gas turbine recuperators with which our company has considerable development experience. This seal type consists of a foil that depends on the seal pressure drop itself to maintain contact. Seals of this type are quite effective in high temperature, high-pressure drop environments of the type experienced in the wave rotor rig.

A number of ideas were brought forward in the development of the idea. We started with a port-shaped seal, as illustrated in Figure 73.

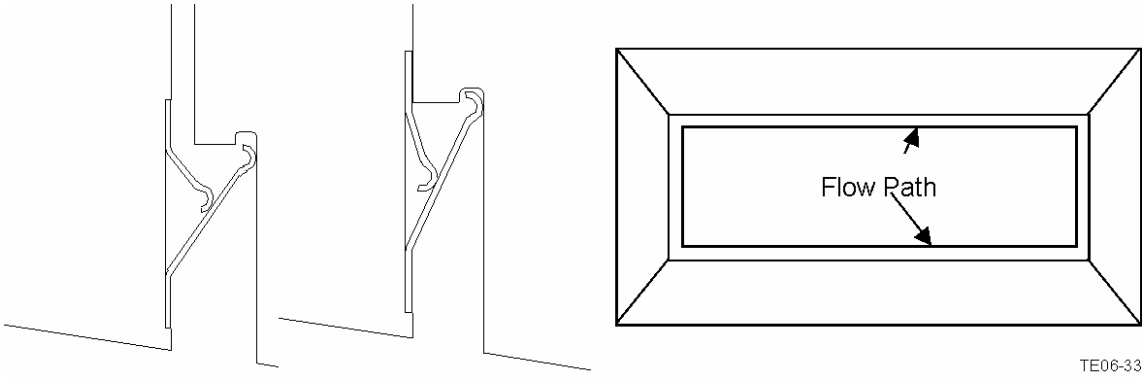

Figure 73. Initial-Recuperator-Type Seal as It Might Be Adapted to a More or Less Rectangular Opening.

The initial foil seal idea employed multiple parts and would have inherent leaks at all four corners.

We progressed from this type foil seal to the type illustrated in Figure 74, in which the seal was continuous and would accommodate the expected motion between the movable plate and the stationary plate by deflection. The seal would maintain contact through the mechanical spring rate of the seal that would be "helped' by the differential pressure across the seal. In this seal with essentially "square" corners, it was suggest that we would wire electrodischarge machine (EDM) cut 0.010-in. slots in the corners to both relieve stress and to permit the seal to function properly.

Secondary flow analysis of the foil-type seal indicated this type seal held more promise to reduce shunt side leakage than did the strip-type seal. Consequently, we proceeded to develop a workable seal design.

Of primary concern, beyond effectiveness in leak-flow reduction, was the stress level in the seal itself. Our desire was that the seal operate in the "Hooks-Law" range, that is, that in the range of the seal's expected deflection, that it would not experience permanent "set" or plastic deformation. To accomplish this, we established that the maximum stress in the sealing element should not exceed 50% of the yield stress at its most extreme deflection condition. We applied this condition at the maximum operating temperature point.

A careful analysis was made of the expected differential travel of the movable plate to the stationary plate. Incremental movement is caused by differential thermal growth between the rotor and stationary elements of the rig. The first number to be established was the cold build clearance. While this was not a truly well established number for the rig, it appears that after several builds, the value being used was 0.046 in. This value appeared in a number of the data sets supplied and was ultimately adopted as a reasonable value for cold-build clearance.

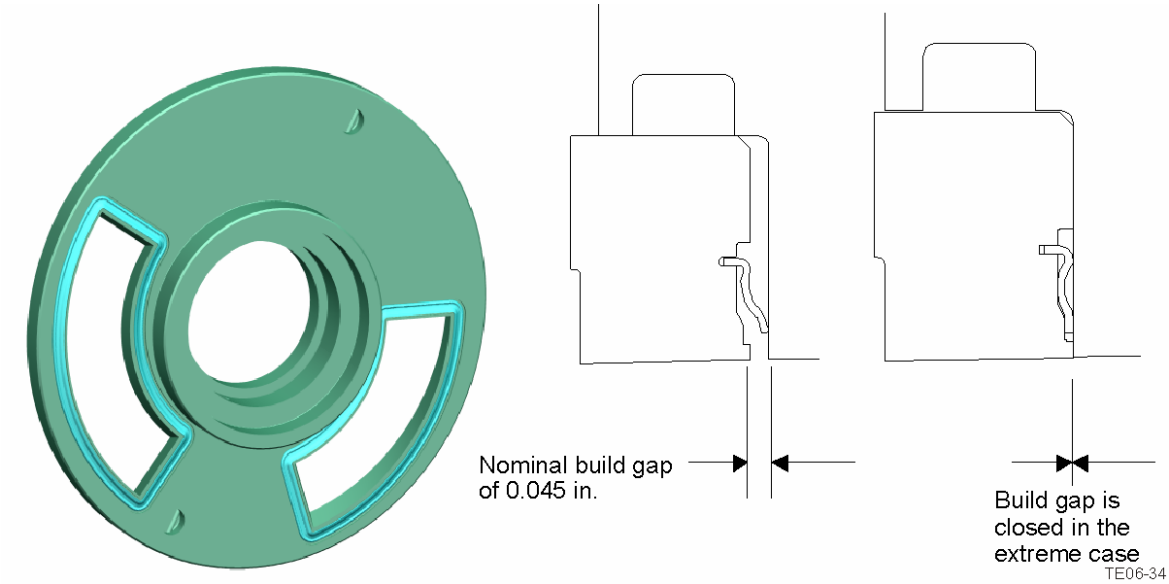

Figure 74. In the Next Generation of Foil Seal, the HP Port and LP Port Would Feature Different Seals Due to the Differential Pressure Direction.

Using the supplied data for maximum gas temperatures, we assumed hot rotor, cold case and hot case, cold rotor to find the extremes of the travel. This work showed that the movement of the plate relative to the stationary structure from cold build to hot running was expected to be of the order of only +0.004 in. However, prior to equilibrium being reached, the minimum clearance condition required a 0.020-in. movement of the foil seal. We established a "free state" of the foil seal to be 0.065 in. From discussions regarding rig cold build clearance experience, it was assumed that the cold build clearance was 0.046 in. This meant that at cold build the foil seal would be deflected 0.019 in. and thus would allow the seal to function properly in the cold state. At full hot and running conditions, the deflection of the seal would then grow to 0.023 in. Using material properties, we determined that at the most extreme condition of hot rotor, cold case (which we could never fully achieve in practice), the deflection of the seal would be 0.039 in.

Using this maximum deflection value, we performed a stress analysis using 0.010-in. thick INCO 718 heat-treated (for strength development) seal material. An initial trail is shown in Figure 75. The maximum stress level is too high to meet the established criteria, implying a different design was needed. The style of design is illustrated in Figure 76.

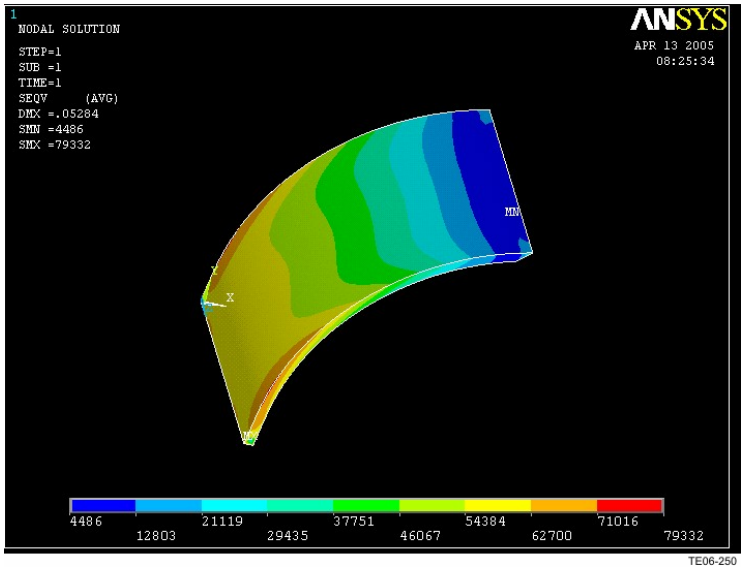

Figure 75. This Analysis Shows That the Seal Maximum Stress Is Too High.

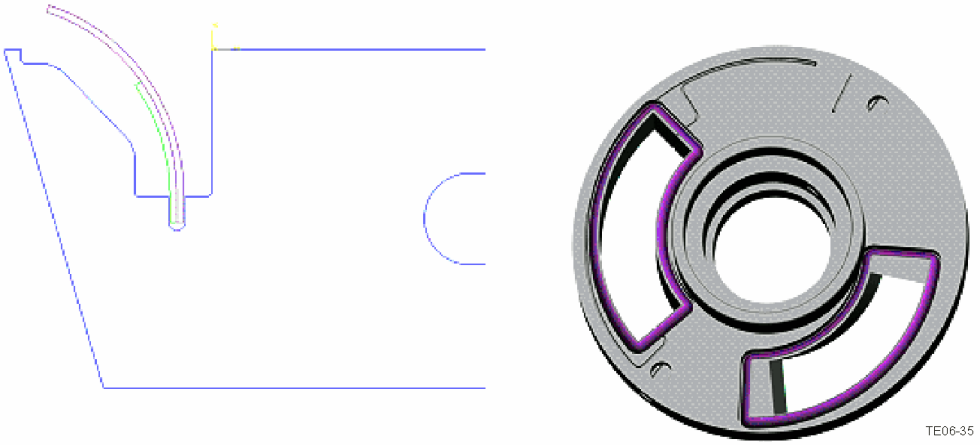

Figure 76. Foil Seal Design for Imbedded-Type Seal.

This implied a design change was required to satisfy the criteria. We tried a number of ideas to improve this stress picture. These ideas included a tapered sheet (expensive) as well as two sheets with the inner sheet being shorter than the prime seal surface to simulate the tapered sheet idea. None of these concepts fully met the criteria for the desired seal deflection. We finally determined that we would have to change the way the seal was restrained at the inner edge. This led to an "ogee" type seal that was fully free on both ends, as shown in Figure 77.

As is evident from this figure, our thinking was changing. We eliminated the "corners" going to a full radius. This changed the stress picture at the corners dramatically and allowed us to meet our stress criteria with a single sheet of foil material, as shown in Figure 78.

A short 0.010-in. wire-cut EDM slot was provided at the center of the corner radius to relieve the stresses in the corner. The maximum stress was at this stress concentration and would not affect seal performance overall. Further, in this refinement of the original ogee seal idea, we trapped one end of the seal in a groove in the movable plate so that the ogee seal just contacted the top of the groove at cold build. Further deflection made this joint and the contact with the movable plate surface more intimate, thus reducing any clearance at these points and reducing leakage.

This pair of foil seals and associated rework of existing parts is being offered by RRNAT as the most reasonable approach to sealing the shunt flow in the SE-17 rig.

3.7.2 Force and Moment Balance

Having satisfied ourselves that the foil seal design held promise, detailed analysis was done to finalize the secondary flow model. Data from this analysis made possible the computation of the moments and axial forces produced by the wave rotor gas path pressures on the movable plate. Of vital interest were the changes that might be introduced by changing the method of sealing of the shunt side of the movable plate. Further, the analysis might be expected to provide insight to NASA regarding rotor-to-stator contact experienced during the exercise of the test program that has been under way for several years.

The movable plate was divided into seven sectors to compute the pressures that result on both sides of the plate from gas path pressures generated by the operation of the wave rotor.

The seven sectors are shown in Figure 79, where many other features of importance to the moment and force balance calculation are depicted. Even though only two wiper seals were actually used in the current program involving the SE-17 rig, all three are shown here and sectors are defined as if they were all in place. Of course, when the wiper seal was removed, no restriction was included in the model and there was no pressure drop from that sector and the adjacent one.

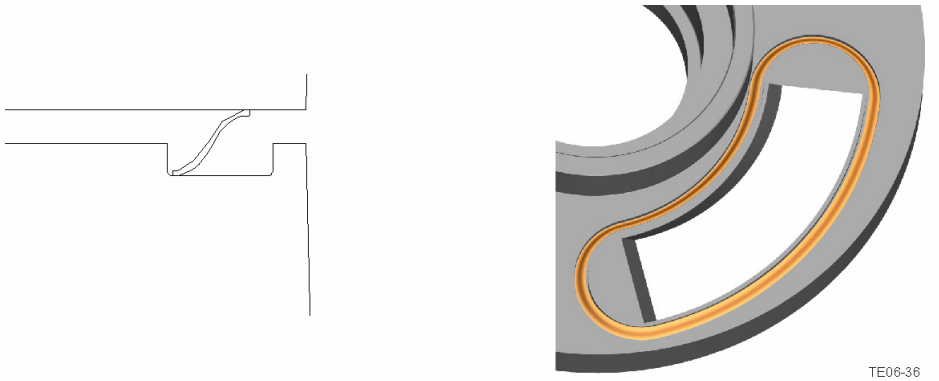

Figure 77. Ogee-Type Foil Seal Concept.

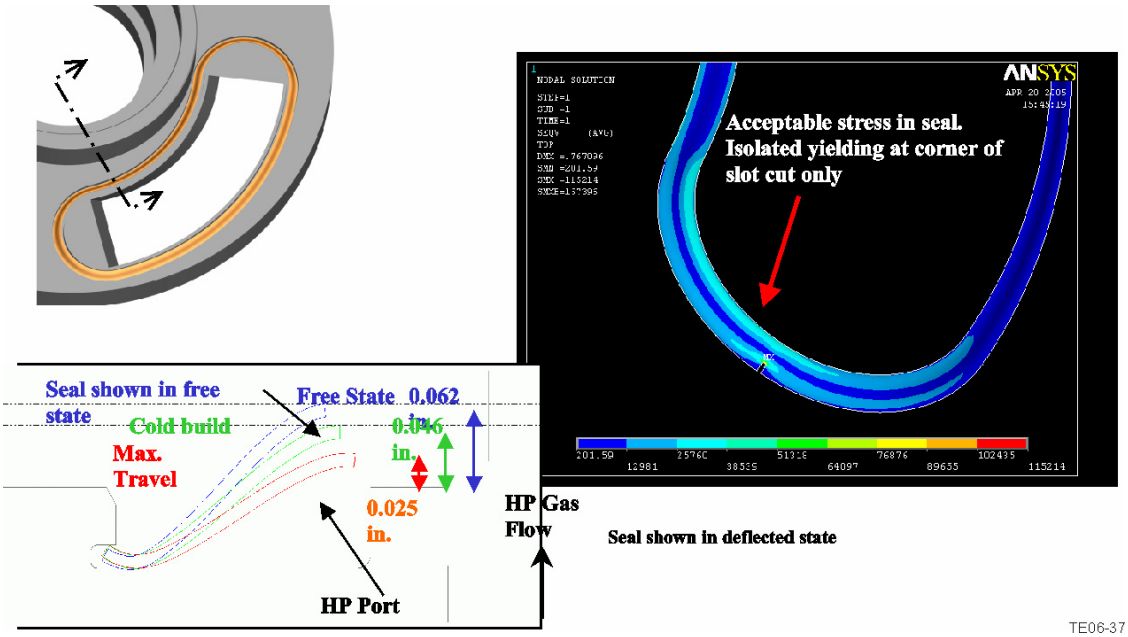

Figure 78. Stress Analysis of Full Ogee (Unconstrained) Foil Seal at Maximum Deflection.

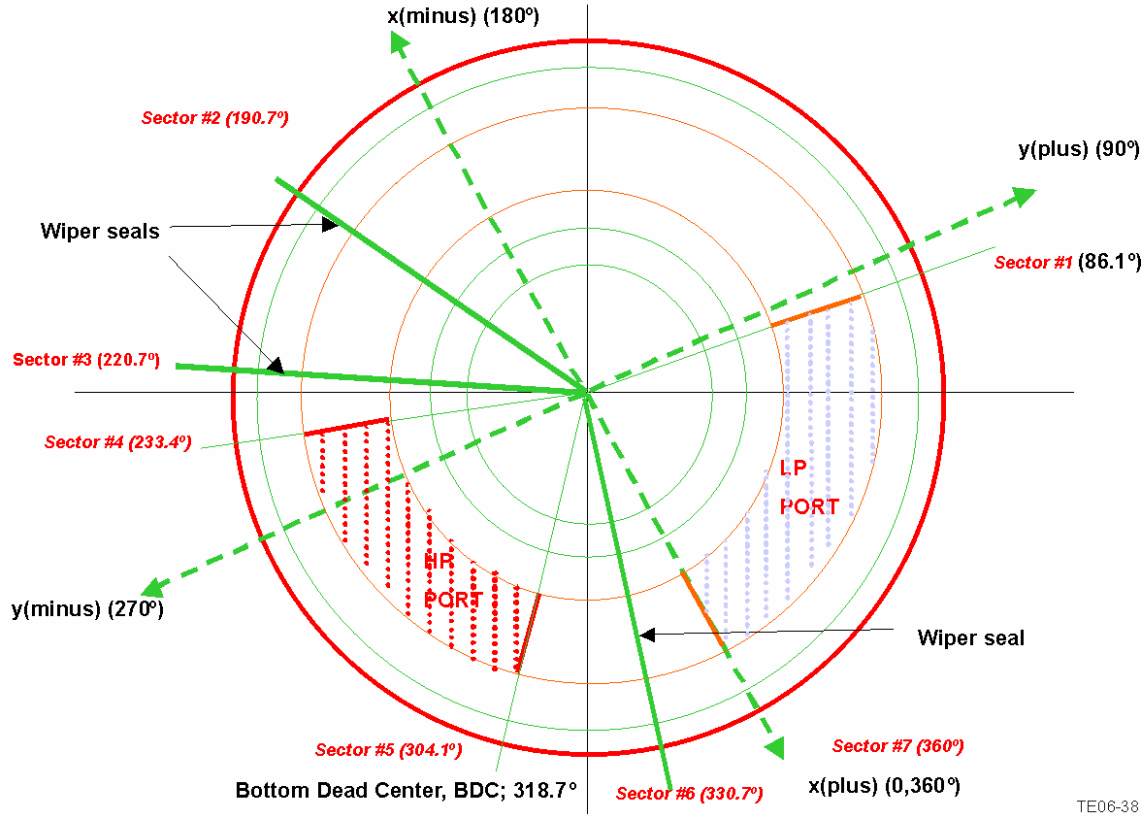

Figure 79. Movable Plate Viewed in Direction of Gas Flow (View of the Side of the Movable Plate That Interfaces the Rotor).

In calculating forces, each sector was further subdivided into six annular strips or rings arrayed radially from the plate centerline to the rim. On the side of the plate interfacing the rotor, the outermost annular ring represents that part of the plate that extended beyond the rotor. It was exposed to gas pressure found in that area—a pressure expected to communicate around the full periphery of the plate. Radially inward, the next ring represents that area that was in direct contact with the outer rim of the rotor. Traveling radially inward, the next ring represents the gas path proper. This annulus presents the driving conditions for the flow and pressure calculation. Next inward is the ring representing the inner rim of the rotor. The next ring is that area below the rotor inner rim but above the moustache seal. The final area, near the center of the plate, did not enter into our calculation since it was inboard of the lowest radius moustache seal. There are corresponding areas on the back or shunt side of the plate, but, of course, they are subdivided into fewer rings, as is appropriate. An Excel® spreadsheet was established to make the calculation straightforward for repetitive cases.

3.7.3 SE-17 Current Configuration Calculation

In developing the condition of the SE-17 as tested by NASA, RRNAT had at its disposal data from three runs. Run 3468 became known as the "Baseline" and formed the basis for much of the work subsequently done to improve the performance of the rig. Late in the program, we also looked at Runs 3677 and 3685. Results are shown for all models.

The "Baseline" case (Run 3468) was run with two sets of conditions we called Case 1 and Case 3, defined as follows:

- Case 1
  - Q1-D result with 0.0025 in. (inlet) and 0.004 in. (exit) gaps
  - Force the measured back pressure onto port 4 by specifying P4 in the input file using the average of the 10 port static taps on the rig
  - Adjust the burner pressure drop parameter BLOSS until achieving the measured loop flow ratio of 1.53
  - Adjust the heat addition parameter QCORR until matching the measured overall temperature ratio TT4BAR/TTOR
  - No shunt leakage (Note that inlet mass flow is not adjusted to test levels.)

- Case 3
  - Same as case 1 with shunt leakage model turned on
  - Adjusted P4/P1 value until the performance looked like the test results
  - Since the shunt leakage actually occurs upstream of where the static pressure measurement is made in the rig, adjust the imposed back pressure until the measured mass flow rate plus 10% for blockage is achieved
  - Adjust the burner pressure drop parameter BLOSS until achieving the measured loop flow ratio of 1.53
  - Adjust the heat addition parameter QCORR until matching the measured overall temperature ratio TT4BAR/TTOR

The computation results in a moment and a force. The moment tends to pitch the endplate about the centerline, while the axial force either pushes toward or away from the rotor, either helping or acting opposed to the Bellville springs. For the SE-17 in its current configuration and for the runs studied, the results are shown in Table 11:

Table 11. Results of Force and Moment Balance Calculation on SE-17 Rig.

Run	Case	Moment vector (ft-lb)	Quadrant from BDC	Location from BDC (deg)	Axial load (lb)
3468	1	27.88	2nd	168	-7.4
3468	3	23.09	2nd	172	6.0
3677	Wiper open	20.58	2nd	165	-40.2
3685	Wiper open	20.18	2nd	160	-42.8
3677	Wiper closed	25.55	2nd	171	-1.9
3685	Wiper closed	24.22	2nd	166	-10.7

For all cases, the moment was reasonably consistent and tended to pitch the movable plate about the rig centerline with the top of the plate moving away from the rotor, thus pushing the bottom of the plate into the rotor at a point about 10 degree past bottom dead center (see Figure 80). The axial load appeared well balanced considering the Bellville springs exerting some 75 lb toward the rotor. The gas loads did not, on the other hand, contribute enough force to cause concern about the loading of the thrust bearing.

For data points 3677 and 3685, we ran the model with the wiper seals left "open", i.e., not in contact. The effect on the axial load was to increase it dramatically in the same direction as the Bellville springs. The effect on pitching moment was, however, to reduce it about 25%.

3.7.4 SE-17 Modified with Foil Seals

Initially, we thought it might be possible to provide a foil seal for the HP port only or for the LP port only allowing the remainder of the backside of the movable plate to come to the gas path pressure of one or the other port. Our work showed this was not possible, largely due to the very high axial loads involved as shown in Table 12.

Table 12. Results of Force and Moment Balance Calculation on SE-17 Rig with Seals.

Run	Case	Moment Vector (ft-lb)	Quadrant from BDC	Location from BDC (deg)	Axial Load (lb)
HP	1	10.78	2nd	132.13	+196.09
HP	3	6.3	2nd	125.44	+170.76
LP	1	25.39	2nd	105.85	-217.22
LP	3	19.66	2nd	105.35	-175.91
HPLP	1	18.75	2nd	101.55	-44.38
HPLP	3	13.92	2nd	99.69	-24.40

Key findings of Tables 11 and 12 are presented graphically in Figures 80 and 81. Note that the arrows representing the moment vectors are to be interpreted as described above.

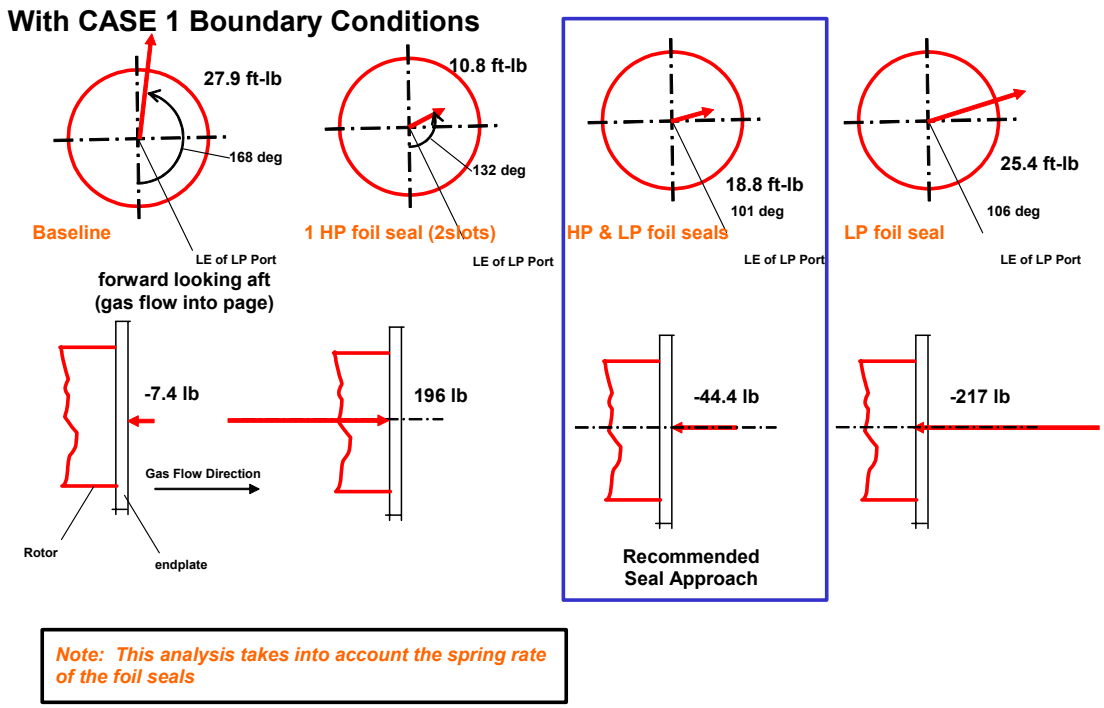

Figure 80. Movable Plate Force and Moment Summary, Case 1.

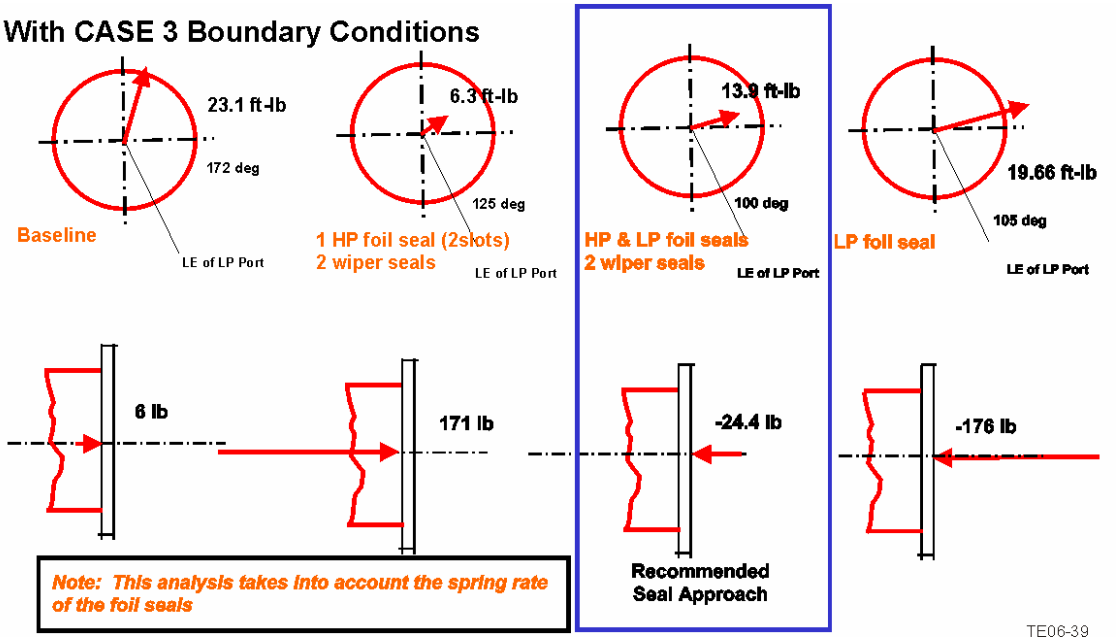

Figure 81. Movable Plate Force and Moment Summary, Case 1.

In the case of the LP-only solution, the axial load would add about 200 lb to the thrust-bearing load in the same direction as the Belleville spring load. This might be tolerated, but is quite a departure from the current setup for SE-17 and was considered an undesirable solution.

For the HP-only case, the situation was much worse. The axial load was just under 200 lb for the two cases and it was in the opposite direction from the Belleville spring load. This tended to open the gap between the rotor and stator and, during operation, would have reversed the thrust direction on the thrust bearing. In fact, one envisioned the thrust being toward the rotor at cold build and startup (due to the load from the Bellville spring) and then changing directions as the rig came up to full pressure, thus causing the rotor to stator gap to increase by the internal clearance of the thrust bearing. Clearly, this was not desirable as a solution.

After due consideration, RRNAT recommends that foil seals be placed around both the HP and LP ports. This should result in a reduced pitching moment on the plate (by 26 to 42%, depending on which case is chosen for comparison). The moment itself should be shifted to more in plane with the centerline (side to side rather than top to bottom). This may or may not be desirable. Certainly the reduced moment is desirable, however. In addition, the axial load will go up, but it is in the "correct" direction to keep the movable plate toward the rotor, in the same direction as the Belleville spring load, and not so high as to challenge the thrust bearing capacity.

Conclusion from Moment Work. This part of the program occurred late in the contract period and provided considerable insight into the operation of the rig. Our work showed that a significant overturning or pitching moment exists to make the movable endplate operate out of plane with the rotor. In the design of the rig, there is little in the way of mechanical features to react this moment. The presence of the moment should result in unequal rubbing of the endplate and rotor in one specific circumferential sector as indicated in the moment information provided. Had this outcome been available earlier in the program, perhaps some means to react the moment could have been devised. This finding, if confirmed by NASA, could form the basis for a further modification to the rig to improve its performance, this time having to do with the primary endwall to rotor sealing.

Detailed drawings of the preferred seals and movable endwall modifications as designed for the LP and HP ports were prepared and delivered to NASA GRC.

IV. References

1. Won, H. T., and Waters, M., "Constant Volume Combustor Implementation on a 50-Passenger Commercial Regional Transport Mission Simulation," AIAA Paper 2002-4413.

2. Paxson, D. E., "A General Numerical Model for Wave Rotor Analysis," NASA TM 105740, 1992.

3. Paxson, D. E., Wilson, J., "Recent Improvements to and Validation of the One Dimensional NASA Wave Rotor Model," NASA TM 106913, 1995.

4. Nalim, M. R., Paxson, D.E., "A Numerical Investigation of Premixed Combustion in Wave Rotors," NASA TM 107242, ASME-96-GT-116.

5. Paxson, D.E., "A Comparison Between Numerically Modeled and Experimentally Measured Loss Mechanisms In Wave Rotors," AIAA-93-2522.

6. Berrak Alparslan, "Performance Analysis of Novel Wave Rotor Pulsed Detonation Engine Cycles," MSME Thesis, Purdue University, IUPUI, Dec. 2002.

7. B. Alparslan, M. R. Nalim, and P. H. Snyder, "Wave Rotor Combustor Test Rig Preliminary Design," 2004 International Mechanical Engineering Congress, ASME Paper IMECE2004-61795, Nov 2004.

8. R. Nalim and K. Pekkan, "Internal Combustion Wave Rotors for Gas Turbine Engine Enhancement," International Gas Turbine Conference, IGTC2003-ABS-146, Tokyo, Japan, Nov 2003.

9. *Proceedings of the 1985 ONR/Navair, Wave Rotor Research and Technology Workshop,* Department of the Navy document NPS-67-85-008, Naval Postgraduate School, Monterey, California, May 1985

10. "Dynamic-Pressure Machine for Charging Internal Combustion Engines," Patent 4,487,552, December 11, 1984, BBC Brown, Boveri & Company, Ltd. Baden, Switzerland.

11. ABB Technical Paper, "Project No. 426; A Pressure-Wave Machine with Integrated Constant-Volume Combustion," undated paper from an European Technical Journal.

12. E. Zauner, and F. Spinnier, *Operational Behavior of a Pressure Wave Machine with Constant-Volume Combustion,* ABB Technical Report, October 1994.

APPENDIX A

Trip report: Visit to NASA GRC July 12, 2004

Eric Donovan, Cal Emmerson and Phil Snyder visited Jack Wilson and Jerry Welch (Dan Paxson was away at JPC) at NASA GRC from ~11:00 AM to 5:30 PM.

Examination of SE-17 rig

The rig was examined especially regarding seal and leakage issues. The rig was completely disassembled and provided an excellent opportunity to examine parts and discuss potential leak paths. Eric took several digital photos of the hardware, and leak-path dimensions were obtained at a number of sites. Particular attention was given to the space between the false endwall and the fixed structure, and to the carbon seals.

Specific rig observations:

1. The "witness marks" on the movable seal plate indicate there is relative motion between the seal plate and the "wiper"-type seals. This movement could be "flapping" of the wiper blades or possibly some complex response of the plate itself. This may require investigation to be understood. This would require modeling the elements and making analytical predictions of the expected response frequencies of the elements. Frequency response testing of the elements would confirm the analytical work and together with the analytical work could be used to estimate the response leading to a better understanding of what is going on. It is possible that the Bellville springs used to position the movable seal plate might be responding to the forcing function of the passage opening and closing. The Belleville spring is inherently damped, but could, nevertheless, be responding. This could lead to loading of the plate that is cyclic rather than steady as desired and might explain the wear we witnessed.

   The matter is less important if a design change eliminates the need for the "wiper" blades. If the plate is responding, a damping coating on the backside might provide enough damping to result in better operation. This would apply background Allison has gained with large gears, and the response of a large gear may in many respects be similar to the response of the seal plate to the passage frequency of the wave rotor.

2. Clearly, the seal of the airflow that must bridge the gap between the stationary and translating endplate is a problem. Consideration should be given to some positive flexible duct:

   a. Possibly a "regenerator-type" leaf seal
   b. Possibly a modified bellows type seal

3. It is believed that the carbon seals should be lubricated to function properly. The fact that they are "dry" may be the leading cause of the fracturing of the seals. It appears that the destruction of the sealing knife may most likely be handling damage.

4. One of the vanes on the rotor was bent. It was proposed that this was caused by the broken instrumentation getting caught in the clearance gap. Perhaps icing buildup on the instrumentation due to wet air had loaded the probe beyond its design capability and caused it to subsequently fail. Regarding the rotor damage, a suggestion would be that NASA Zyglo inspect the vanes to reveal any microcracking that might be associated with the damage to the rotor before proceeding with additional testing. If microcracking is discovered, the microcrack can be removed by scalloping a small thumbnail of material out of the vane. This is commonly done with damaged titanium fan blades in service with no ill effects and should work here just fine.

General Conclusions

Some aspects of sealing the CVC will be more difficult than sealing the four-port wave rotor rig due to higher-pressure level, higher temperature, and higher loads.

We will pursue the objective of designing a product-type solution to the sealing problem for the CVC and then apply that same concept to the NASA rig.

Our intent would be to definitively eliminate the NASA rig problem and allow NASA to obtain the data they desire and removing the objection that this problem is unsolvable.

We will work toward settling on our approach and then work to adapt the best approach to the existing NASA rig without a complete tear up.

Overview of the Allison Leakage Modeling Methodology

Discussions were held regarding the rig data best suited for study using the model. Of the test results available, it was determined that 5 data points were of greatest usefulness. Each point needs to have the qualification of a well defined geometry (seal and other configuration information, data regarding anticipated endwall clearance, ...), an adequate set of recorded P, T, N, flow data, relevance regarding operating point, and usefulness regarding either calibration or predictive use of model.

According to my understanding, the 5 points targeted are:

1. Point # 235 recorded 1999. This is a point Dan has taken greatest effort to analyze.
2. The peak pressure gain point of the 1999 data
3. An Aug 2003 (? Jerry, feedback confirmation on this please) point with carbon seals and with no rotation (a "cold flow" point in Allison terminology)
4. A June 2004 point with carbon seals, high mass flow and good performance but at a low temperature ratio
5. A low temp ratio point from previous testing corresponding to the June 2004 point above in map position.

These are points for which a leakage analysis will be performed. Q1-D modeling of the 4 test points should be undertaken. (no Q1-D analysis of the non-rotating point) The intent for Q1-D modeling is to arrive at modeling of performance accounting for all losses, particularly leakage from rotor passages to multiple chambers around the circumference to include the effects of communication with discreet circumferential chambers of differing pressure. The Q1-D modeling will also provide pressures at the endwalls that will be used in the leakage modeling analysis to fill in wall pressures in regions where no pressure data was measured. The overall goal of the Q1-D analysis is to establish sensitivities of 4PWR performance to leakage entities as identified by the leakage analysis.

A discussion was held with Leo Burkardt late in the afternoon regarding the accomplishments of the day, the overall Allison CVC development strategy, Allison participation in the IHPTET symposium in Sept, and the potential LEAP workshop in approximately the same time frame.

Phil Snyder
Monday, July 19, 2004

APPENDIX B

Utilizing the results of Cases 1 and 3 described in section 3.5, and utilizing the average rotor passage pressures for the 5 inlet and 7 exit segments calculated for these cases, the detailed leakage prediction tool BC88 was applied. The cases considered are outlined below. For all cases the rotor-to-stator gap was modeled as 0.0025 in. on the inlet end and 0.004 in. on the exit end; movable endplate to stationary end wall gap was modeled at 0.042 in. and two wiper seals were present with 0.001-in. contact gap.

1. Run 3468 baseline
2. Run 3468 with hp foil seal having 1 slot
3. Run 3468 with hp foil seal having 2 slots
4. HP foil seal with 2 slots and LP foil seal with 4 slots
5. LP foil seal with 4 slots
6. Minimum circumferential flow with gap in annulus outside rotor-to-stator interface: 0.0025 in. (inlet) and 0.004 in. (exit)
7. No circumferential flow by modeling perfect circumferential seals between segments
8. Perfect carbon seals present, carbon seals modeled as in perfect condition
9. Run 3677
10. Run 3685

For each geometry, both case 1 (no shunt flow) and case 3 (with shunt flow) were predicted. Within the pair of cases, the results are presented in 2 sheets, with the first presenting the plane of elements between the movable endplate and the stationary endplate, and the second showing the flow solutions at each end of the rotor, inlet and exit.

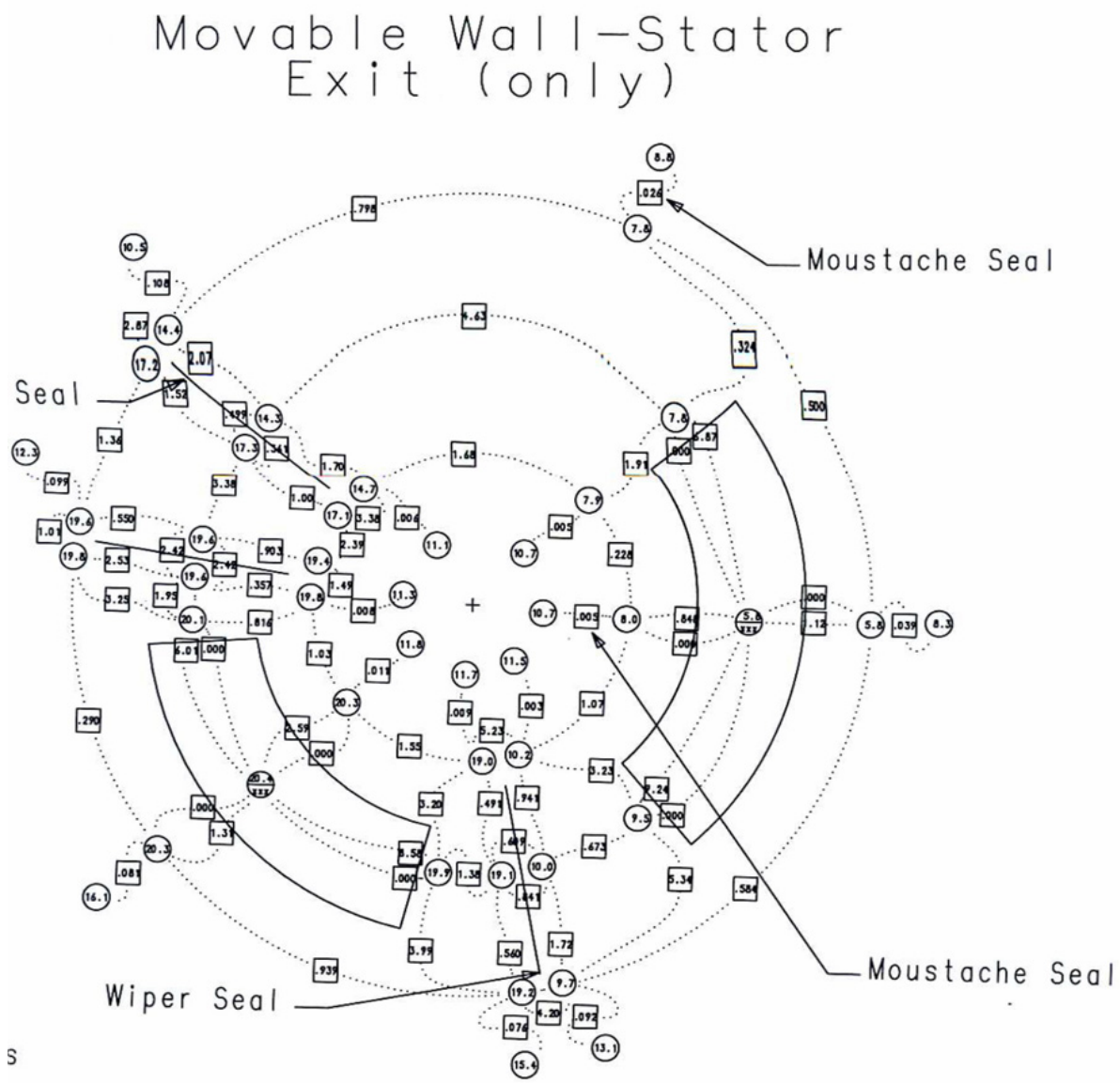
Movable Wall—Stator
Exit (only)
Moustache Seal
Seal
Moustache Seal
Wiper Seal
S
Run 3468
Baseline Case 1
Inlet Gap = 0.0025"
Exit Gap = 0.004"
MEW-Stator Gap = 0.042"
2 Wiper Seals
Seal Contact Gap = 0.001"

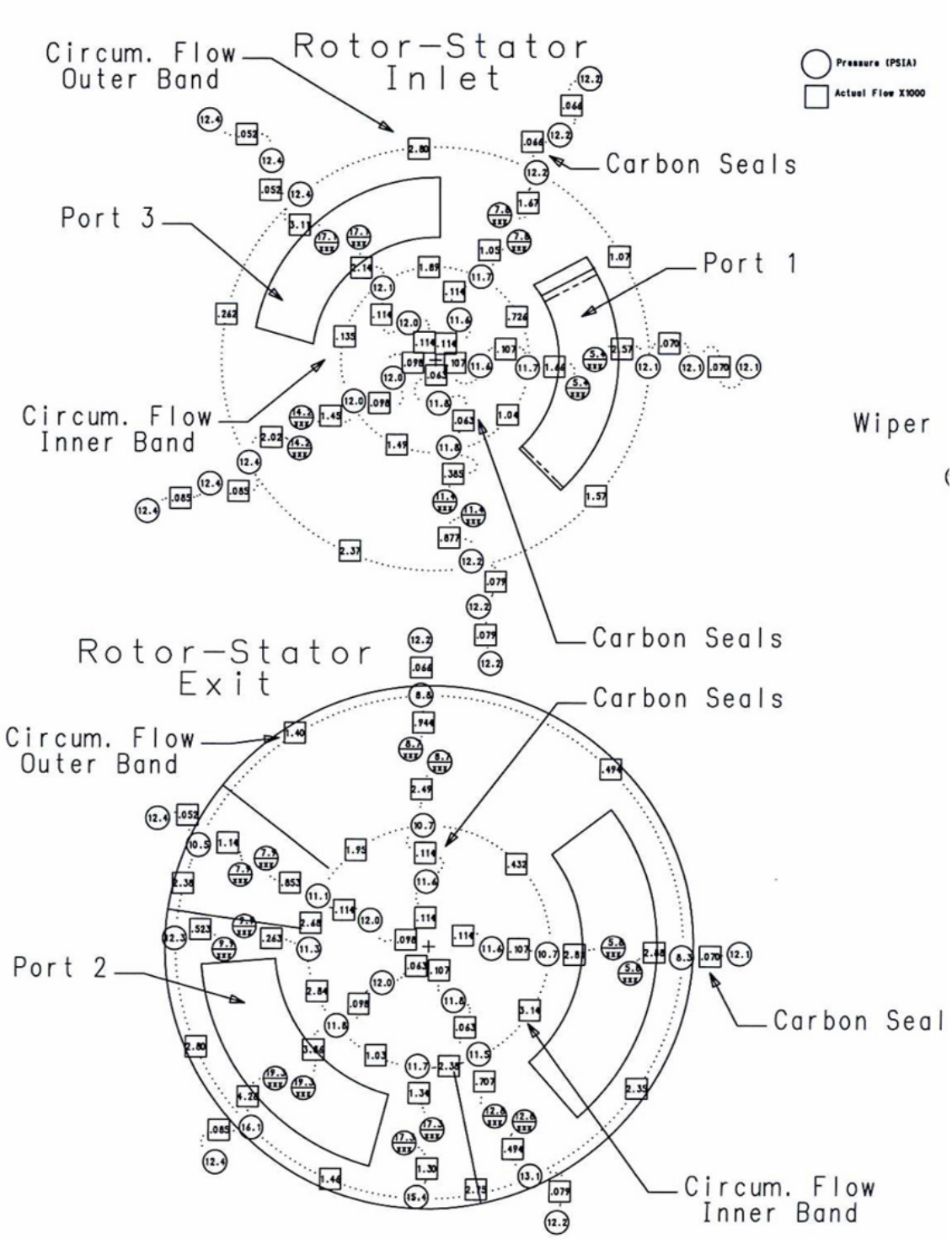
Rotor–Stator
Inlet
Circum. Flow
Outer Band
Carbon Seals
Port 3
Port 1
Circum. Flow
Inner Band
Carbon Seals
Rotor–Stator
Exit
Carbon Seals
Circum. Flow
Outer Band
Port 2
Carbon Seal
Circum. Flow
Inner Band
Pressure (PSIA)
Actual Flow X1000
Wiper

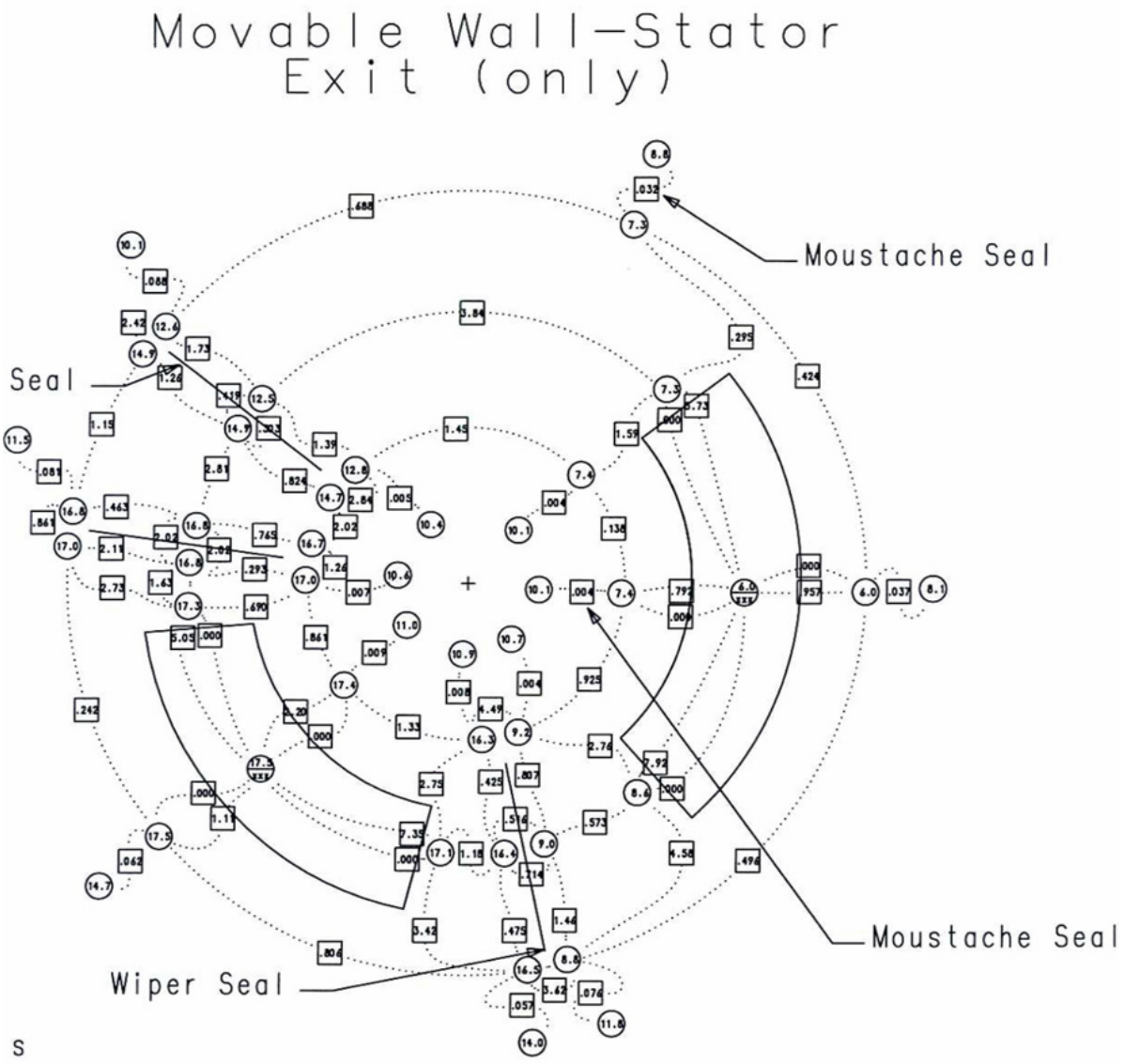

Run 3468
Baseline Case 3
Inlet Gap = 0.0025"
Exit Gap = 0.004"
MEW-Stator Gap = 0.042"
2 Wiper Seals
Seal Contact Gap = 0.001"

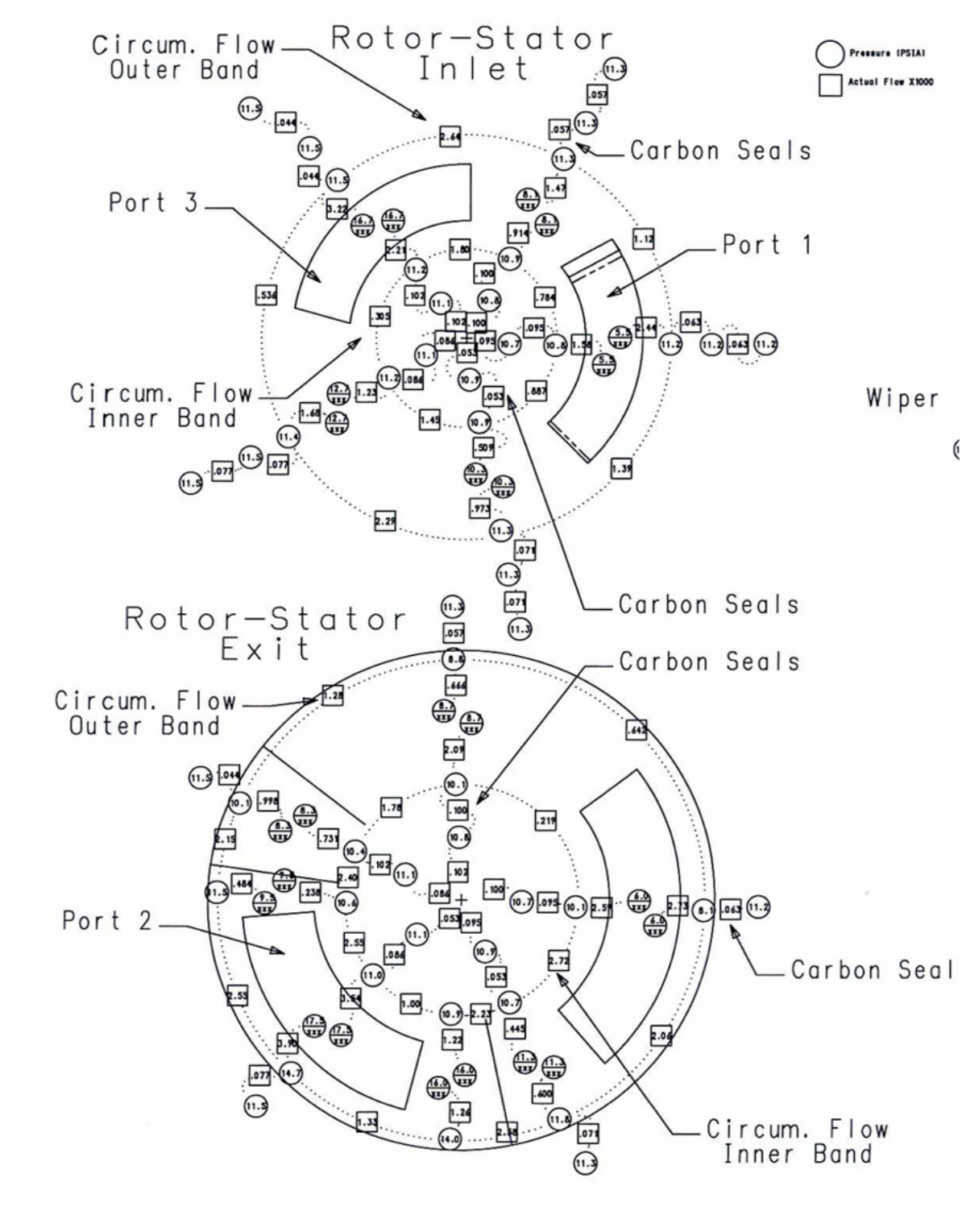
Rotor–Stator
Inlet
Circum. Flow
Outer Band
Carbon Seals
Port 3
Port 1
Circum. Flow
Inner Band
Wiper
Carbon Seals
Rotor–Stator
Exit
Carbon Seals
Circum. Flow
Outer Band
Port 2
Carbon Seal
Circum. Flow
Inner Band

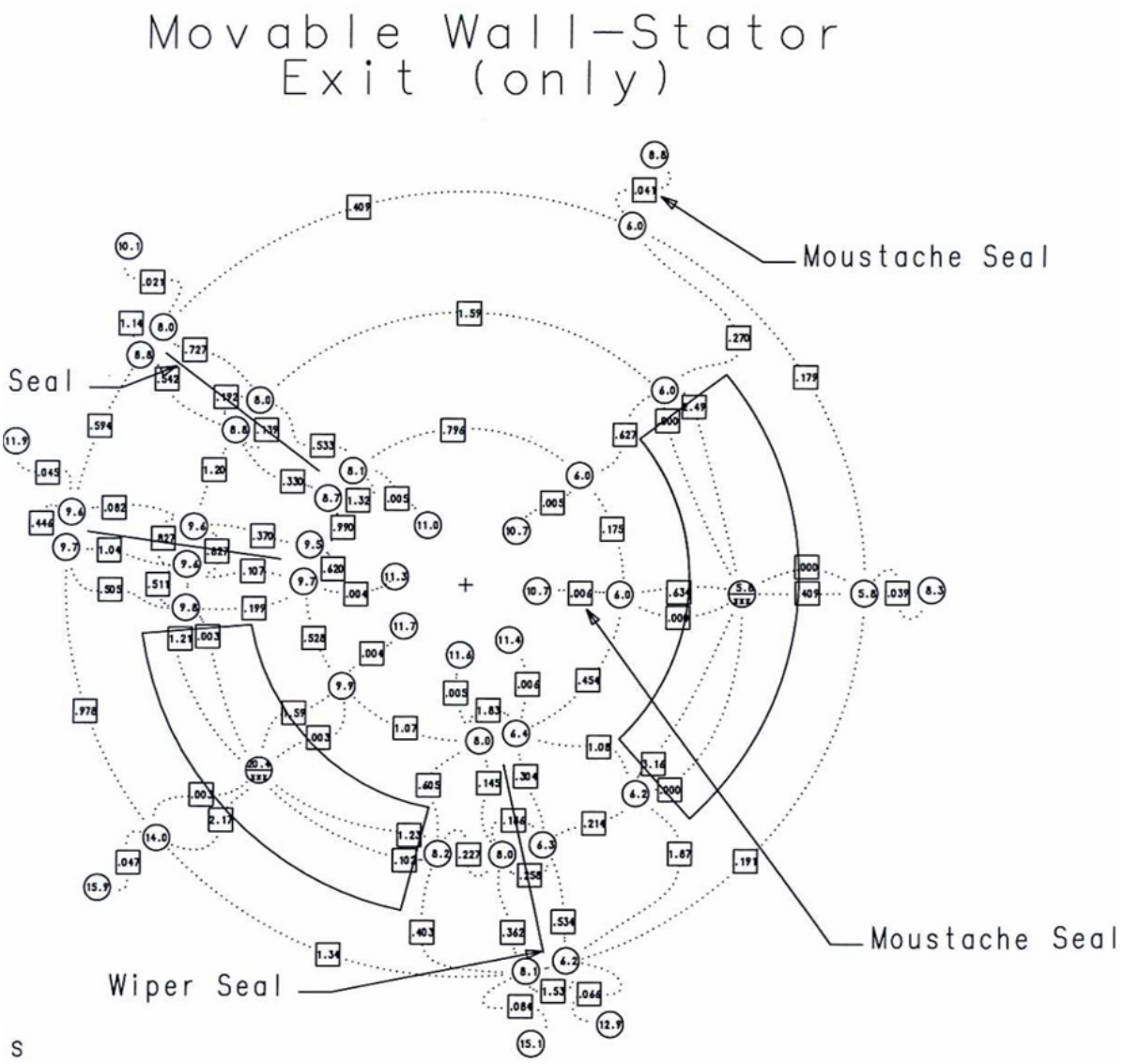

Run 3468 Case 1
HP Foil Seal 1 Slot
Inlet Gap = 0.0025"
Exit Gap = 0.004"
MEW-Stator Gap = 0.042"
2 Wiper Seals
Seal Contact Gap = 0.001"

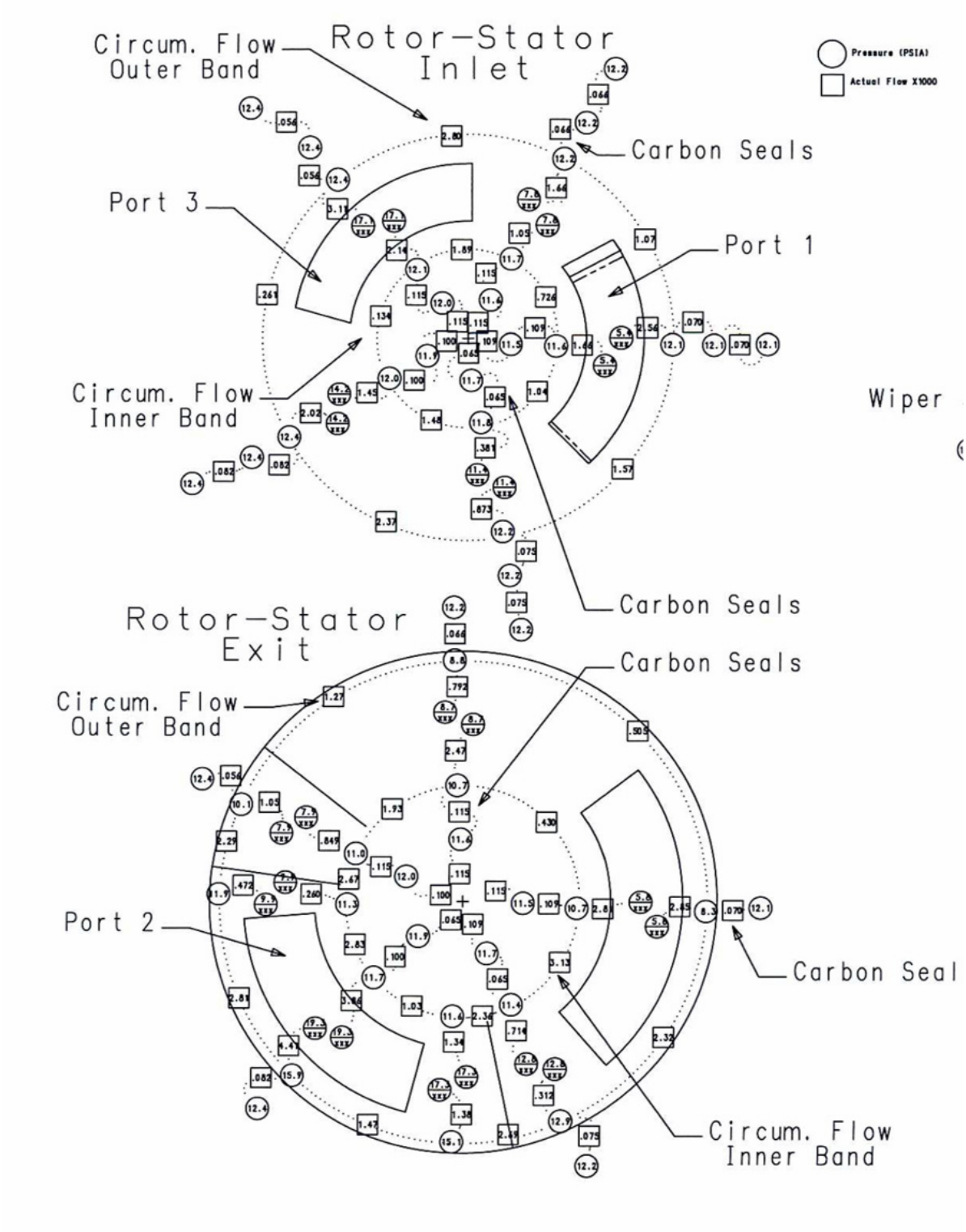
Rotor–Stator
Inlet
Circum. Flow
Outer Band
Carbon Seals
Port 3
Port 1
Circum. Flow
Inner Band
Carbon Seals
Rotor–Stator
Exit
Carbon Seals
Circum. Flow
Outer Band
Port 2
Carbon Seal
Circum. Flow
Inner Band

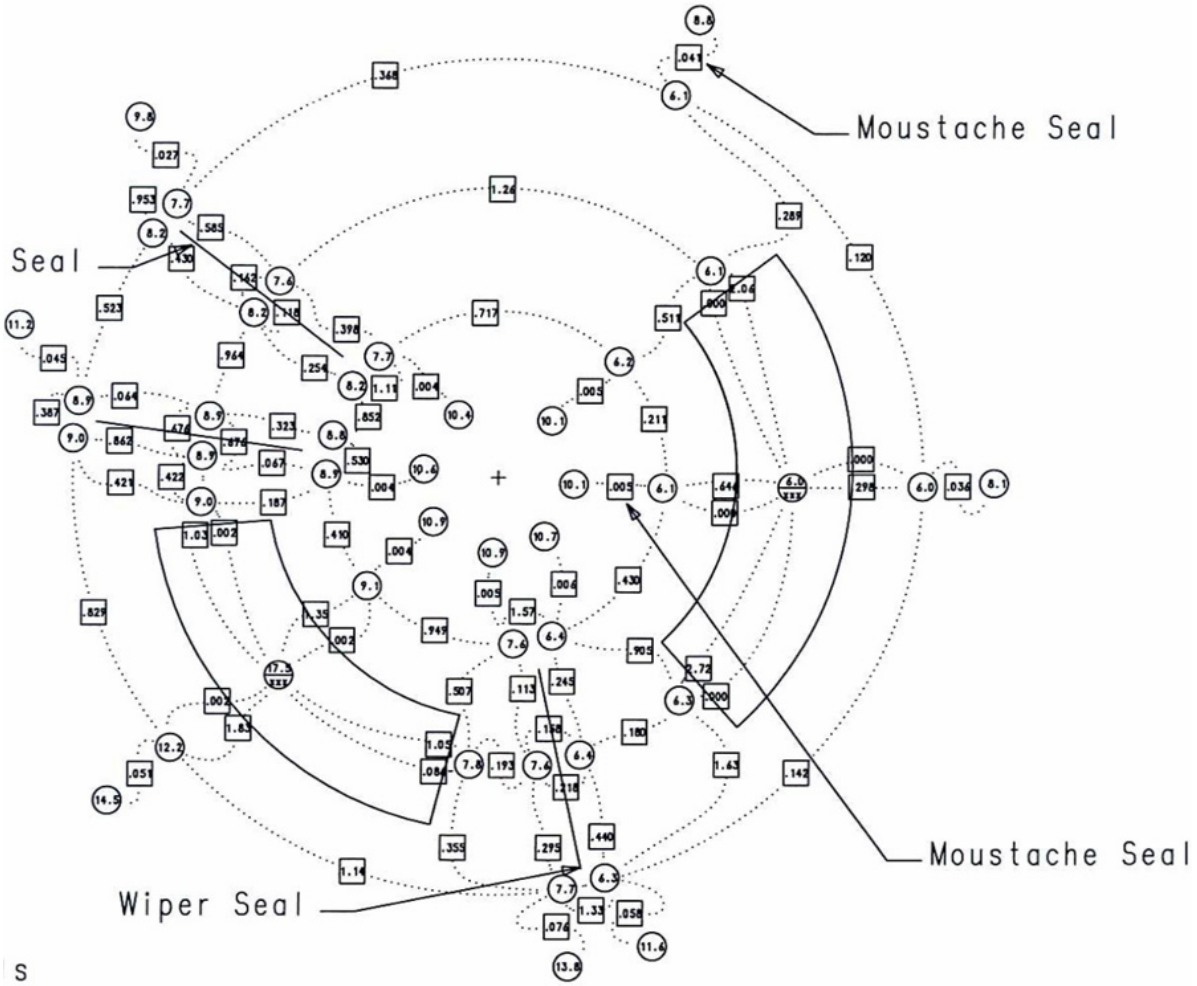

Run 3468 Case 3
HP Foil Seal 1 Slot
Inlet Gap = 0.0025"
Exit Gap = 0.004"
MEW-Stator Gap = 0.042"
2 Wiper Seals
Seal Contact Gap = 0.001"

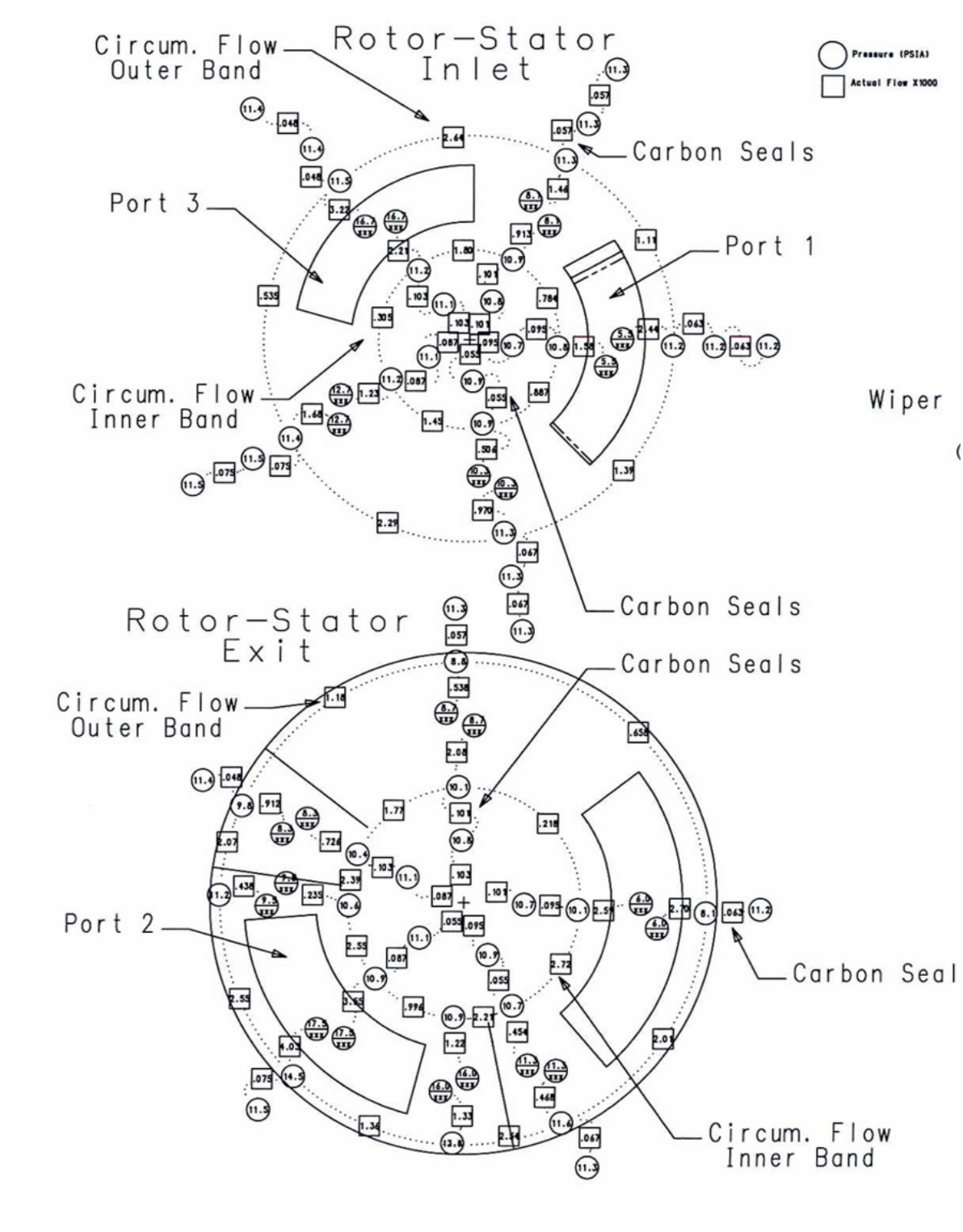
Rotor–Stator
Inlet
Circum. Flow
Outer Band
Carbon Seals
Port 3
Port 1
Circum. Flow
Inner Band
Wiper
Carbon Seals
Rotor–Stator
Exit
Carbon Seals
Circum. Flow
Outer Band
Port 2
Carbon Seal
Circum. Flow
Inner Band
Pressure (PSIA)
Actual Flow X1000

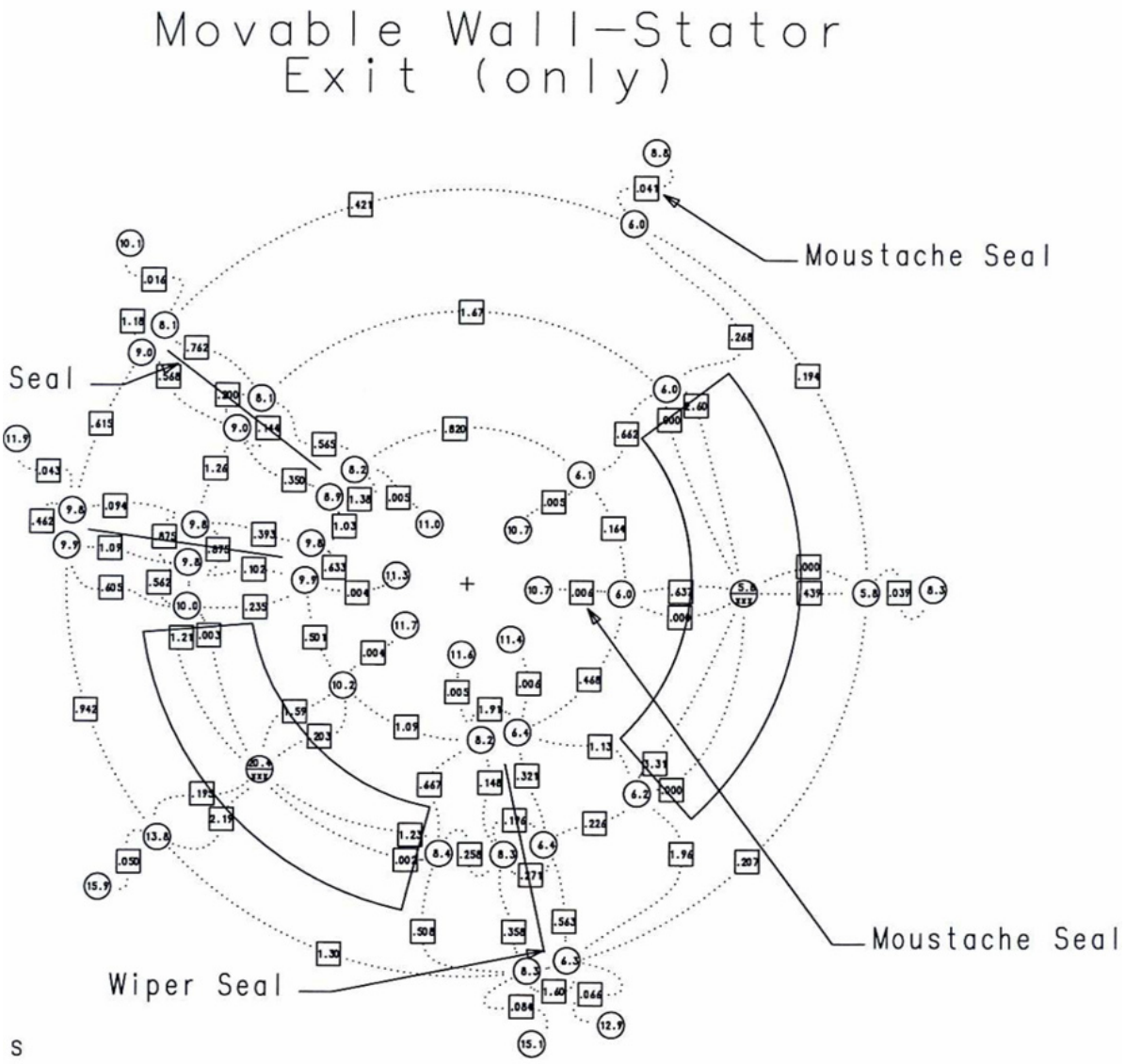

Run 3468 Case 1
HP Foil Seal 2 Slots
Inlet Gap = 0.0025"
Exit Gap = 0.004"
MEW-Stator Gap = 0.042"
2 Wiper Seals
Seal Contact Gap = 0.001"

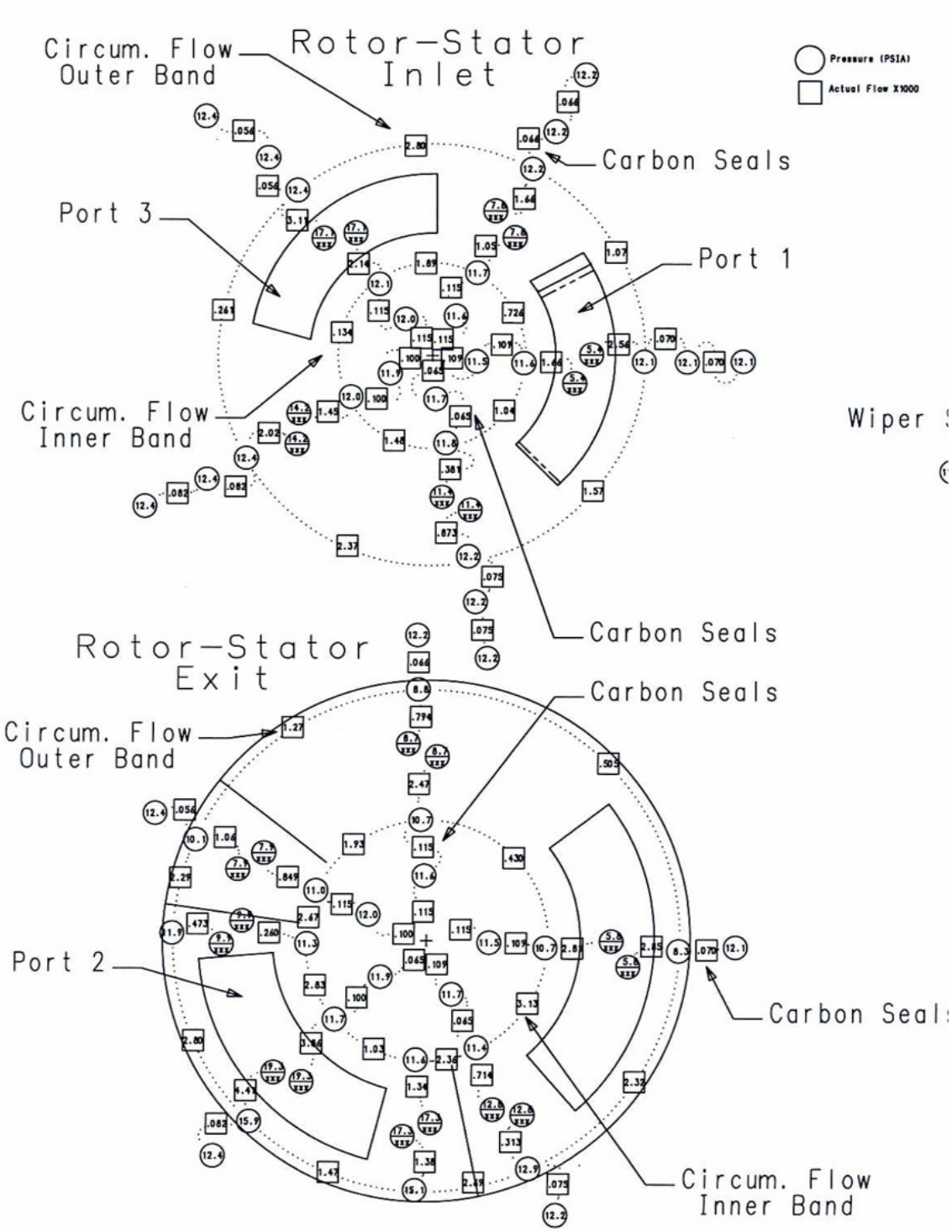
Rotor–Stator
Inlet
Circum. Flow
Outer Band
Carbon Seals
Port 3
Port 1
Circum. Flow
Inner Band
Carbon Seals
Rotor–Stator
Exit
Carbon Seals
Circum. Flow
Outer Band
Port 2
Carbon Seal
Circum. Flow
Inner Band

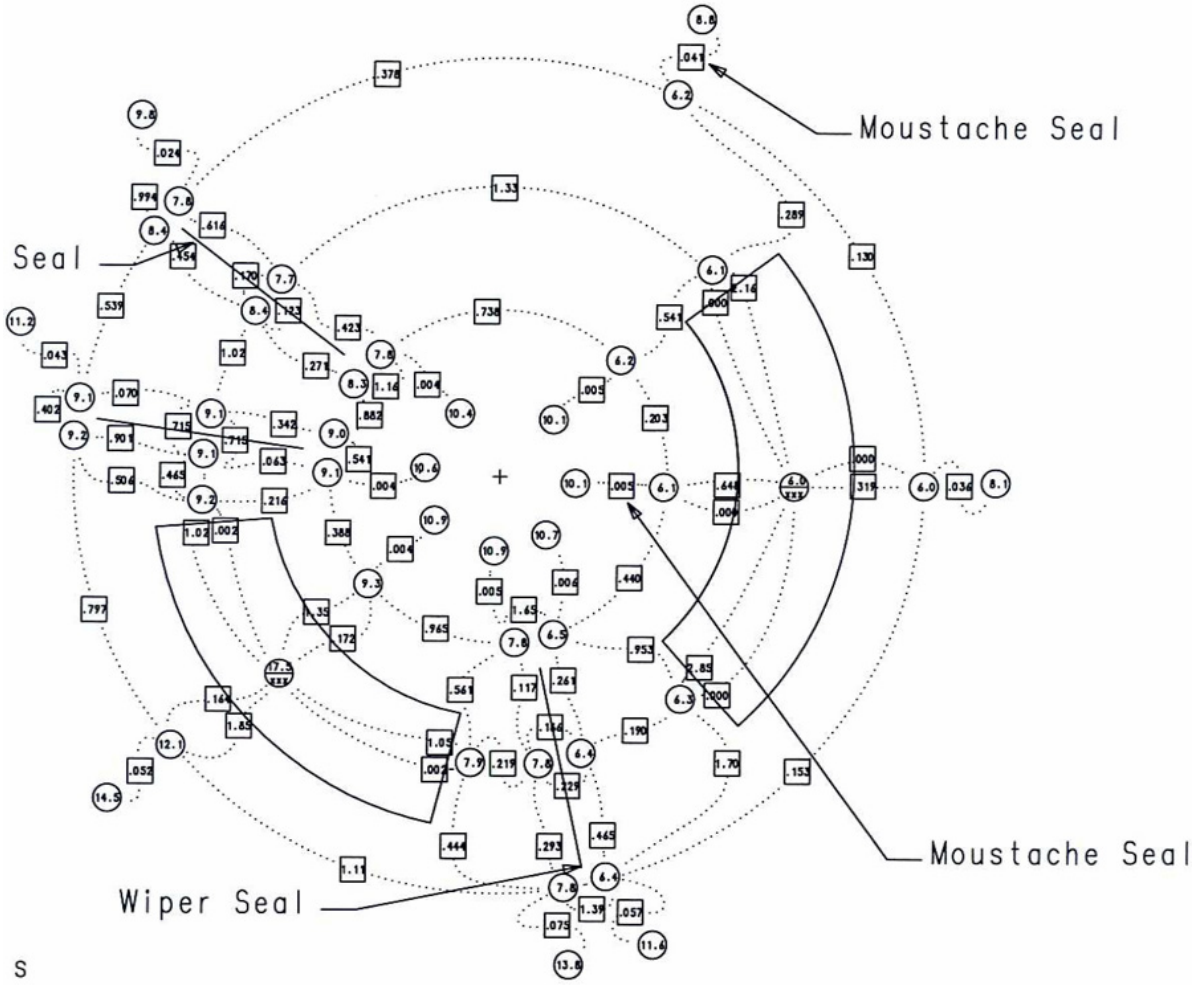

Run 3468 Case 3
HP Foil Seal 2 Slots
Inlet Gap = 0.0025"
Exit Gap = 0.004"
MEW-Stator Gap = 0.042"
2 Wiper Seals
Seal Contact Gap = 0.001"

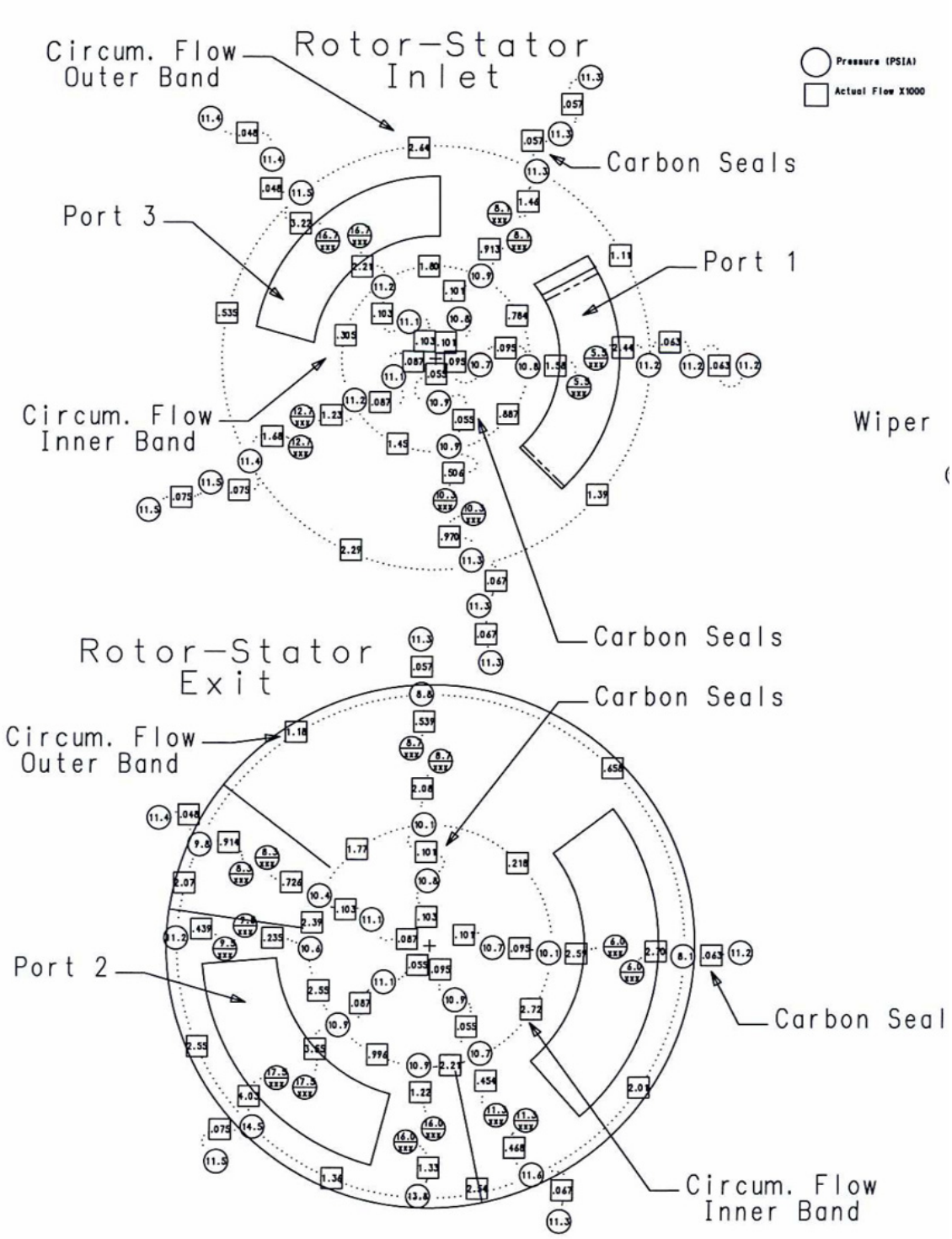
Rotor–Stator
Inlet
Circum. Flow
Outer Band
Carbon Seals
Port 3
Port 1
Circum. Flow
Inner Band
Carbon Seals
Rotor–Stator
Exit
Carbon Seals
Circum. Flow
Outer Band
Port 2
Carbon Seal
Circum. Flow
Inner Band

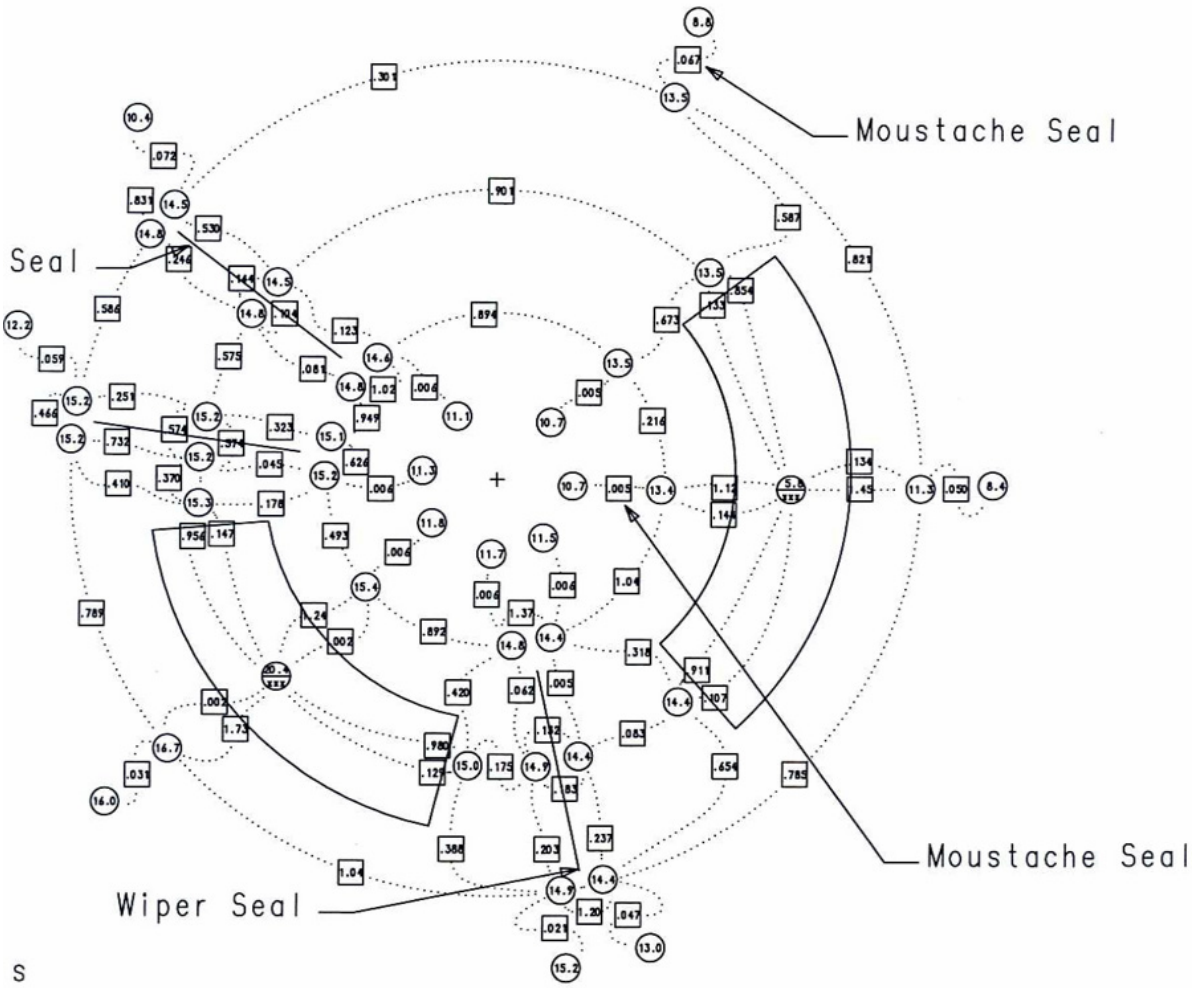

Run 3468 Case 1
HP Foil Seal 2 Slots + LP Foil Seal 4 Slots
Inlet Gap = 0.0025"
Exit Gap = 0.004"
MEW-Stator Gap = 0.042"
2 Wiper Seals
Seal Contact Gap = 0.001"

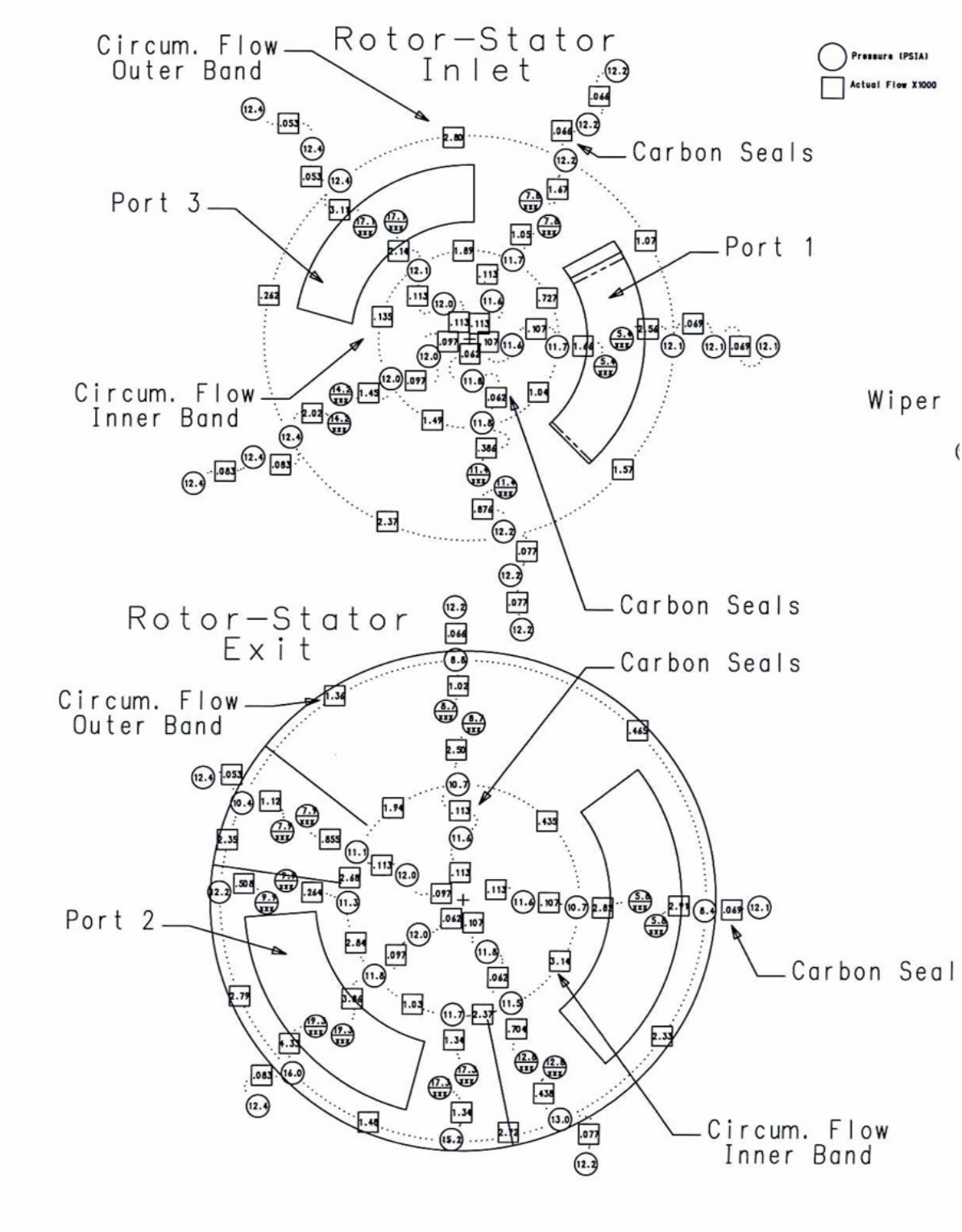
Rotor–Stator
Inlet
Circum. Flow
Outer Band
Carbon Seals
Port 3
Port 1
Circum. Flow
Inner Band
Wiper
Carbon Seals
Rotor–Stator
Exit
Carbon Seals
Circum. Flow
Outer Band
Port 2
Carbon Seal
Circum. Flow
Inner Band
Pressure (PSIA)
Actual Flow X1000

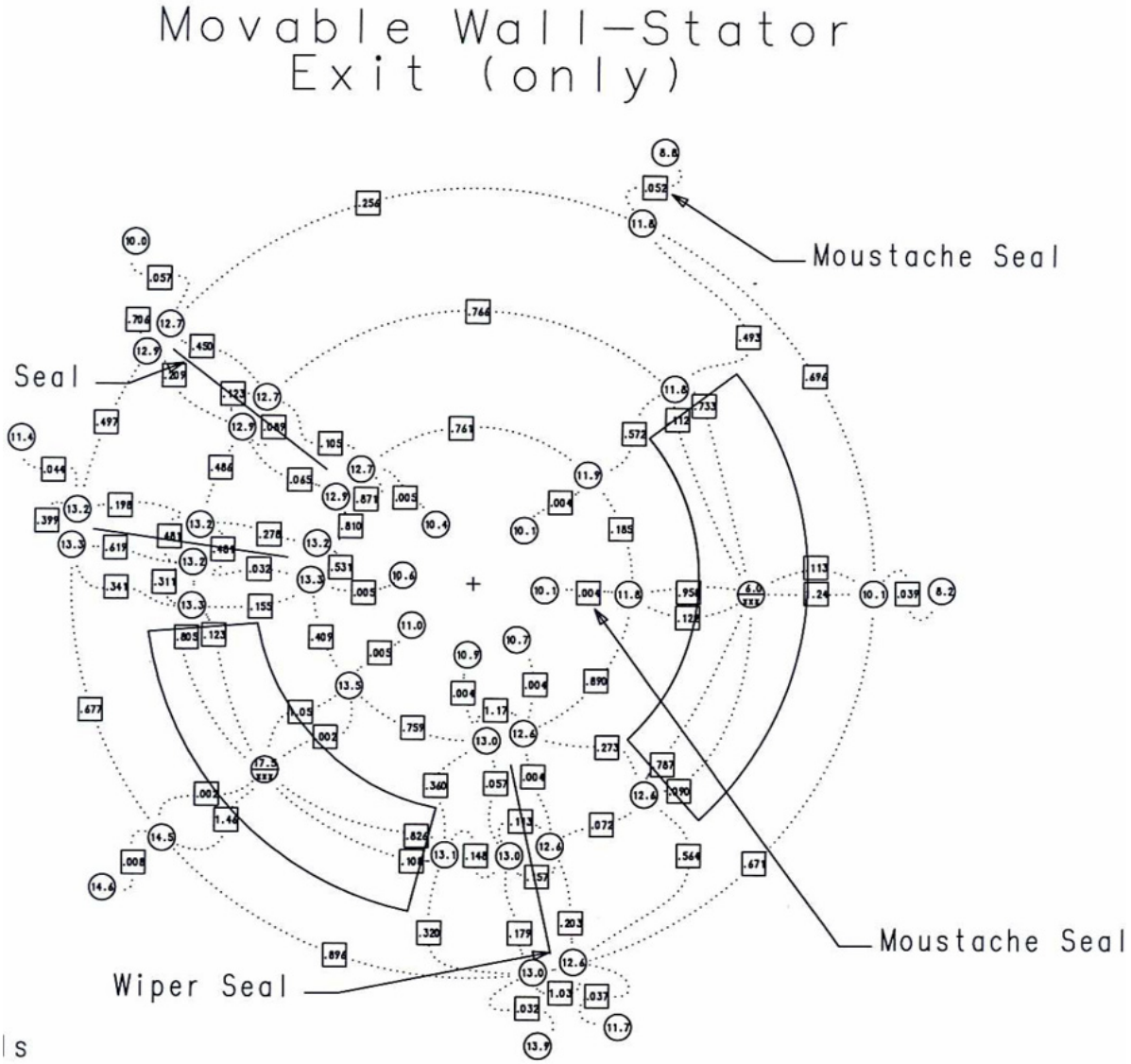

Run 3468 Case 3
HP Foil Seal 2 Slots + LP Foil Seal 4 Slots
Inlet Gap = 0.0025"
Exit Gap = 0.004"
MEW-Stator Gap = 0.042"
2 Wiper Seals
Seal Contact Gap = 0.001"

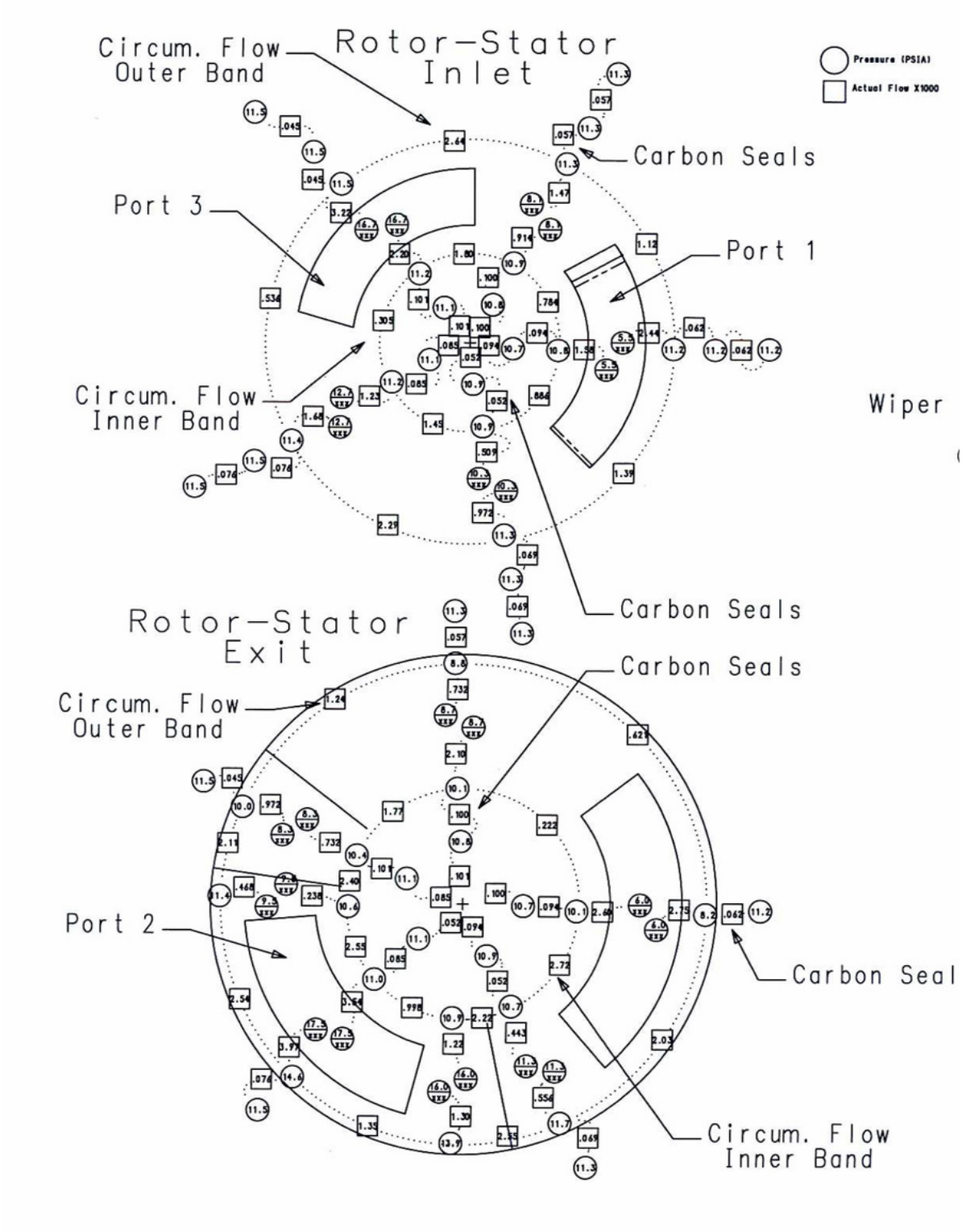
Rotor–Stator
Inlet
Circum. Flow
Outer Band
Carbon Seals
Port 3
Port 1
Circum. Flow
Inner Band
Wiper
Carbon Seals
Rotor–Stator
Exit
Carbon Seals
Circum. Flow
Outer Band
Port 2
Carbon Seal
Circum. Flow
Inner Band
Pressure (PSIA)
Actual Flow X1000

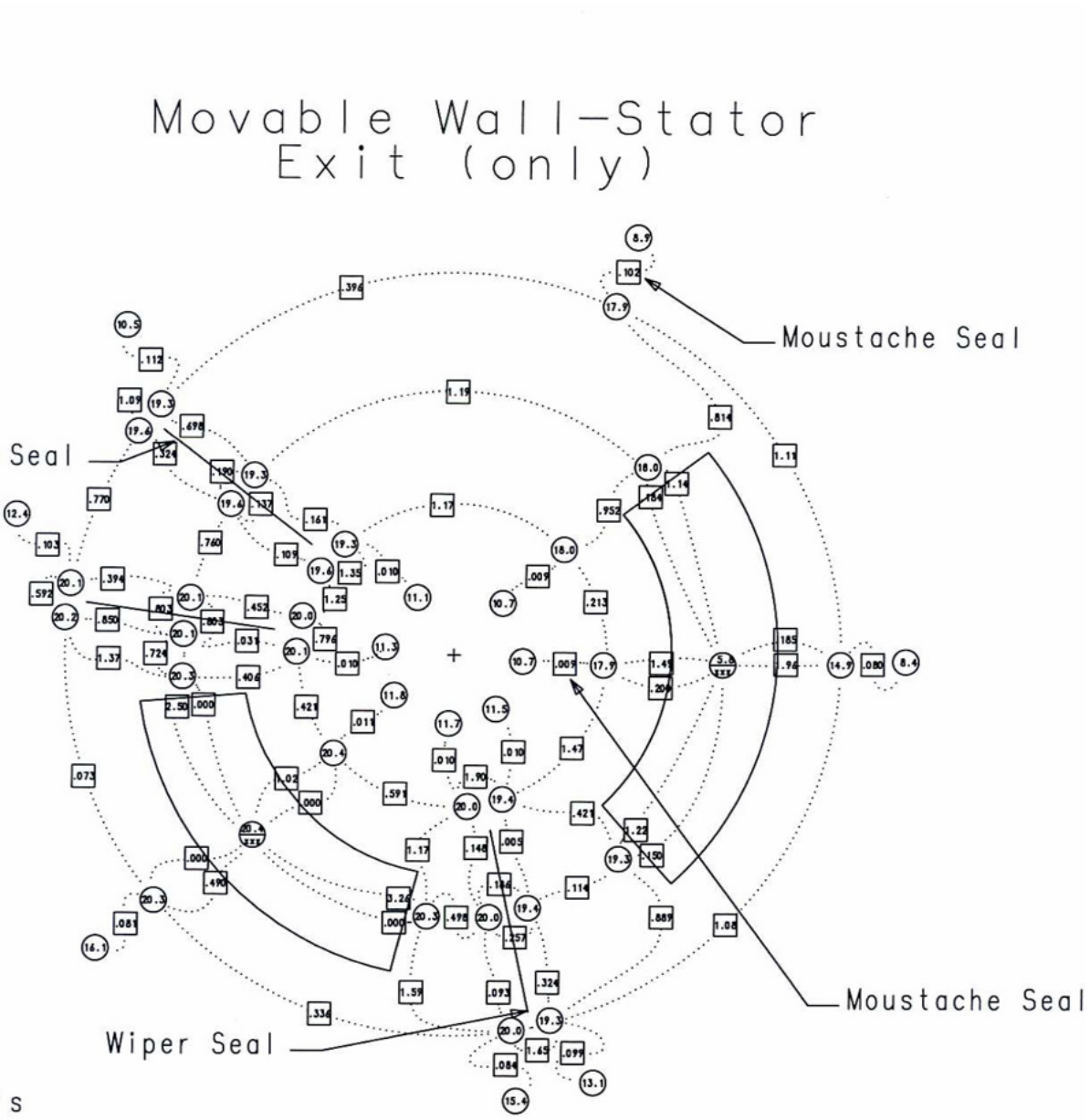

Run 3468 Case 1
LP Foil Seal 4 Slots
Inlet Gap = 0.0025"
Exit Gap = 0.004"
MEW-Stator Gap = 0.042"
2 Wiper Seals
Seal Contact Gap = 0.001"

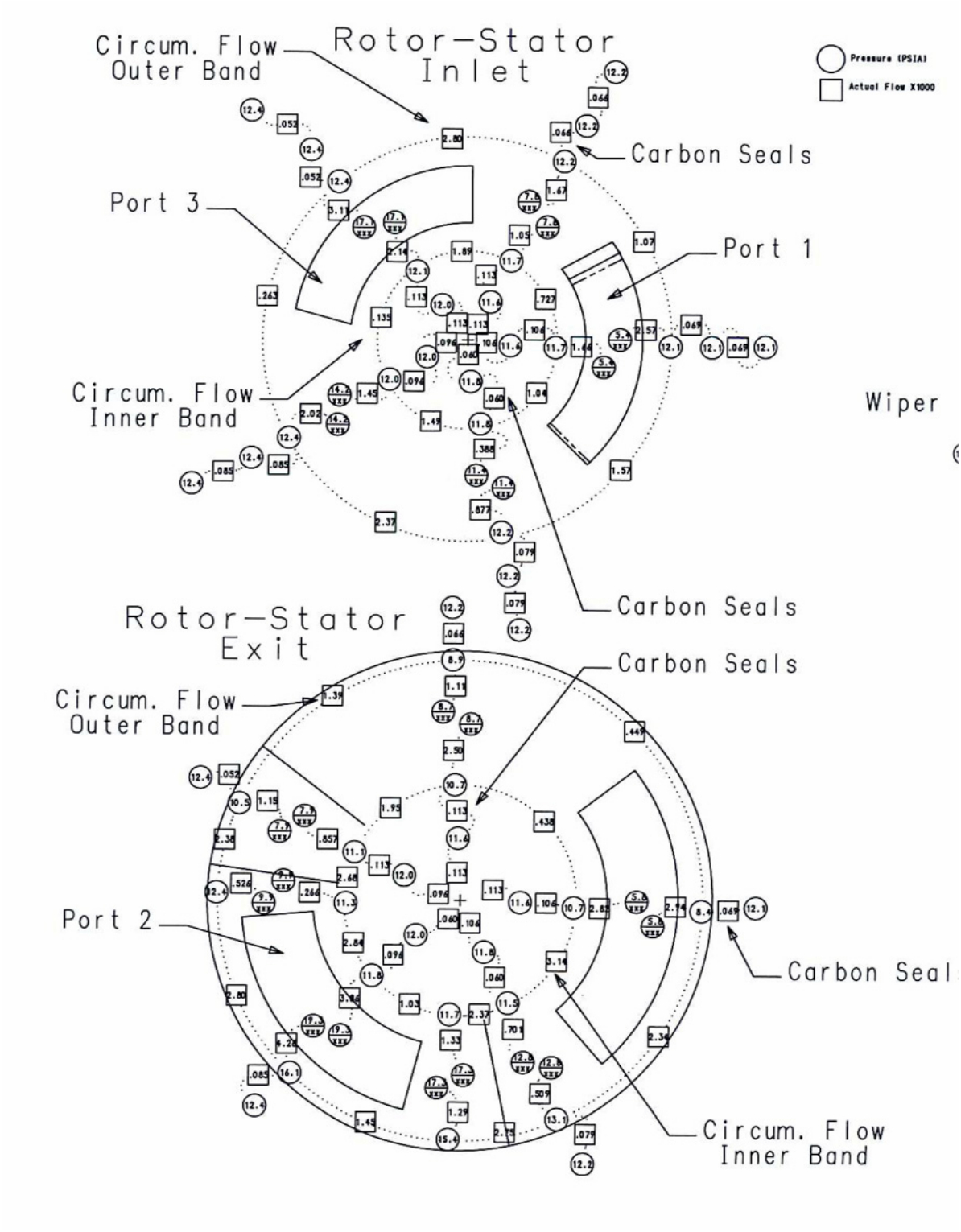
Rotor–Stator
Inlet
Circum. Flow
Outer Band
Carbon Seals
Port 3
Port 1
Circum. Flow
Inner Band
Carbon Seals
Wiper
Rotor–Stator
Exit
Carbon Seals
Circum. Flow
Outer Band
Port 2
Carbon Seal
Circum. Flow
Inner Band
Pressure (PSIA)
Actual Flow X1000

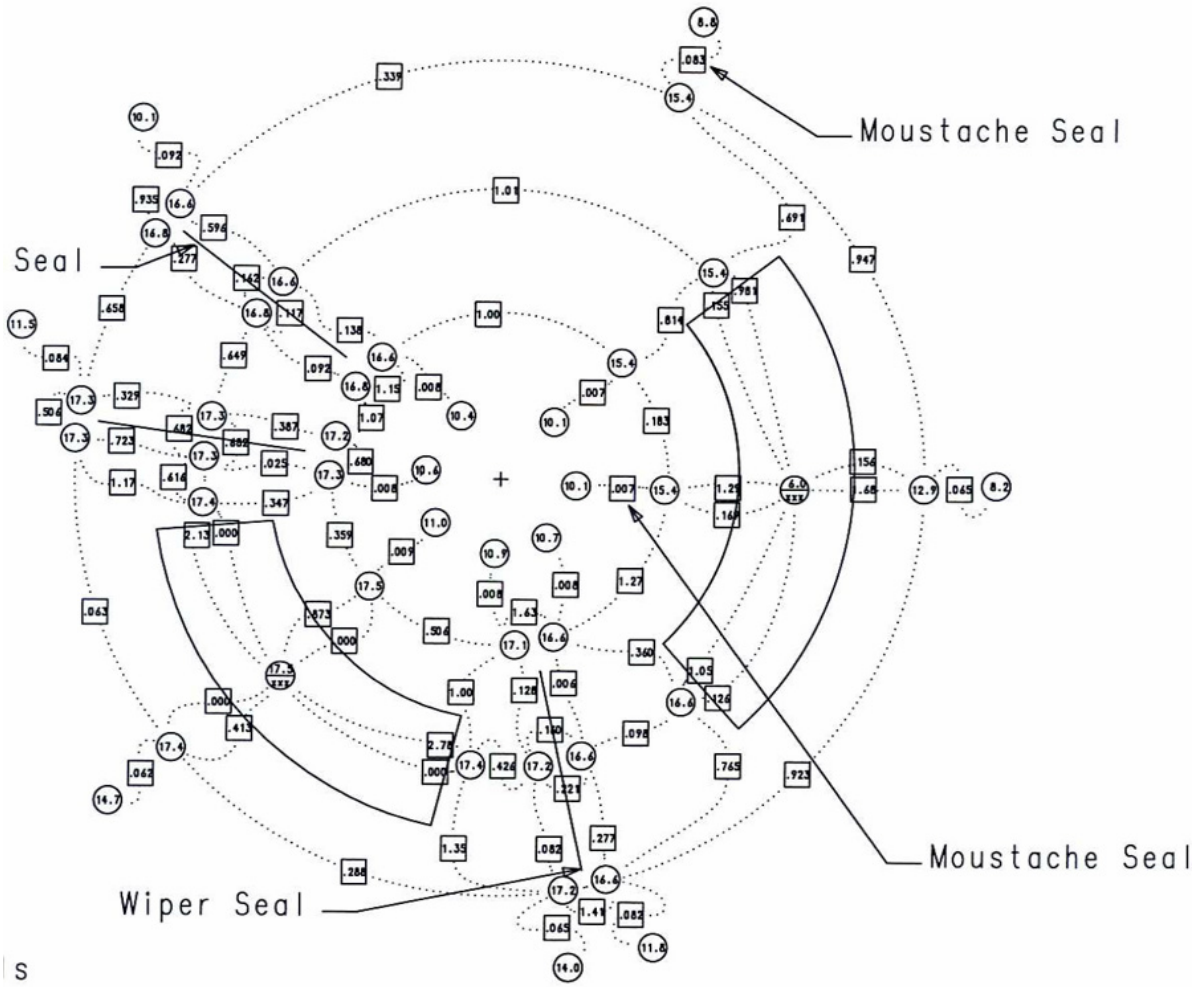

Run 3468 Case 3
LP Foil Seal 4 Slots
Inlet Gap = 0.0025"
Exit Gap = 0.004"
MEW-Stator Gap = 0.042"
2 Wiper Seals
Seal Contact Gap = 0.001"

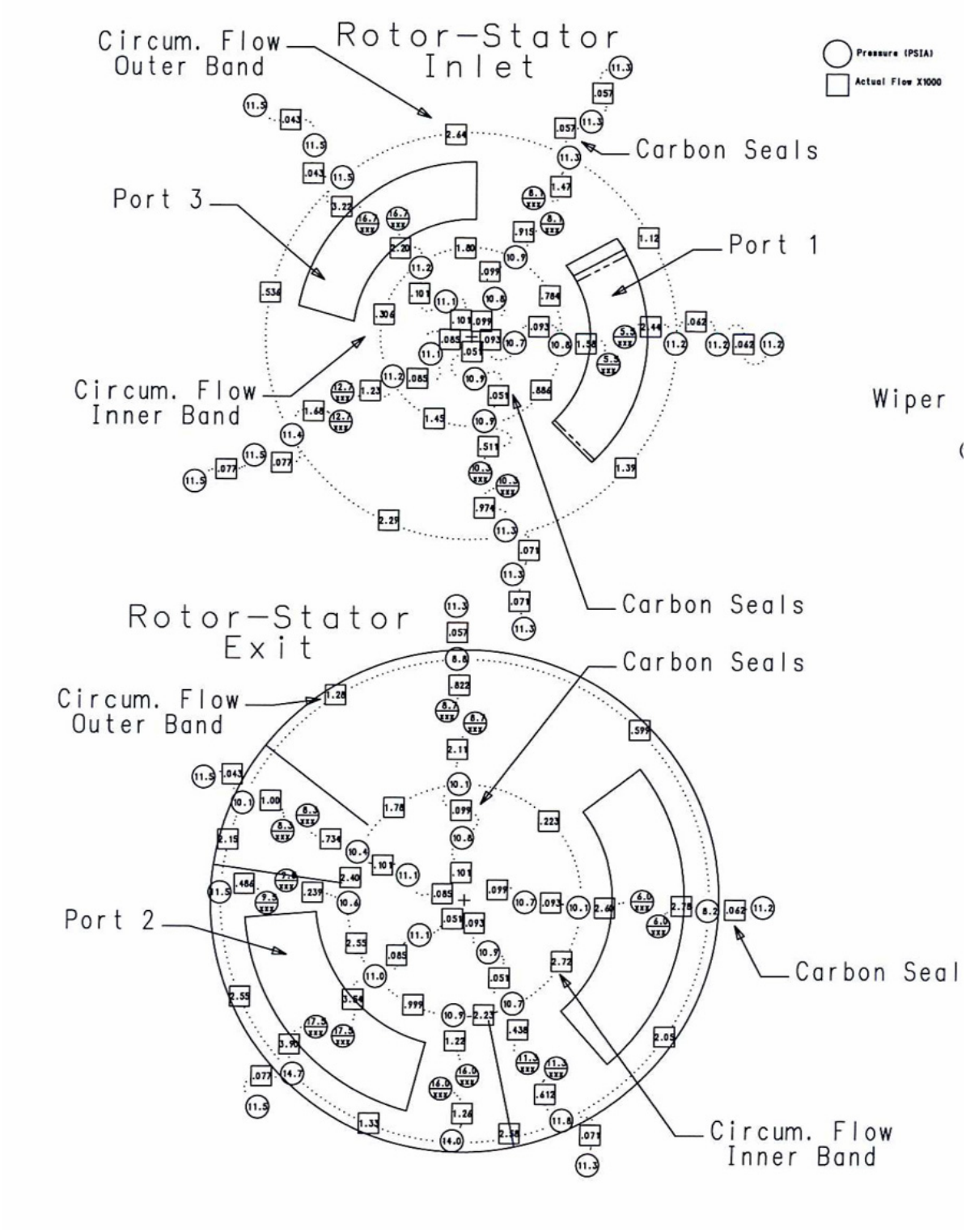
Rotor–Stator
Inlet
Circum. Flow
Outer Band
Carbon Seals
Port 3
Port 1
Circum. Flow
Inner Band
Wiper
Carbon Seals
Rotor–Stator
Exit
Carbon Seals
Circum. Flow
Outer Band
Port 2
Carbon Seal
Circum. Flow
Inner Band
Pressure (PSIA)
Actual Flow X1000

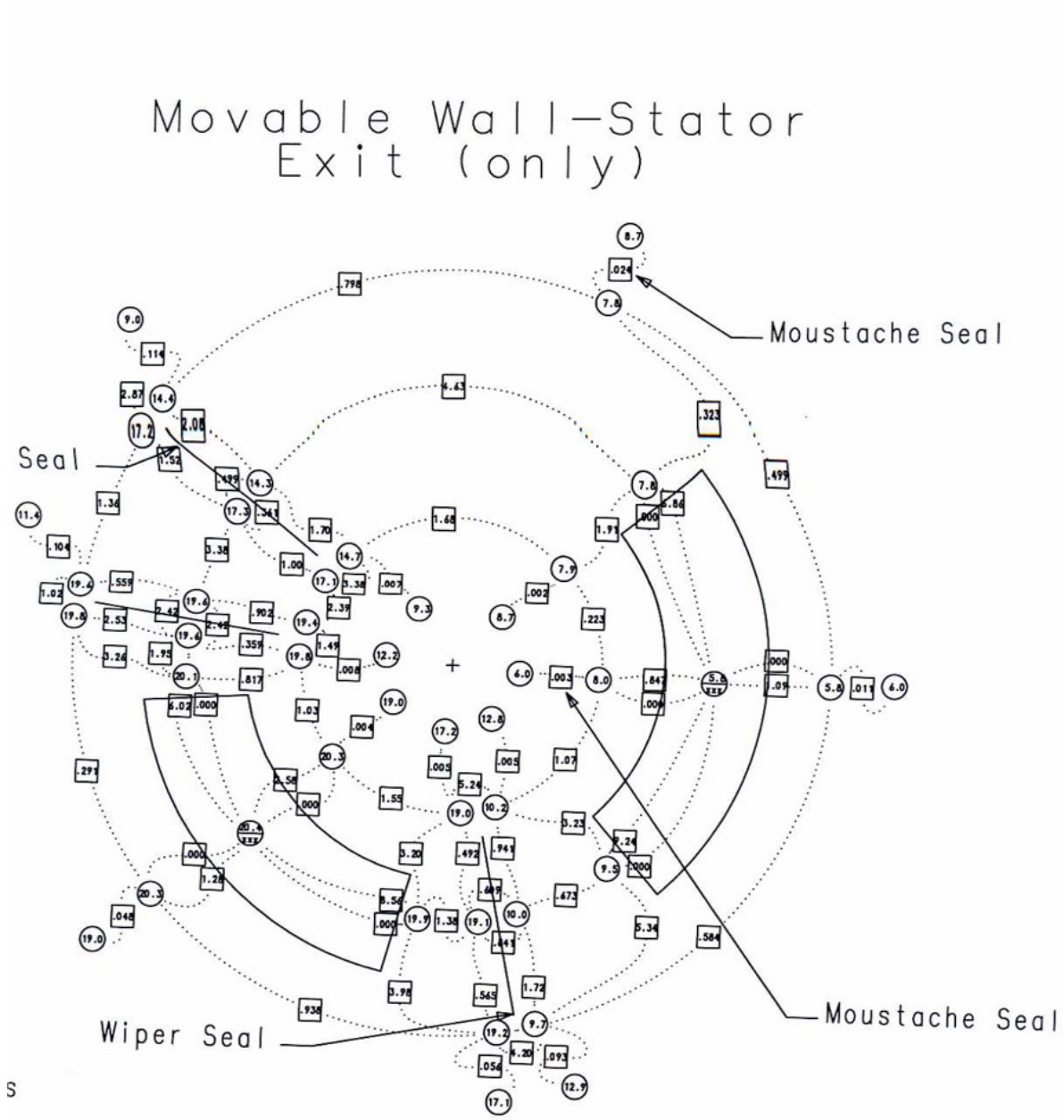

Run 3468 Case 1
Minimum Circumferencial flow (gap = RS gap)
Inlet Gap = 0.0025"
Exit Gap = 0.004"
MEW-Stator Gap = 0.042"
2 Wiper Seals
Seal Contact Gap = 0.001"

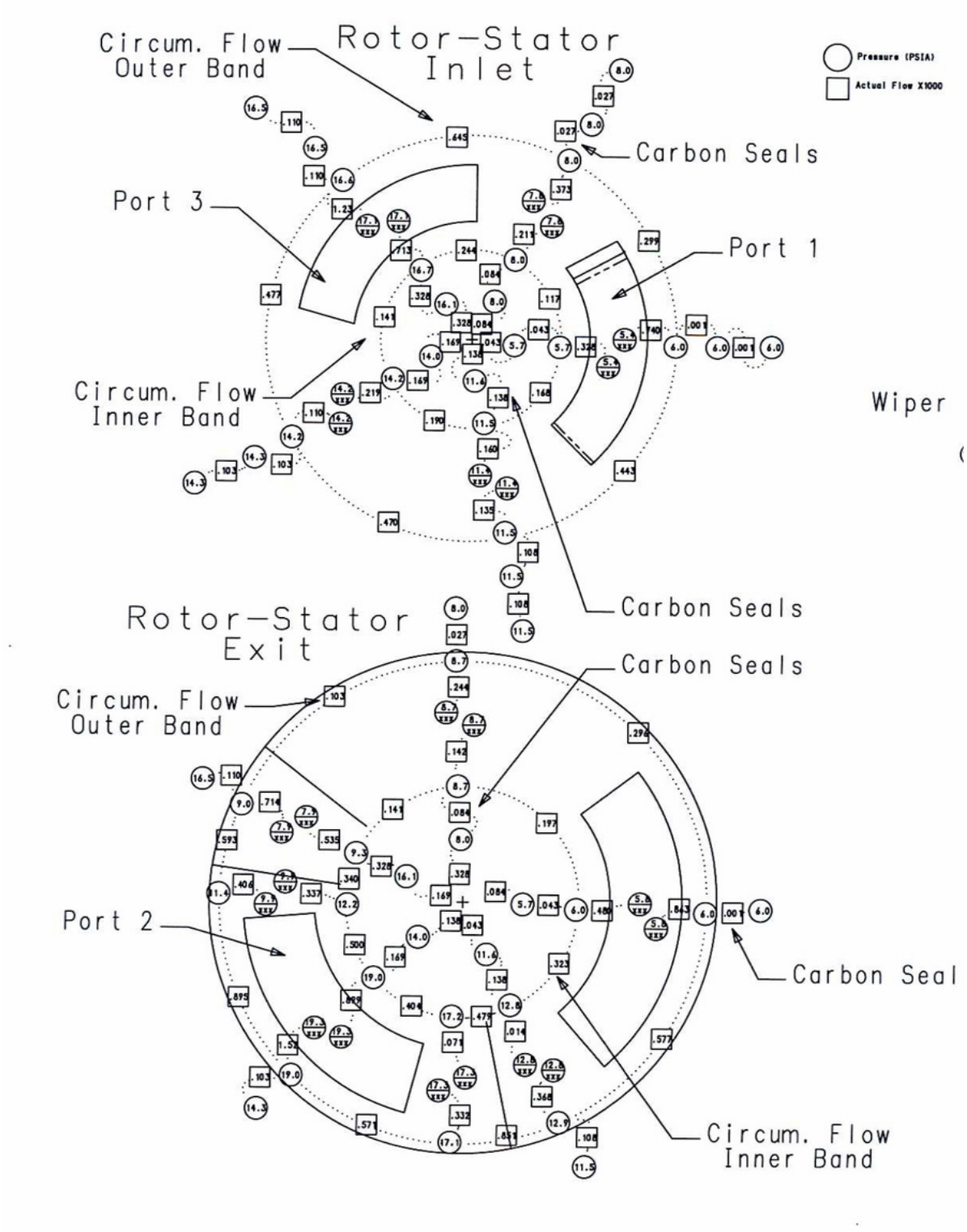
Rotor–Stator
Inlet
Circum. Flow
Outer Band
Pressure (PSIA)
Actual Flow X1000
Carbon Seals
Port 3
Port 1
Circum. Flow
Inner Band
Wiper
Carbon Seals
Rotor–Stator
Exit
Carbon Seals
Circum. Flow
Outer Band
Port 2
Carbon Seal
Circum. Flow
Inner Band

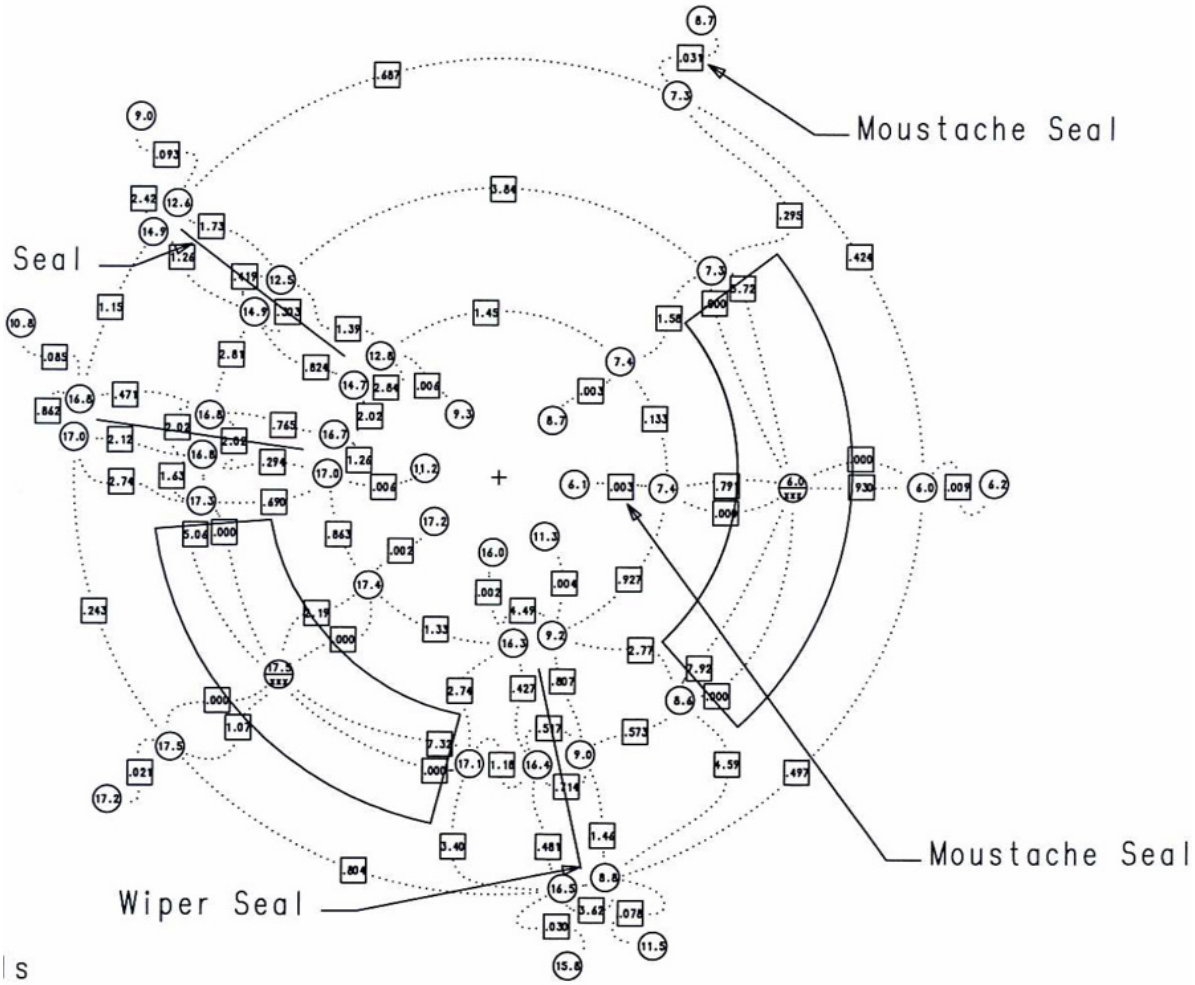

Run 3468 Case 3
Minimum Circumferencial flow (gap = RS gap)
Inlet Gap = 0.0025"
Exit Gap = 0.004"
MEW-Stator Gap = 0.042"
2 Wiper Seals
Seal Contact Gap = 0.001"

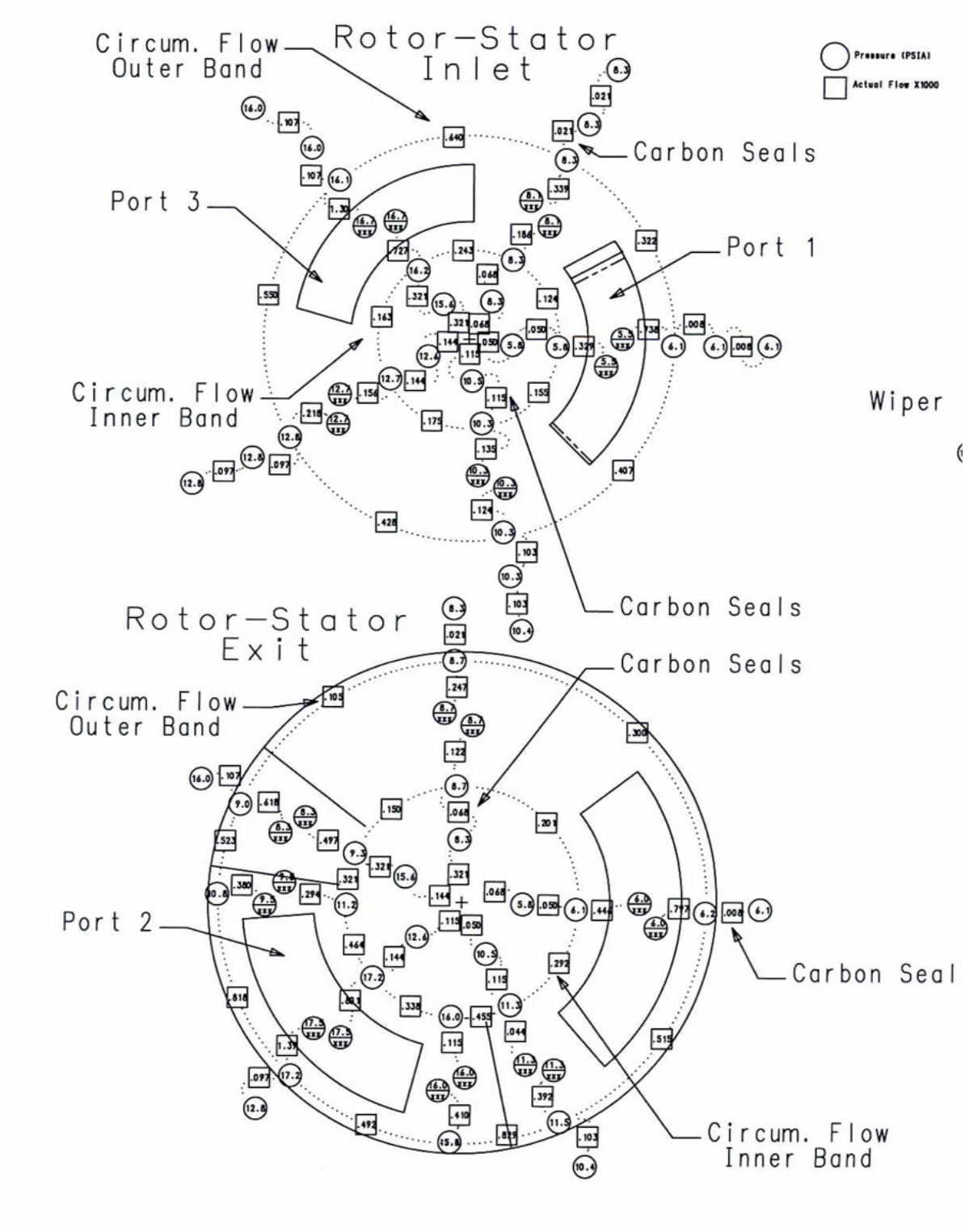
Rotor–Stator
Inlet
Circum. Flow
Outer Band
Pressure (PSIA)
Actual Flow X1000
Carbon Seals
Port 3
Port 1
Circum. Flow
Inner Band
Wiper
Carbon Seals
Rotor–Stator
Exit
Carbon Seals
Circum. Flow
Outer Band
Port 2
Carbon Seal
Circum. Flow
Inner Band

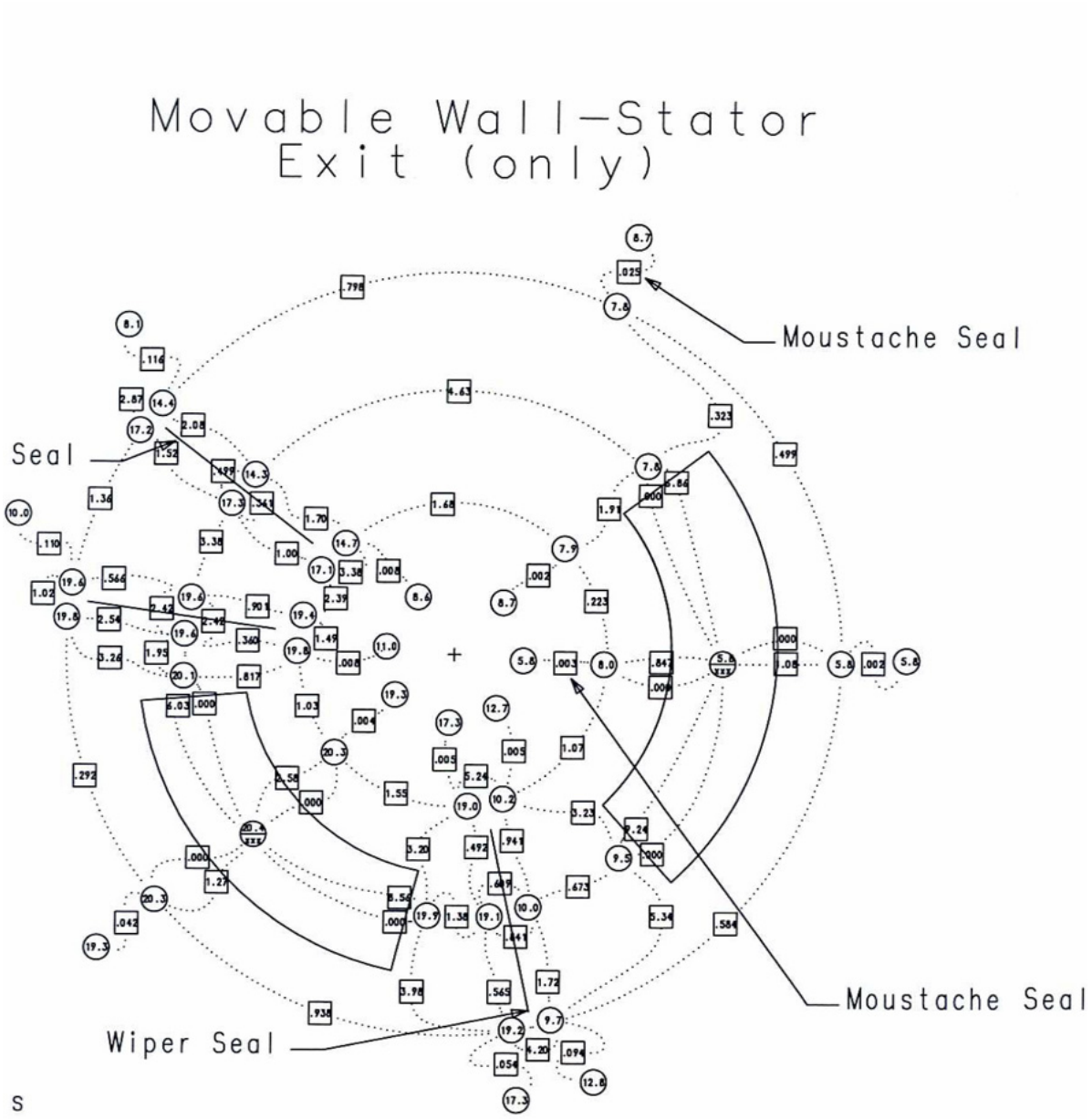

Run 3468 Case 1
No Circumferencial Communication (RS gaps)
Inlet Gap = 0.0025"
Exit Gap = 0.004"
MEW-Stator Gap = 0.042"
2 Wiper Seals
Seal Contact Gap = 0.001"

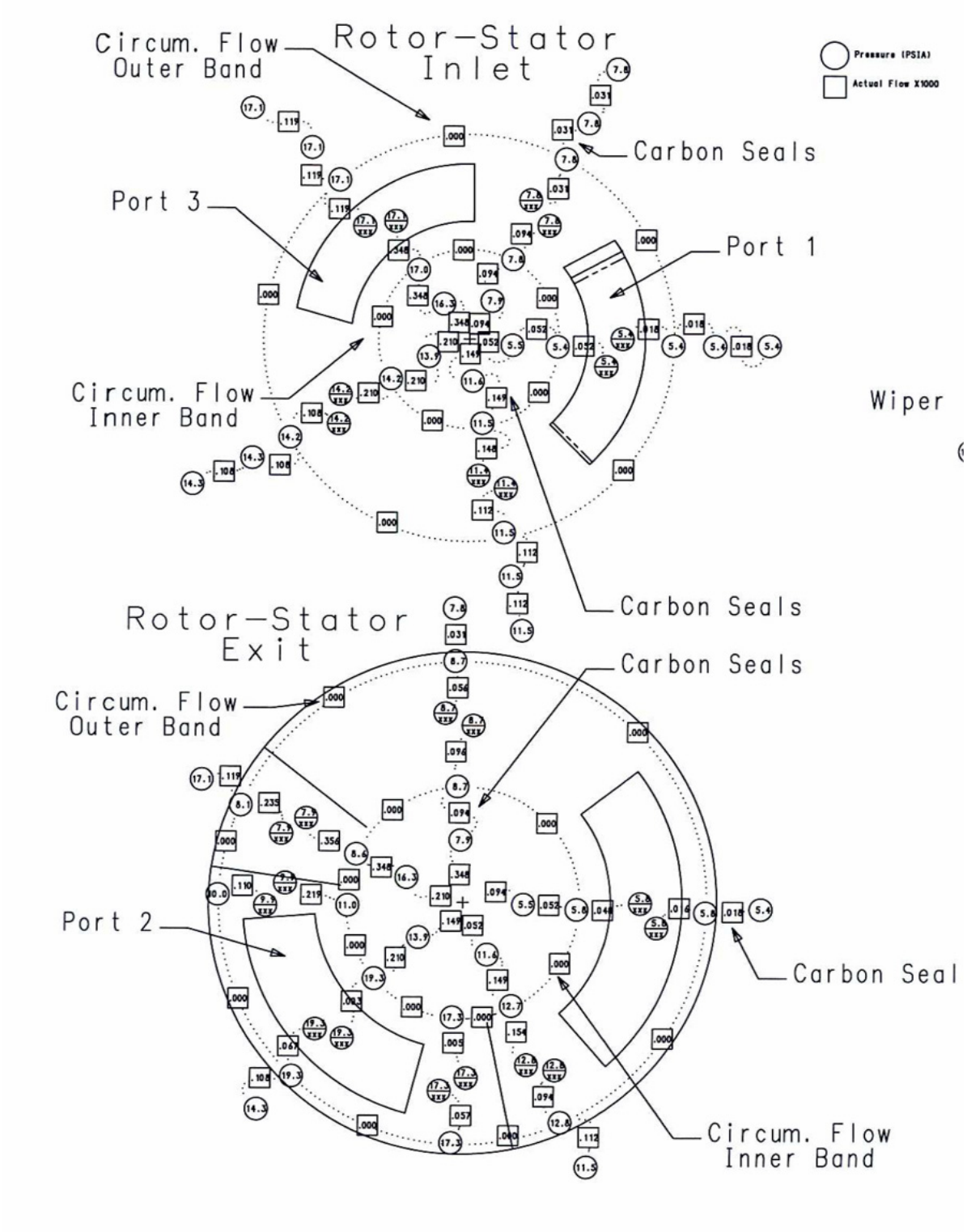
Rotor–Stator
Inlet
Circum. Flow
Outer Band
Pressure (PSIA)
Actual Flow X1000
Carbon Seals
Port 3
Port 1
Circum. Flow
Inner Band
Wiper
Carbon Seals
Rotor–Stator
Exit
Carbon Seals
Circum. Flow
Outer Band
Port 2
Carbon Seal
Circum. Flow
Inner Band

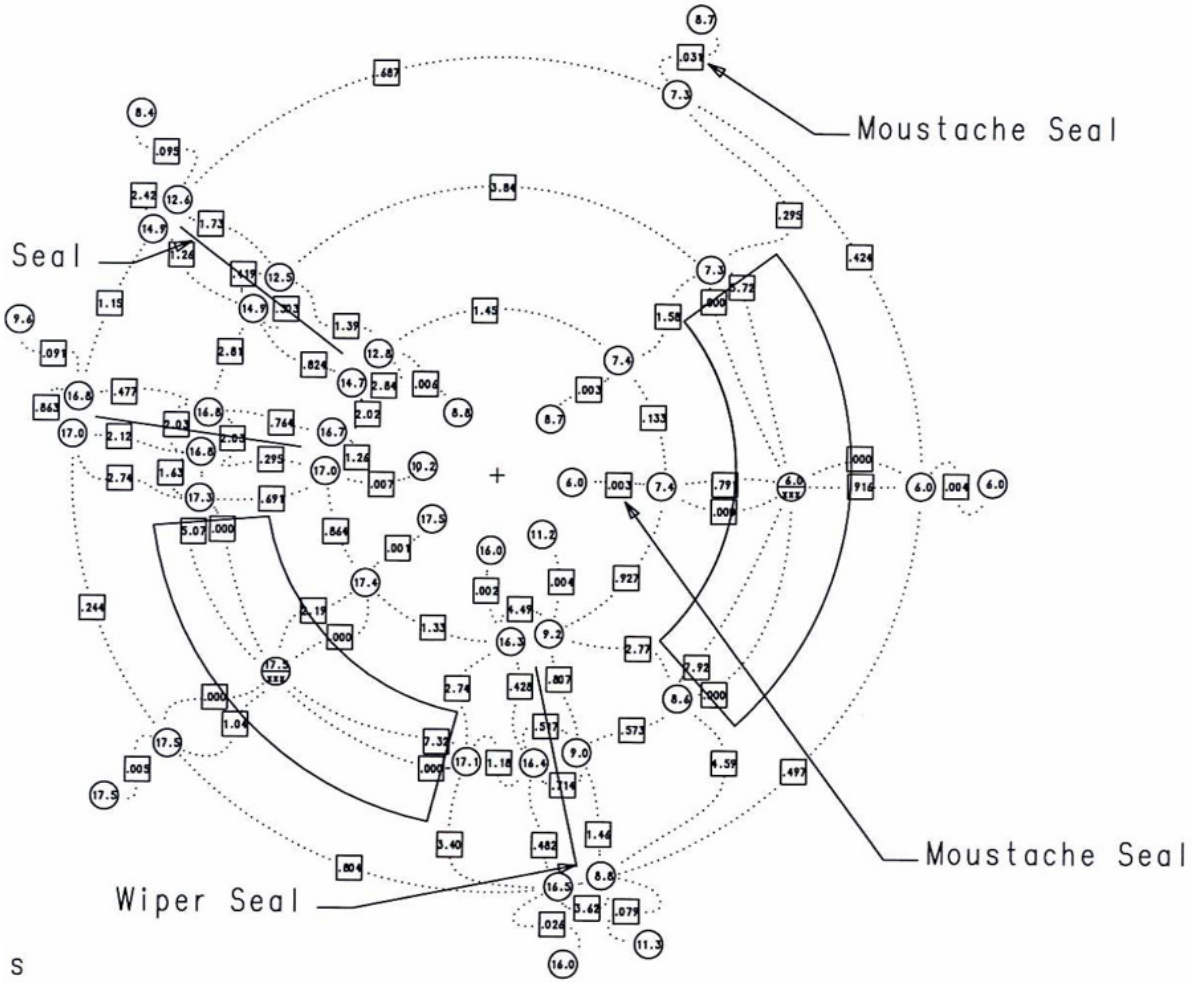

Run 3468 Case 3
No Circumferencial Communication (gap = RS gap
Inlet Gap = 0.0025"
Exit Gap = 0.004"
MEW-Stator Gap = 0.042"
2 Wiper Seals
Seal Contact Gap = 0.001"

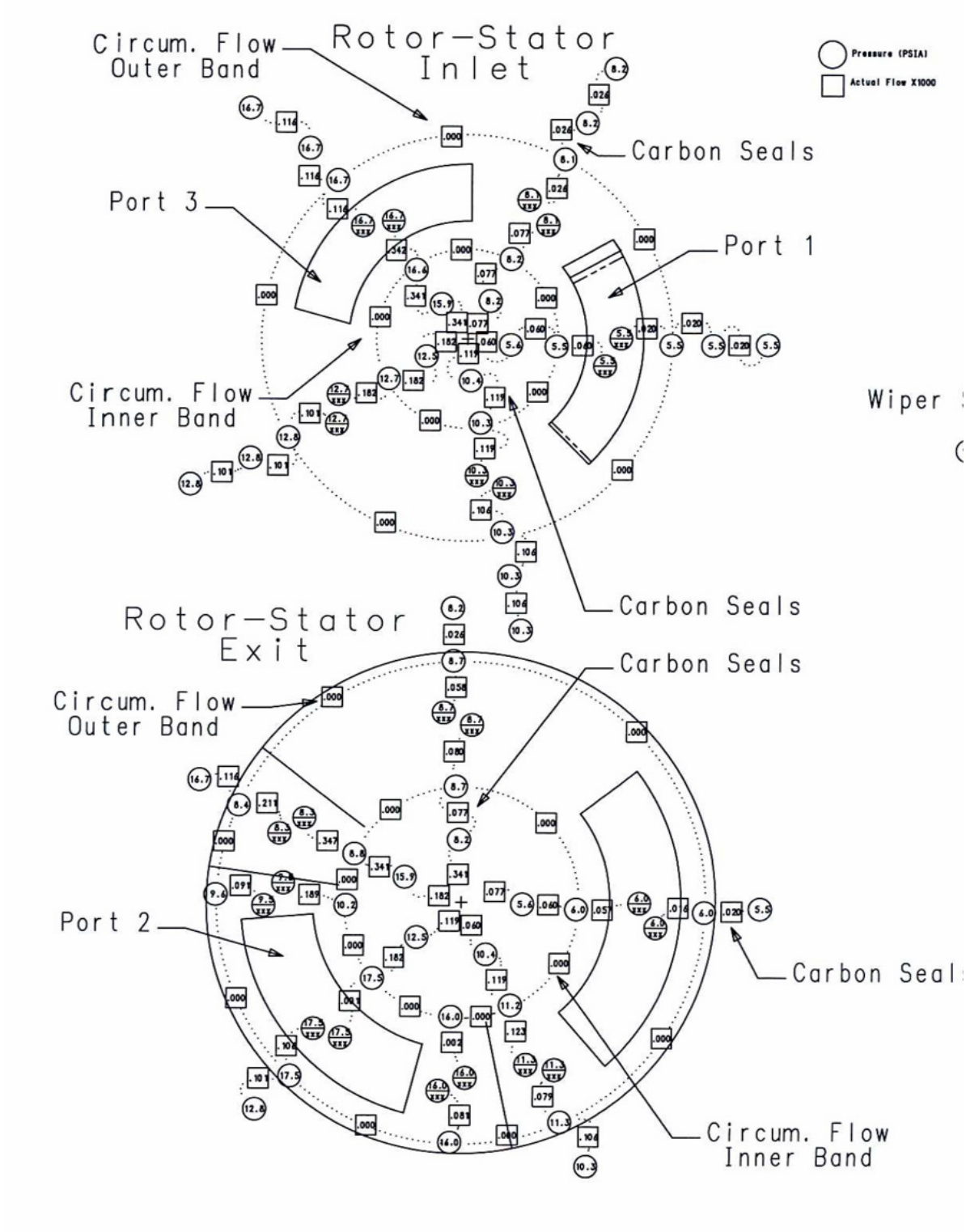
Rotor–Stator
Inlet
Circum. Flow
Outer Band
Pressure (PSIA)
Actual Flow X1000
Carbon Seals
Port 3
Port 1
Circum. Flow
Inner Band
Wiper
Carbon Seals
Rotor–Stator
Exit
Carbon Seals
Circum. Flow
Outer Band
Port 2
Carbon Seal
Circum. Flow
Inner Band

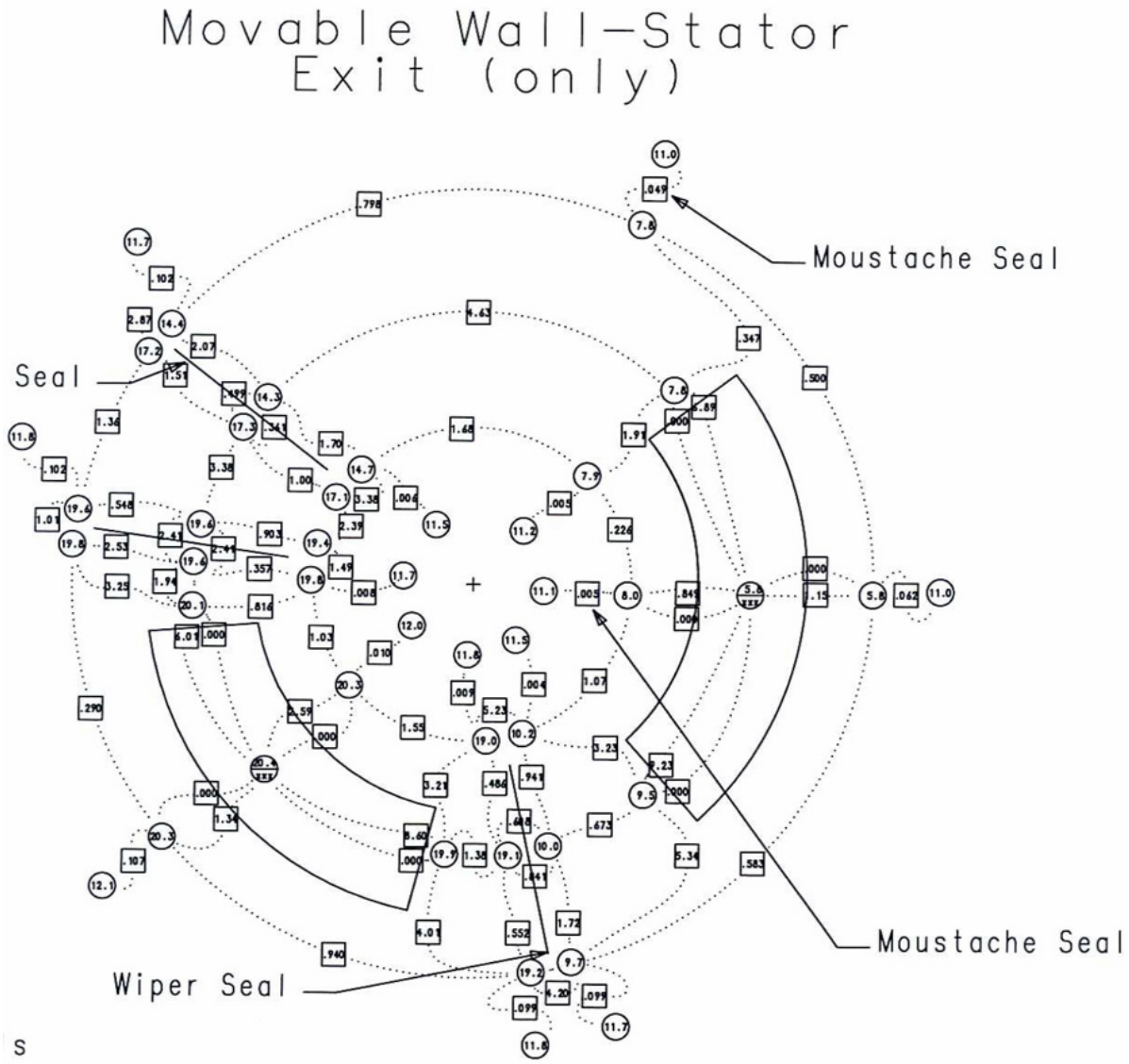

Run 3468 Case 1
No Carbon Seals Present
Inlet Gap = 0.0025"
Exit Gap = 0.004"
MEW-Stator Gap = 0.042"
2 Wiper Seals
Seal Contact Gap = 0.001"

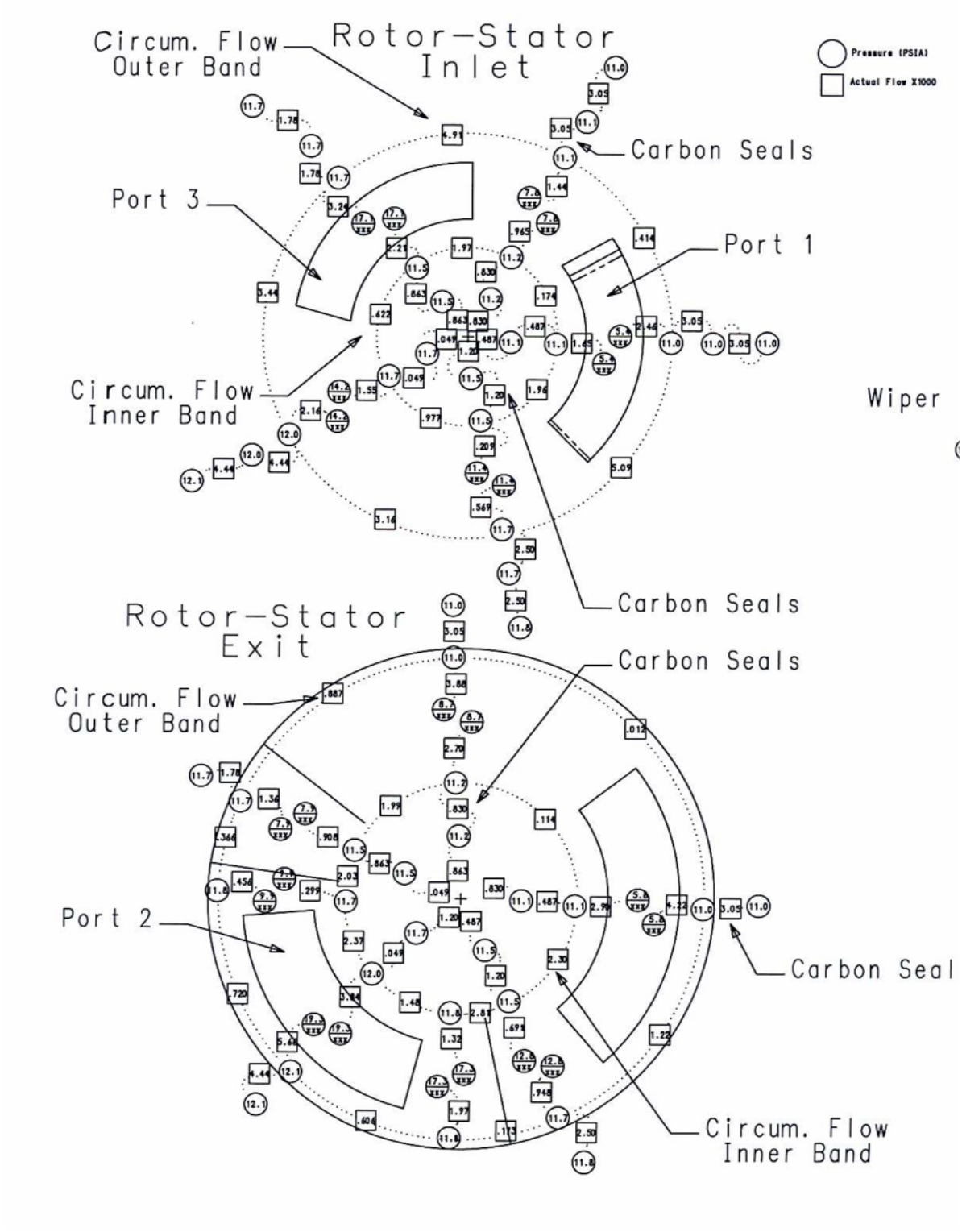
Rotor–Stator
Inlet
Circum. Flow
Outer Band
Carbon Seals
Port 3
Port 1
Circum. Flow
Inner Band
Wiper
Carbon Seals
Rotor–Stator
Exit
Carbon Seals
Circum. Flow
Outer Band
Port 2
Carbon Seal
Circum. Flow
Inner Band

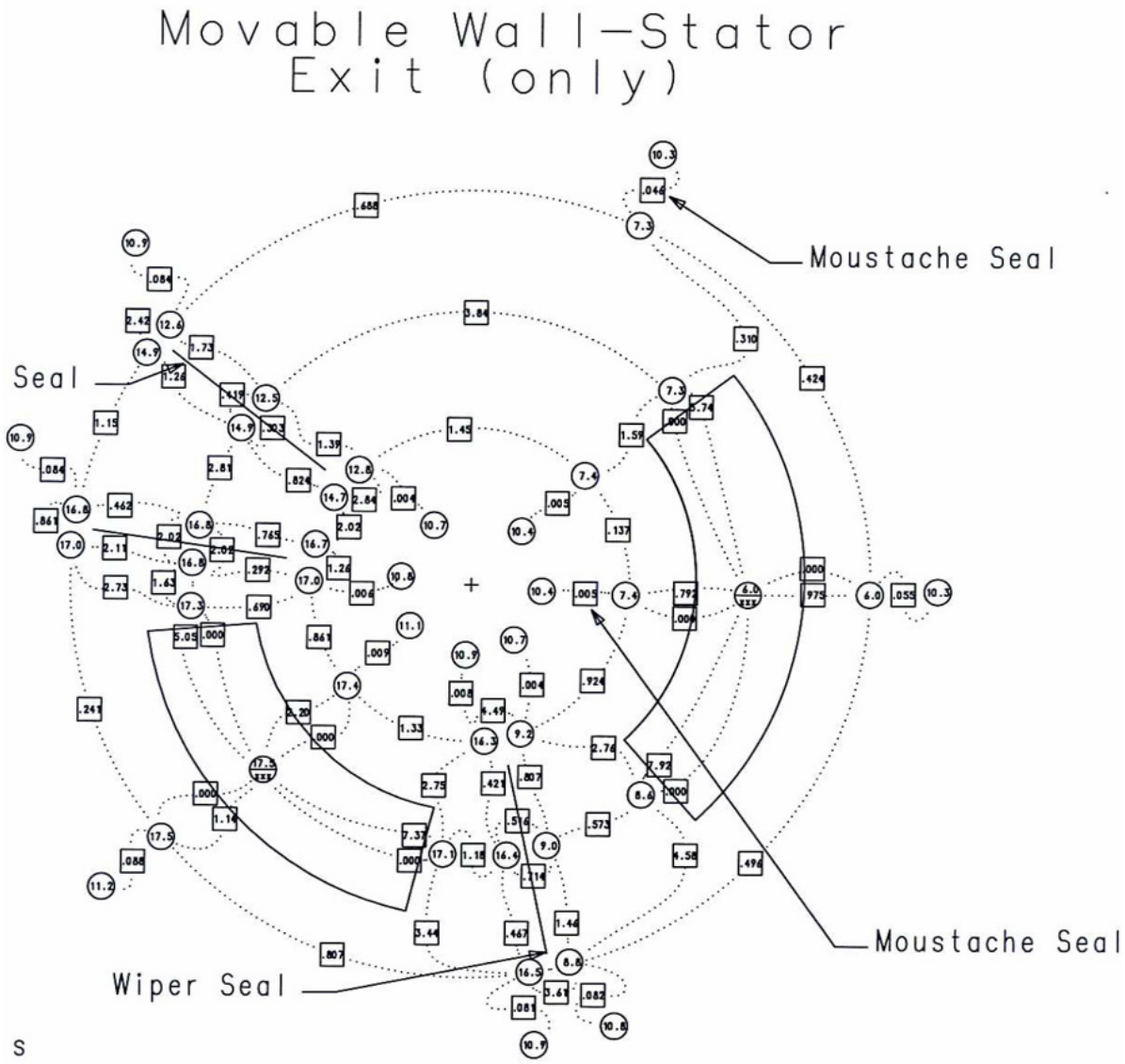

Run 3468 Case 3
No Carbon Seals Present
Inlet Gap = 0.0025"
Exit Gap = 0.004"
MEW-Stator Gap = 0.042"
2 Wiper Seals
Seal Contact Gap = 0.001"

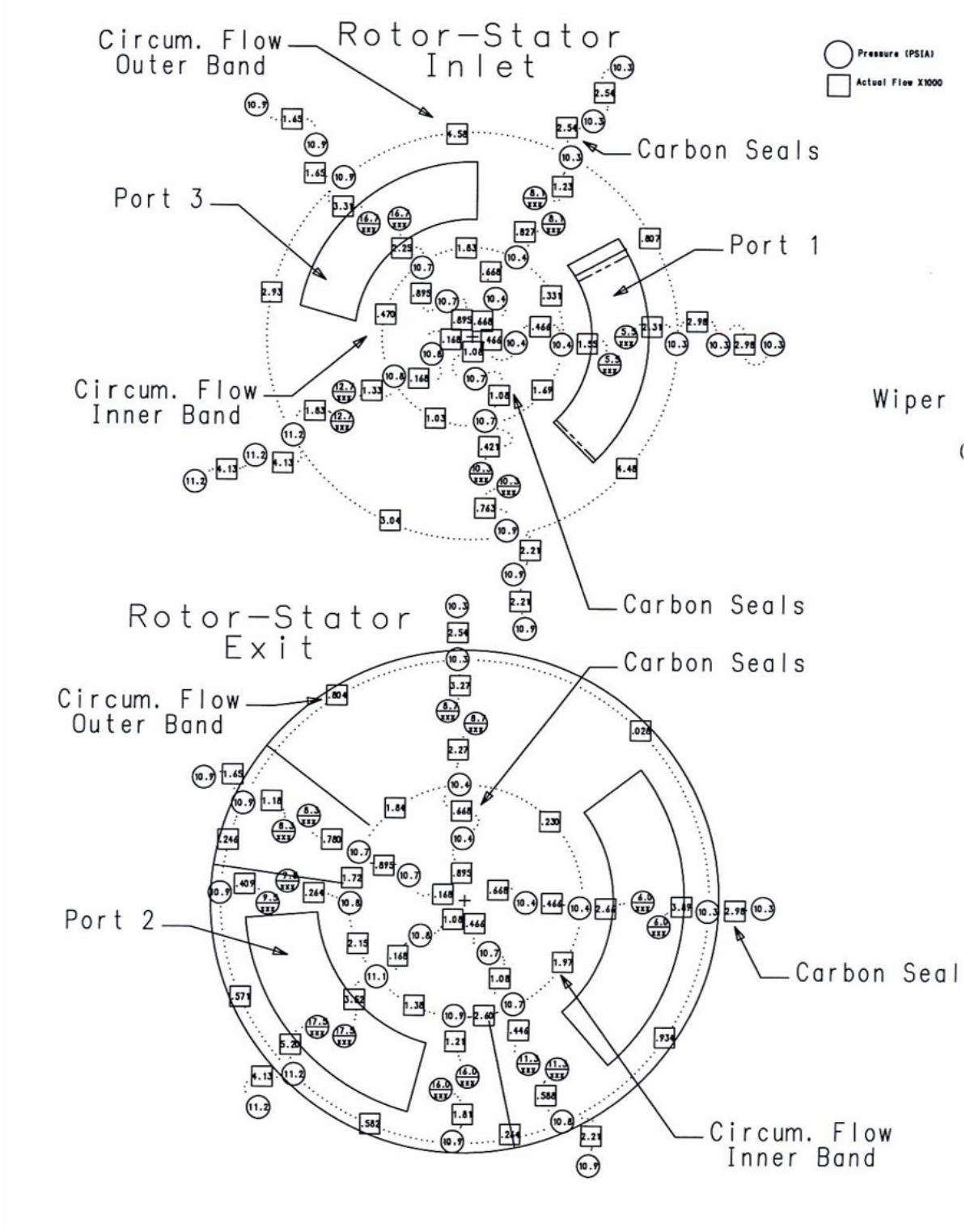
Rotor–Stator
Inlet
Circum. Flow
Outer Band
Carbon Seals
Port 3
Port 1
Circum. Flow
Inner Band
Wiper
Carbon Seals
Rotor–Stator
Exit
Carbon Seals
Circum. Flow
Outer Band
Port 2
Carbon Seal
Circum. Flow
Inner Band

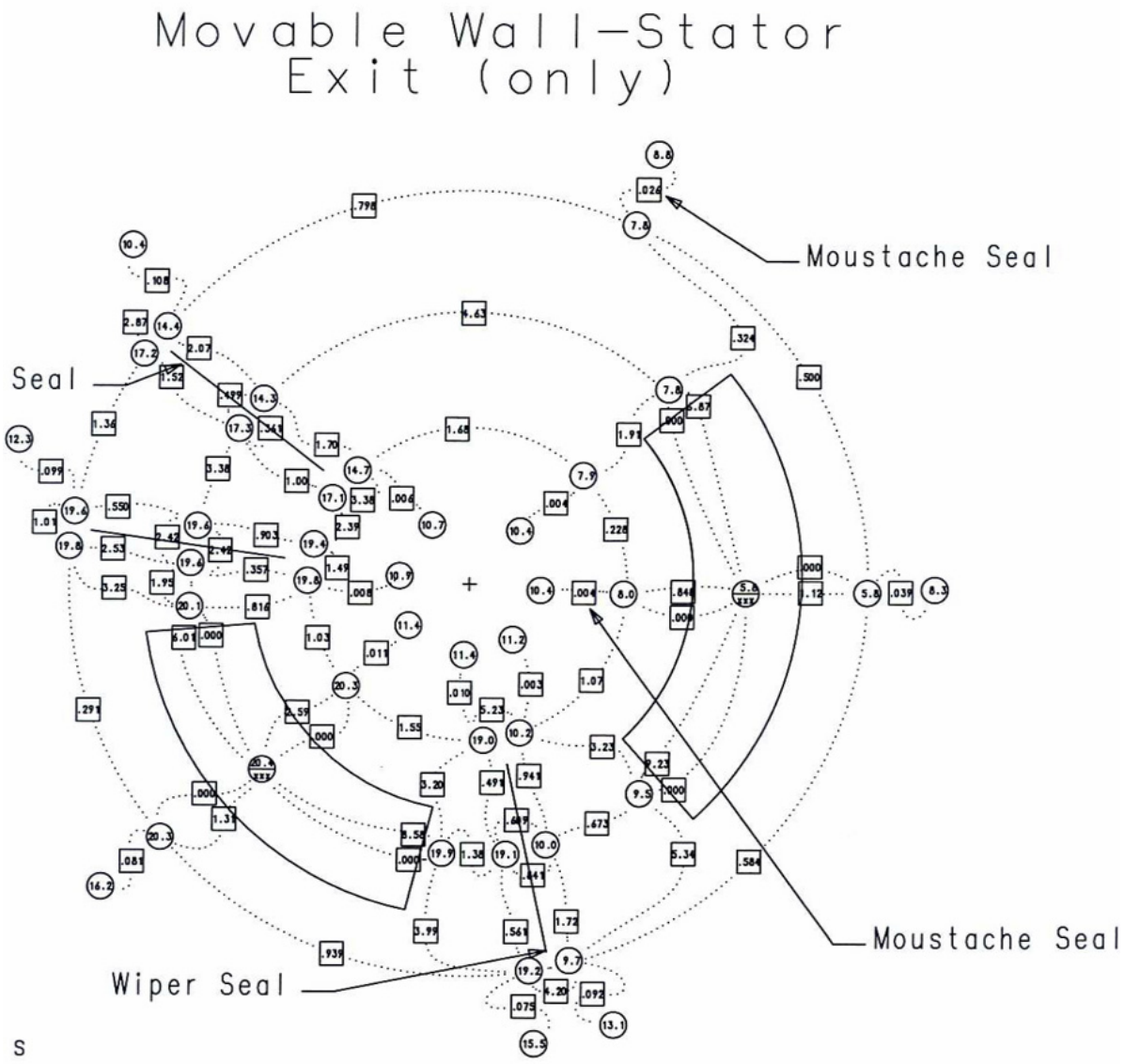

Run 3468 Case 1
Perfect Carbon Seals Present
Inlet Gap = 0.0025"
Exit Gap = 0.004"
MEW-Stator Gap = 0.042"
2 Wiper Seals
Seal Contact Gap = 0.001"

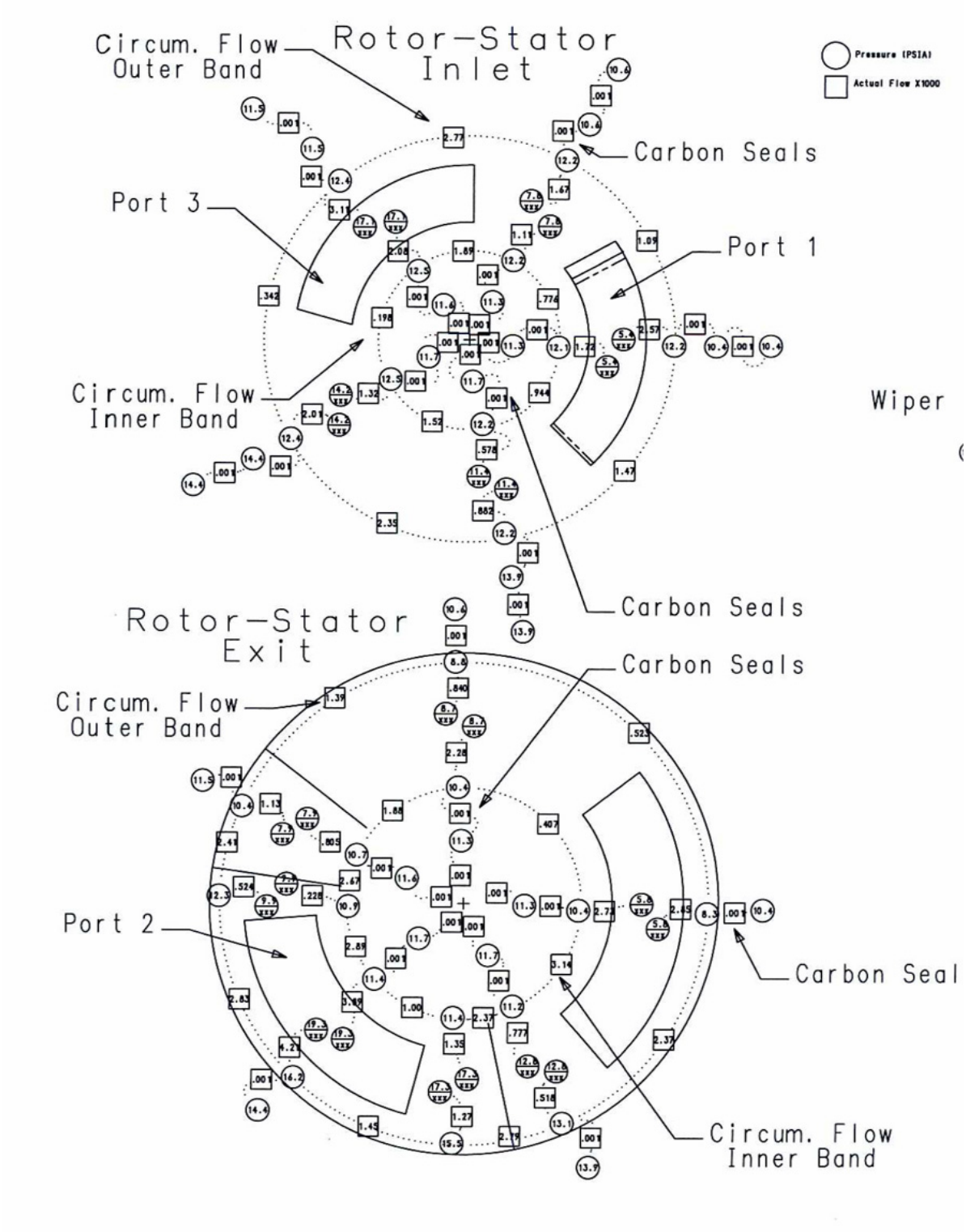
Rotor–Stator
Inlet
Circum. Flow
Outer Band
Pressure (PSIA)
Actual Flow X1000
Carbon Seals
Port 3
Port 1
Circum. Flow
Inner Band
Wiper
Carbon Seals
Rotor–Stator
Exit
Carbon Seals
Circum. Flow
Outer Band
Port 2
Carbon Seal
Circum. Flow
Inner Band

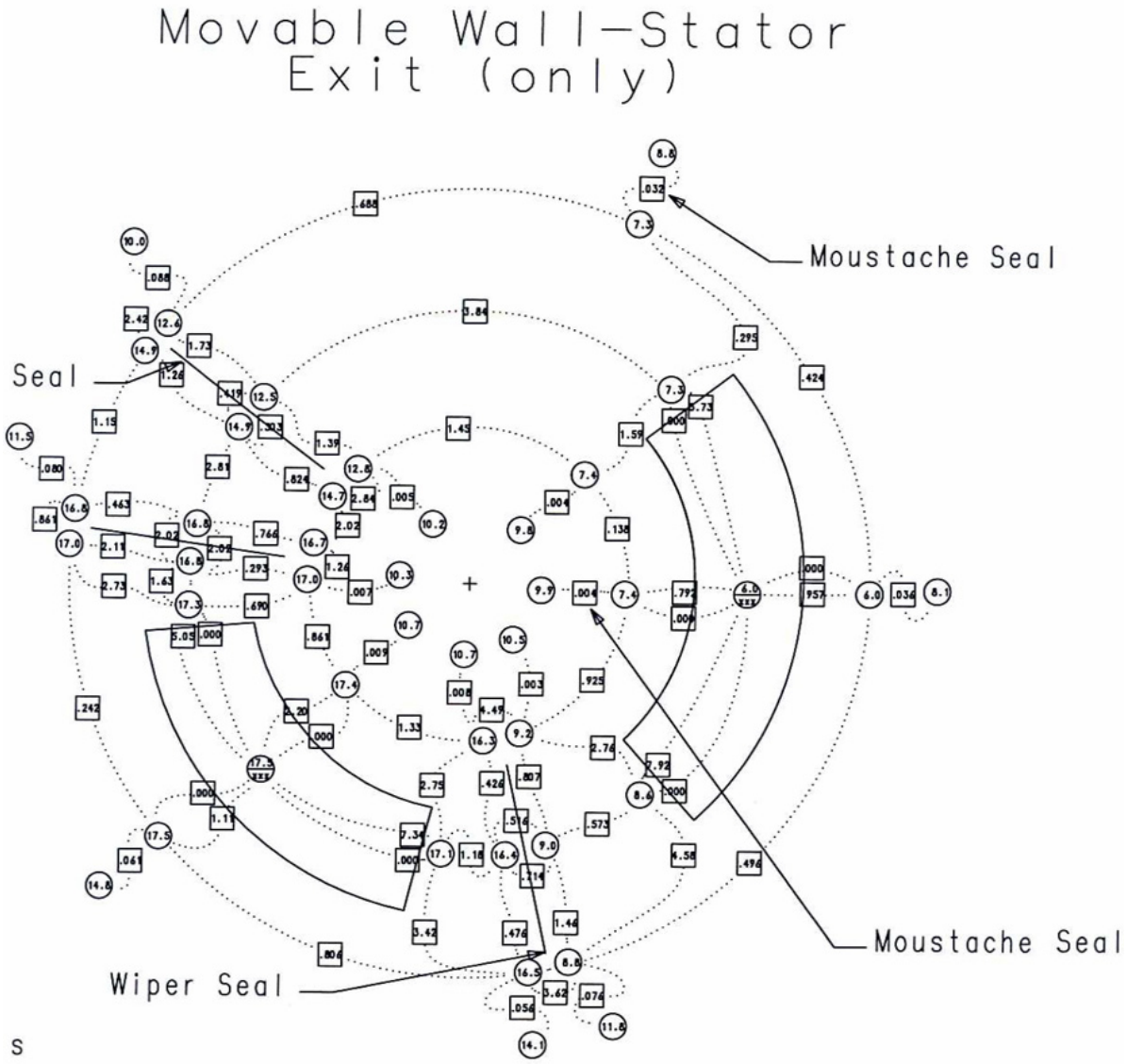

Run 3468 Case 3
Perfect Carbon Seals Present
Inlet Gap = 0.0025"
Exit Gap = 0.004"
MEW-Stator Gap = 0.042"
2 Wiper Seals
Seal Contact Gap = 0.001"

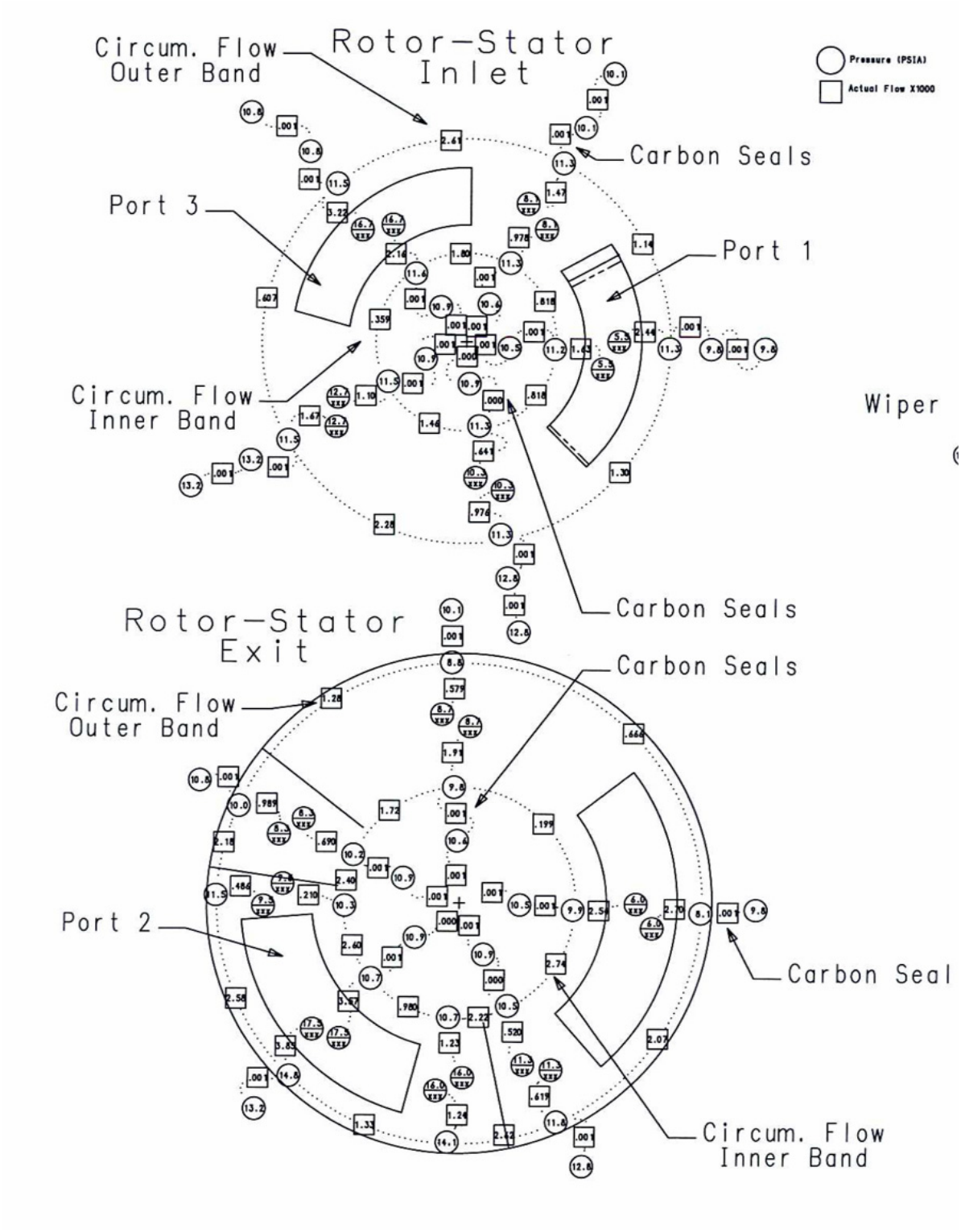
Rotor–Stator
Inlet
Circum. Flow
Outer Band
Carbon Seals
Port 3
Port 1
Circum. Flow
Inner Band
Wiper
Carbon Seals
Rotor–Stator
Exit
Carbon Seals
Circum. Flow
Outer Band
Port 2
Carbon Seal
Circum. Flow
Inner Band
Pressure (PSIA)
Actual Flow X1000

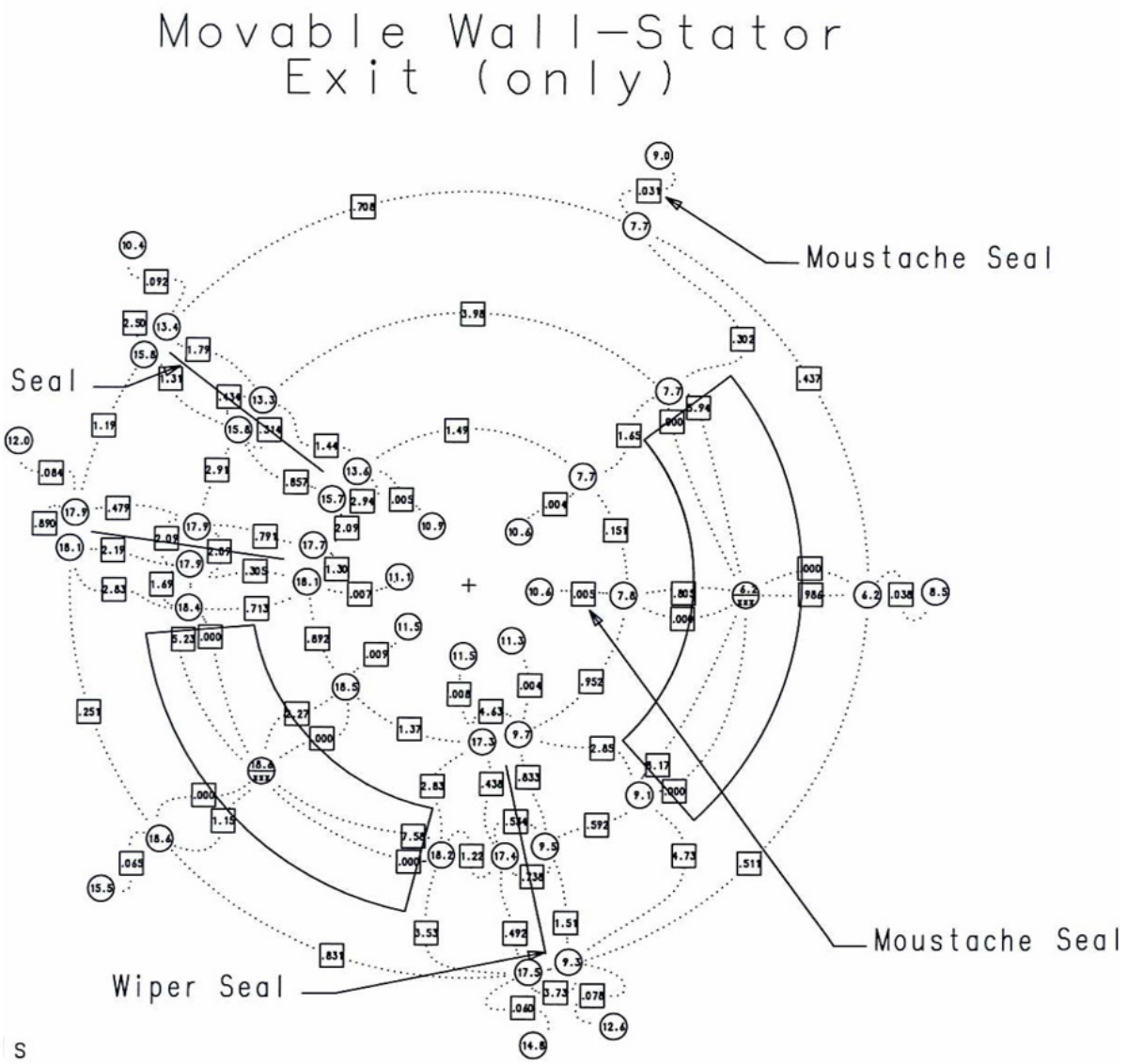
Movable Wall—Stator
Exit (only)
Moustache Seal
Seal
Moustache Seal
Wiper Seal
Run 3677
Inlet Gap = 0.0025"
Exit Gap = 0.004"
MEW-Stator Gap = 0.042"
2 Wiper Seals
Seal Contact Gap = 0.001"

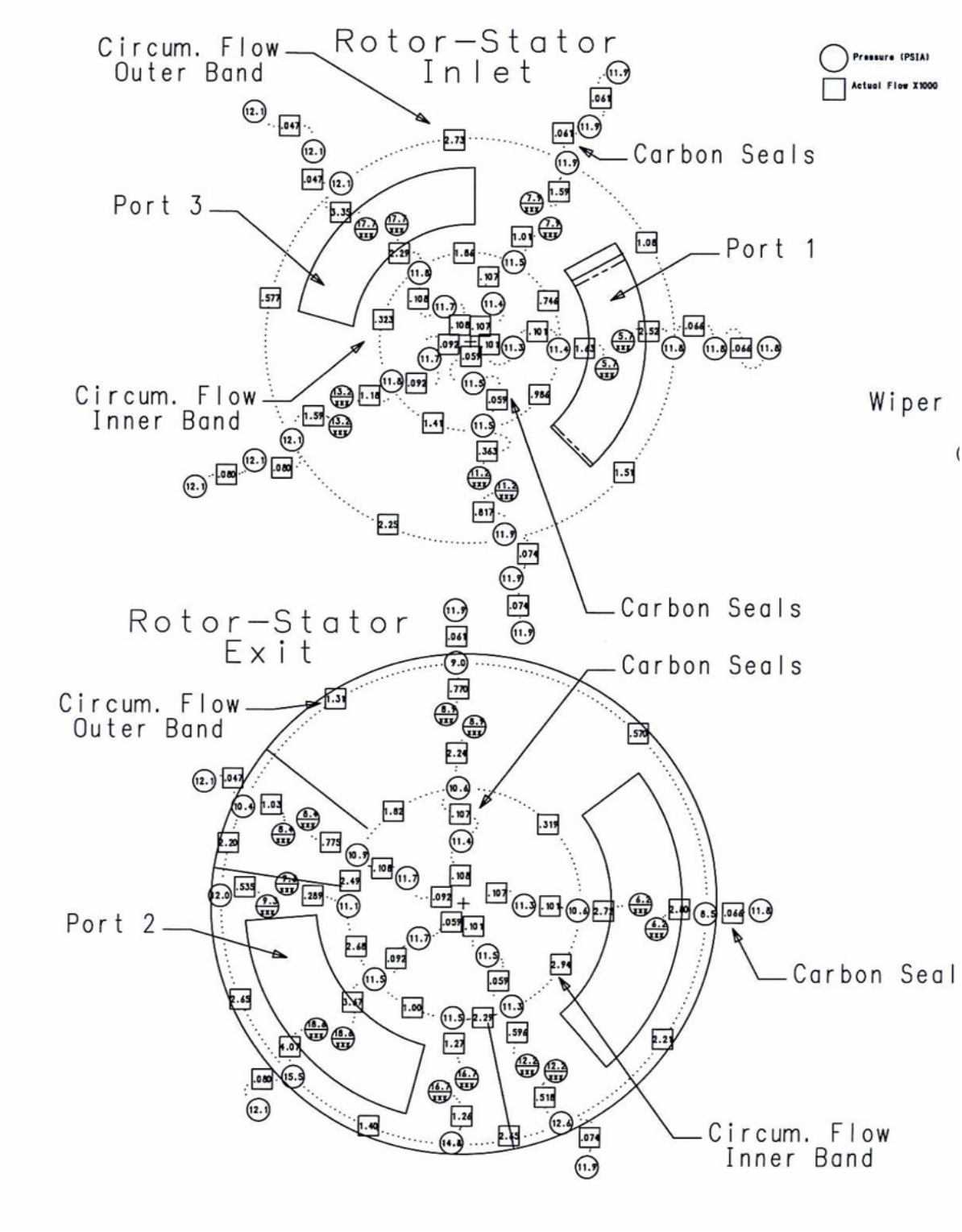
Rotor–Stator
Inlet
Circum. Flow
Outer Band
Carbon Seals
Port 3
Port 1
Circum. Flow
Inner Band
Wiper
Carbon Seals
Rotor–Stator
Exit
Carbon Seals
Circum. Flow
Outer Band
Port 2
Carbon Seal
Circum. Flow
Inner Band
Pressure (PSIA)
Actual Flow X1000

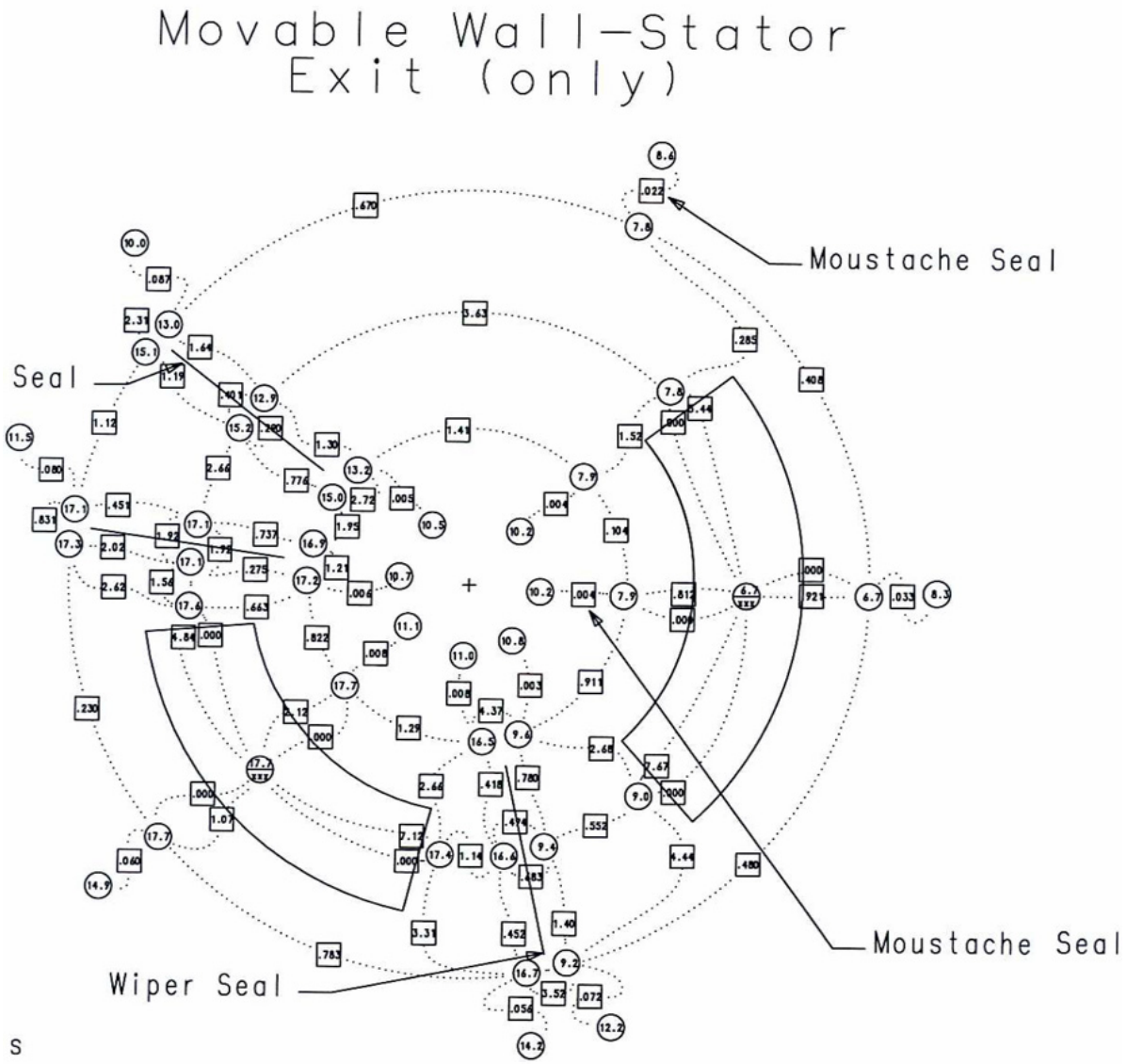

Run 3685
Inlet Gap = 0.0025"
Exit Gap = 0.004"
MEW-Stator Gap = 0.042"
2 Wiper Seals
Seal Contact Gap = 0.001"

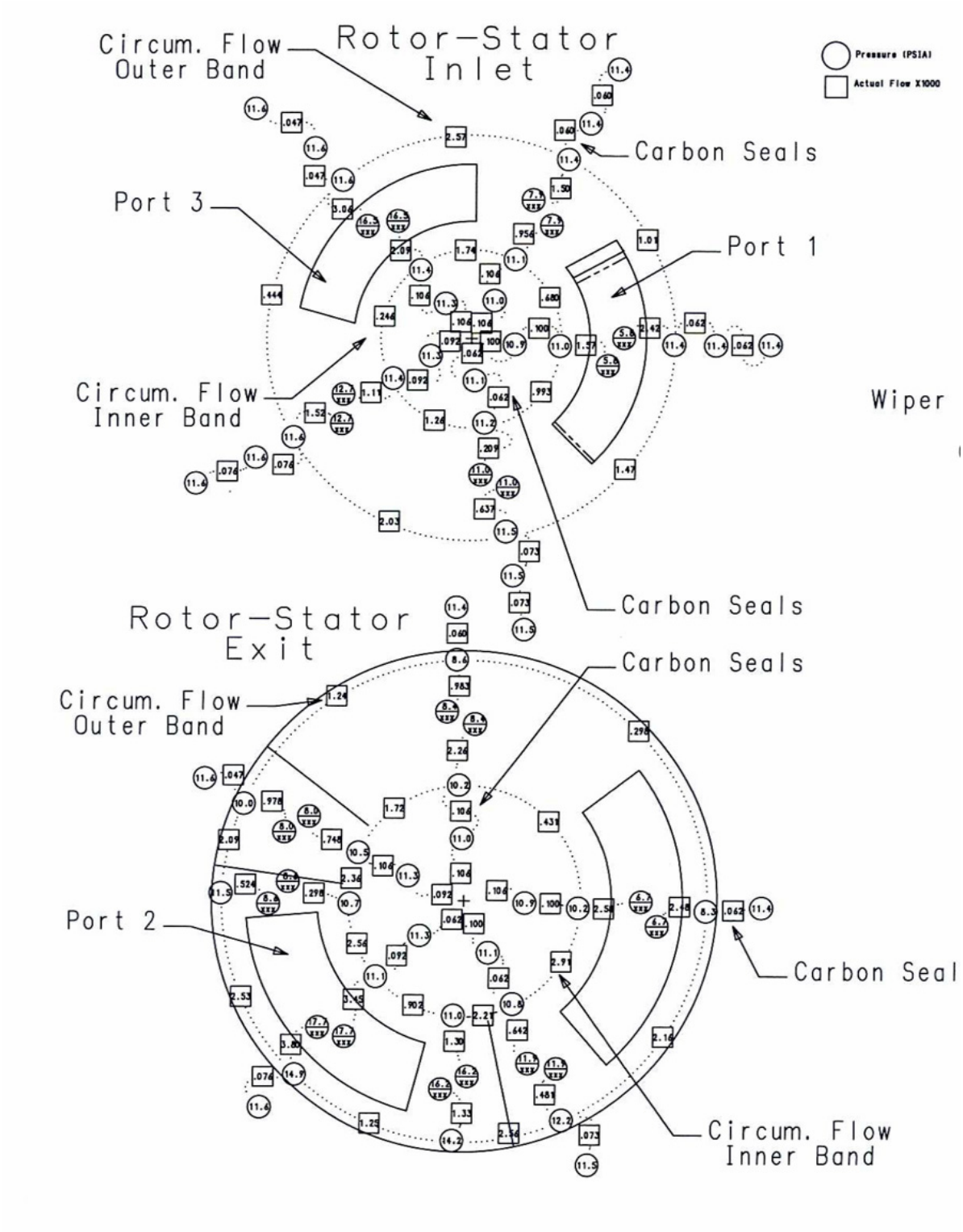
Rotor–Stator
Inlet
Circum. Flow
Outer Band
Carbon Seals
Port 3
Port 1
Circum. Flow
Inner Band
Wiper
Carbon Seals
Rotor–Stator
Exit
Carbon Seals
Circum. Flow
Outer Band
Port 2
Carbon Seal
Circum. Flow
Inner Band

REPORT DOCUMENTATION PAGE		Form Approved OMB No. 0704-0188

1. REPORT DATE *(DD-MM-YYYY)*	2. REPORT TYPE	3. DATES COVERED *(From - To)*
01-12-2008	Final Contractor Report	

4. TITLE AND SUBTITLE
Seal Technology Development for Advanced Component for Airbreathing Engines

5a. CONTRACT NUMBER
NAS3-01143

5b. GRANT NUMBER

5c. PROGRAM ELEMENT NUMBER

6. AUTHOR(S)
Snyder, Philip, H.

5d. PROJECT NUMBER

5e. TASK NUMBER

5f. WORK UNIT NUMBER
WBS 984754.02.07.03.11.02

7. PERFORMING ORGANIZATION NAME(S) AND ADDRESS(ES)
Rolls-Royce North American Technologies, Inc.
Indianapolis, Indiana 46207-7162

8. PERFORMING ORGANIZATION REPORT NUMBER
E-16656

9. SPONSORING/MONITORING AGENCY NAME(S) AND ADDRESS(ES)
National Aeronautics and Space Administration
Washington, DC 20546-0001

10. SPONSORING/MONITORS ACRONYM(S)
NASA

11. SPONSORING/MONITORING REPORT NUMBER
NASA/CR-2008-215479

12. DISTRIBUTION/AVAILABILITY STATEMENT
Unclassified-Unlimited
Subject Category: 07
Available electronically at http://gltrs.grc.nasa.gov
This publication is available from the NASA Center for AeroSpace Information, 301-621-0390

13. SUPPLEMENTARY NOTES

14. ABSTRACT
Key aspects of the design of sealing systems for On Rotor Combustion/Wave Rotor (ORC/WR) systems were addressed. ORC/WR systems generally fit within a broad class of pressure gain Constant Volume Combustors (CVCs) or Pulse Detonation Combustors (PDCs) which are currently being considered for use in many classes of turbine engines for dramatic efficiency improvement. Technology readiness level of this ORC/WR approaches are presently at 2.0. The results of detailed modeling of an ORC/WR system as applied to a regional jet engine application were shown to capture a high degree of pressure gain capabilities. The results of engine cycle analysis indicated the level of specific fuel consumption (SFC) benefits to be 17 percent. The potential losses in pressure gain due to leakage were found to be closely coupled to the wave processes at the rotor endpoints of the ORC/WR system. Extensive investigation into the sealing approaches is reported. Sensitivity studies show that SFC gains of 10 percent remain available even when pressure gain levels are highly penalized. This indicates ORC/WR systems to have a high degree of tolerance to rotor leakage effects but also emphasizes their importance. An engine demonstration of an ORC/WR system is seen as key to progressing the TRL of this technology. An industrial engine was judged to be a highly advantageous platform for demonstration of a first generation ORC/WR system. Prior to such a demonstration, the existing NASA pressure exchanger wave rotor rig was identified as an opportunity to apply both expanded analytical modeling capabilities developed within this program and to identify and fix identified leakage issues existing within this rig. Extensive leakage analysis of the rig was performed and a detailed design of additional sealing strategies for this rig was generated.

15. SUBJECT TERMS
Turbine engines; Pulse detonation engines; Combustion; Detonation; Wave rotor

16. SECURITY CLASSIFICATION OF:			17. LIMITATION OF ABSTRACT	18. NUMBER OF PAGES	19a. NAME OF RESPONSIBLE PERSON
a. REPORT	b. ABSTRACT	c. THIS PAGE			STI Help Desk (email:help@sti.nasa.gov)
U	U	U	UU	128	19b. TELEPHONE NUMBER *(include area code)* 301-621-0390